DAMCO CONSULTING

Government of South Australia

SA Water

Deltares
Enabling Delta Life

Development of the Adelaide Receiving Environment Model

Development of the Adelaide Receiving Environment Model

Jos van Gils
Paul Erftemeijer
Milena Fernandes
Rob Daly

1210877-000

Deltares

Title
Development of the Adelaide Receiving Environment Model

Client	Project	Reference	Pages
SA Water	1210877-000	1210877-000-ZKS-0030	152

Keywords
Seagrass, habitat suitability model, biogeochemical model, hydrodynamics, waves, Adelaide, Delft3D

Summary
Some 6,000 hectares of seagrass were lost in Adelaide's Coastal Waters between the 1949 and 2007. The Adelaide Coastal Waters Study (ACWS, 2001-2007) comprised a multidisciplinary scientific study by a large group of research institutes and universities that provided valuable insights and data related to this issue. The present report summarises the development of the Adelaide Receiving Environment Model (AREM), a modelling instrument intended to provide a quantitative assessment of the relation between coastal discharges and seagrass health. AREM relies on the ACWS insights and data as well as on newly collected data gathered within the context of the present modelling study. AREM uses a habitat suitability index (HSI) approach to quantify the impact of 8 locally most relevant environmental parameters (light penetration to the canopy, shading by epiphyte cover, substrate, temperature, salinity, extreme waves, currents and tidal exposure) on the nine seagrass species in the study area (4 *Posidonia* spp., 2 *Amphibolis* spp., *Heterozostera tasmanica*, *Zostera muellerii* and *Halophila australis*). The relevant environmental parameters are quantified using well-established coupled wave-hydrodynamics, suspended sediments and biogeochemistry models. By feeding these into the HSI method, habitat suitability maps are compiled that express where and to what degree current environmental conditions are favouring/preventing seagrass growth and survival. The HSI has been validated by hindcasting the period of earliest seagrass mapping (1940s), the period of maximum anthropogenic pressure (1970s) and the present period (based on 2011 data). The results of the model confirm that light availability is the most critical pathway for coastal discharges to affect seagrass health, both through direct shading (particles, CDOM, phytoplankton) and by stimulating rapid growth of filamentous epiphytic algae on the seagrass leaves. The light availability for seagrasses is also affected by wave-induced resuspension of the seabed, especially in shallower nearshore areas without seagrass cover, which releases fines that cause periods of relative darkness before they re-settle. This leads to an atypical low light zone in-shore. Recent mapping data (2013) demonstrated that no further net losses of seagrass have occurred since 2007 and revealed the first signs of seagrass recovery at some sites. Further load reduction scenarios will be tested with AREM to devise the most cost-effective management strategy to prevent any further seagrass loss and promote seagrass recovery along Adelaide's coastline.

State
final

Contents

Executive Summary

SA Water is developing targeted coastal waters modelling capabilities, in support of the optimisation of their operations. The first step in this process was the development of a pilot version of the Adelaide Receiving Environment Model (AREM) in 2014. This resulted in a range of recommendations for activities to address knowledge and data gaps. These activities have been carried out and, on the basis of the results, an upgraded and calibrated version of the AREM has been developed. The development and application of the new AREM lead to a better understanding of the present conditions in the Adelaide coastal waters with respect to avoiding further losses of seagrasses and creating conditions for recolonisation. The current report discusses the upgrade of the AREM and the results obtained from its first applications.

Quantifying discharges to the Adelaide metropolitan coastal waters

The results from the AREM pilot model revealed that there were several data gaps with respect to the quantity and quality of discharges to the Adelaide metropolitan coastal waters. These data gaps have been successfully resolved by targeted surveys.

The composite samples collected and analysed by the Adelaide and Mount Lofty Ranges Natural Resources Management Board (AMLR NRM) accurately measure the loads of constituents from the rivers over periods of 2-4 weeks. They do not resolve short time fluctuations of loads however, which are relevant for quantifying conditions for seagrass in the coastal waters. A series of surveys during flood events in the Gawler, Torrens and Onkaparinga Rivers pointed out that the concentrations of suspended solids (SS) are by good approximation proportional to the square of the river flows, which implies that the loads are proportional to the third power of the river flows. For other relevant water quality parameters (e.g. nitrogen, coloured dissolved organic matter or CDOM) no strong correlations with the river flow were found. These new data allowed us to quantify realistic time variable SS concentrations in Adelaide's rivers, fully consistent with the AMLR NRM recorded loads.

In addition, the particle size distribution of the suspended solids in coastal discharges, which determines their fate as well as their effect on seagrasses, was unknown. It has been successfully characterised in the Gawler, Torrens and Onkaparinga Rivers and in all Wastewater Treatment Plant (WWTP) effluents.

The concentrations of CDOM are best characterized by the light absorption at one specific wavelength in the UV spectrum. Such information was not yet available for discharges to the Adelaide coastal waters. It has been successfully quantified in 13 river outflows and in all WWTP effluents.

All together, the targeted surveys allowed for an adequate quantification of (the variability with time) of the discharges to the Adelaide metropolitan coastal waters.

The relation between water quality and PAR downward attenuation in the Adelaide Coastal Waters

The Adelaide Coastal Waters Study (ACWS) concluded that discharges of SS, CDOM and nutrients have an effect on the clarity of the water and therefore on the amount of sunlight penetrating the water column and reaching the seagrass canopy. To quantify this effect, AREM uses a commonly applied model that expresses the vertical light attenuation coefficient K_d (relative loss of light per meter of water column) as a function of the concentrations of key water quality parameters: inorganic particles, chlorophyll-*a* (Chla, a measure for algae biomass), non-algal organic particles and CDOM. For the pilot version of AREM, the contribution of these components to the vertical attenuation coefficient per unit of their

concentration was derived from field studies and model applications elsewhere in the world. By dedicated coastal surveys, field data have been collected to derive these parameters for the Adelaide Coastal Waters.
Samples were collected between November 2014 and September 2015 from three stations along two transects: one off Bolivar with stations at water depths of 3, 7 and 12 m, and one off Grange with stations at water depths of 5, 10 and 15 m. Each site was visited 17 times or more. Paired water quality and light data were obtained to calibrate the vertical light attenuation model. At the same time, the water quality data served to calibrate the biogeochemical model (see below).
The light model derived from the collected field data works remarkably well. It explains 65% of the variability in K_d by using concentrations of four water quality constituents: CDOM, Chla, fine and coarse SS. The constituents having the strongest impact on K_d were found to be CDOM and fine SS.

A hydrodynamics, waves, sediment and biogeochemical model for the Adelaide Coastal Waters
The AREM contains interconnected models describing the hydrodynamics, waves, fine sediment dynamics and biogeochemistry of the Adelaide Coastal waters. These models have the objective of quantifying relevant environmental conditions for seagrass habitat suitability evaluation (see below), as affected by local river discharges and discharges of treated wastewater and stormwater, taking into account the morphology, meteorology and oceanography of the study area.

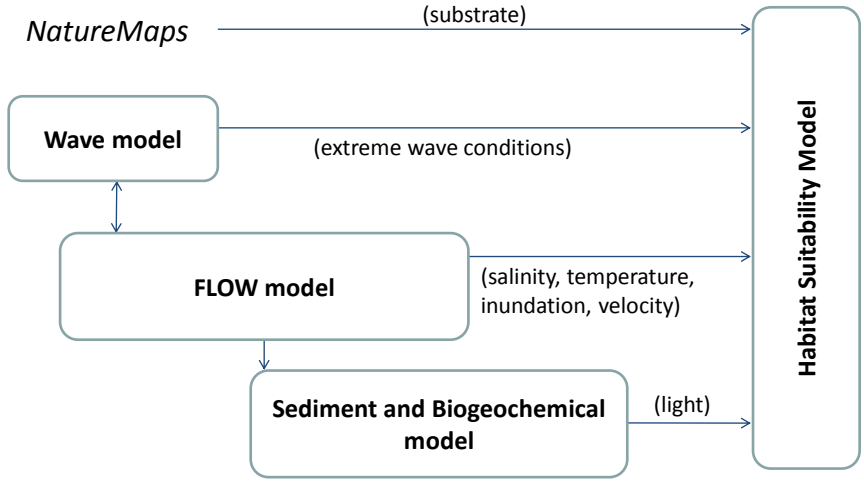

The currents, salinity and temperature of the coastal waters in the study area are simulated by 3D mathematical hydrodynamics modelling, taking into account the feedback mechanisms induced by horizontal and vertical density differences driven by the water temperature and salinity. The impact of waves on near-shore residual currents is included by an online coupling between the hydrodynamics and wave models. The effect of the presence of seagrass on currents and waves is represented by a spatially variable bottom roughness using the large scale *NatureMaps* habitat map provided by DEWNR as input.

The sediment/biogeochemistry model quantifies the light reaching the seagrass leaves, and is driven by currents, shear stress, temperature and salinity calculated by the coupled hydrodynamics and wave models. The sediment model uses a newly created map of the fine particles content of the top sediment layer (based on ACWS data) as input. This map determines the amount of fine particles released as a result of wave-induced resuspension events. The presence of seagrass also affects the mobilization of fine particles during resuspension events: the denser the seagrass cover, the more resuspension is inhibited. The biogeochemistry model contains a sub-model that quantifies the amount of potential nuisance epiphyte growth on the seagrass leaves and the subsequent effect on the amount of light reaching the seagrass leaves. A dedicated literature survey was conducted to select the parameters of this sub-model.

The available data were used to calibrate and validate the AREM components discussed above. The new coastal data collected as a part of the present study were essential, because this dataset is the only one that includes all parameters that contribute to the downward attenuation of light and because it has a high enough frequency to make the results independent of the timing of sampling relative to individual weather events.

This study established for the first time a complete and quantitative relation between coastal discharges and downward light attenuation in the Adelaide coastal waters. On an annually averaged basis, CDOM is the most relevant component over large parts of the study area. Close to the metropolitan coast, inorganic suspended matter is the most relevant, while phytoplankton and organic particles are the most relevant close to the shore north of the Port River outlet.

For both inorganic particles and CDOM we found that there are more sources than coastal discharges alone. Relevant background contributions stem from outside the project area (CDOM), mangroves and seagrasses (CDOM) and sediments (CDOM and inorganic particles). This implies that the relation between the coastal discharges and the concentrations of water quality parameters affecting downward light attenuation is not direct and linear, under the influence of these background contributions.

The relation between coastal discharges and seagrass habitat suitability for the Adelaide Coastal Waters

Habitat Suitability Index (HSI) models are commonly used to predict habitat quality and species distributions based on known relationships between environmental conditions and the tolerances/requirements of plant or animal species. The AREM quantifies the HSI for all nine different species of seagrasses known to occur in the Adelaide Coastal Waters. For each species, the suitability is quantified in relation to 7 environmental conditions, being (a) light reaching the seagrass leaves, (b) salinity, (c) water temperature, (d) substrate, (e) extreme wave exposure, (f) flow velocity and (g) tidal exposure. For all nine seagrass species, a literature survey provided their requirements and tolerance related to these conditions. As indicated above, models were used to quantify 6 of these 7 conditions, while a substrate map was obtained from field data.

The overall seagrass HSI is obtained by overlaying all species specific suitability maps and finding the maximum value. If the environment is suitable for at least one species, we consider it suitable for seagrass. In this process, also information is obtained about the most suitable species (or best adapted species) and the most limiting environmental factor for that most suitable species.

Light availability is the dominant environmental factor determining seagrass habitat suitability, together (locally) with substrate, extreme wave conditions and tidal exposure.

The simulated habitat suitability was found to correlate well with 2013 seagrass cover. The validity of the AREM was further tested by simulating seagrass habitat suitability for the 1940s (prior to human impact) and the mid 1970s (maximum seagrass loss rate), and comparing the

results to seagrass maps obtained from that period. The observed temporal gradients in seagrass cover in the study area are reproduced remarkably well.
By a sensitivity assessment we provided further insights in the relation between the coastal discharges and the habitat suitability for seagrasses. The simulation results are evaluated in the Central Metropolitan Coast area ("central"), in the area north of it and in the area south of it. In the north and central zones, results are presented for the area presently without seagrass ("sand"), for the south zone this difference could not be made due to lack of data on seagrass cover.

	Effect of Penrice removal in 2013 (change of suitable area (ha), relative to 2011)	**Effect of all WWTPs removed (change of suitable area (ha), relative to 2013)**	**Effect of all rivers removed (change of suitable area (ha), relative to 2013)**	**Effect of reduced resuspension (change of suitable area (ha), relative to 2013)**
North-sand	2221	1204	517	391
Central-sand	572	985	430	886
South	13	561	80	245
Total	2806	2751	1027	1521

The results show that the removal of Penrice has already had a strong positive effect, which is concentrated in front of Port River, in the north. The (hypothetical) removal of all WWTP discharges is expected to have a similar additional positive effect, but more equally distributed. The (hypothetical) removal of all rivers would have a marked effect too, but significantly smaller. Finally, resuspension from areas which are currently bare sand but used to have seagrass cover in the 1940s, has a significant effect on the area suitable for seagrasses, especially in the central part.
A high HSI does not automatically imply the immediate recovery of seagrass. Successful recruitment, assuming sufficient seed supply, is determined by the probability of uprooting of seedlings because seedlings are not as well-established and anchored as mature plants. Thus, recovery is primarily a matter of "windows of opportunity", when seedlings will manage to successfully establish during a window of time with sufficiently calm conditions without major perturbations.

Area specific loads (ASLs) as an indicator for pressure from coastal discharges
The Adelaide Coastal Waters Study used the concept of area specific loads (ASL) for the coastal area as a whole, as an indicator for the pressure from coastal discharges on seagrasses, and stipulated a threshold value of 1 t km^{-2} of nitrogen. We explored it as a second line of evidence. A method to derive spatially explicit maps of simulated ASLs has been developed and applied. The results obtained for the mid 1970s were overlayed with areas of recorded seagrass loss. A correlation was found, which indicated that the area of inshore continuous seagrass losses is characterised by 3 months rolling average ASL values exceeding 1.5 tN km^{-2}. Assuming that this value represents a historically based threshold value for coastal discharges, we evaluated current conditions against this threshold and found that it is only exceeded in small areas in the direct vicinity of the present WWTP outfalls. This would imply that current conditions would be sufficient for almost complete recovery of previous seagrass losses.
The AREM simulation results explain why this is not the case. The ASL based threshold expresses which coastal discharges could kill seagrass in an otherwise "pristine" environment (without enhanced resuspension due to seagrass losses). The AREM simulations reveal a so-called positive feedback loop: seagrass losses cause enhanced resuspension, which causes further losses if the discharges remain high and prevents recovery after discharges have been reduced. Only after the discharges have been reduced far enough to compensate the

resuspension-induced turbidity, recovery may start. This is all included in the habitat suitability maps produced by AREM. The ASL threshold neglects this positive feedback loop.

Use of the AREM

The upgraded and validated AREM can now be used to evaluate various management scenarios, which could refer to changes in one or more discharges (constant or variable in time), changes in the composition of discharges, relocation of discharges etc. The AREM output will not only provide changes in area suitable for seagrass relative to a chosen reference, but also a wide spectrum of maps and time series plots (as provided in this report) that support the interpretation of the results.

1 General introduction

Bolivar Wastewater Treatment Plant – Photograph by SA Water

1.1 Background

Over decades, seagrass cover in the Adelaide coastal waters has declined. Studies like the Adelaide Coastal Waters Study (ACWS; Fox et al., 2007) have attributed this deterioration to high nutrient loads that stimulate phytoplankton and epiphyte growth and as such decrease the availability of light for seagrass photosynthesis. High suspended sediment concentrations (e.g. from stormwater drains) are considered to have a similar effect, whereas low sediment stability is considered an issue for seagrass recovery. In response to these studies, the Adelaide Coastal Water Quality Improvement Program (ACWQIP) aims at a reduction in nitrogen loads of 75% of 2003 levels (2,400 t) and a reduction in sediment loads of 50% of 2003 levels (8,400 t), as well as an unquantified reduction of coloured dissolved organic matter (CDOM) for 2020-2030. This has evident consequences for SA Water operations. By 2013, a substantial reduction in emissions from wastewater treatment plants (WWTP) has already been realised, but further reductions require considerable investments. Moreover, the population of Adelaide is expected to grow by up to 45-50% between 2006 and 2036, resulting in higher volumes of wastewater to treat and a larger drained urbanised area. An efficient use of (financial) resources is required to keep SA Water's services at an acceptable cost level. However, by the end of 2012, SA Water concluded that understanding of system functioning as a whole is limited, hindering the capacity to target investment into initiatives for specific areas and periods of the year that would provide clear and measurable environmental outcomes. To overcome this situation, SA Water is developing targeted coastal waters modelling capabilities, in support of the optimisation of their operations. As a first step in this process, SA Water completed the development of a pilot version of the Adelaide Receiving Environment Model in 2014 (AREM; Zijl et al., 2014). The development of the pilot model resulted in a range of recommendations for activities to address knowledge and data gaps

(van Gils and Barbara, 2014). These activities have been carried out and the results are compiled in the present report.

1.2 This study

The overall objectives for this study are:

- Expanding and evaluating the pilot version of AREM in a way that as far as possible creates conditions for acceptance by local stakeholders.
- Using the AREM to answer the following questions, all directed towards avoiding further seagrass loss and promoting conditions for recolonisation:
  - To what extent are the present conditions likely to cause further losses of seagrasses (short-term), or halt recolonisation (long-term)? What is the relative contribution by continuous discharges, intermittent discharges and resuspension? What is the relative contribution by direct shading and epiphyte growth?
  - What are the potential benefits of loads reduction in this respect? Is there a difference between the continuous or the intermittent discharges? To what degree has the removal of the Penrice discharge contributed to improved conditions for seagrasses?

The way forward with respect to the expansion and evaluation of AREM has been explored during an Inception Phase (Deltares & Jacobs, 2015) and has been discussed with the Scientific Advisory Group (SAG) appointed by SA Water. These explorations and discussions have contributed to the results compiled in the present report.

The project has been carried out by a Deltares team lead by Jos van Gils, Firmijn Zijl and Dr Sofia Caires. Damco Consulting, in particular Dr Paul Erftemeijer, acted as a subcontractor to Deltares. Parts of the overall scope of work have been carried by Dr Milena Fernandes, Dr Rob Daly and Tim Kildea of SA Water. The work compiled in this report has been carried out between May 2015 and June 2016.

Figure 1.1 Area of interest (blue box)

This study addresses the Adelaide coastal waters, from 20 km north of Port Gawler in the north to Sellicks Beach in the south, extending over about 80 km in a north-south direction and 20 km off the coastline (see blue rectangle in Figure 1.1). The study area is part of Gulf St Vincent, which is connected to the open ocean via Investigator Strait and Backstairs Passage.

1.3 AREM availability

At the end of this study, the AREM files and supportive programs have been transferred by Deltares to SA Water.

1.4 Acknowledgements

The authors of this report acknowledge the advice and recommendations by the Scientific Advisory Group and by the Stakeholder Board appointed by SA Water as a part of the present project. Furthermore, we acknowledge the support by Peter Pfennig and Clive Jenkins of EPA in finding information related to the Penrice discharges, Sam Gaylard of EPA for making available coastal water quality data and Ying He of EPA for processing sediment composition data. We thank the SA Water staff that contributed to collecting data, including Tim Kildea and Scott Kraft. We thank the Deltares staff that contributed to the work presented in this report, including Sofia Caires, Jasper Dijkstra, Gerrit Hendriksen, Peter Herman, Tony Minns, Joana van Nieuwkoop, Joao de Lima Rego, Willem Stolte, Meinard Tiessen, Tineke Troost and Firmijn Zijl. In addition we acknowledge the assistance from other institutes and individuals to identify and access historical datasets, in particular Chari Pattiaratchi (UWA), James Cameron, Matthew Royal and Christopher Botting (DEWNR), Elaine Miles (BoM), Jason Tanner (PIRSA-SARDI), Jochen Kaempf (Flinders University), Gayani Dharmasena (Penrice), and Sally Edwards (Geological Survey of Queensland). We thank the Scientific Advisory Group for their guidance and input in the development of this final version of the model: Anthony Cheshire (SMU), Mark Baird (CSIRO), Chari Pattiaratchi (UWA), Michelle Waycott (DEWNR, UoA) and Sam Gaylard (EPA). We thank the internal SA Water working group for advice and review: James Crocker, Alex Donald, Tara Hage, Nirmala Dinesh, Olaf Richter, Liz Roder and Karen Rouse. We also acknowledge the support from stakeholder engagement advisors Jane Wilson and Matthew Bonnett (SA Water), and Georgina House (GH Planning).

1.5 This report

This report is divided into 4 main chapters, which deal with specific topics of the AREM development. Chapter 2 “Quantifying discharges to the Adelaide metropolitan coastal waters” discusses the characterisation of coastal discharges on the basis of additional data collected by SA Water. Chapter 3 “The relation between water quality and PAR downward attenuation in the Adelaide Coastal Waters” discusses how AREM models downward attenuation of light on the basis of additional coastal water quality data collected by SA Water. Chapter 4 “A hydrodynamics, waves, sediment and biogeochemical model for the Adelaide Coastal Waters” discusses the dynamic water system models that quantify essential environmental conditions for seagrass. Chapter 5 “The relation between coastal discharges and seagrass habitat suitability for the Adelaide Coastal Waters” discusses the habitat suitability model that provides a quantitative cause-effect relation between coastal discharges and habitat suitability in the study area. Each one of these chapters is organised in Materials & Methods, Results and Discussion sections. The final Chapter 6 provides a summary of the relevant outcomes of the project.

1.6 Abbreviations used

Abbreviation	Explanation
ACWQIP	Adelaide Coastal Water Quality Improvement Program
ACWS	Adelaide Coastal Waters Study
ADCP	Acoustic Doppler Current Profiler
ANMN	Australian National Moorings Network
AREM	Adelaide Receiving Environment Model
ASL	Area Specific Load
BGC	biogeochemical (model)
BLOOM	phytoplankton sub-model in Delft3D
BoM	Bureau of Meteorology
CDOM	coloured dissolved organic matter, fraction of DOM
Chla	Chlorophyll-a
CSIRO	Commonwealth Scientific and Industrial Research Organisation
Delft3D	generic coastal modelling software
DEWNR	Department of Environment, Water and Natural Resources
DO	Dissolved Oxygen
DOM	dissolved organic matter
DOC	dissolved organic carbon
DW	dry weight
EF	emission factor
EMC	Event Mean Concentration
EPA	Environmental Protection Agency of South Australia
GOF	goodness of fit
HSI	habitat suitability index
IM	(particulate) inorganic matter (sand and silt)
IMOS	Integrated Marine Observing System
MSL	Mean Sea Level
N	nitrogen
NH4	ammonium (free and ionised)
NO3, NO2	nitrates, nitrites
NOx, OxN	oxidised nitrogen (sum of nitrates and nitrites)
NRSKAI	National Reference Station Kangaroo Island (SAIMOS)
OC	organic carbon
P	phosphorus
PAR	photosynthetically active radiation (400-700 nm)
PIM	particulate inorganic matter (= IM)
PIP	particulate inorganic P
PO4	ortho phosphates
POC	particulate organic carbon
PON	particulate organic nitrogen
POP	particulate organic phosphorus
RA	rolling average
RMSE	root mean square error
RMSD	root-mean square deviation
SAG	Scientific Advisory Group

Abbreviation	Explanation
SAIMOS	South Australian Integrated Marine Observing System
SARDI	South Australian Research and Development Institute
std	standard deviation
Si	(dissolved) silica
SiO2	silicates
SI	suitability index
SS	suspended solids (= TSS)
STP	sewage treatment plant, used as a synonym for WWTP
SWAN	wave modelling software
TOC	total organic carbon
TotN, TN	total nitrogen
TotP, TP	total phosphorus
TDS	total dissolved solids
TSS	total suspended solids (= SS)
UTC	Coordinated Universal Time
UV-abs	absorption of light measured at a frequency of 254 nm
WWTP	wastewater treatment plant

2 Quantifying discharges to the Adelaide metropolitan coastal waters

Discharge Channel of Bolivar Wastewater Treatment Plant – Photograph by SA Water

2.1 Introduction

Light available to seagrasses in the Adelaide coastal waters is influenced by the discharge of suspended solids (SS) and coloured dissolved organic matter (CDOM) from land sources (Figure 2.1). The pilot phase of the Adelaide Receiving Environment Model (AREM) used composite sampler data from the Adelaide and Mount Lofty Ranges Natural Resources Management Board (AMLR NRM)(http://amlr.waterdata.com.au/) to define the concentration of SS in the rivers discharging to the coast, with SS separated into two fractions of inorganic particles settling either rapidly (IM1, >63 µm) or slowly (IM2, <63 µm) (Zijl et al. 2014). IM2 was assumed to contribute 20% of river inputs, and 80% of inputs from wastewater treatment plants (WWTPs).

The AMLR NRM composite samples for SS are collected using an automatic sampler linked to measured flows with samples collected at regular intervals of discharge. These samples are combined in a large container and are intended to represent the average concentration over the period of collection; typically 1 month. Sampling is more frequent with increasing flows so any events that occur during this period have a stronger effect on the concentration in the composite sample. This sampling method is intended to accurately represent the loads

of constituents from the river over the sampling period to derive a flow-weighted mean concentration. SS has a strong correlation with flow however and large events can deliver much of the load for the monthly period over only a few days or hours. The pilot phase model used daily total flow and composite sample concentration to define the loads to the coast. While this will provide the correct load from the river it tends to “flatten out” the dynamics of the SS discharge causing the model to underestimate the short term impacts of large flow events.

Figure 2.1 Overview of discharge points in the AREM

The pilot phase of AREM also assumed a constant value of 10 mg L^{-1} for the discharge of dissolved organic carbon (DOC) from both rivers and WWTPs as a proxy for CDOM (Zijl et al. 2014). The use of DOC as a proxy might be hindered by its variable composition making it difficult to predict light attenuation. A better alternative is to measure light absorption in one particular wavelength in the UV part of the spectrum (UV-abs) (Coble 2007). UV-abs can then be extrapolated to derive overall light attenuation in the photosynthetically active part of the spectrum (PAR, 400-700 nm).

The main goal of this work was to improve the parameterisation of land inputs of SS and CDOM into AREM. We used grab (snapshot) samples collected from three major rivers (Gawler, Torrens, Onkaparinga) to define CDOM inputs, the particle size distribution of SS, and flow relationships to SS. These relationships were then used together with the measured composite sample data, to define river inputs with more dynamic concentrations for SS. This is intended to provide more realistic SS concentrations while still being based on the recorded load for the year. The riverine data was further used to tune the speciation of nutrient and organic matter inputs in AREM. The particle size distribution of SS and CDOM concentrations in effluents from the WWTPs discharging to the coast were also measured, and industrial inputs from the Penrice soda ash plant were parameterised based on historical data.

2.2 Materials and methods

2.2.1 Rivers

2.2.1.1 Sampling

Hourly time series of the river discharges and constituent concentrations were derived from the AMLR NRM water quality monitoring network in Adelaide's rivers (http://amlr.waterdata.com.au/). These data comprise analyses of continuous monthly or biweekly flow-proportional composite water quality samples for SS, total phosphorus (TP), total Kjeldahl nitrogen (TKN) and oxidised nitrogen (NO_x). The data derived from the composite sampling are expected to be representative for the river loads of substances, but do not capture the short term variability of the concentrations.

To estimate temporal variability of river inputs, grab surface water samples were collected during the hydrograph for significant rain events (>7 mm rain) from the main rivers discharging to the Adelaide coast: Gawler, Torrens and Onkaparinga (Table 2.1, Figure 2.1). Samples were collected between July 2014 and September 2015. Due to less urbanised catchments, there were no significant flows in the Gawler and Onkaparinga rivers except in winter. The Gawler river did not have any significant flows during 2015 because the catchment never became saturated (BOM dryness index for Mt Crawford). The grab samples were analysed for the absorption of light at 254 nm (UV-abs), SS (concentration and particle size distribution), as well as particulate organic carbon (POC) and nutrients, i.e. ammonia, NO_x, TKN, soluble reactive P and TP.

Because UV-abs is not routinely monitored in Adelaide's rivers, additional composite samples were collected as part of the AMLR NRM water quality monitoring network, in order to estimate spatial variability of river CDOM inputs. This concerned sampling in the wet season during June-September 2015 (one composite sample per month).

Table 2.1 River grab sampler locations.

Site Code	Site Name
A5041014	Torrens River @ Seaview Road Bridge
A5050510	Gawler River @ Virginia Park
A5031005	Onkaparinga River 1.1 km u/s Ford Old Noarlunga

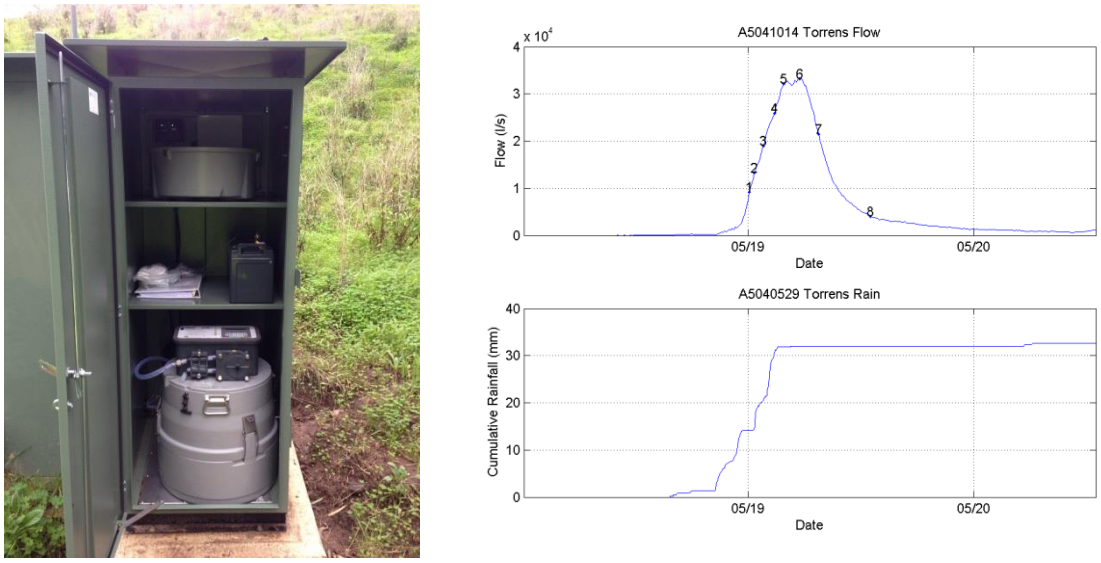

Figure 2.2 Automatic sampler installation (left), and example hydrograph with sample collection times shown (right).

2.2.1.2 *Flow correlations and AREM input time-series*

Results from grab samples were used to examine correlations between flow and SS in each river using a power function:

$$C_{ss} = aQ^b + c \quad (1)$$

where C_{ss} is the SS concentration and Q is flow. Model parameters were fitted to the observed data using Excel solver by minimising a least squares objective function.

The power-law fit describes the long-term character of the SS load in a river but does not reproduce the natural variability in SS concentrations. Scatter around the regression line is, among other things, caused by variations in sediment supply due to, e.g. seasonal effects controlled by weather patterns, previous conditions in the river basin, channel recovery from extreme precipitation events and differences in sediment availability at the beginning and end of a flood. In an attempt to stay true to the observed loads from the rivers the modelled SS was combined with the composite sample data.

Observed hourly flow data was used to model a time series for SS in each river. The flow and modelled SS data was divided into sections to represent the period each composite sample was collected over (~1 month). The flow-weighted mean concentration for the modelled data was calculated for each period ($\bar{C}_{model}$). The ratio between this value and the observed composite concentration ($\bar{C}_{obs}$) was used to derive a scale factor for SS concentration derived from the power function (C_{SS}):

$$C_{AREM} = C_{ss} \frac{\bar{C}_{obs}}{\bar{C}_{model}} \quad where \quad \bar{C}_{model} = \frac{\sum C_{ss(i)} Q_{(i)}}{\sum Q_{(i)}} \tag{2}$$

2.2.1.3 *Bad or missing data*

There was a problem with the Range Wetland Outlet (AMLR NRM site A5041024) where flow data was reported as >0.5 ML d^{-1} for the entire period between 2010 and 2011. The flow for this site was replaced by flow from the nearby Magazine Wetland Outlet (A5041025) scaled by an annual factor of 0.3382. The scale factor was determined by comparing annual totals for 2013 and 2014 at each site.

For sites where composite data was not available, data from a similar or nearby site was used as an estimate for the concentrations at those sites. Helps Drain 100m d/s Summer Rd Bolivar (A5051013) concentrations were used for Dry Creek @ Bridge Road (A5041052), Sturt River d/s Anzac Highway (A5040549) concentrations were used for Patawalonga Creek u/s Barcoo Outlet (A5041022), Gawler River @ Virginia Park (A5050510) concentrations were used for Light River at Pt Wakefield Rd Bridge (A5051003).

Some sites had periods of missing flow data; during these periods the flow was assumed to be zero.

2.2.2 Wastewater treatment plants

2.2.2.1 *Sampling*

SA Water routinely records daily flow volumes of effluents and collects periodic samples for SS, TP, TKN, ammonium, NO_x, silicates and dissolved oxygen. These data were supplemented by samples to determine CDOM (UV-abs) and the particle size distribution of SS in effluents.

Samples were collected from each WWTP discharging to the Adelaide's coast: Bolivar (effluents from the stabilisation lagoons and from the High Salinity Plant), Glenelg (effluents from Plants A/B and C/D), and Christies Beach (effluents from Plants A/B and C). Weekly composite samples were collected from each of these effluent streams in November 2014, February, April, May, July, August and September 2015.

2.2.2.2 *Laboratory analysis*

Samples for the analysis of CDOM were filtered through a 0.45 µm syringe filter. Absorbance was measured at 254 nm by comparison with an ultrapure water blank in a UV-1700 PharmaSpec Spectrophotometer equipped with a 10 mm quartz cell (Standards Australia 1990). The absorption coefficient a, used as a proxy of CDOM concentration, was calculated as:

$$a = 2.303 \times \frac{A}{l} \tag{1}$$

where A is the absorbance and l is the path length (Hu et al. 2002; Coble 2007).

Samples for the analysis of SS were filtered through a pre-weighed glass fibre filter (GF/C, 47 mm diameter), and dried at 103-105 °C (APHA-AWWA-WEF 2012a).

Samples for the determination of the particle size distribution of SS were analysed in a LISST laser diffraction particle size analyser (Sequoia Scientific, USA), and the results integrated into size fractions.

Samples for the analysis of organic carbon were either analysed unfiltered for the determination of total organic carbon (TOC) or filtered through a 0.45 µm syringe filter for the determination of dissolved organic carbon (DOC). Samples were acidified to release inorganic carbon, then digested with sodium persulphate at 98-100 °C and the resulting carbon dioxide measured in a OI Analytical Organic Carbon Analyser 1030 (APHA-AWWA-WEF 1995). POC was determined as the difference between TOC and DOC.

The concentrations of TKN and TP were determined in a KoneLab AQUAKEM discrete analyser after digestion of unfiltered samples with sulphuric acid and potassium sulphate (APHA-AWWA-WEF 2012b, e). Samples for the analysis of dissolved nutrients were filtered through a 0.45 µm syringe filter in the field. The concentrations of ammonium were determined in a KoneLab AQUAKEM discrete analyser (APHA-AWWA-WEF 2012c). The concentrations of soluble reactive P (orthophosphate) and NO_x were determined by flow injection analysis (FIA) in a Lachat Quickchem 8500 Automated Ion Analyser (APHA-AWWA-WEF 2012f, d).

2.3 Results

2.3.1 Rivers

2.3.1.1 Correlation between flow and SS

For both the Torrens and Gawler rivers the power model used for the correlation between flow and SS explains more than 80% of the variability in the data (Figure 2.3 and Figure 2.4, Table 2.2). In the case of the Onkaparinga River there was no consistent relationship between flow and SS.

For the purposes of creating a dynamic time series of SS in AREM, we decided to use the model from the Gawler River to describe non-urban catchments including the Onkaparinga River. This model is compared against observed values in the Onkaparinga River in Figure 2.5, falling between the two extremes of observed values. As will be outlined later, the actual loads are linked to the observed composite sample data so the model used only affects the dynamics of the inputs but not the loads.

Table 2.2 Model parameters (Q in L s^{-1} and Css in mg L^{-1})

Parameter	Torrens	Gawler
a	7.97E-08	2.00E-06
b	2.08	1.76
c	14.4	11.24
Mean Absolute Error	5.41	9.23
r^2	0.906	0.806

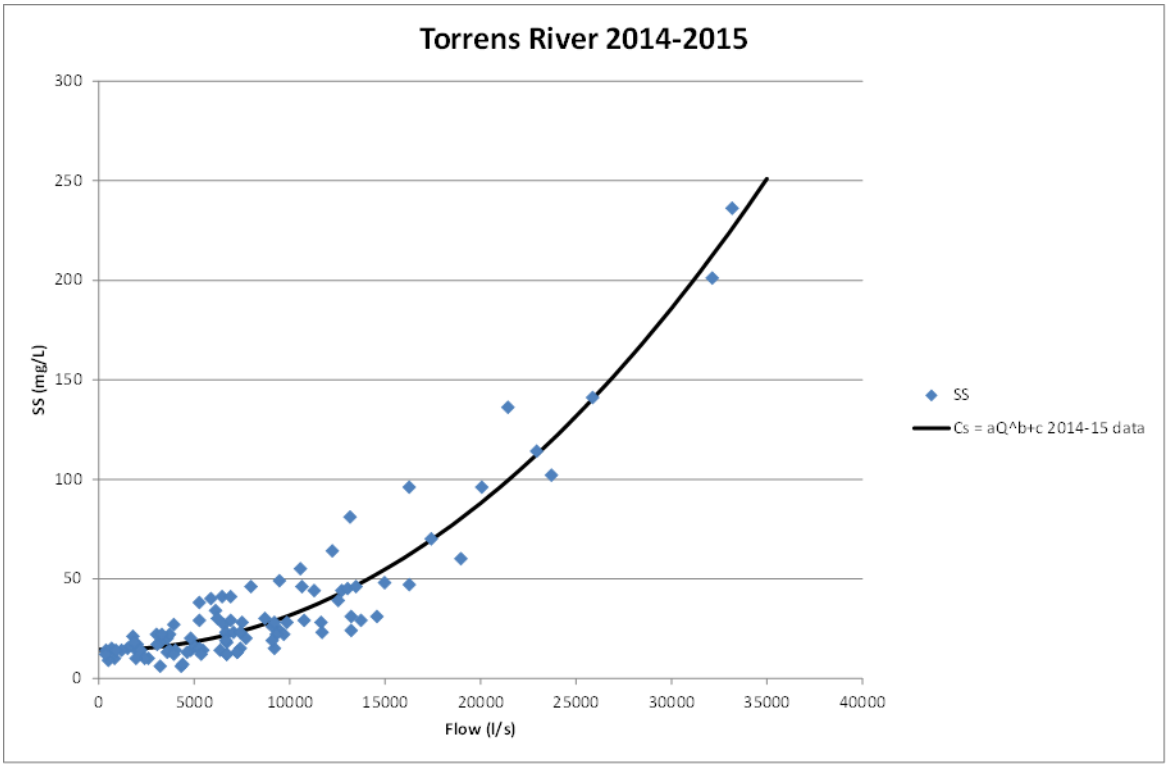

Figure 2.3 Fit of model curve to Torrens River grab sample data.

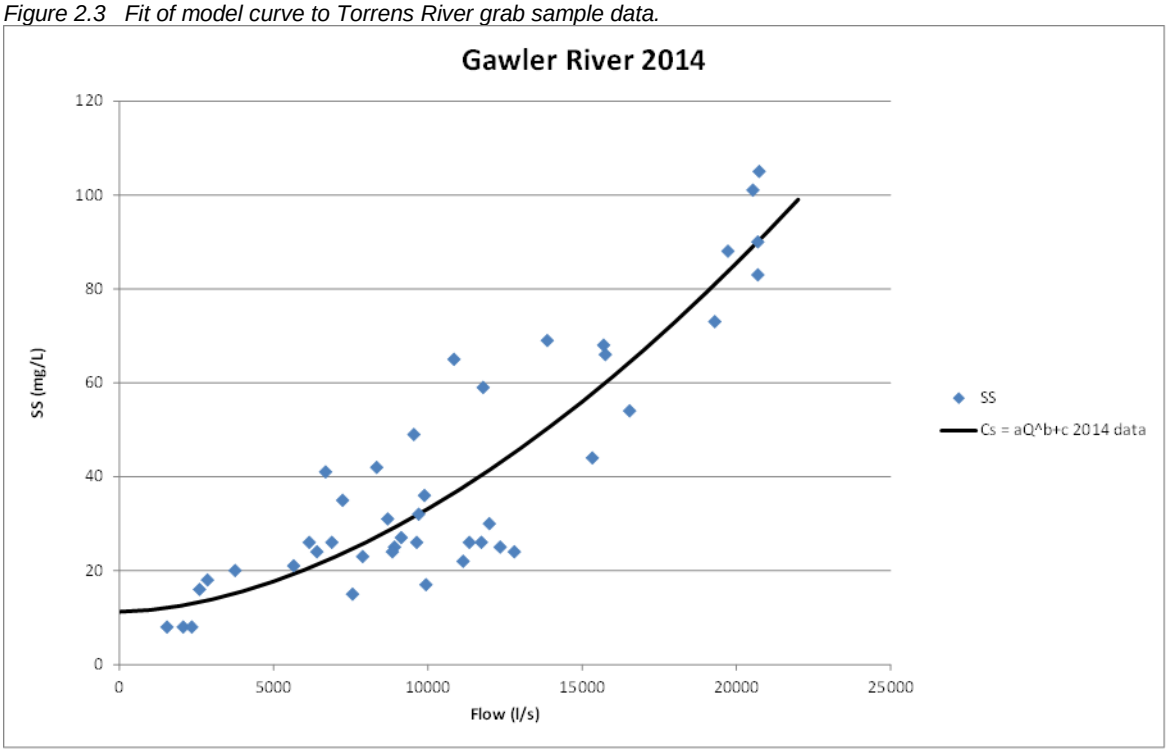

Figure 2.4 Fit of model curve to Gawler River grab sample data.

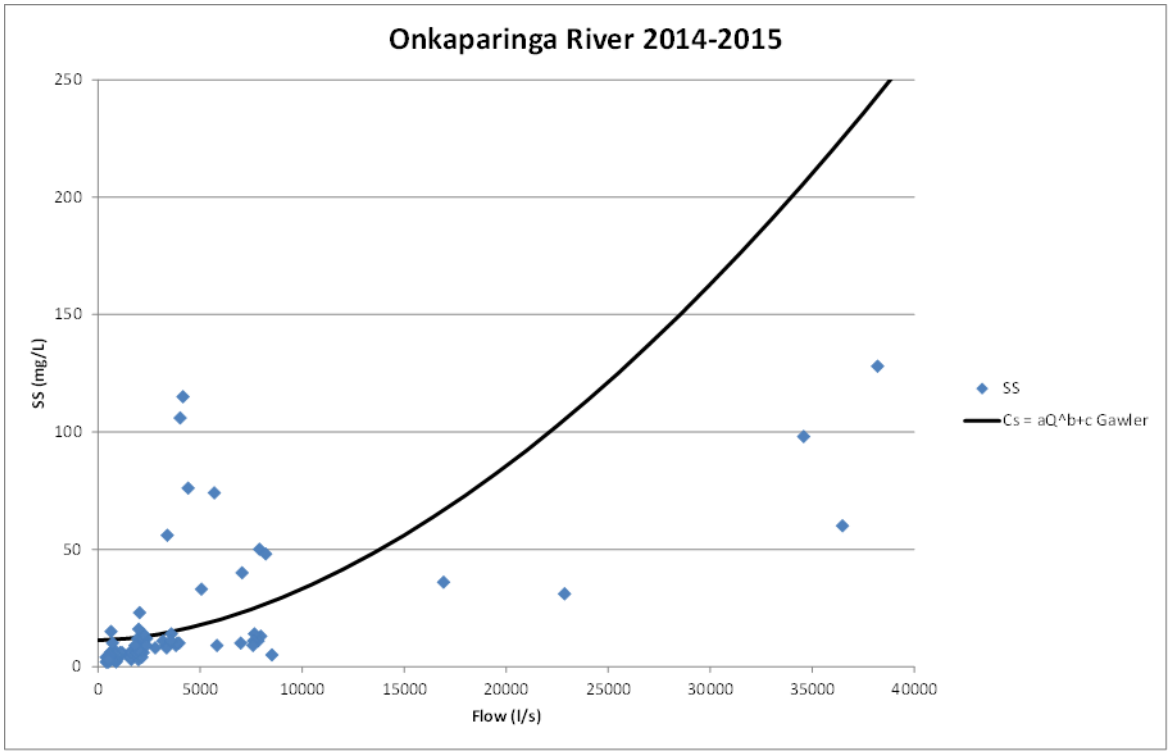

Figure 2.5 Plot of Gawler River model curve against Onkaparinga grab sample data.

The results of scaling SS concentrations to measured loads are shown in Figure 2.6. The procedure also allowed the power model to be applied to other rivers where flow versus SS correlations are not known. The assumption is that the b parameter for each river is similar to the model chosen to represent it (Table 2.3). Since the results are scaled to the observed loads the a parameter has no effect on the result. To avoid radical step changes in the scaled concentrations the c parameter in the power function was reduced to 1. Using the c values from Table 2.2 for smaller rivers resulted in very little dynamics in the output and sudden step changes from one composite sample period to another. Similarly, using a value of zero resulted in unrealistic dynamics with peak values much higher than would be expected (once scaled to observed load). A value of 1 was fitted to provide results in line with expected SS concentrations.

Table 2.3 Coastal discharge sites and model used to estimate SS discharges.

Site Number	Site Name	Model
A5041014	Torrens River @ Seaview Road Bridge	Torrens
A5050510	Gawler River @ Virginia Park	Gawler
A5051003	Light River at Pt Wakefield Rd Bridge	Gawler
A5041022	Patawalonga Creek u/s Barcoo Outlet	Torrens
A5031010	Field River u/s Mouth	Gawler
A5030547	Christie Creek d/s Galloway Road	Gawler
A5031005	Onkaparinga River 1.1 km u/s Ford Old Noarlunga	Gawler
A5031009	Pedler Creek u/s Mouth	Gawler
A5041006	Little Para River d/s Pt Wakefield Rd	Gawler
A5051013	Helps Drain 100m d/s Summer Rd Bolivar	Torrens
A5041016	Kirkcaldy Wetland @ Nash Street East Grange	Torrens
A5041052	Dry Creek @ Bridge Road	Torrens
A5041024	Range Wetland Outlet	Torrens
A5041025	Magazine Wetland Outlet	Torrens
A5041009	Barker Inlet @ Barker Wetland at Outlet	Torrens
A5041017	Barker Inlet Wetland @ North Outlet No 2	Torrens
A5040549	Sturt River d/s Anzac Highway	Torrens
A5040583	Brownhill Creek @ Adelaide Airport	Torrens

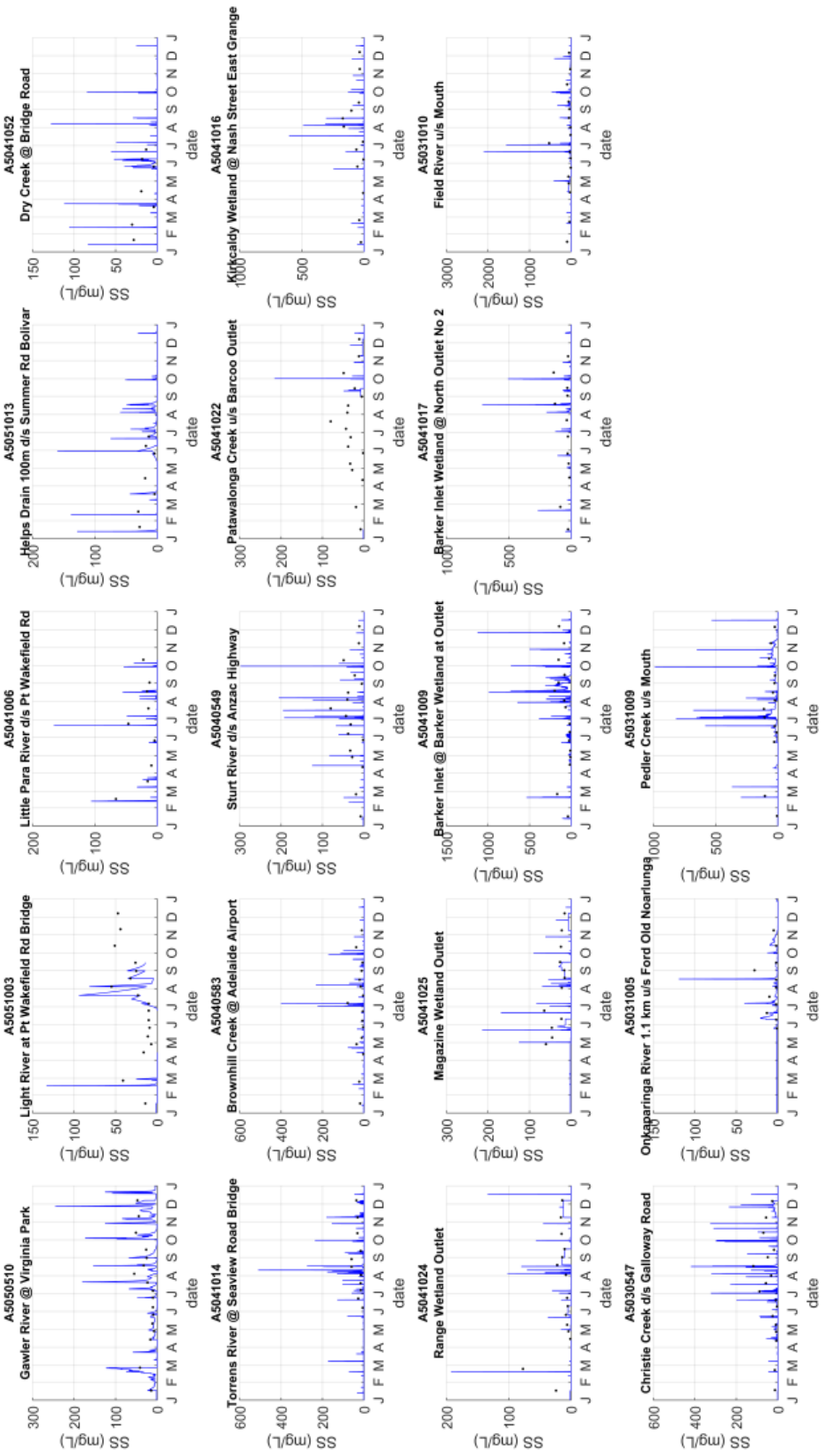

Figure 2.6 AREM input time series for SS (blue line), observed composite sample data (black dots).

In summary, there was a consistent and strong correlation between river flow and SS concentration but no consistent correlation with the other parameters investigated, i.e. ammonia, NO_x, TKN, total nitrogen (TN = TKN + NO_x), soluble reactive P, TP, TOC, DOC and UV-abs. Furthermore, from the additional sampling, we established certain characteristics of the water quality of Adelaide's rivers needed to specify river loads in AREM that cannot be derived from the regular monitoring (Table 2.4). The organic fraction of SS was 16% for the Torrens and Gawler rivers, but only 7% for the Onkaparinga. Soluble reactive P was around 18% of TP for the Torrens and Onkaparinga rivers, but ~39% in the Gawler River. The contribution of ammonium to riverine TN was less than 5%.

Table 2.4 Selected characteristics of the quality of Adelaide's rivers, derived from specific surveys carried out by SA Water.

	Torrens samples	**Gawler samples**	**Onkaparinga samples**	**All samples**
N-NH4 as a fraction of total Kjeldahl N	4.1% (n = 99)	1.1% (n = 42)	0.5% (n = 82)	2.9% (n = 223)
Soluble reactive P as a fraction of total P	18% (n = 99)	39% (n = 42)	17% (n = 82)	22% (n = 223)
organic fraction of SS (1)	16% (n = 14)	16% (n = 8)	7% (n = 24)	11% (n = 46)

1 Only high flow samples were used, because these deviated substantially from values during low or no flow, and since these are representative for events delivering the particle loads.

2.3.1.2 *Coloured Dissolved Organic Matter*

For the three sites were flood events were monitored throughout the year, CDOM was highest than measured in composite samples during the spatial survey (Table 2.5). We note however that the values obtained from flood events do not show a dependency on the river discharge. The highest UV-abs values (> 0.24 cm^{-1}) were recorded for the Gawler River, Sturt River and Onkaparinga River. Apart from these sites, UV-abs did not show marked spatial differences, generally varying in the range 0.11-0.19 cm^{-1}.

Table 2.5 Summary of available data for UV-absorption (cm^{-1}) in Adelaide's rivers.

River	**UV-abs (cm^{-1}), composite samples**	**UV-abs (cm^{-1}), flood event samples**
Gawler	0.26 ± 0.01	0.74 ± 0.17 (n = 42)
Barker Outlet 1	0.12 ± 0.01	
Barker Outlet 2	0.17 ± 0.03	
Range	0.13 ± 0.02	
Magazine	0.13 ± 0.03	
Kirkcaldy	0.13 ± 0.04	
Torrens	0.11 ± 0.01	0.19 ± 0.08 (n = 98)
Brownhill	0.18 ± 0.05	
Sturt	0.24 ± 0.09	
Field	0.13 ± 0.01	
Christies	0.13 ± 0.01	
Onkaparinga	0.26 ± 0.09	0.37 ± 0.11 (n = 85)
Pedler	0.18 ± 0.04	

2.3.1.3 *Particle size distribution of SS*

The particle size distribution was found to be different to some degree for the three rivers studied (Table 2.6). Sediments in the Torrens River were finer in winter (IM2 <63 µm up to 73%) than in summer/autumn (IM2 ~54%). For the other rivers, there were no flow events outside the winter period.

The particle size distribution also varied between the rising and falling limbs of the hydrograph in winter, with the falling phase associated with a higher percentage of fines, IM2 rising from 49-62% to 65-75%. No clear relations were found between the particle size distribution of SS and its organic content.

Table 2.6 Mean contribution of each size class to the total particle pool, in rivers.

River / Stage	n	<16 µm (%)	16-63 µm (%)	>63 µm (%)
Torrens Rising	4	16	38	46
Torrens Falling	33	29	44	27
Torrens Summer/Autumn	37	16	38	46
Gawler Rising	15	27	35	38
Gawler Falling	19	39	36	25
Onkaparinga Rising	38	17	32	51
Onkaparinga Falling	31	26	39	35

2.3.2 River loads in AREM

Table 2.7 provides an overview of how the concentrations of the modelled substances were derived for river inputs. Correlations of the concentration of SS with the river flows were implemented. For UV-abs, results from grab sampling were used where available, supplemented by results obtained from the composite samples. For the other substances, we used the results from the composite samples to characterise the loads with any exceptions noted in Table 2.7. The particle size distribution data were used to distribute inorganic particles over the three size fractions distinguished in the model: for rivers with an urban catchment based on Torrens data and for rivers with a rural catchment based on Gawler (flat) or Onkaparinga (hilly) data.

Table 2.7 Conversion rules for river loads.

Full name of substance(s)	Name in the model	Assumption
Dissolved oxygen (mg/L)	OXY	9.5 [1]
Particulate organic carbon (mgC/L)	POC	X * SS [2, 6]
Coloured dissolved organic matter (cm^{-1})	DOC	UV-abs [8]
Particulate inorganic matter (mg/L)	IM	(1-X) * SS [2, 7]
Particulate organic nitrogen (mgN/L)	PON	TKN * 0.97 *0.5 [9,3,6]
Dissolved organic nitrogen (mgN/L)	DON	TKN * 0.97 *0.5 [9,3]
Nitrate (mgN/L)	NO_3	NO_x
Ammonium (mgN/L)	NH_4	TKN * 0.03 [9]
Particulate organic phosphorus (mgP/L)	POP	TP * 0.56 * 0.4 [4, 6]
Dissolved organic phosphorus (mgP/L)	DOP	TP * 0.22 [4]
Ortho-phosphate (mgP/L)	PO_4	TP * 0.22 + TP * 0.56 * 0.6 [4]
Silica (mgSi/L)	Si	5.6 [5]

1 Concentration at 100% saturation, fresh water of 18°C (Thoman & Mueller, 1987).

2 Organic fraction X as in Table 2.4.

3 Assumption: 50% of organic N is in dissolved form.

4 Share of soluble reactive P in TP as in Table 2.4. We assume that there is a similar amount (22%) of P in dissolved organic form, and that 40% of the remaining particulate fraction (56%) is organic (Meybeck, 1982).
5 High end value of streams draining common rock types (Meybeck and Helmer, 1989).
6 The distribution over the rapidly decaying fraction 1 and the slowly decaying fraction 2 of organic C, N and P is 50:50, based on the assumption that the material will be moderately degradable.
7 Distribution over the size fractions as in Table 2.6, assuming discharges in summer/autumn from the Onkaparinga and Gawler rivers have the same distribution as the rising flow in winter (as observed for the Torrens River).
8 Mean value for the grab samples where available (Table 2.5), since they include results obtained for a range of discharges. Otherwise, we use the mean value for the composite samples where available, and a value of 0.2 cm^{-1} for rivers without data.
9 Share of NH_4 in TKN as in Table 2.4.

2.3.3 Wastewater Treatment Plants

2.3.3.1 Coloured Dissolved Organic Matter

CDOM values were highest for the Bolivar effluents, and lowest for Glenelg (Table 2.8). There was little variation in CDOM between the different effluent streams for each WWTP.

Table 2.8 Mean (SD) of UV-absorption (cm^{-1}) in WWTP effluents.

WWTP (sampling point)	n	UV-abs (cm^{-1})
Bolivar (4007) No 1 Weir	9	0.27 (0.03)
Bolivar (4281) High Salinity Plant	9	0.23 (0.01)
Glenelg (40555) Plant A/B	9	0.19 (0.01)
Glenelg (40556) Plant C/D	9	0.19 (0.01)
Christies Beach (4101) Plant A/B	9	0.20 (0.02)
Christies Beach (41073) Plant C (operational since April 2012)	17	0.22 (0.02)

2.3.3.2 Particle size distribution of SS

The Bolivar Lagoon effluent ("Bolivar weir") had the highest percentage of fines, with IM2 (<63 μm) comprising 65% of the total, almost half of which from particles <16 μM (Table 2.9). In contrast, fines <16 μm varied between 5 and 9% in the other effluents. The lowest percentage of IM2 was found in the Bolivar High Salinity Plant effluents (20%) and the Christies Beach Plant (30-40%). The Glenelg effluents had intermediate values for IM2 (40-50%).

Table 2.9 Mean (SD) contribution of each size class to the total SS pool, in wastewater effluents.

Effluent	n	<16 μM (%)	16-63 μM (%)	>63 μM (%)
Bolivar (4007) No 1 Weir	7	26 (7)	39 (6)	35 (10)
Bolivar (4281) High Salinity Plant	7	5 (2)	15 (6)	80 (8)
Glenelg (40555) Plant A/B	7	7 (1)	42 (8)	51 (9)
Glenelg (40556) Plant C/D	7	6 (1)	35 (7)	58 (7)
Christies (4101) Plant A/B	7	6 (2)	25 (7)	69 (7)
Christies (41073) Plant C	7	9 (4)	28 (11)	63 (11)

2.3.4 WWTP loads in AREM

For the WWTPs, the loadings are derived from routine measurements of DO, SS, TKN, ammonium, NO_x, TP and Si. CDOM and particle size distribution were derived from the data discussed in the previous section. The concentrations of the modelled substances were calculated as shown in Table 2.10.

Table 2.10 Conversion rules for WWTP loads.

Full name of substance(s)	Name in the model	Assumption Bolivar Lagoon	Assumption other effluents
Dissolved oxygen (mg/L)	OXY	DO	DO [1]
Particulate organic carbon (mgC/L)	POC	SS * 0.5 * / 2.5 [2, 6]	SS * 0.2 * / 2.5 [2, 6]
Coloured dissolved organic matter (cm^{-1})	DOC	UV-abs [5]	UV-abs [5]
Particulate inorganic matter (mg/L)	IM	SS * 0.5 [7]	SS * 0.8 [7]
Particulate organic nitrogen (mgN/L)	PON	(TKN-NH_4)*0.5 [3, 6]	(TKN-NH_4)*0.5 [3, 6]
Dissolved organic nitrogen (mgN/L)	DON	(TKN-NH_4)*0.5 [3]	(TKN-NH_4)*0.5 [3]
Nitrate (mgN/L)	NO_3	NO_x	NO_x
Ammonium (mgN/L)	NH_4	NH_4	NH_4
Ortho-phosphate (mgP/L)	PO_4	TP * 0.4 [4]	TP * 0.9 [4]
Particulate organic phosphorus (mgP/L)	POP	TP * 0.6 * 0.5 [3, 4, 6]	TP * 0.1 * 0.5 [3, 4, 6]
Dissolved organic phosphorus (mgP/L)	DOP	TP * 0.6 * 0.5 [3,4]	TP * 0.1 * 0.5 [3,4]
Silica (mgSi/L)	Si	Si	Si

1 A value of 5.0 mg/L has been assumed for Bolivar HS (average value of DO measured at Christies and Glenelg)

2 For Bolivar Lagoon, POC was estimated by subtracting ammonium from TKN to obtain organic nitrogen, multiplying by a C:N ratio of 6 to obtain organic carbon, and subtracting DOC. A similar approach was unsuccessful for the other plants, probably because of the approximate nature of this procedure in combination with very low SS levels. For all discharges except Bolivar Lagoon, 20% of SS is assumed to be organic matter. This is converted to carbon equivalents by division by 2.5.

3 Distribution over particulate and dissolved fractions derived from (Servais et al 1999, Zawilski & Brzezinska 2009).

4 Additional data collected by SA Water reveal that the fraction of soluble reactive P is about 90% for all effluents, except the No 1 Weir Effluent where that fraction is about 40%. Further assumptions are that the remaining P is equally distributed over particulate and dissolved organic species.

5 Mean values listed in Table 2.8.

6 The distribution over the rapidly decaying fraction 1 and the slowly decaying fraction 2 of organic C, N and P is 20:80, based on the assumption that most of the material will be relatively slowly degradable.

7 Size fractions distribution as in Table 2.9. For Glenelg WWTP we use the average of Glenelg A/B and C/D. For Christies WWTP we use Christies A/B values, since Christies C plant is only operational since 2012.

2.3.5 Penrice loads

The Penrice soda ash plant is situated on the west bank of the Port River. For the Penrice loads, data are available for the water discharge and the NH3, SS and TP loads. The modelled substances loads are derived from the quantities effectively measured at Penrice according to Table 2.11. Note that organic loads have been assumed negligible (Jadeka & Tewari, 2007).

Table 2.11 Scaling loads for Penrice loads.

Full name	Name in the model	Derived from
Particulate inorganic matter	IM	SS * 0.5 (see text) [1]
Ammonium	NH4	NH3
Ortho-phosphate	PO4	TP

1 Distributed over the size fractions <16µm:16-63µm:>63µm = 65:10:25 (derived from development application for the settlement ponds of Penrice, see text)

The available data indicate that the quantity of particulate matter discharged to the environment from the Penrice facilities has been very substantial. The Adelaide Coastal Waters Quality Improvement Plan (ACWQIP) reports about 100,000 t/y between 1975 and 1985. A large reduction of this load occurred when Penrice developed settlement ponds in 2002 to remove the solids from their wastewater discharges. The ACWQIP indicates that the load dropped to 1780t in 2003 and 810t in 2008. Data collected during phase 1 indicate a load of 8749t in 2011. According to a development application for the settlement ponds of Penrice, the particulate inorganic matter retained in test ponds was mostly fine grained calcite ($CaCO_3$) (~65% < 20µM, ~75% < 63µM). This mineral is very poorly soluble at a normal sea water pH. Its specific density is 2.71 kg m^{-3}.

Prior to the installation of the settling ponds, much of the discharged solids remained in the Port River close to the discharge point, eventually impeding the passage of ships, with only a fraction of the material travelling to Adelaide's coast. This local trapping is the result of small scale physical processes that are affected by the discharge characteristics (i.e. density of the slurry substantially higher than seawater) in combination with the local Port River cross section and bathymetry. Historically, Penrice used to dredge this material from the Port River main channel every few years and discharge it directly into Adelaide's coastal waters near Outer Harbor. This practice ceased in 1993.

The AREM cannot resolve these so-called near field processes and the local retention of particles needs to be prescribed as input. To really estimate this factor, we would need detailed information about the discharge geometry, volume, salinity, temperature and particle content as a function of time, as well as detailed information about the local Port River cross section and the ambient salinity and temperature as a function of space, depth and time. Such an analysis goes beyond the scope of this study. The fraction of the discharged particles that would not be trapped inside Port River and would find its way to Adelaide coastal waters prior to the installation to the settling ponds is estimated at 5% (best guess based on expert knowledge, Peter Pfennig, EPA). This implies a load of 5,000 t y^{-1}.

It is likely that after the installation of the settling ponds, the fraction of particles escaping to the coastal waters increased, because the overall density of the discharge as well as the average particle size probably decreased. Initial calculations indicate that the 2011 Penrice load of 8,749 t, if allowed to move to the coastal waters, would have an unreasonably high effect on the seagrass habitat suitability in the coastal area affected by the Port River outflow.

Consequently, we still assume a retention in Port River causing a noticeable reduction of the load. We have adopted a working hypothesis of 50% retention.

The dumping grounds for the material dredged from the Port River are in deeper water (8-10 m) which has probably limited resuspension. Based on observations during diving, a large fraction of the dumped material is still there (personal communication, Peter Pfennig, EPA). On these grounds, we consider resuspension of this material as less relevant, and we will consider it included in our overall representation of resuspension.

2.3.6 2011 loads summary

SS loads (8,872 t) were dominated by Penrice (48%), with noticeable contributions from rivers (30%) and WWTPs (22%) (Table 2.12, Figure 2.6). N loads (1,817 t) were dominated by WWTPs (61%), with a noticeable contribution by Penrice (33%). CDOM loads (393 10^3 m^2) are from rivers (59%) and WWTPs (41%). The loads from WWTPs were primarily from Bolivar, for SS (91% of WWTPs total), N (63%) and CDOM (69%). The loads from rivers were primarily from Torrens River, for SS (28% of rivers total), N (23%) and CDOM (16%) and from Gawler River, for SS (18%), N (24%) and CDOM (51%).

Table 2.12 Overview of estimated annual loads in 2011

	Suspended Solids (t/y)	**Total Nitrogen (t/y)**	**CDOM (Mm^2/y)[1]**
Light	51	2.8	26
Gawler	473	24.8	1178
Helps	21	1.9	50
Little Para River	21	1.7	23
Dry Creek	58	8.2	138
Barker Inlet 1	434	10.1	70
Barker Inlet 2	69	1.7	20
Range Wetland	4	0.3	2
Magazine	11	4.0	7
Kirkaldy	29	1.6	12
Torrens	749	23.9	366
Patawalonga	0	0.0	2
Sturt	83	5.1	80
Brownhill	65	4.4	79
Field	403	8.2	61
Christies Creek	123	2.6	32
Onkaparinga	45	3.8	173
Pedler	18	0.3	7
Subtotal Rivers	*2657*	*105.3*	*2326*
Bolivar Lagoon	1722	620.6	920
Bolivar High Salinity	61	80.8	197
Glenelg	120	180.6	297
Christies	64	224.6	191
Subtotal WWTPs	*1966*	*1106.5*	*1605*
Penrice	4249	605.0	0.0
TOTAL	8872	1816.9	3931

[1] The concentration of CDOM is represented by the UV-absorption at 254 nm, expressed in cm^{-1}. The unit for the mass of CDOM is obtained by first converting cm^{-1} to m^{-1} and then by multiplying with a volume in m^3, which yields m^2.

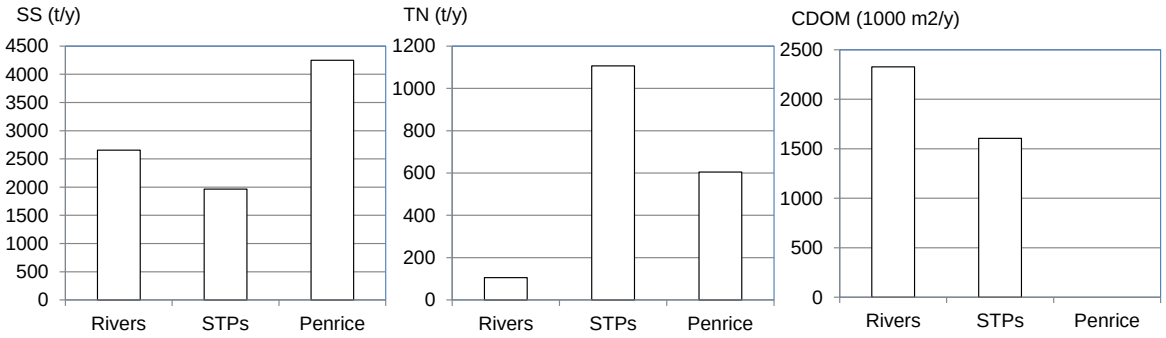
SS (t/y)
4500
4000
3500
3000
2500
2000
1500
1000
500
0
Rivers
STPs
Penrice
TN (t/y)
1200
1000
800
600
400
200
0
Rivers
STPs
Penrice
CDOM (1000 m2/y)
2500
2000
1500
1000
500
0
Rivers
STPs
Penrice

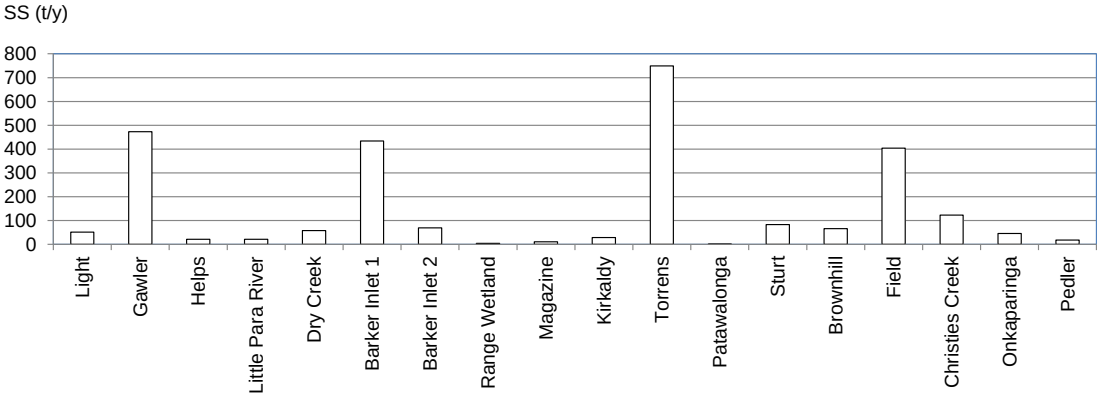
SS (t/y)
800
700
600
500
400
300
200
100
0
Light
Gawler
Helps
Little Para River
Dry Creek
Barker Inlet 1
Barker Inlet 2
Range Wetland
Magazine
Kirkaldy
Torrens
Patawalonga
Sturt
Brownhill
Field
Christies Creek
Onkaparinga
Pedler

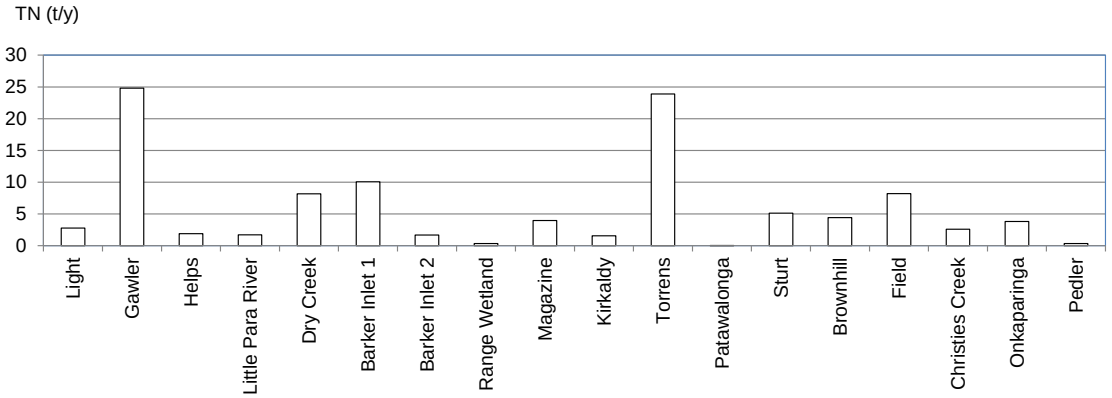
TN (t/y)
30
25
20
15
10
5
0
Light
Gawler
Helps
Little Para River
Dry Creek
Barker Inlet 1
Barker Inlet 2
Range Wetland
Magazine
Kirkaldy
Torrens
Patawalonga
Sturt
Brownhill
Field
Christies Creek
Onkaparinga
Pedler

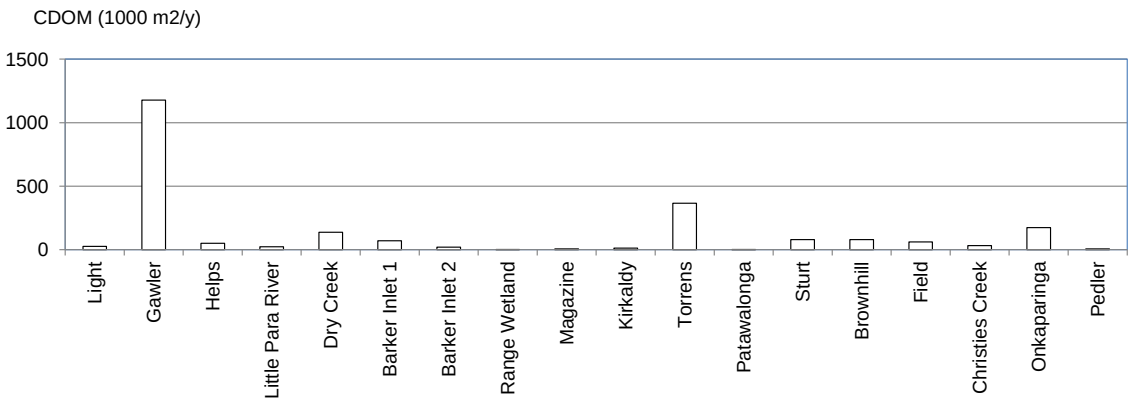
CDOM (1000 m2/y)
1500
1000
500
0
Light
Gawler
Helps
Little Para River
Dry Creek
Barker Inlet 1
Barker Inlet 2
Range Wetland
Magazine
Kirkaldy
Torrens
Patawalonga
Sturt
Brownhill
Field
Christies Creek
Onkaparinga
Pedler

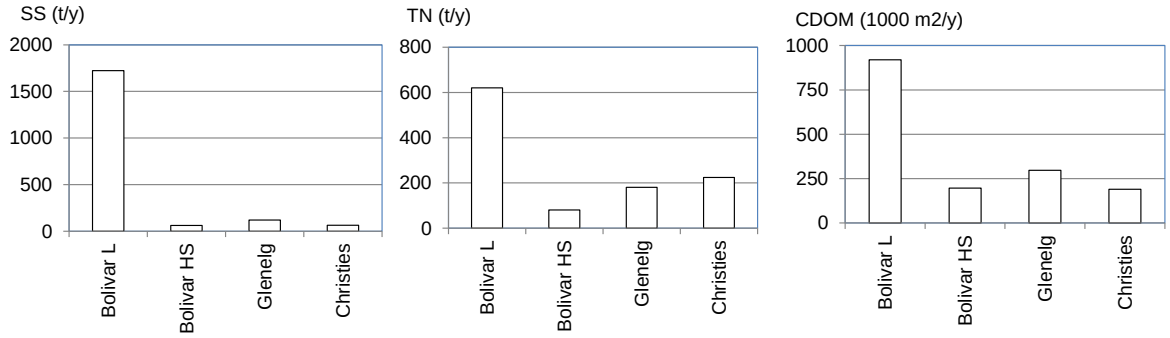

Figure 2.7 Overview of 2011 estimated loads of total suspended solids (SS), total nitrogen (TN) and CDOM, per category (top), river totals subdivided by river (middle) and WWTP totals subdivided by plant (bottom).

2.4 Discussion

CDOM concentrations in rivers and WWTPs were higher in the north of the study area, where values in the Gawler River were higher than in effluents from the Bolivar WWTP. The high values recorded at the latter are likely related to the use of open air stabilisation lagoons at this site, where phytoplankton comprises ~50% of SS. In the central metropolitan coast, CDOM values were similar between the Torrens River and the Glenelg WWTP. Further south, CDOM concentrations were generally higher in effluents from the Christies Beach WWTP than in rivers draining the southern catchments.

The particle size distribution of SS also varied between sources. In the pilot AREM, IM2 (<63 µm) was assumed to contribute 80% of inputs from WWTPs, but only 20% of inputs from rivers. IM2 in WWTP effluents was found to be much lower than set up in the pilot model, generally less than 50%, with the exception of the Bolivar lagoon effluents, where it reached 65%. For the rivers, the inverse was noted, with IM2 typically representing on average more than half of the total, and increasing during falling flows to up to 75% of the total. Hence, fine particles dominate river inputs, but not WWTP inputs.

The particle size distribution of riverine SS further changed in space and time. The contribution of fine particles decreased from catchments with a gentle topography in the north to southern rivers receiving inputs from the Mount Lofty Ranges. Topography, different land uses and geology are all likely to play a role in defining the composition of the SS pool (Walling et al. 2000)

The particle size distribution in the rising limb of the hydrograph was similar between rivers, IM2 contributing about 50-60% of total SS, with the fraction <16 µm representing ~17% in the Torrens and Onkaparinga, and 27% in the Gawler. Particle size decreased during falling flows, with IM2 reaching 65-75% of the total, mostly in the size class 16-63 µm, except for the Gawler river, where particles <16 µm remained dominant.

The higher contribution of larger particles in the Torrens River during summer/autumn when soil is dry is possibly a consequence of a greater fraction deriving from channel bed resuspension rather than surface runoff (Walling et al. 2000). When soil moisture is low, infiltration capacity is larger than rainfall and runoff is limited (Barma & Varley 2012). The contribution of channel bed resuspension is likely to be compounded by phytoplankton during the warmer months. In contrast, catchment soil is closer to saturation during winter, and a larger fraction of particles is likely to derive from catchment runoff, particularly during falling flows.

The development of correlations between SS and flow allowed a more dynamic input of SS in AREM. The parameters obtained in the power function between flow and SS are empirical coefficients and have no physical meaning. In studies of other rivers, the exponent b typically varies between 0.5 and 1.5 and rarely exceeds 2.0 (Syvitski et al. 2000). This puts both the Torrens (b = 2.08) and Gawler rivers (b = 1.76) in the upper range reported for rivers, with a strong nonlinear response of SS to flow and increased loads during large events. The lack of correlation between flow and SS for the Onkaparinga River could relate to water management practices upstream of the sampling site. In particular, the upper reaches of the Onkaparinga River is dammed for drinking water storage (Mt Bold Reservoir). During 2014 there was a release of water from the reservoir in accordance with the Dam safety rules. This water would likely have a lower SS load with residence time in the reservoir allowing for settling. The Clarendon weir also plays a role, given the existing diversion to Happy Valley Reservoir. Depending on the state of reservoir levels and flow rates, discharge from the Scott Creek part of the catchment may or may not be diverted for storage. This means the flow in the river is not necessarily linked to the rainfall intensity/duration. Since the erosional processes producing SS are also linked to rainfall there is usually a correlation between flow and SS. Diversions will weaken this correlation. In addition, there is a large volume of water (270,000 m^3) in the weir usually derived from the Mt Bold reservoir that would effectively dilute the water coming from a catchment inflow.

Overall, the north of the study area was affected by the largest SS loads. Penrice and Bolivar combined accounted for 68% of the total load to the coast. Since the closure of Penrice in 2013, Bolivar and the Torrens River are the largest individual sources of SS to the coast, representing 37 and 16% of the total (based on 2011 data), respectively. The combined input from rivers however still dominates SS loads in the situation without Penrice (57%), with impact concentrated in winter/early spring. The total SS load without Penrice decreased to 4,623 t, a value close to the target of 4,200 t recommended by the ACWS (Fox et al. 2007).

The north of the study area also received the largest N loads, with Penrice and Bolivar accounting for 68% of the total. Bolivar is the single largest source of N to the coast, delivering 43% of the total. The 2011 N loads without Penrice (1,212 t) imply a 50% reduction relative to 2003 loads, going a significant way to reach the ACWS-based target of 75% reduction (Fox et al. 2007).

For CDOM, again the north of the study area received the largest loads, with Gawler and Bolivar accounting for 58% of the total, in about equal shares. For CDOM, the closure of Penrice is not expected to have caused a significant reduction of the total loads. The present study is the first to quantify all relevant CDOM sources in terms of their UV-adsorption, so comparison to older results is not possible. Also, there are no quantitative load reduction targets in place. Finally, in Chapter 4 we will discuss that mangroves, marine sediments and seagrass meadows are also relevant sources of CDOM in the study area.

2.5 Conclusions

By means of a series of targeted surveys, the necessary information was collected to adequately quantify the discharges to the Adelaide metropolitan coastal waters and the variability with time thereof. River loads of suspended solids were found to be highly dependent on the river flow. An algorithm was developed and applied that consistently disaggregates the composite sampler data from the Adelaide and Mount Lofty Ranges Natural Resources Management Board (AMLR NRM). Without affecting the observed loads of SS, hourly time series of concentrations are derived from hourly flow records. For other water

quality variables (e.g. nitrogen, CDOM), no clear relation with the river flow was observed and the above procedure was therefore not necessary. These new discharge time series contribute to the ability of AREM to reproduce the strong temporal and spatial water quality gradients typical for the Adelaide Coastal Waters.
Further data gaps were successfully addressed as well. This concerns in particular the particle size distribution of suspended solids and the concentrations of CDOM discharged by rivers and WWTPs. The latter have been consistently quantified by measuring the absorption of UV light at a single wavelength. The new data contribute to the ability of AREM to simulate the fate of suspended solids in the marine environment and the impact on downward light attenuation of suspended solids and CDOM.

3 The relation between water quality and PAR downward attenuation in the Adelaide Coastal Waters

Seagrass wreck on Adelaide beaches – Photograph by Paul Erftemeijer

3.1 Introduction

Anthropogenic inputs of nutrients and sediments reduce light available to key habitat forming species in coastal regions (Burkholder *et al.* 2007, de Boer 2007, van der Heide *et al.* 2011). While light limitation of phytoplankton occurs at 1% surface irradiance (Sverdrup 1953, Strickland 1958), seagrasses have high respiratory demands and require as much as 10-15% for optimal growth (Duarte 1991, Ralph *et al.* 2007). High light requirements affect the ability of seagrasses to survive chronic turbidity and epiphyte cover associated with continuous land inputs, as well as to cope with and recover from stochastic disturbance from extreme events such as storms. Changes in seagrass habitat in turn affect sedimentary nutrient fluxes, wave attenuation, water residence time and other buffering and feedback mechanisms that impact on the susceptibility of coastal ecosystems to eutrophication (Hendriks *et al.* 2008, Eyre *et al.* 2011, Koftis *et al.* 2013, Adams *et al.* 2016).

The development of models to predict the effect of management scenarios on habitat suitability for seagrasses is a necessary step for cost-effective investment in initiatives for the conservation and restoration of meadows. This study is based on one such a model developed for Adelaide, a 1.3 million metropolitan centre spanning 70 km along the east coast of Gulf St Vincent, South Australia. The region, considered a hotspot for seagrass

diversity in temperate Australia (Short *et al.* 2007, Bryars and Rowling 2009, Erftemeijer 2014), has progressively lost ~60 km^2 of its original seagrass cover since the 1940s (Tanner *et al.* 2014). These changes have prompted management agencies to set aspirational load reductions in the mid-2000s for both nitrogen and suspended solids (SS) to achieve 1 and 7 t/km^2 in the coastal zone, respectively (Fox *et al.* 2007). More recently, the Adelaide Receiving Environment Model (AREM) has been developed to provide further definition of sustainable loads in time and space. AREM is based on the Delft3D modelling suite, and includes four modules: hydrodynamic, waves, water quality and seagrass habitat suitability (Zijl *et al.* 2014). This paper provides an overview of the development of an empirical light attenuation model for inclusion in the water quality module of AREM.

The empirical light model is based on the relationship between water quality and the vertical attenuation coefficient (K_d). The latter quantifies the exponential decay of light with depth from absorption and scattering of photons by both living (phytoplankton) and non-living particulate matter (detritus and inorganic sediments), coloured dissolved organic matter (CDOM), and seawater molecules. Assuming that the effects of each optically active constituent are additive in nature (Gordon 1989, Gallegos 2001), K_d is commonly approximated as:

$$K_d = K_{sw} + K_{CDOM} + K_{Chla} + K_{Det} + K_{IM} \quad (1)$$

where K_{sw}, K_{CDOM}, K_{Chla}, K_{Det} and K_{IM} are the partial attenuation coefficients of pure seawater, CDOM, chlorophyll *a* (Chla, as a proxy for phytoplankton), detritus and inorganic matter, respectively. The partial attenuation coefficient of each constituent i (K_i) is calculated as a function of its specific attenuation coefficient k_i and concentration [I]:

$$K_i = k_i \times [I] \quad (2)$$

In this study, we used an empirical approach to estimate local k values for CDOM, Chla, detritus, and both fine (<63 μm) and coarse suspended solids (SS). Water quality and light data were obtained at fixed sites between summer and winter and used to estimate and optimize k values for the region using both stepwise multiple linear regression and a sequential evaluation of simple linear regressions. The calculated partial attenuation coefficients were then used to identify the main drivers controlling light attenuation in the system. This optical model, applied to the water quality module of AREM, will allow the estimation of the intensity of light available in the photosynthetically active radiation (PAR) part of the spectrum (400-700 nm) and the identification of areas where seagrass presence or recovery might be inhibited by light. This information will help target improvements into the precise locations and periods of the year most likely to deliver ecological gains for seagrasses. The study's approach can be extended to address similar problems in other metropolitan regions, with the local derived k values particularly relevant for southern Australia.

3.2 Materials & Methods

3.2.1 Study area

The coast of Adelaide borders Gulf St Vincent, a large embayment opening to the Southern Ocean. The Gulf is an inverse estuary, with salinity increasing towards its upper reaches as a result of minimal surface runoff and a semi-arid regime where evaporation is in excess of precipitation. Gulf waters are vertically well mixed except for brief periods during neap tides. The mean annual wave height decreases from south to north following a broadening of the bathymetry towards the upper Gulf (Pattiaratchi *et al.* 2007). Catchments in the north and south of the Adelaide coast are mainly agricultural with the usual pattern of flow restricted to

pulse events around winter (June-September) (Wilkinson *et al.* 2005b). The urbanized river systems in the central coast flow more frequently due to a large proportion of impervious surfaces in these catchments (Wilkinson *et al.* 2005a). Tidal currents parallel to the coast dominate the circulation and trap land-based inputs in water depths <10 m (Pattiaratchi *et al.* 2007). In 2014/15, rivers were the main source of suspended solids (53%) to the coast, while wastewater treatment plants (WWTPs) were the main source of nitrogen (82%) (Jones 2015; SA Water data). Two rivers discharged more than half of the annual riverine load of 3,831 t of suspended solids (SS): the central Torrens River (60%) and the northern Gawler River (10%) (Jones 2015). The load of 650 t of nitrogen from WWTPs was delivered by the outfalls of Bolivar (68%), Glenelg (22%) and Christies Beach (10%) (Katherine Reid, SA Water, personal communication).

3.2.2 Sampling

Between November 2014 and September 2015, 97 paired water quality and light data were obtained at fixed sites ranging from shallow to deep waters in two different locations of the Adelaide coast (Figure 3.1). Shallow sites were located in fragmented/sparse seagrass whilst the deeper sites were located in dense seagrass meadows. One location at the mouth of Barker Inlet is impacted by effluents from the Bolivar WWTP, the largest in Adelaide (~40 GL year^{-1}). The Bolivar transect had 3 sites located at 3 m (B3), 7 m (B7) and 12 m (B12) mean tide depth. The other location, near Grange Beach, is impacted by inputs from the Torrens River, the single largest source of suspended solids to the metropolitan coast. This transect also had three sites, located at 5 m (G5), 10 m (G10) and 15 m (G15). Each site was visited over 17 different days or more.

Samples were collected with a van Dorn water sampler from 1 m below the surface and 1 m above the bottom, for the analysis of CDOM, Chla, particulate organic carbon (POC), and SS. Samples for Chla were collected in dark plastic bottles, and the other samples in clear plastic bottles. Samples were transported on ice in the dark, stored in a refrigerator, and usually analysed the day after collection.

For the measurement of light, two Odyssey PAR 2π cosine light sensors (Dataflow Systems, New Zealand) were deployed 0.7-1 m apart at each site, with the lowest light meter placed 0.6-0.9 m from the bottom to avoid sediment interference, while approximating the height of the seagrass canopy (Collings *et al.* 2006, Pedersen *et al.* 2012). The light meters were attached to a steel frame with arms separated by 180^{o} to preclude shading of the lower light meter. The light meters recorded average light intensity for each 30 min period and were deployed for periods of time from two weeks to over a month, in November 2014, January/February, March, April/May and August/September 2015. The light meters were retrieved and/or cleaned on an approximately fortnightly basis to avoid interference from fouling. Calibration against a 2π LI-190R Licor sensor was used to convert data obtained from the Odyssey sensors to µmol photons m^{-2} s^{-1}. Two Odyssey light meters were also deployed on land (sites L1 and L2 in Figure 3.1), together with a 2π LI-190R Licor sensor. For periods were land-based light data was not available, data was obtained from a site maintained by the Adelaide and Mount Lofty Ranges NRM Board at Virginia (site L3) and rescaled to µmol photons m^{-2} s^{-1} by comparison with LiCor data during available concurrent periods.

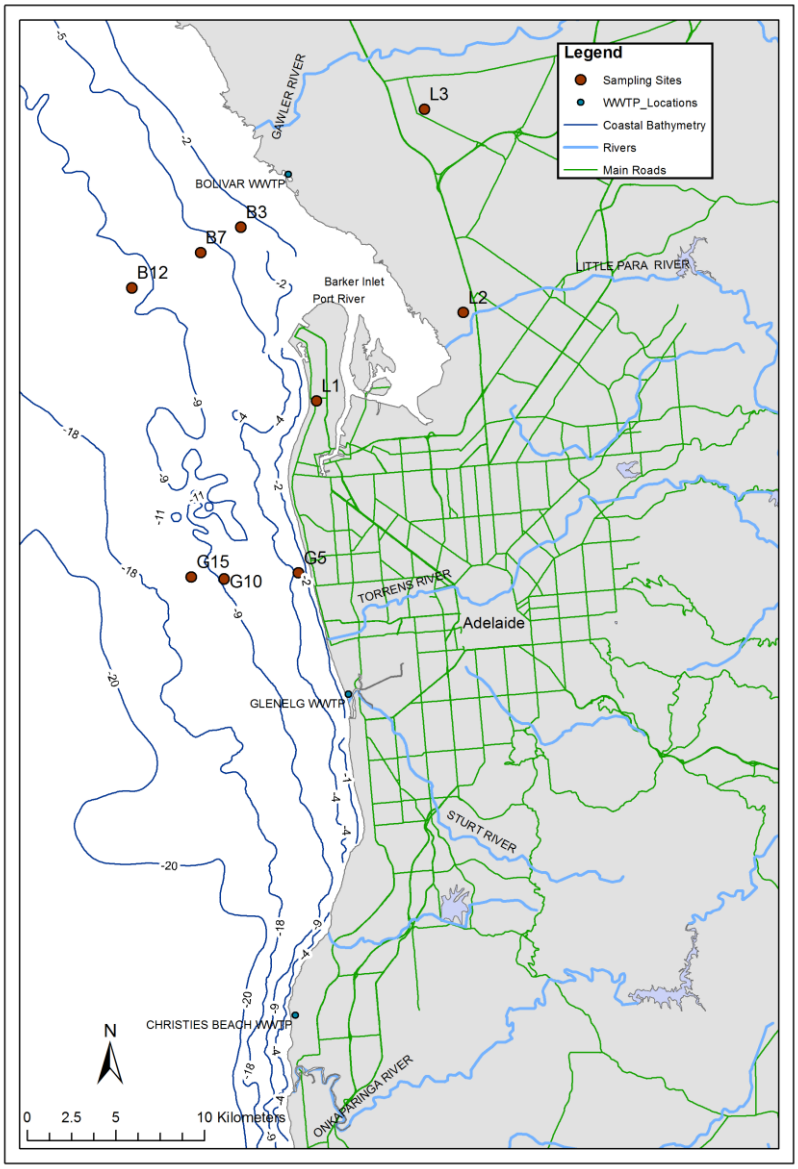

The location at the mouth of Barker Inlet had 3 sites located at 3 m (B3), 7 m (B7) and 12 m depth (B12). The location off Grange Beach also had three sites, located at 5 m (G5), 10 m (G10) and 15 m (G15). Sites L1, L2 and L3 were used to obtain irradiation intensity reaching the water surface.

Figure 3.1 Sampling sites along the Adelaide coast.

Two Xylem Exo2 sondes were also deployed at sites G5 and B3 adjacent to the light loggers, anchored by a steel frame such that they were 1 m from the seabed. Sondes recorded turbidity and water depth every 15 min. Sensors were automatically wiped every 12 h and cleaned at the same time as the light sensors. Two Nortek Aquadopp 1 MHz Acoustic Doppler Current Profilers (ADCPs) were deployed at sites G10 and B7. Instruments were anchored 0.25 m from the seabed in a stainless steel frame with a flat plate on the bottom to preclude interference from seagrass. Wave burst data were collected at 6 h intervals with 1024 samples collected at 1 Hz frequency. Significant wave height and mean wave period were derived using Nortek Storm software.

Wind data was obtained from the Bureau of Meteorology for site 023052 “Black Pole” which was located between the Bolivar and Grange sampling sites.

3.2.3 Laboratory analysis

Samples for the analysis of CDOM were filtered through a 0.45 μm syringe filter. Absorbance was measured at 254 nm by comparison with an ultrapure water blank in a UV-1700 PharmaSpec Spectrophotometer equipped with a 10 mm quartz cell (Standards Australia 1990). The absorption coefficient (*a*), used as a proxy of CDOM concentration, was calculated as:

$$a = 2.303 \times \frac{A}{l} \quad (3)$$

where *A* is the absorbance and *l* is the path length (Hu *et al.* 2002, Coble 2007).

Samples for the analysis of Chla were filtered onto 1.20 μm glass fibre filters (GF/C, 47mm) and extracted with 96% cold ethanol. Chla concentrations were determined at 665 nm in a UV-Vis Thermo Evolution 300 spectrophotometer equipped with a 40 mm glass cuvette (Wintermans and Mots 1965).

Samples for the analysis of organic carbon were either analysed unfiltered for the determination of total organic carbon (TOC) or filtered through a 0.45 μm syringe filter for the determination of dissolved organic carbon (DOC). Samples were acidified to release inorganic carbon, then digested with sodium persulphate at 98-100 ^{o}C and the resulting carbon dioxide measured in a OI Analytical Organic Carbon Analyser 1030 (APHA-AWWA-WEF 1995). POC was determined as the difference between TOC and DOC.

Samples for the determination of SS were analysed in a LISST laser diffraction particle size analyser (Sequoia Scientific, USA), and the results integrated into fine (< 63 μm) and coarse fractions. LISST results in μL L^{-1} were translated into concentrations in mg L^{-1} by applying a density of 2.6 g mL^{-1}, typical for particles in coastal waters (Babin *et al.* 2003).

3.2.4 Calculation of K_d and wave-induced bed shear stress

K_d was calculated by rearranging the Lambert-Beer equation into:

$$K_d = -\frac{1}{z} ln \frac{I_z}{I_0} \quad (4)$$

where I_0 is PAR below the water surface, I_z is PAR at depth z, and z is the depth of the sensor in meters. I_0 was calculated from land-based sensor data corrected for ocean surface reflection according to the solar zenith angle (Kirk 1983), adjusted for wind and overcast conditions (Walsby 1997). Overcast conditions were considered when the incident radiation was less than half the clear sky radiation expected for that time/day. K_d values were similar for each underwater sensor and therefore were averaged. For comparison with water quality results, K_d values were averaged over the period that water quality samples were collected (i.e. between 8:30am and 2:00pm).

Wave-induced bed shear stress was calculated from significant wave height and mean wave period according to Jones et al. (2012). The wave friction factor was solved iteratively using the formulation of Jonsson (1966). Wave height and period at nearshore sites G5 and B3 were obtained from data measured at sites G10 and B7, respectively, based on statistical relationships obtained from simulated data for 2011 using SWAN version 40.85 applied in non-stationary, third-generation mode (see also Chapter 4).

3.2.5 Statistical analysis

The results for surface and bottom water quality samples were averaged to represent conditions throughout the water column. Statistical analysis was undertaken with the software package STATISTICA (StatSoft, Tulsa, OK). One-way analysis of variance (ANOVA) was used to identify statistical differences ($\alpha = 0.05$) between sites for each water constituent, and two-way ANOVA to identify interactive effects of season and site. Variables were log-transformed when there was a need to improve normality and heterogeneity of variances. Tukey post-hoc tests were performed when significant differences were detected. Specific attenuation coefficients for water constituents were estimated based on a multiple regression of K_d against constituent concentrations. These specific attenuation coefficients were optimized using Excel solver by minimising the sum of residuals between measured and calculated K_d.

3.3 Results

3.3.1 Spatial and temporal variability of water quality and K_d

CDOM had a mean value of 0.047 ± 0.013 cm^{-1} (mean ± SD), and lower variability than the particulate constituents of Chla (0.72 ± 0.64 mg m^{-3}), fine (4.5 ± 3.7 g m^{-3}) and coarse SS (20.3 ± 25.6 g m^{-3}). Assuming C/Chla = 50, and dry matter/C = 2.5 (Parsons et al. 1984, Xu et al. 2005), phytoplankton was estimated to contribute on average 2% of fine SS. POC concentrations were also low, with approximately half of all samples having DOC concentrations as high as TOC, resulting in negligible POC, and the other half having a mean POC concentration of 0.15 ± 0.12 gC m^{-3}. The latter values suggest that POC contributed on average 11% of fine SS or less.

K_d ranged from 0.12 to 0.89 m^{-1}, with a mean value of 0.35 ± 0.17 m^{-1}. The water constituent that best explained K_d was fine SS ($r^2 = 0.49$, $p < 0.001$), followed by CDOM ($r^2 = 0.41$, $p < 0.001$) and Chla ($r^2 = 0.41$, $p < 0.001$) (Figure 3.2). Coarse SS in contrast was not a good predictor of K_d ($r^2 = 0.10$, $p = 0.001$).

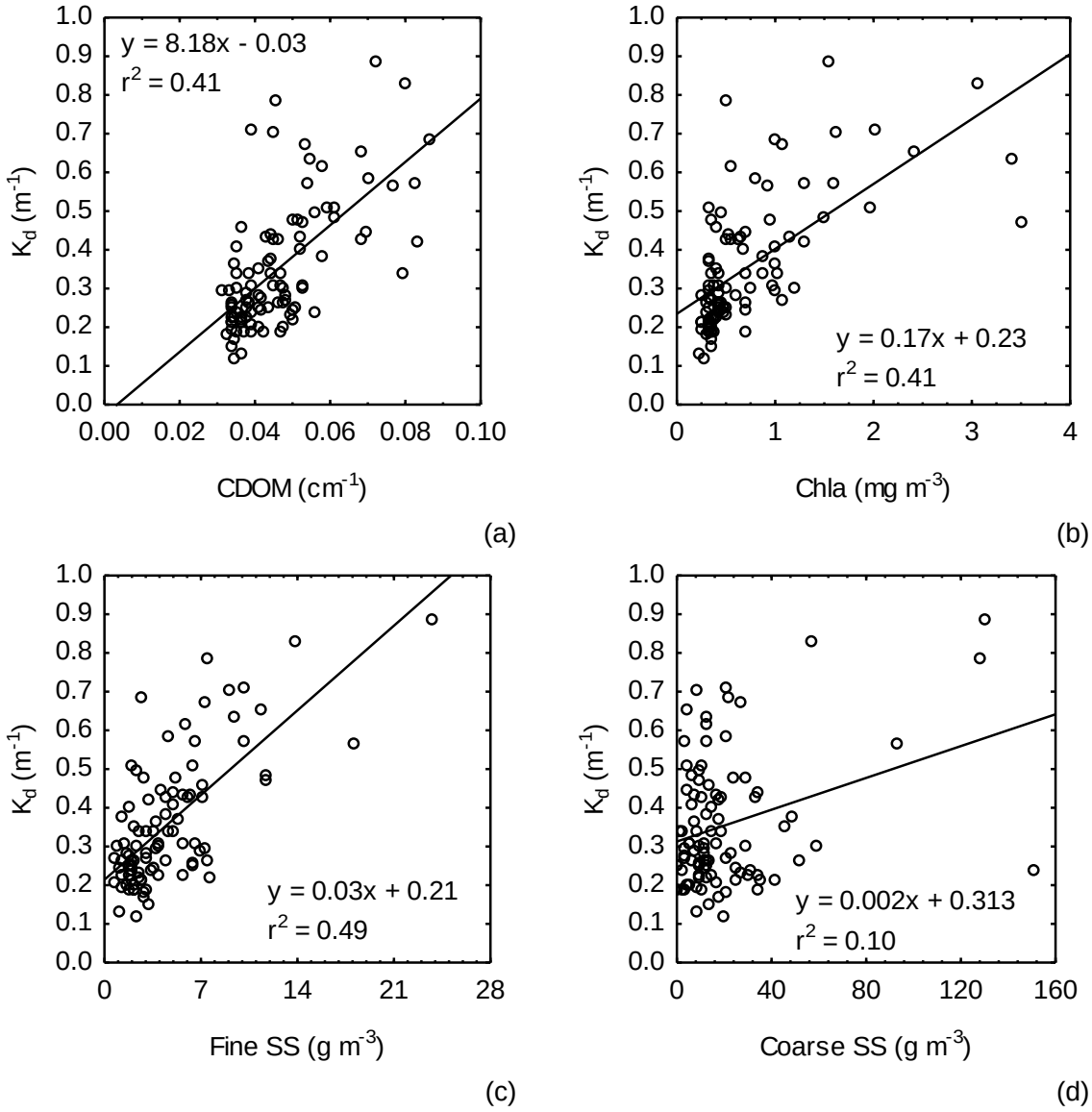

Figure 3.2 Regression between measured K_d and CDOM (a), Chla (b), fine (c) and coarse SS (d).

Turbidity explained 82% of the variability in K_d averaged over daylight hours (Figure 3.3a). Wave-induced bed shear stress was a good predictor of turbidity obtained as instantaneous measurements every 6 h (Figure 3.3b). Time series of turbidity, wave-induced bed shear stress, and wind indicate that strong winds with a westerly or southerly component generate bed shear stress > 1-2 Pa associated with an increase in turbidity (Figure 3.4).

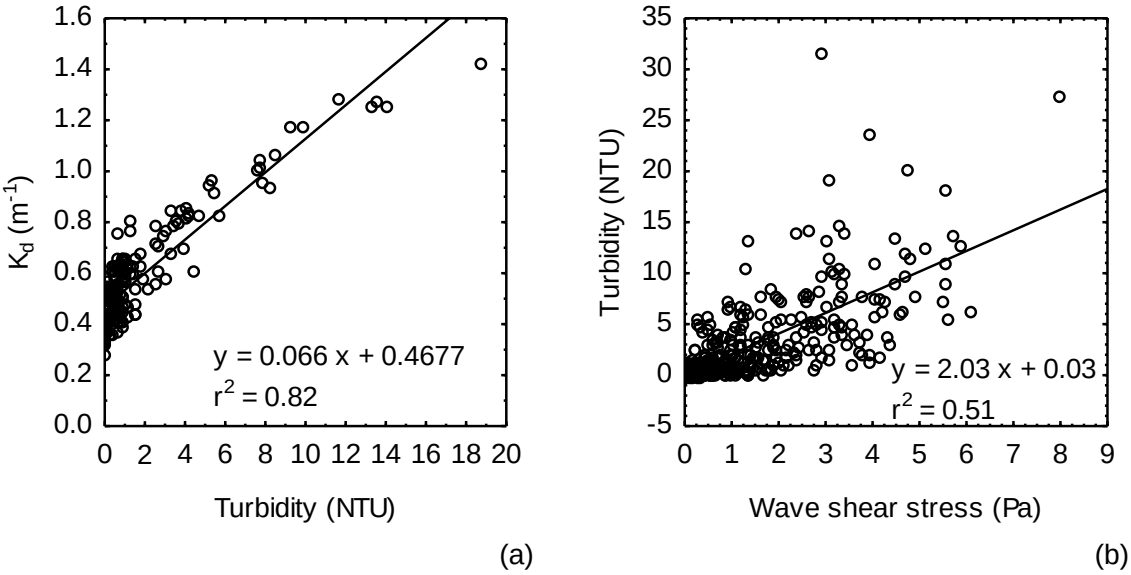

Figure 3.3 Regression between measured K_d and turbidity averaged over daylight hours (a), and instantaneous turbidity and wave-induced bed shear stress (b).

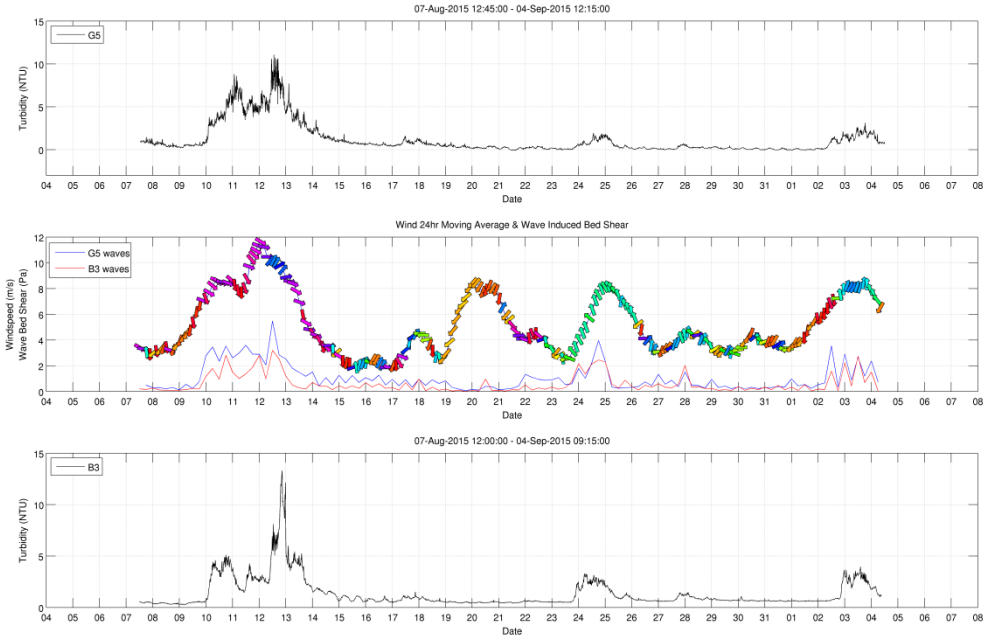

Figure 3.4 Temporal evolution of turbidity at site G5 (top) and B3 (bottom) compared to wind intensity and direction, and wave-induced bed shear stress (middle).

Site had a significant effect on the concentrations of CDOM, Chla and fine SS (one-way ANOVA, $p < 0.001$), but not coarse SS ($p=0.23$) (Figure 3.5). CDOM concentrations were higher and generally more variable at the inshore sites B3 and G5, while Chla and fine SS concentrations were only significantly higher at site G5 (Tukey post-hoc tests). The highest K_d values were also recorded at the inshore sites (one-way ANOVA, $p < 0.001$), with the lowest K_d recorded at the deeper sites in the Grange transect. The inshore-offshore decrease in concentrations was more marked for CDOM and Chla than for the highly variable SS

fractions. The decrease was also more gradual for the Bolivar transect than for the Grange transect.

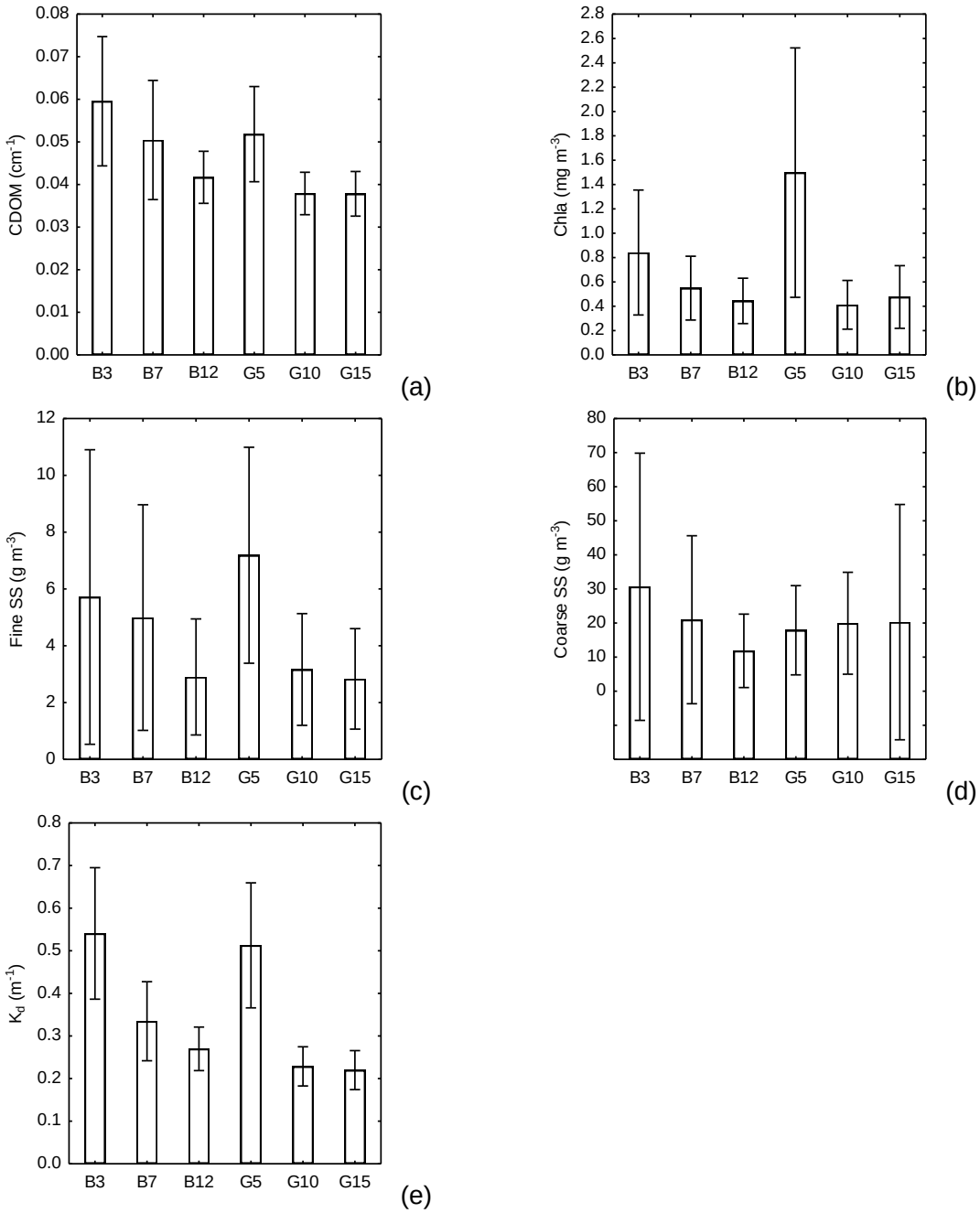

Figure 3.5 Mean (±SD) CDOM (a), Chla (b), fine (c) and coarse SS (d), and K_d (e) for the Bolivar (3, 7 and 12 m) and Grange transects (5, 10 and 15 m).

There was a significant interaction between site and season for CDOM (two-way ANOVA, $p < 0.05$), with higher concentrations in winter at sites B3, B7 and G5 (Tukey post-hoc tests) (Table 3.1). There was no interaction between site and season for Chla, fine and coarse SS, and K_d. There was a trend for higher concentrations of Chla (and lower concentrations of coarse SS) in the Bolivar transect in winter in comparison to summer (Table 3.1). The

concentrations of fine SS tended to be lower at the offshore sites B12, G10 and G15 in winter.

Table 3.1 Concentrations of water quality constituents and K_d in the Bolivar (3, 7 and 12 m) and Grange (5, 10, 15 m) transects. Values are presented as the seasonal mean (±SD).

	CDOM (cm^{-1})	Chla ($mg\ L^{-1}$)	Fine SS ($mg\ L^{-1}$)	Coarse SS ($mg\ L^{-1}$)	K_d (m^{-1})
B3					
Summer	0.046 (0.005)	0.42 (0.07)	4.90 (2.70)	65.62 (54.99)	0.54 (0.22)
Autumn	0.049 (0.008)	0.85 (0.68)	5.54 (3.23)	21.03 (15.82)	0.50 (0.15)
Winter	0.070 (0.012)	0.98 (0.45)	6.09 (6.80)	24.34 (40.39)	0.56 (0.15)
B7					
Summer	0.040 (0.005)	0.28 (0.04)	3.96 (1.86)	26.40 (12.08)	0.29 (0.11)
Autumn	0.042 (0.007)	0.62 (0.27)	4.90 (2.11)	20.57 (18.24)	0.34 (0.07)
Winter	0.058 (0.014)	0.57 (0.26)	5.31 (5.30)	19.86 (31.52)	0.34 (0.11)
B12					
Summer	0.034 (0.001)	0.33 (0.02)	3.82 (1.62)	19.54 (7.04)	0.28 (0.09)
Autumn	0.039 (0.006)	0.56 (0.28)	4.20 (2.85)	16.30 (10.69)	0.28 (0.05)
Winter	0.044 (0.004)	0.40 (0.11)	1.98 (1.09)	7.67 (10.39)	0.26 (0.05)
G5					
Summer	0.046 (0.007)	1.55 (1.61)	6.24 (3.17)	16.97 (5.28)	0.45 (0.18)
Autumn	0.047 (0.010)	1.23 (0.62)	7.01 (2.95)	12.72 (4.27)	0.52 (0.13)
Winter	0.056 (0.011)	1.63 (1.09)	7.60 (4.64)	21.09 (17.27)	0.53 (0.16)
G10					
Summer	0.037 (0.002)	0.59 (0.42)	3.82 (1.63)	17.64 (2.86)	0.22 (0.05)
Autumn	0.033 (0.001)	0.34 (0.07)	5.50 (2.34)	13.86 (6.01)	0.25 (0.06)
Winter	0.040 (0.005)	0.37 (0.10)	2.17 (1.18)	22.73 (18.86)	0.22 (0.05)
G15					
Summer	0.039 (0.007)	0.64 (0.49)	3.12 (0.75)	24.08 (9.43)	0.23 (0.07)
Autumn	0.038 (0.007)	0.50 (0.28)	4.63 (2.23)	8.94 (3.36)	0.24 (0.04)
Winter	0.037 (0.004)	0.41 (0.13)	1.74 (0.52)	25.30 (47.32)	0.21 (0.04)

3.3.2 Estimation of specific attenuation coefficients

There were 97 measurements of K_d paired with water quality, 16 in summer, 28 in autumn and 53 in winter. In a first approach, we used the measured parameters of CDOM, Chla, fine and coarse SS in a stepwise multiple linear regression against K_d to derive specific attenuation coefficients for these optically active fractions. This approach is unconstrained and therefore takes into account the influence and/or covariance of unmeasured parameters. The multiple linear regression derived from these constituents was significant (r^2 = 0.70, standard error = 0.09 m^{-1}), with each specific attenuation coefficient (scenario 1, Table 3.2) having a p-value <0.005, except for coarse SS (p = 0.01). Detritus was excluded from this initial assessment because of the very low POC levels.

Repeating the above calculations by including a detritus term, the specific attenuation coefficients of the different water quality constituents remain significant (p < 0.005) and largely unchanged (scenario 2, Table 3.2), with a lower significance for coarse SS (p = 0.01) and detritus (p = 0.11). Detritus was calculated as the difference between POC and carbon in Chla (assuming C/Chla = 50) and therefore constitutes the fraction of non-algal detritus. Fine SS was corrected to account only for inorganic SS by calculating the difference between fine SS and the sum of carbon in detritus and Chla (assuming dry matter/C = 2.5). POC was assumed to be concentrated in the fine size fraction because >75% of phytoplankton in metropolitan Adelaide is <5 μm (van Ruth 2010, 2012), and the sorption of organic matter to SS is typically controlled by surface area (Middelburg and Herman 2007). The organic fraction of coarse SS was considered negligible.

Both scenarios 1 and 2 in Table 3.2 give slightly negative intercepts for the background of pure seawater (K_{sw}), which were however not significant (p > 0.8). Fixing K_{sw} to the widely accepted value of 0.0384 m^{-1} (Lorenzen 1972, Atlas and Bannister 1980, Christian and

Sheng 2003, Kelble *et al.* 2005) yields a lower specific attenuation for CDOM, but similar values for Chla, fine and coarse SS (scenario 3, Table 3.2).

Table 3.2 Specific attenuation coefficients (k) derived for CDOM (cm m^{-1}), Chla (m^2 mg^{-1}), detritus (m^2 g C^{-1}), fine and coarse SS (m^2 g^{-1}), as well as the partial attenuation coefficient of pure seawater K_{sw} (m^{-1}).

Scenario	k_{CDOM}	k_{Chla}	k_{Det}	k_{fineSS}	$k_{coarseSS}$	K_{sw}	Constraint
1	4.710	0.068	---	0.015	0.001	-0.0041	none
2	4.692	0.069	0.151	0.015[a]	0.001	-0.0088	none
3	3.831	0.071	---	0.015	0.001	0.0384	K_{sw}
4	2.623	0.071	---	0.032	0.001	0.0384	k_{Chla}, $k_{coarseSS}$ and K_{sw} as in scenario 3, slope in Fig. 4 ≥0.85

[a]Corrected to account only for inorganic SS.

In order to further verify the estimate of the specific attenuation coefficient for CDOM, a mechanistic approach was employed based on the simple linear regression between K_d and fine SS:

$$K_d = 0.0312 \times [fine\ SS] + 0.2143 \quad (5)$$

Since fine SS includes all particulate components affecting light (inorganic SS, phytoplankton, detritus), the intercept of the equation accounts for the influence of all non-particulate components (K_{sw} + K_{CDOM}), thus allowing for the determination of K_{CDOM} (0.1759 cm^{-1}). Fine SS was used instead of total SS (coarse plus fine) as the latter is not a good predictor of K_d, explaining only 16% of the variance in the dataset, while fine SS accounts for 49%. From K_{CDOM} and the mean concentration of CDOM (0.047 cm^{-1}), the specific attenuation of CDOM is calculated as 3.767 cm m^{-1}, a value close to that obtained from the multiple linear regression (scenario 3, Table 3.2).

The comparison of measured versus calculated K_d when using the specific attenuation coefficients derived above however leads to an overall overestimation of K_d for values <0.4 m^{-1} and an underestimation for higher values (Figure 3.6a; sum of residuals = 0.81). This reflects the higher number of points measured in the low K_d range (65 out of 97), where the partial attenuation from CDOM has a larger contribution to K_d (see next section). In contrast, fine SS plays a key role in the high K_d range. In order to avoid strong biases in K_d in both low and high ranges, we further optimized CDOM and fine SS coefficients to obtain the lowest sum of residuals when constraining the slope of the linear regression (Figure 3.6b; sum of residuals = 1.14). The optimized coefficients are lower for CDOM, but higher for fine SS (scenario 4, Table 3.2). Prediction of K_d values with these coefficients has an standard error of 0.10 m^{-1}, which is 29% of the mean K_d value of 0.35 m^{-1}, and 11% of the maximum K_d of 0.89 m^{-1}.

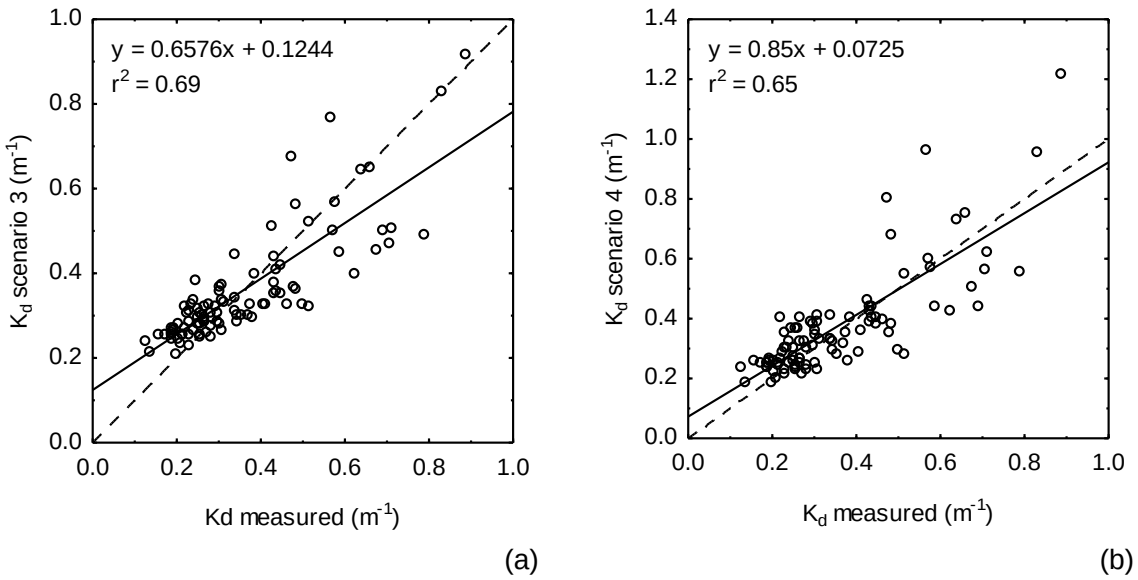

Figure 3.6 Calculated versus measured K_d by using the specific attenuation coefficients in scenarios 3 (a) and 4 (b) of Table 3.2. The dotted line indicates the regression with a slope of 1.

3.3.3 Contribution of each constituent to K_d

The most important driver of light attenuation was SS, which contributed on average 40% of calculated K_d. Fine SS contributed 6 times as much to attenuation (34%) as coarse SS (6%). CDOM was the second largest contributor to light attenuation, accounting on average for 36% of K_d. Phytoplankton had a modest impact on light (~ 13%), only marginally higher than the background imparted by seawater (12%). Overall, the contribution of particulate constituents to K_d was 53%.

The relative importance of each water constituent over the entire range of K_d observed in this study (Figure 3.7) indicates the key role of CDOM at K_d values < 0.4 m^{-1}. When K_d increases above this value, fine SS becomes the main driver of light attenuation, rising from less than 20% to over 60%. Chla is also a contributor at high K_d values, but the range of variation is much smaller (~10-30%). Coarse SS had a near constant contribution to K_d around 5%, only increasing to 10% or more for K_d values above 0.9 m^{-1}.

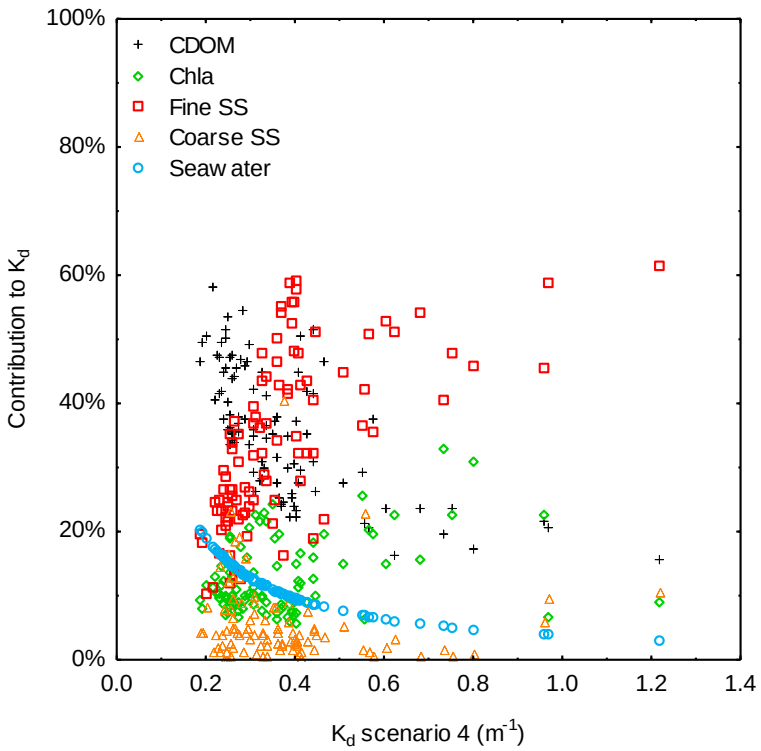

Figure 3.7 Contribution of each water constituent to light attenuation as a percentage of the total.

The changes in the contribution of the different constituents to K_d reflects the inshore-offshore gradient in concentrations. The partial attenuation of CDOM was typically 50% higher nearshore, while the partial attenuation of fine SS was double or more nearshore. As a consequence, the importance of SS to light attenuation was more marked at the shallow sites, where its contribution was 41-45% of K_d, as opposed to 34-37% at the deeper sites. The contribution of CDOM to K_d was inversely related to the contribution of fine SS: while the CDOM contribution increased from a minimum value of 16% nearshore to a maximum of 58% at deeper sites, the contribution of fine SS decreased from 62% to 10%. Similarly to CDOM, the seawater background accounted for around 8-9% of K_d at the shallow sites, but increased to 14% at the deeper sites. Particulate constituents were responsible for 54-64% of K_d at the shallow sites, while dissolved constituents contributed to 51-54% at the deeper sites.

Spatial variability was not as evident for the contribution of phytoplankton to K_d (~11%), except for site G5, where it reached 19%. Fine SS was also a greater contributor to light attenuation at this site (41% as opposed to 33% elsewhere). CDOM in contrast had a larger effect on light in the northern Bolivar transect (37-40%) than in the central Grange transect (28-37%).

3.4 Discussion

The Adelaide coast is an oligotrophic system with low Chla concentrations and relatively low K_d values despite its location at the edge of a large metropolitan area. A range of factors is likely to contribute to maintain water quality in the region, including the prevalence of rainfall (and land runoff) between June and September, when flushing from the Southern Ocean is intensified (Samarasinghe *et al.* 2003). This seasonality in rainfall also affects the inputs from WWTPs, with the lower volume of effluents in the dry summer months further reduced by the greater demand for recycled water used in irrigation. This balance between seasonal inputs and time of flushing helps to explain low Chla levels throughout the year, and the modest

influence of this parameter on light attenuation in the water column, contributing to ~13% of K_d, with little spatial or temporal variability.

In contrast to Chla, CDOM and fine SS were large contributors to light attenuation, and combined accounted on average to 70% of K_d. Both constituents peaked nearshore, fine SS more markedly than CDOM. Two processes act to accentuate the gradient for fine SS: (1) sediments settling from the water column with distance from shore, and (2) resuspension in shallow waters compounding SS concentrations from direct land-derived inputs . Periods of low light were invariably preceded by high wave-induced bed shear stress and high turbidity measurements indicative of sediment resuspension. Strong winds with a westerly or southerly component provided the longest overwater fetch distance and hence bed shear stress, causing elevated water turbidity.

As a consequence of high SS concentrations nearshore, SS had the largest effect on light overall and was the dominant parameter in the determination of the highest K_d values. When considering that the range of K_d values for which water quality was available (K_d up to 1 m^{-1}) was about half of that measured by deployed loggers over longer time scales (K_d up to 2 m^{-1}), the importance of SS in light attenuation can be expected to be even higher than estimated here. This is similar to patterns observed for other shallow systems such as the Indian River Lagoon or Chesapeake Bay (Christian and Sheng 2003, Xu *et al.* 2005). In the case of the Adelaide coast, the separation of SS into fine and coarse fractions likely afforded the empirical light model greater predictive ability than reported in other studies with a similar number of samples.

The unresolved K_d variability in the empirical model possibly stems from changes in the composition and size of particles within the fine SS fraction. The absorption and scattering of light by SS is size dependent, with smaller particles not only being more optically active, but also having a longer residence time in the water column before settling (Baker and Lavelle 1984, Campbell and Spinrad 1987). Albeit coarse SS represented on average 72% of total SS, this fraction contributed only to ~6% of K_d. The accurate simulation of fine SS therefore becomes crucial to the modelling of light availability close to shore.

The other main contributor to light attenuation, CDOM, has a different spatial distribution to fine SS, with values decreasing more gradually with distance offshore. The importance of CDOM in light attenuation is likely accentuated by the fact that Adelaide waters are relatively clear, with K_d typically <1 m^{-1}, as opposed to values as high as 4 m^{-1} or more in other shallow coastal systems where light attenuation is controlled by particulate fractions (e.g. Christian and Sheng 2003, Obrador and Pretus 2008). CDOM concentrations measured here (mean of 0.047 cm^{-1}) were intermediate between coastal (typically <0.030 cm^{-1}) and estuarine waters (>0.050 cm^{-1}) (Vant 1990, Clark *et al.* 2002, Pfannkuche 2002, Clementson *et al.* 2004, Branco and Kremer 2005, Kostoglidis *et al.* 2005, Le *et al.* 2013, Yamaguchi *et al.* 2013). This comparison assumed an exponential decay of CDOM absorption with wavelength, and an exponential decay constant S of 0.016 nm^{-1} (Pfannkuche 2002, Clementson *et al.* 2004, Le *et al.* 2013), to translate measurements in other studies to CDOM absorption at 254 nm. The specific attenuation coefficient for CDOM (2.623 cm m^{-1}) was also intermediate between values reported in New Zealand and Australia (<2 cm m^{-1})(Pfannkuche 2002, Kostoglidis *et al.* 2005) and those reported in US and UK estuaries (>5 cm m^{-1}) (Branco and Kremer 2005, Moate *et al.* 2012), corroborating the idea that CDOM coefficients are highly variable depending on composition and need to be tuned to translate local conditions. Internal sources of CDOM might contribute to the value calculated for Adelaide, as the region has shallow seagrass beds and is fringed by mangroves in the north, both known sources of CDOM (Stabenau *et al.* 2004, Shank *et al.* 2010).

Detritus is the only fraction that was not specifically taken into account in the coefficients derived from the empirical model given the overall low values of POC measured in the samples. This fraction is implicitly quantified in either the fine SS or Chla coefficients, with

multiple lines of evidence indicating the latter to be more relevant. The coefficient calculated for Chla (0.071 m^2 mg^{-1}) is higher than values from similar studies (Pfannkuche 2002, Christian and Sheng 2003, Branco and Kremer 2005, Xu *et al.* 2005, Obrador and Pretus 2008, Yamaguchi *et al.* 2013), with the coefficient for several phytoplankton families reported to vary in a narrow range, with a mean value of 0.014 m^2 mg^{-1} (Lorenzen 1972, Atlas and Bannister 1980, Kelble *et al.* 2005). In contrast, the specific attenuation coefficient calculated for fine SS (0.032 m^2 g^{-1}) is similar to values reported in the literature for carbon-free ash centred around 0.030 m^2 g^{-1} (Bowers and Binding 2006, Stramski *et al.* 2007, Blauw *et al.* 2008, Devlin *et al.* 2009, Los 2009, Moate *et al.* 2012). Chla is also better correlated with variables governed by land inputs, such as phosphate (r^2=0.40; data not shown), and hence is more likely to translate the variability of land-derived POC, as opposed to fine SS (e.g. r^2=0.13 for the correlation with phosphate), which more closely followed benthic shear stress and sediment resuspension. Chla as measured here is further uncorrected for its degradation product phaeophytin, and therefore also includes an algal detritus component. The slightly higher contribution of Chla to light attenuation (up to 33%) at high K_d values might thus be compounded by the effect of non-algal POC on the specific attenuation coefficient calculated for Chla.

The estimation of the detritus component in k_{Chla} requires a mechanistic approach. By multiplying the mean Chla concentration (0.72 mg m^{-3}) by its optimized specific attenuation coefficient (0.071 m^2 mg^{-1}), the average partial attenuation from Chla (K_{Chla}) is estimated as 0.051 m^{-1}. Assuming that detritus is included in this value, K_{Chla} = K_{live} + K_{det}, where K_{live} relates to living phytoplankton. Additional data collected in two of our sampling trips (November and January) indicate that on average phaeophytin accounts for 37% of the measured Chla. Correcting the mean Chla concentration for phaeophytin to calculate the concentration of living phytoplankton, and multiplying this value by the experimentally-based specific attenuation coefficient of 0.014 m^2 mg^{-1}, results in a mean K_{live} of 0.006 m^{-1}. By difference, K_{det} is calculated as 0.044 m^{-1}. The mean concentration of detritus is estimated as 0.18 g C m^{-3} by assuming a C/Chla ratio of 50 and using a ratio of detritus to Chla on a carbon-basis of 5 (calculated from the field data where POC>0). From K_{det} and the mean concentration of detritus, the specific attenuation of detritus was estimated as 0.25 m^2 g C^{-1}, a value in the 0.1-0.3 m^2 g C^{-1} range reported for POC in mixed coastal particles (Blauw *et al.* 2008, Woźniak *et al.* 2010, van Gils and Tatman, 2003). Additional data collected in two of our sampling trips (November and January) indicate that on average phaeophytin accounts for 37% of the measured Chla.

The application of the specific attenuation coefficients derived here in the AREM modelling suite developed for Adelaide (Zijl *et al.* 2014) will allow the prediction of the effect of changes in land-derived inputs will have on the attenuation of light via changes in SS, CDOM, phytoplankton and detritus. Although the empirical model has limited spatial coverage, some of these changes are already evident from the data, with fine SS having a more pronounced effect on light in the central metropolitan coast, and CDOM in the north.

Along the central coast, river inputs trapped close to shore due to the dominant north-south tidal movement (Pattiaratchi *et al.* 2007), together with intense wave action and sediment resuspension, dictate the current role of fine sediments in defining seagrass suitability. The K_d values measured here, when applied to published relationships between K_d and seagrass colonization depth, indicate that seagrasses in the region would survive in water depths up to 2.5-5 m, or if using a model developed more specifically for *Posidonia*, up to 14-19 m (Duarte *et al.* 2007). Yet the current distribution of seagrasses in the region shows no seagrasses at depths of *less* than about 5 m, and dense meadows from 10 to 20 m (Hart 2013). The average light climate therefore might not be the most useful tool to assess the light requirements of seagrasses in this case, with the magnitude of extreme events and the duration of low light conditions in relation to critical growth stages perhaps being more

relevant to predict seagrass survival (Moore *et al.* 1997, Gallegos 2001), particularly for species with low below-ground reserves such as *Amphibolis* spp, which was selectively lost from the region (Bryars and Rowling 2009).

The high contribution of CDOM in the north appears to be partly modulated by WWTP inputs, as both CDOM concentrations in effluents (0.27 cm^{-1}) and volume of inputs (~40 GL per year) is higher than in the central coast (0.19 cm^{-1} and ~20 GL) (Chapter 2). The same holds for river inputs, with the Gawler River in the north having CDOM values almost four times higher than Torrens River in the central zone (0.74 vs 0.19 cm^{-1}) (Chapter 2) despite less than half the discharge volume (11 vs 26 GL) (Jones 2015). This analysis suggests different management levers to ameliorate the light climate in the north vs the central zone. In the latter, initiatives to decrease SS inputs and wave resuspension, and SS residence time, might lead to the best outcomes, while in the north management of river and effluent colour would also produce good results.

The use of management levers to ameliorate water quality nearshore is an avenue for promoting restoration and bringing the seagrass edge to its former position closer to shore. Comparison of current water quality to historical data suggests a significant improvement in the light climate from values recorded between the 1970s up to the late 1990s (Lewis 1975, Steffensen 1985, Gaylard 2004). Turbidity in the central coast has been reduced from mean values of 2-6 NTU, to 1-2 NTU currently. Chla concentrations also dropped from 2-5 mg m^{-3}, to less than 1 mg m^{-3}. Corroborating this trend in water quality, the latest seagrass survey indicated no further losses since 2007, but only limited natural recolonisation (Hart 2013). Hence it appears that the challenge now is no longer in halting seagrass decline, but promoting its return in areas where fine SS resuspension defines a new alternate state (Adams *et al.* 2016).

3.5 Conclusions

New data have been collected from the Adelaide coastal waters that allow the construction of a linear model that relates the observed downward attenuation of light to the observed concentrations of key water quality parameters.

The empirical light model derived here works remarkably well in the coastal waters of Adelaide. The model explains 65% of the variability in K_d by using concentrations of four water quality constituents: CDOM, Chla, fine and coarse SS. The model predictive ability could be further refined if the dataset was extended to include measurements of water quality, particularly changes in the composition of fine SS, for events were K_d reaches values > 0.4 m^{-1}.

The specific attenuation coefficients calculated for the optically active fractions used in this empirical model can be easily extrapolated to a more complex biogeochemical model of the region to estimate the effect of potential management initiatives on light available to seagrasses. Fine SS and CDOM are the main determinants of K_d, and good predictive ability for these parameters becomes paramount in biogeochemical model validation. Coarse SS accounts for most of the SS mass but only a negligible fraction of light attenuation.

Fine SS is a particularly relevant management lever nearshore, where major seagrass losses were recorded since the 1970s. CDOM is equally important further north, where highly coloured discharges affect a more broadly shallow region. Given significant improvement in water quality since the early 2000s, management initiatives can now shift their focus from halting seagrass loss to promoting seagrass recolonisation through the control of fine SS and CDOM.

4 A hydrodynamics, waves, sediment and biogeochemical model for the Adelaide Coastal Waters

Port River mouth seen from the North – Photograph by Paul Erftemeijer

4.1 Introduction

The current chapter discusses the final versions of the hydrodynamics, waves and sediment/biogeochemistry sub-models of the AREM. These models have the objective of quantifying relevant environmental conditions for seagrass habitat suitability evaluation, as affected by local river discharges and discharges of treated wastewater and stormwater, taking into account the morphology, meteorology and oceanography of the study area. The area of interest for the modelling covers the Adelaide coastal waters, from 20 km north of Port Gawler in the north to Sellicks Beach in the south, extending 20 km off the coastline (see blue rectangle in Figure 1.1). For a discussion of the Habitat Suitability Model, we refer to Chapter 5. The currents, salinity and temperature of the coastal waters in the study area are simulated by 3D mathematical hydrodynamics modelling, taking into account the feedback mechanisms induced by horizontal and vertical density differences driven by the water temperature and salinity. Following the approach adopted in the ACWS (Pattiaratchi, Newgard and Hollings, 2007), the impact of waves on near-shore residual currents is included in the modelling by an online coupling between the hydrodynamics and wave models. The sediment/-biogeochemistry model quantifies the light reaching the seagrass leaves, and is driven by currents, temperature and salinity calculated by the coupled hydrodynamics and wave models.

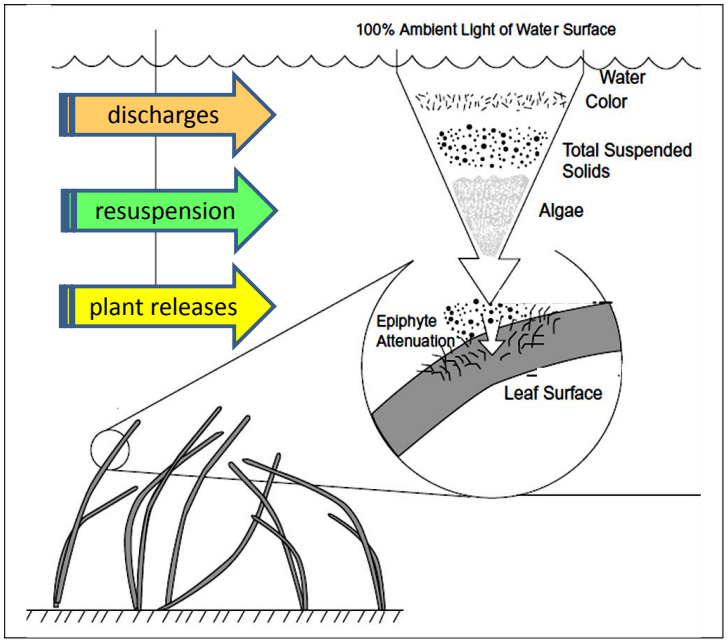

Figure 4.1 Conceptual diagram of water column- and epiphyte attenuation of light before reaching a seagrass leaf (adapted from Batiuk, et al., 2000)

The conceptual model for modelling available light is shown in Figure 4.1. Incident solar radiation, corrected for reflection, penetrates into the water towards the seagrass canopy. The available light is attenuated by absorption and scattering by suspended particles that include algae, and by water colour affected by CDOM. During Phase 1 of the AREM development we concluded that the observed concentrations of particles in the study area cannot be quantitatively explained by coastal discharges alone. This conclusion was partly based on an observation that simulated concentrations resulting from coastal discharges alone were much smaller than observed concentrations. In addition, detailed high frequency light measurements over a year along a transect off Grange (Collings, et al., 2006) revealed regular low light episodes lasting several days. Such episodes sometimes coincided with rain events, but not always. However, all low light episodes coincided with strong winds, which led to the conclusion that wave induced resuspension provides a substantial part of the coastal water particle concentrations. Petrusevics (2005) also found that local winds were positively related to suspended matter variability at stations about 5 km offshore. Finally, in situ observations by SA Water in 2015 at inshore stations off Bolivar and off Grange confirmed that high water turbidity is not always connected to runoff events. These observations revealed that strong winds with a westerly or southerly component correlated with elevated water turbidity. During the present project, we also concluded that the observed concentrations of CDOM in the study area cannot be quantitatively explained by coastal discharges alone. This conclusion was possible due to the availability of measured data of the UV-absorption in coastal discharges (Chapter 2) and in receiving coastal waters (Chapter 3). Model simulations showed that simulated concentrations resulting from coastal discharges are much smaller than observed concentrations. In our conceptual model, there are additional CDOM releases from seagrass, mangroves and sediment resuspension.

4.2 Materials & Methods

4.2.1 Model software

The AREM makes use of the Delft3D open source software (oss.deltares.nl/web/delft3d). Delft3D is a modelling system that consists of several modules that can simulate flows, waves, sediment transport, morphological developments and ecological processes (Roelvink & Van Banning, 1994; Lesser et al., 2004). Delft3D has a wide range of previous applications world-wide. ScienceDirect and Google Scholar together hold more than 4,000 articles discussing Delft3D modelling. There is a wide pool of Delft3D users available at numerous universities, scientific institutes, consultancy firms and government bodies all over the world. This makes Delft3D a suitable basis for the development of the AREM.

4.2.2 Model domain and grids

The selection of the model domain and the grids was based on different and sometimes contradicting requirements. Firstly, the AREM needs to represent strong spatial and temporal concentration gradients inside the study area, especially nearshore, driven by highly variable river inflows (Chapter 2) and currents and winds. This requires a high resolution. Secondly, the residual currents entering and leaving the study area are determined by transport patterns on the scale of St Vincent Gulf as a whole, which makes it necessary to have a model domain spanning the whole gulf. Thirdly, the use of annual simulations is an essential element in the AREM modelling strategy. Replacing such annual simulations by a set of shorter simulations capturing seasons and characteristic events, and extrapolating these shorter simulations to annual time scales, would strongly affect the quality of the overall AREM concept. It would make the results less objective, since they would depend strongly on our choice of events and the weight we attribute to them. Based on these considerations, we used a two domain approach, with a high resolution “detail” local model nested in an “overall” model covering St Vincent Gulf (Figure 4.2). Both grids are curvilinear, i.e. they have the regular structure of a rectangular grid but with variable dimensions. They are defined in the WGS 84 co-ordinate system.

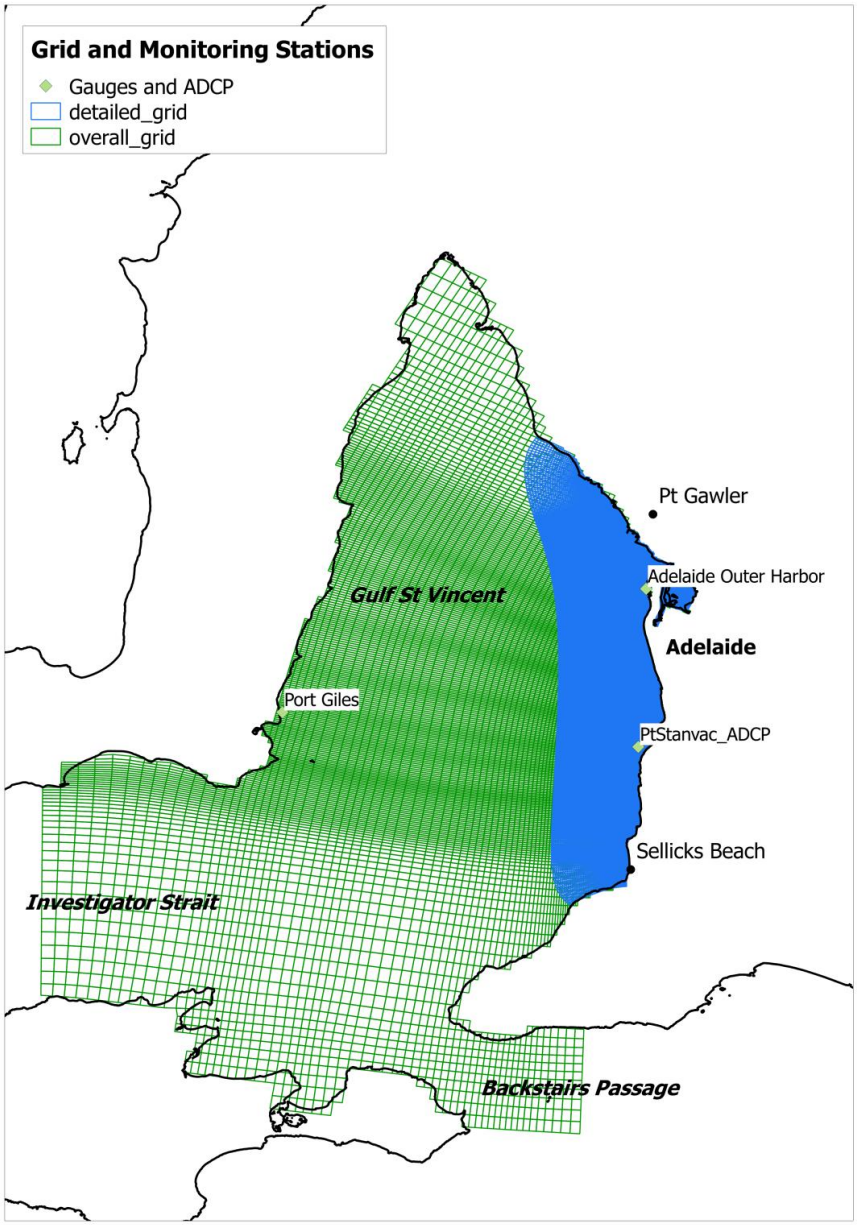

Figure 4.2 High resolution "detail" local model grid (blue) and "overall" model grid (green)

The detailed domain is designed to cover the area of interest reaching from 20 km north of Pt Gawler to Sellicks Beach, encompassing the extent of coastal discharges plumes as they were determined during Phase 1 of the AREM development (Zijl et al., 2014). The resolution of the detailed grid was selected to satisfy as much as possible all requirements without presenting an unacceptable computational burden for performing annual simulations. The detail model has a 50m east-west resolution over the first km near the beach, widening out in a western direction to about 400m at the open sea boundary (see Figure 4.3, right panel). In the north-south direction, the resolution is about 200m. An area with higher north-south resolution exists in front of the Port River outlet to better resolve the outflow plume (see Figure 4.3, left panel).

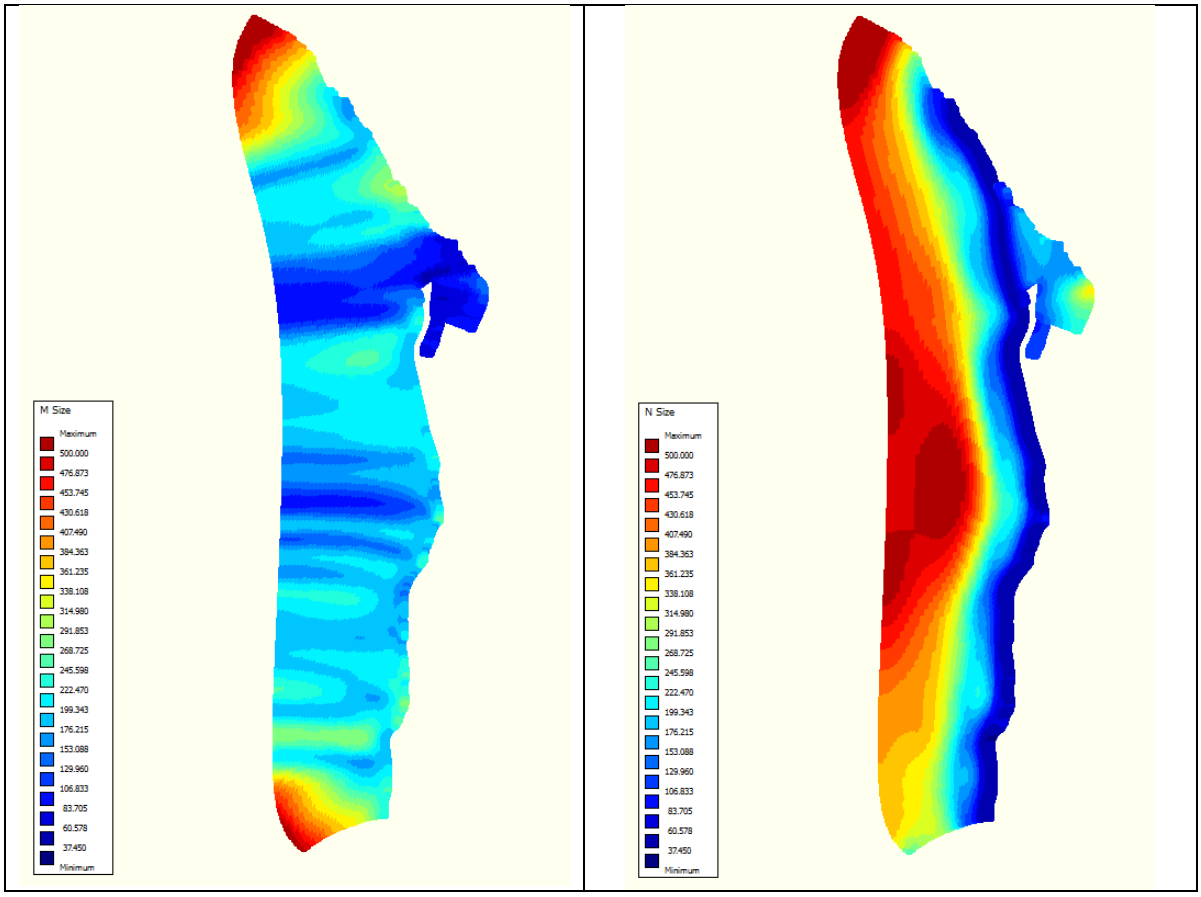

Figure 4.3 North-South (left) and East-West (right) resolution of the detail model grid.

The overall model has open boundaries in Backstairs Passage and Investigator Strait (Figure 4.2). This implies that the degree of realism of the flow patterns and fluxes in the south part of Gulf St. Vincent depends on the definition of realistic boundary conditions.

The vertical grid schematization uses a so-called “sigma layer” approach, where the water column is divided into a fixed number of layers. The thickness of each layer is defined as a constant and homogeneous fraction of the total water depth. 20 sigma layers are used in the detail and in the overall model, with a uniform thickness of 5 % of the local water depth.

4.2.3 Bathymetry

The bathymetry has been derived from the 250 m resolution Australian bathymetry and topography grid, June 2009 (Whiteway, 2009), which covers the whole Gulf St Vincent, and from the 50 m resolution ACWS bathymetry dataset (Pattiaratchi, Newgard and Hollings, 2007), which covers the study area. The latter was used in the Port Adelaide & Barker Inlet area, the former everywhere else in the model domains, see Figure 4.4. Bathymetry processing was done using the Delft3D-QUICKIN tool[1]. First, grid cell averaging was performed for the area where there are several data points per grid cell, and using triangular interpolation for the remaining grid cells. This lead to discontinuities along the borders of the area where the fine resolution dataset was used (Figure 4.5, left panel), which could cause false circulation patterns. Therefore, the bathymetry in the area within the magenta polygon (Figure 4.5, left panel) was smoothed. Furthermore, the area marked by the black polygon

[1] *(https://oss.deltares.nl/documents/183920/185723/QUICKIN_User_Manual.pdf)*

(Figure 4.5, left panel) showed elevations up to levels exceeding 1m above MSL. Inspection via Google Earth suggests that those elevations are unrealistically high. This was corrected in the area east of the 2m depth contour line by setting the depth along the shoreline to 0m, and by interpolating and smoothing using Delft3D-QUICKIN. The resulting bathymetry is shown in Figure 4.6.

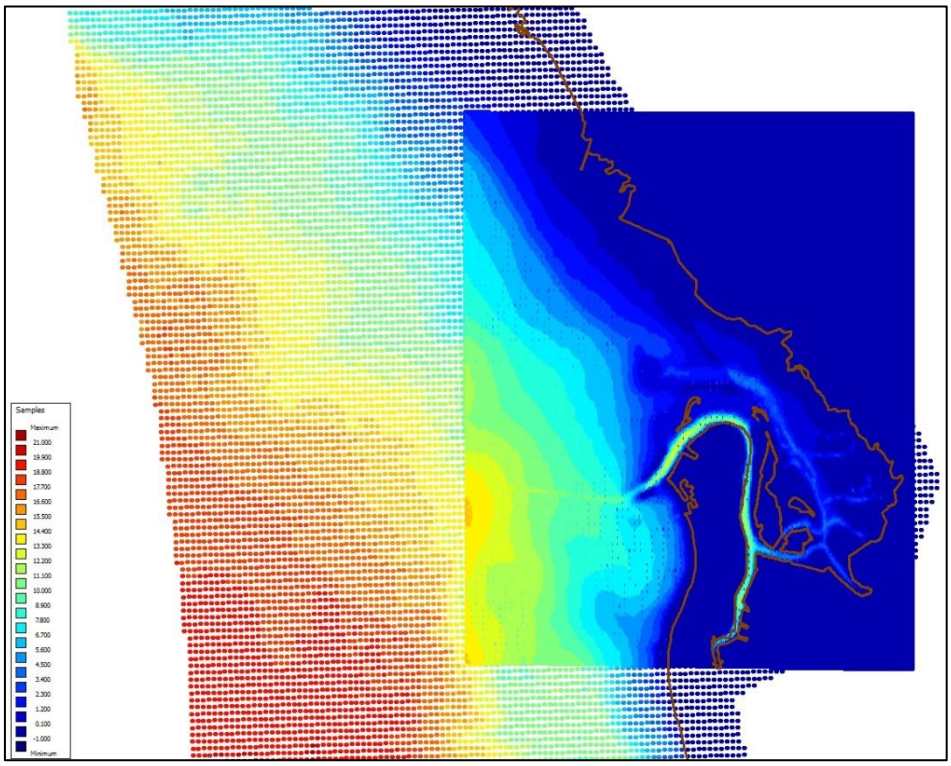

Figure 4.4 Depth data used in the Port River and Barker Inlet area. The densely dotted area shows data from (Pattiaratchi, Newgard and Hollings, 2007); the sparsely dotted area shows the Australian bathymetry and topography grid data (Whiteway, 2009).

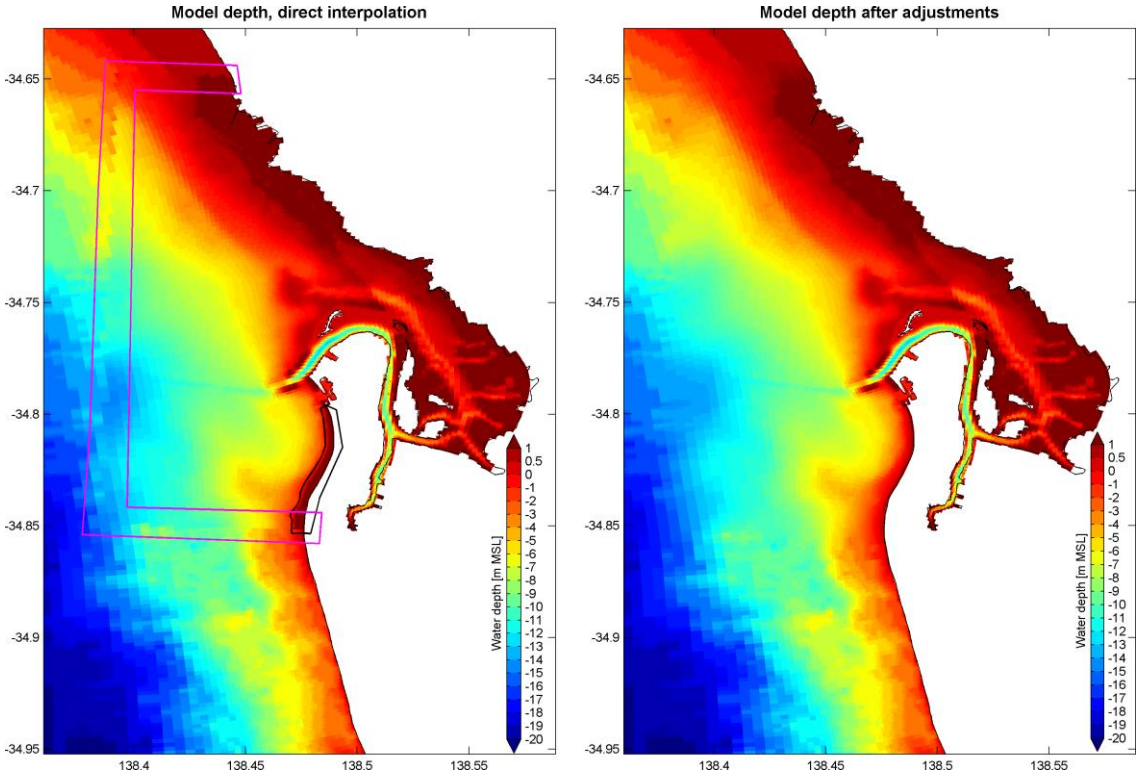

Figure 4.5 Computational depths, interpolated onto finer model grid: directly (left) and after the adjustments described here (right).

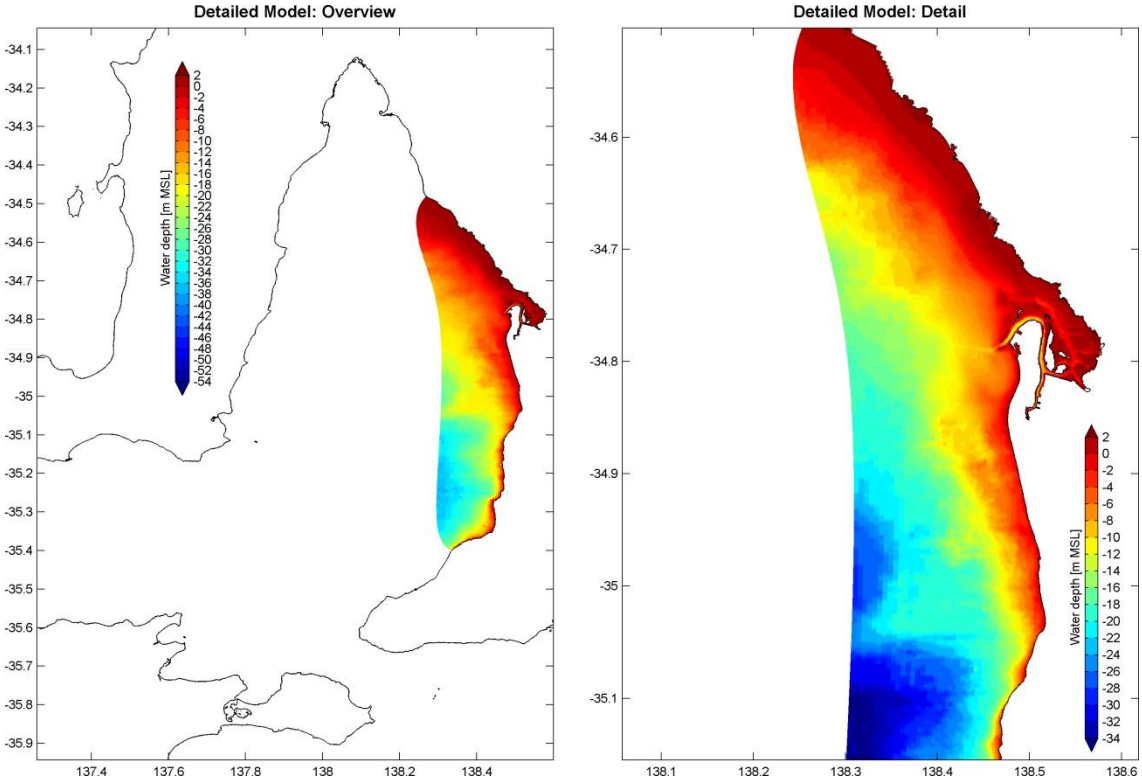

Figure 4.6 Final bathymetry used in the detailed model.

4.2.4 Meteorological forcing

The phase 2 model is driven by detailed meteorological data obtained from the Australian Bureau of Meteorology. In particular we used half hourly data for total rainfall, wind, air temperature, relative humidity, cloud cover and solar radiation for the station Adelaide Airport, as well as daily evaporation data. Figure 4.7 shows the rose of the wind data for 2011. The bar lengths indicate the occurrence percentages. Directions are defined towards the centre of the rose. The numbers in the centre of the rose segments are the percentage of occurrences in the lowest class. It can be seen that wind velocities from the southwest are the most dominant and the strongest, with velocities up to 15 m/s. About 20% of the time the wind comes from a north-easterly direction (from land).

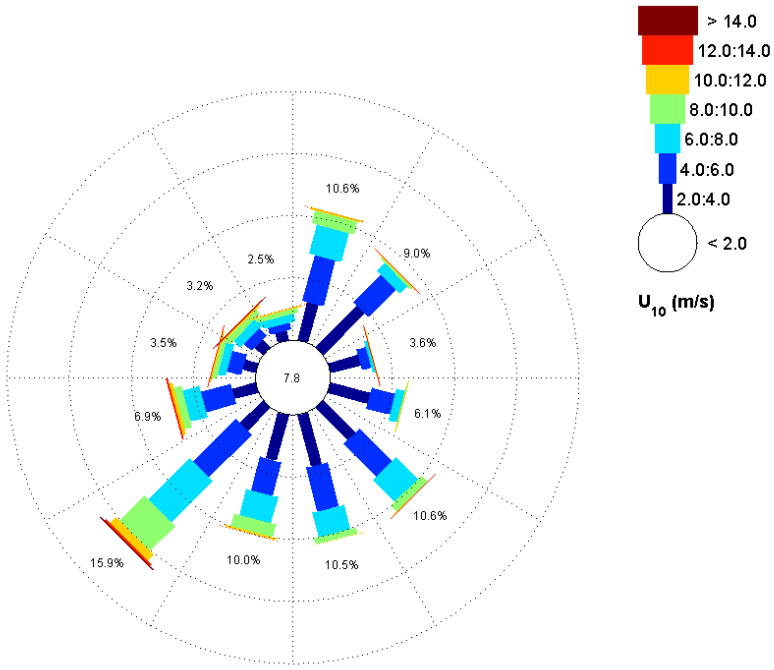

Figure 4.7 Wind rose; the bars display the occurrence of wind velocities U_{10} (m/s) for 12 wind sectors. The number in the centre of the wind rose segments shows the occurrence of wind velocities in the lowest wind class.

4.2.5 Hydrodynamics model

Three-dimensional unsteady flow and transport phenomena are simulated in Delft3D-FLOW by solving the well-known shallow-water hydrostatic pressure equations (Stelling, 1983; Lesser et al., 2004; Twigt, et al. 2009). It uses an orthogonal curvilinear horizontal grid and terrain-following vertical coordinates (σ-transformation) or horizontal z-layers (Stelling, 1983; Leendertse, 1987). In addition, it calculates transport of heat and salinity. A wind-induced shear stress is applied at the water surface, with the wind drag coefficient formulated according to Smith and Banke (1975). The surface heat flux is calculated according to the Ocean Heat Flux Model (Lane, 1989). At the bed, a friction force is applied driven by a specified bottom roughness. This roughness is spatially variable under the influence of seagrass cover. This will be discussed in section 4.2.7.

4.2.5.1 Boundary conditions

Tidal water level boundary conditions at the open boundaries are specified in the frequency domain. The tidal conditions of 13 constituents (MM, MF, Q1, O1, P1, K1, N2, M2, S2, K2, MN4, M4, MS4) were obtained from the TPXO 7.2 Global inverse tide model database

(Oregon State University; http://volkov.oce.orst.edu/tides/TPXO7.2.html) using the Delft Dashboard package (https://publicwiki.deltares.nl/display/OET/DelftDashboard). A conversion was applied from the UTC reference used in this data source to the local time zone (GMT +09:30h). During calibration, adjustments were made to the amplitudes and phases of these 13 constituents. In addition, 5 constituents (MSF, MU2, L2, T2 and S1) were added to better represent the tidal elevations inside the study area. This was done using water level data from the Bureau of Meteorology (BoM) at Port Giles and Outer Harbor (Figure 4.2).

No complete field dataset was available to specify the non-tidal water level signal (surge) on the AREM model boundaries. Such information is available only for a part of the simulated period and only for a station in Investigator Strait (Australian National Moorings Network (ANMN)). The surge signals observed at Adelaide Outer Harbour and Port Giles (Figure 4.2) are very similar. This suggests that the surge in the whole Gulf St Vincent is following the open sea surge in a uniform way. Following this hypothesis, we defined the non-tidal water level signal (surge) on the AREM model boundaries equal to the low pass filtered non-tidal part of the observed water levels at Port Giles. This signal is consistent with the available ANMN data.

To confirm the reproduction of circulation patterns in the study area, the model validation includes a comparison of simulated currents and observed ADCP currents at Port Stanvac (Figure 4.2). We acknowledge that the choice of the model domain and the applied surge forcing is not adequate to correctly represent circulation patterns and upwelling events in the outer parts of the Gulf near Investigator Strait and Backstairs Passage. This would require detailed water level observations in both Investigator Strait and Backstairs Passage or, alternatively, nesting in a larger scale, ocean model. In view of the strongly localised character of the problem at hand, we consider this limitation acceptable. The salinity and the temperature at the open boundaries have also been set pragmatically to a homogeneous and constant salinity of 34.8 ppt and a homogeneous time-dependent temperature varying between 14ºC (July-August) to 23ºC (February) based on IMOS data and SA Water data.

4.2.5.2 Physical and numerical parameters

For accurately modelling of the vertical velocity and temperature gradients, a two-equation k-ε vertical turbulence closure model is used. Apart from the vertical eddy viscosity and vertical eddy diffusivity computed by the k-ε model, a background value of 5×10^{-5} m^2/s has been applied for the vertical eddy viscosity, to account for breaking of internal waves and to prevent decoupling of layers. In our experience with this type of application and grid resolution, horizontal viscosity and diffusivity values of approximately 0.1-0.5 m^2/s are applicable. Based on Cox, Kaempf and Fernandes (2013), who computed lateral dispersivity from drifter experiments, we have set the values for horizontal viscosity and diffusivity to 0.2 m^2/s. Cox, Kaempf and Fernandes (2013) note that in the analysis of the longer time series, they find higher apparent dispersivity values of about 3 m^2/s, presumably due to the presence of mesoscale eddies, which were absent in their model. Since these eddies are presumably resolved in our detailed hydrodynamic model, we have kept a uniform value of 0.2 m^2/s, also in offshore waters. The Stanton number for the convective (forced) heat flux and the Dalton number for the evaporative heat flux are set to 1.3×10^{-3} (Gill, 1982; Lane, 1989). For the Secchi depth, a measure of the transparency of the water that affects the penetration of heat in the water column and the formation of temperature stratification, a typical value of 8 m for clear coastal waters has been applied. This is a homogeneous parameter in the hydrodynamics model, and it can therefore not be directly derived from the simulated water quality. The selected value is equivalent to a total downward attenuation of 0.21 m^{-1}. This is in good agreement with the measured values in the study area (see Chapter 3). The air density

was set to 1.2 kg/m^3. The time step in the overall model is 2 minutes, in the detail model 0.5 minute.

4.2.5.3 *Initialisation*

For water levels and currents, a spin-up period of approximately 5 days is in principle sufficient. For the salinity and, to a lesser extent, for the water temperature, the model responds to the applied boundary conditions under the influence of the transport of water masses within the model domain. This is a slow process. Therefore, the initial conditions for salinity and water temperature were derived from a repeated 12 month simulation with the overall model.

4.2.6 Wave model

The wave model has been set up using the same detail grid as the flow model, in order to avoid instability in the models. An extra, stand-alone SWAN-based wave model has been set up to transform high quality off-shore wave hindcasts available from the Australian Bureau of Meteorology (BoM) to the boundaries of the detail model (see Figure 4.8).

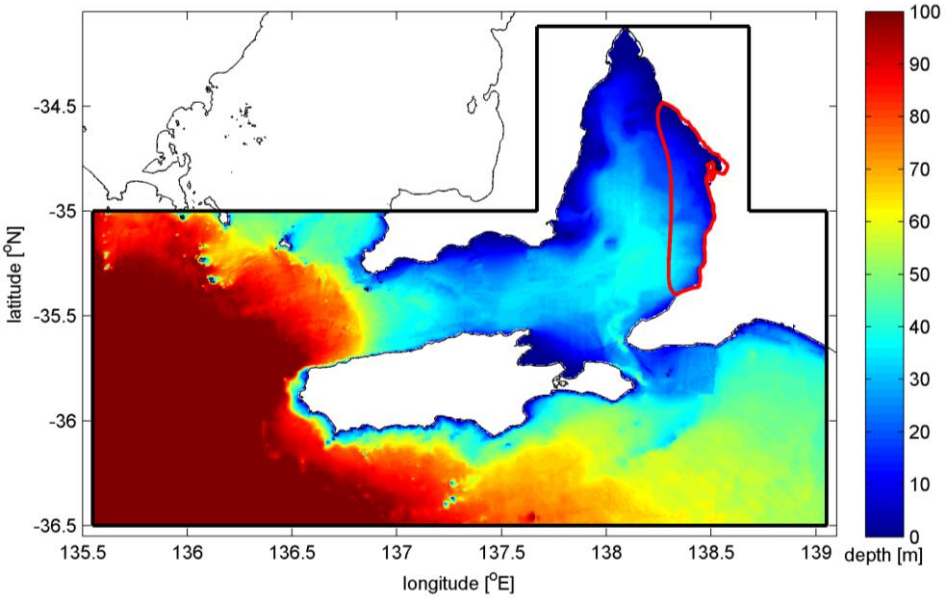

Figure 4.8 Region covered by the Extended Wave Model (outlined in black) and the detail model (outlined in red).

Directional and spectral grids have been defined based on the wave characteristics, wind characteristics and geometry of the region. The wave climate includes rather long waves that can propagate into the region and shorter wind waves that are generated at sea with rather short fetches. For the directional space, waves from all possible directions are considered, divided in 48 sectors of 7.5° each. The frequency domain discretisation goes from 0.02 to 2.5 Hz (0.4 – 50 s), with the frequencies logarithmically divided in 51 bins. At the open water boundaries of the detail model, the hourly 2D wave spectra computed by the Extended Wave Model have been imposed (see Appendix C).

4.2.6.1 *Physical and numerical parameters*

The SWAN version 40.85 has been applied in non-stationary, third-generation mode. For whitecapping, the saturation-based whitecapping is used (Van der Westhuysen et al., 2007). Quadruplet nonlinear interaction is modelled using the Discrete Interaction Approximation (DIA) (Hasselmann et al., 1985). The shallow water source terms include bottom friction according to Madsen, Poon and Graber (1988) and depth-induced breaking according to

Battjes and Jansen (1978), with γ (the ratio of maximum individual wave height over depth) equal to 0.73 (default). A spatially varying bottom roughness length scale (K_n) is applied, see section 4.2.7. Triad wave-wave interactions are not activated.

The backward space, backward time (BSBT) numerical scheme is used. In the numerical settings, a curvature stopping criterion of 0.001, on at least 99% of the wet grid points, with a maximum number of iterations of 60 is set. Furthermore, to assist the model convergence when the waves are low, a small degree of under-relaxation (alfa = 0.01; http://swanmodel.sourceforge.net/online_doc/swanuse/node29.html) is applied. The time step of the on-line coupling between the flow and wave models is 60 minutes. The online coupling between the flow and the wave models allows the wave model to receive water level and current input from the flow model. The wave conditions (i.e. wave forces based on the radiation stresses and orbital bottom velocity) computed in the wave model are used as input to compute wave driven currents, enhanced turbulence and bed shear stress in the flow model. The flow-wave coupling implemented in Delft3D is described in the respective manuals of the Delft3D-FLOW and the Delft3D-WAVE models (see https://oss.deltares.nl/documents/183920/185723/Delft3D-FLOW_User_Manual.pdf, Section 9.7; http://swanmodel.sourceforge.net/online_doc/swantech/node22.html).

4.2.7 Representation of seagrasses

Seagrasses create hydraulic roughness for both flow and waves. Ignoring this plant-induced drag would lead to an overestimation of flow velocities (and bed shear stresses and fluxes) in vegetated areas. Quantification of this drag is not straightforward because it depends on the shape, the size and the spatial density of the plants. The plant shape varies during the tidal cycle because the plants are flexible; and their bending is related to the depth and flow velocity. In addition, the different species throughout Gulf St. Vincent have different biomechanical properties that are relevant to reconfiguration. Spatial density will differ as well. A realistic representation of these effects can be achieved in a relatively simple way by using a single drag value, thus avoiding a highly complex model and the associated computational effort (Dijkstra, 2012). This single drag value is derived by using Dynveg, a model specifically developed for these purposes, which takes into account the plant properties and reconfiguration (bending) in the flow (Dijkstra and Uittenbogaard, 2010).

We consider *Posidonia spp*. the most representative for the Adelaide seagrass meadows, with a representative stem or leaf thickness of 1 mm, a leaf width of 7.5 mm, a leaf length of 50 cm and approximately 1000 leaves per m^2 (Erftemeijer, 2015). The elasticity modulus is 4.7×10^{-8} N m^{-2}, and the plant density is 910 kg m^{-3}, derived from measurements on *P. oceanica* (Folkard, 2005). We have derived the drag values for a depth of 7.5 m and a current velocity of 0.1 m/s, as typical values for the nearshore seagrass meadows. The results obtained for a situation with and without plants are compiled in Table 4.1.

Table 4.1 Flow conditions, reconfigured seagrass properties and representative hydraulic roughness coefficients for Adelaide seagrasses

water depth (m)	velocity (m/s)	plant height (m)	drag coefficient (-)	Chézy[1]	Manning[2]
7.5	0.1	0.38	0.54	26.4	0.053
7.5	0.1	-	-	58.0	0.024

[1] equivalent hydraulic roughness expressed as a Chézy coefficient in $m^{1/2}$ s^{-1}, formula 74 (Baptist et al., 2007)
[2] equivalent hydraulic roughness expressed as a Manning coefficient in s $m^{-1/3}$.

The presence of seagrass was derived from the NatureMaps database (EnviroDataSA, 2015). In particular, we distinguished areas with different density and patchiness, as compiled in Table 4.2 and plotted in Figure 4.9.

Table 4.2 Naturemaps derived seagrass density and patchiness classes and adopted roughness in FLOW and WAVE models

Seagrass Density	Seagrass Patchiness	Index	Manning roughness in FLOW model	Equivalent Madsen roughness in WAVE model
no seagrass	no seagrass	0	0.024	0.05
Sparse	Patchy	1	0.024	0.05
Medium	Patchy	2	0.024	0.05
Dense	Patchy	3	0.024	0.05
Sparse	Continuous	4	0.024	0.05
Medium	Continuous	5	0.0385	0.09
Dense	Continuous	6	0.053	0.23

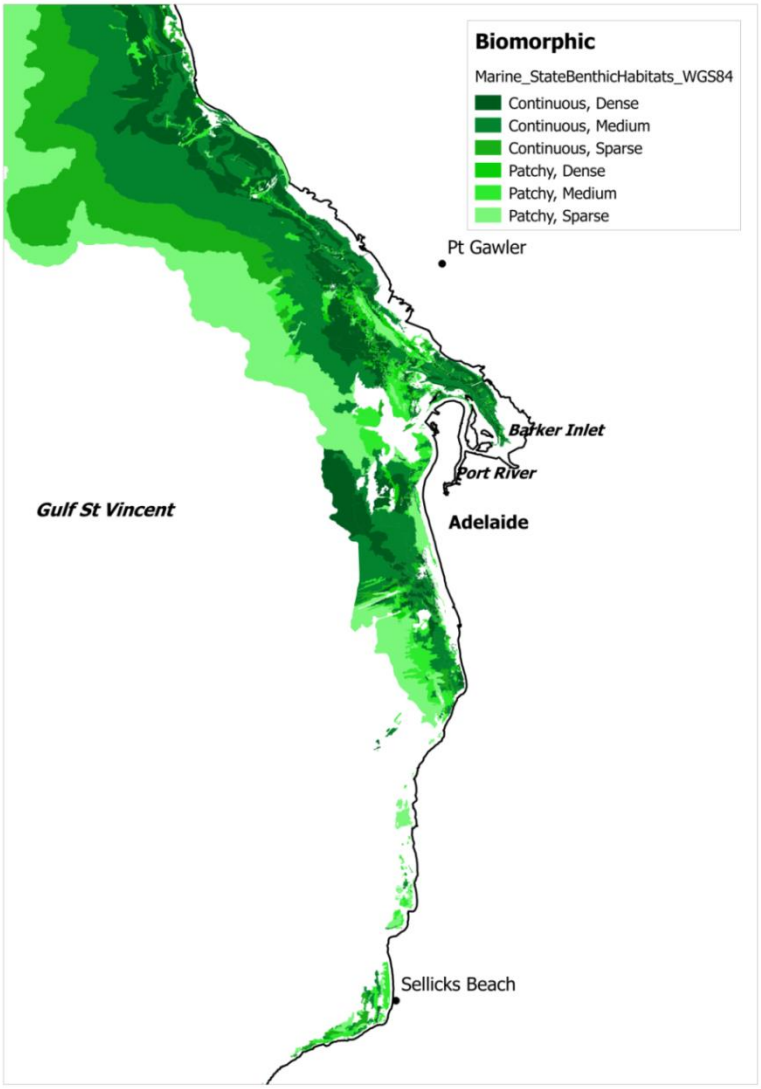

Figure 4.9 Characterisation of seagrass coverage (density, patchiness) as derived from NatureMaps data

4.2.8 Sediment Model

The sediment model includes three size fractions of inorganic matter (IM1 <16 µm, IM2 16-63 µm and IM3 >63 µm) and two fractions of particulate organic matter (POM1 rapidly decaying and POM2 slowly decaying). If suspended in the water column, the total of these substances is called “suspended solids” together with phytoplankton. These substances are undergoing settling and resuspension (Krone, 1962; Partheniades, 1962), the latter induced by shear stresses that are exerted by currents and waves. The resuspension flux F_{res} (g m^{-2} d^{-1}) is calculated as $Z_{res}(\tau/\tau_{cr,res}-1)$, where Z_{res} is the resuspension rate parameter (g m^{-2} d^{-1}), τ is the shear stress (N m^{-2}) and $\tau_{cr,res}$ is the critical shear stress for resuspension. Especially close to shore, the presence of waves increases these shear stresses notably. This is illustrated by Figure 4.10, which shows the simulated probability that simulated shear stresses exceed a value of 1 N m^{-2} during 2011, with and without wave action.

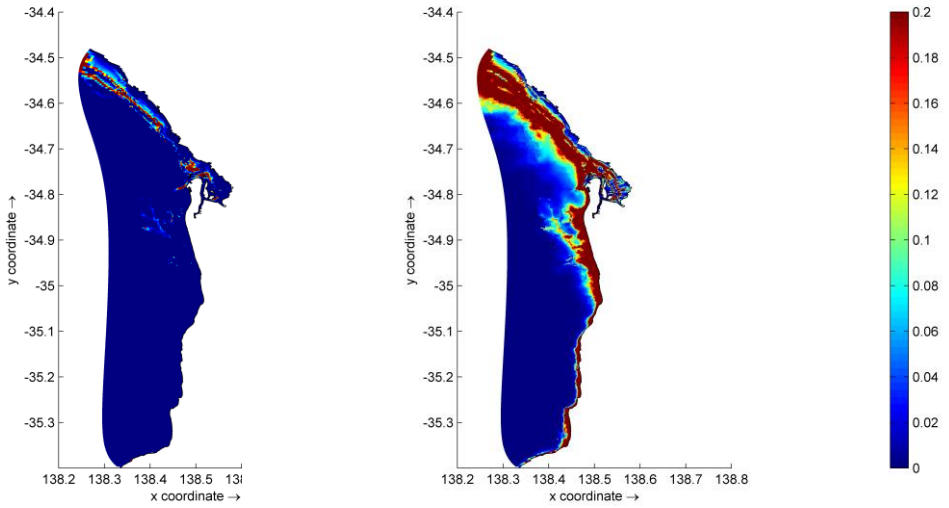

Figure 4.10 Probability (-) that 2011 simulated shear stress exceeds 1.0 N m^{-2}, without (left) and with (right) effect of waves included.

The seabed in the study area is sandy. The fraction < 63 µm (silt), which is expected to remain suspended for some time after resuspension, is commonly small (Bone et al., 2006). The top sediment layer composition data from the work of Bone and collaborators have been interpolated to produce a map of the fraction < 63 µm within the study area, see Figure 4.11. The results reveal silt fractions below 3% over large parts of the study area, with the exception of an area in front of the Port River outflow, where there is a silt fraction of 5-10%. We note that the extreme north and south parts of the detailed model domain are outside the spatial domain covered by Bone and collaborators and have therefore been attributed a homogeneous value of 4%.

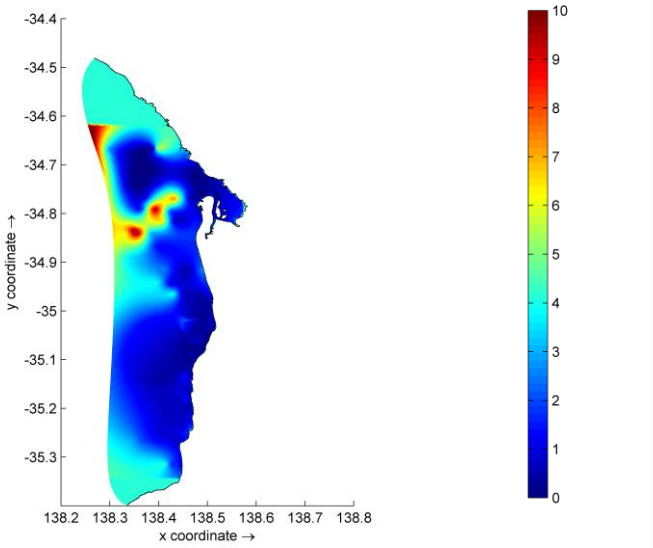

Figure 4.11 Share of particles < 63 µm in %, interpolated from data by (Bone, et al. 2006) and projected on the detailed model domain.

The critical shear stress for resuspension expresses the susceptibility of the sediments to be resuspended from the seabed into the water column. For the bare sediment encountered in the study area, the median grain sizes were estimated from Bone et al. (2006) and range from several hundred µm to 1000 µm. The critical shear stress for resuspension ($\tau_{cr,res}$) is expected to be in the range of 0.5-2.0 N m^{-2} (van Rijn, 1993). The relevant scientific literature provides evidence that seagrass covered sediments are significantly less susceptible to resuspension than bare sediments (Erftemeijer, 2015). To reflect this, the critical shear stress for resuspension has been made dependent of the presence of seagrasses (see section 4.2.7). Based on expert judgement, we attributed areas of continuous dense or continuous medium seagrass cover a critical shear stress of 10 N m^{-2}, areas with continuous sparse or patchy dense seagrass cover a critical shear stress 2.5 times higher than bare sediment and areas with patchy medium and sparse seagrass cover the same value as bare sediment. Thus, the spatially variable critical shear stress for resuspension in the model reflects the degree of seagrass cover, as shown in Figure 4.12 for a bare sand value of 1 N m^{-2}. In the model, any resuspension of bottom material leads to a release of the fractions < 63 µm (IM1 and IM2) that is proportional to their presence as shown in Figure 4.11. Larger particles are assumed not to remain in suspension and are neglected.

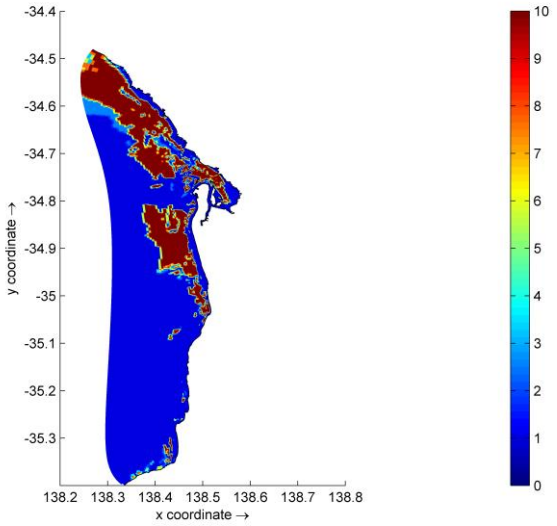

Figure 4.12 Spatially variable critical shear stress for resuspension.

By means of a sensitivity analysis it was established that effectively the same simulation results could be obtained by using different combinations of the resuspension rate parameter Z_{res} and the $\tau_{cr,res}$ for bare sand if the latter is in the expected range of 0.5-2.0 N m^{-2}. This is initially counterintuitive, but it is correct and caused by three factors: (a) the resuspension is limited to areas without seagrass cover, (b) shear stresses without wave action are generally lower than 0.5 N m^{-2} and do not cause resuspension, (c) shear stresses with wave action causing resuspension are generally significantly higher than 2.0 N m^{-2} in areas without seagrass cover. In the model, we used $\tau_{cr,res}$ = 1 N m^{-2} for bare sediment. The value of Z_{res} = 500 g m^{-2} d^{-1} was found by calibration.

We could not explicitly model the build-up of the silt content of the top sediment layer. The presence of silt in the top sediment layer is possibly partly natural and probably the result of discharges of fine particles from rivers, stormwater, and effluent and sludge from treatment plants. The total mass of silt in the top sediment layer of the detailed model is 9.7 million tonnes (1573 km^2, a 20 cm layer with 0.5 porosity, 2.38% of silt according to data shown in Figure 4.11 and a density of 2600 kg/m^3). The baseline model simulation shows an annual net export of fines from the model domain of 0.15 million tonnes per year. We note that the overall sediment balance of the study area, showing accretion, is determined by the coarser size fractions that are not transported in suspension. The net export of fines is much higher than the annual discharge of particles (about 0.01 million tonnes in 2011). Dividing the pool by the export, we obtain a time scale of 64 years. Thus, it is likely that the time scales governing the change of silt content of the top sediment layer are in the order of decades. This implies that the present silt content is the cumulative result of discharges and processes over the past decades, whilst the reduction of coastal discharges in recent years can be expected to lead to changes of the silt content of the top sediment layer in the coming decades.

4.2.9 Biogeochemical model

The biogeochemical (BGC) model is based on well-established concepts implemented in the Delft3D open source suite. It is based on the transport equation, or advection-diffusion equation, and includes a source term that represents coastal discharges and substance specific biogeochemical sources and sinks (Chapra 1996; Thomann and Mueller, 1987).

Numerous applications have been developed world-wide since the early 1980s, often just published in grey literature (e.g. van Gils et al., 2007). Some recent journal publications are provided by Blauw et al. (2008) and Smits and van Beek (2013).

The AREM BGC model is driven by the AREM flow and wave models. In particular, the grid, cell geometry, water fluxes between cells, vertical dispersion coefficients, shear stress, water temperature and salinity are provided by the AREM flow and wave models. The AREM BGC model uses the same horizontal grid as the flow model. In the vertical direction, the original 20 layers are aggregated to 5 layers of equal thickness. This approach enhances model performance, while maintaining a proper representation of shear dispersion (mixing in the direction of flow caused by vertical velocity gradients). We note that the vertical mixing in the study area is so intense that significant stratification is not observed in the AREM flow model. As a consequence, vertical resolution can safely be reduced in AREM BGC model.

The AREM BGC model is based on the Generic Ecological Model for estuaries and coastal waters by Blauw et al. (2008). The substances and processes included in the model are schematically shown in Figure 4.13. The AREM substances are listed in Table 4.3. We note that the substances related to particulate organic matter represent both organic matter from coastal discharges and detritus formed after phytoplankton mortality. They are represented by a rapidly and a slowly decaying fraction. All sediment associated substances, including epiphytes, are not subject to transport (i.e. they are fixed on the grid) and they are restricted to the lowest grid layer.

Coloured Dissolved Organic Matter (CDOM) is expected to be a relevant contributor to light attenuation in the Adelaide coastal waters. The most obvious way to quantify CDOM in relation to its light attenuation properties is to measure light absorption at one particular wavelength in the UV part of the spectrum (UV-absorption or UV-abs). The scientific literature commonly assumes an exponential relation of UV-abs with wavelength (Coble, 2007). This allows the linking of UV-abs to an overall light attenuation in the photosynthetically active part of the spectrum (PAR, 400-700 nm wavelength range) (Lee et al., 2005). CDOM is part of the pool of dissolved organic carbon (DOC). This parameter however, represents a diverse range of compounds with different light absorption properties, and it may therefore not show a marked relation with the light attenuation properties of local waters. For this reason, we chose to let UV-absorption directly represent DOC, as the former is measured in the various coastal discharges.

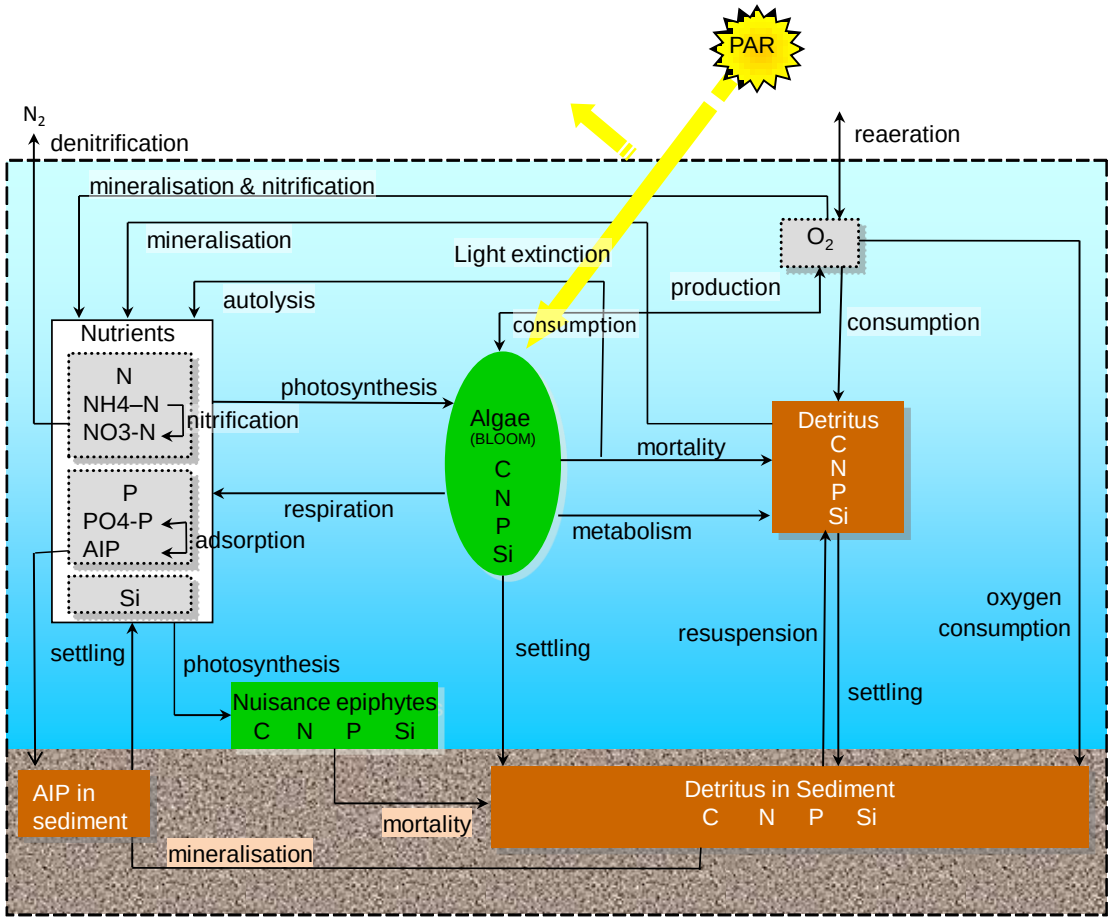

Figure 4.13 Schematic overview of all state variables and processes in AREM (modified from Blauw et al,. 2008).

Table 4.3 List of substances in the sediment and BGC model.

Full name	**Name in the model**
Dissolved oxygen (DO)	OXY
Two fractions of particulate organic matter (C, N, P, Si)	POC1, POC2, PON1, PON2, POP1, POP2, Opal (1 = fast decaying, 2 = slowly decaying)
Dissolved organic matter	DOC, DON, DOP
Three fractions of particulate inorganic matter	IM1, IM2, IM3 (slow-medium-rapid settling)
Dissolved inorganic matter / Particulate inorganic P	NH4, NO3, PO4, Si / PIP
Pelagic phytoplankton	2 functional groups (marine diatoms, marine flagellates), each represented by 3 phenotypes (6 components)
Epiphytes	1 functional group, represented by 3 phenotypes (3 components)
Two fractions of particulate organic matter in sediment (C, N, P, Si)	POC1S1, POC2S1, PON1S1, PON2S1, POP1S1, POP2S1, OpalS1 (1 = fast decaying, 2 = slowly decaying)
Particulate inorganic P in sediment	PIPS1

Each of the phytoplankton functional groups, in this case marine diatoms, marine flagellates and epiphytes, are represented by 3 substances representing 3 phenotypes of algae, see below. The epiphytes are modelled in the same generic way as phytoplankton, but are different in that they are fixed in space horizontally, and vertically in the deepest water layer, and have different properties. They experience nutrient concentrations and light availability at the lower part of the water column. Depending on the type of application, the potential shading effect of epiphytes on seagrass can be simulated either in a limited area where there is seagrass (model validation), or without limitation over the whole model domain (habitat suitability assessment scenario).

The physical and biogeochemical processes formulations as shown in Figure 4.13 are provided by Blauw et al. (2008). The phytoplankton and epiphytes sub-model, called BLOOM, simulates primary production, respiration and mortality of phytoplankton. Within each functional group represented in the model, three phenotypes are defined to account for adaptation to changing environmental conditions:

1. an energy type, with relatively high growth rate, low mortality rate and high N/C and P/C ratio, higher settling velocity and higher chlorophyll content;
2. a nitrogen type, with typically lower internal N/C ratio, lower maximum growth rate, higher mortality rate, lower settling velocity and lower chlorophyll-a content;
3. a phosphorus type, similar to the nitrogen type with typically lower internal P/C ratio.

When conditions in the water change, one phenotype can be instantaneously converted into another phenotype of the same functional group. This represents the rapid adaptation of individual algal cells. Further details can be obtained from Los (2009). The water quality model uses process representations selected from the Delft3D-WAQ process library. Appendix B provides an overview of all formulations and parameters that deviate from the published version of the model by Blauw, et al. (2008). A full account is available in the Delft3D-WAQ documentation (Deltares, 2014).

Especially relevant is the representation of the downward attenuation of light. It is expressed by a linear function of relevant water quality variables:

$$k_d = k_b + \sum_{i=1}^{3} e_{IMi}\, IMi + \sum_{i=1}^{N} e_{Phyti}\, Phyti + \sum_{i=1}^{2} e_{POCi}\, POCi + e_{CDOM} CDOM$$

where k_d is the total downward light attenuation (m^{-1}), k_b is a background value (m^{-1}), *IMi* are the simulated concentrations of inorganic suspended matter (g m^{-3}), *Phyti* are the simulated concentrations of pelagic algae phenotypes (gC m^{-3}), N is the number of simulated pelagic algae phenotypes, *POCi* are concentrations of particulate organic non-algal carbon (gC m^{-3}) and *CDOM* is the simulated concentration of CDOM (cm^{-1} absorption at 254 nm). The parameters *e* are specific downward attenuation parameters expressed as m^{-1}(g m^{-3})$^{-1}$ or equivalent units. These specific downward attenuation parameters have been attributed site specific values based on a dedicated survey, see Chapter 3.

The boundary conditions have been applied at the open-sea boundaries of the overall model and were derived from measurements performed at the NRSKAI buoy in 2011, operated by the Integrated Marine Observing System website node for South Australia (SAIMOS; http://imos.org.au/saimos.html). By analysing the various data sets used for model evaluation (see section 4.2.12), we found that a variable background concentration of dissolved organic nitrogen needed to be added to the boundary condition (0.09-0.13 mgN/L) as well as a

background UV-absorption of 0.015 cm^{-1}. The background concentration for DON turned out to be different in the two datasets used for model evaluation. Neither DON nor UV-abs is included in the SAIMOS data, and it is not possible to determine whether these backgrounds are stemming from the open ocean or from sources and processes within Gulf St Vincent. Furthermore, a background concentration of inorganic suspended matter of 0.7 mg/L needed to be applied, most probably due to sources and processes within Gulf St Vincent.

4.2.10 Sources of particles, nutrients and CDOM

The AREM-BGC is forced by land-based sources of particles, nutrients and CDOM, as discussed in Chapter 2. Using the CDOM inputs to the Adelaide coast, the concentrations simulated by AREM in coastal waters were approximately 1 order of magnitude lower than measured values, and the predicted gradient between inshore and offshore waters about 3 times smaller than measured. In order to better parameterise the dynamics of CDOM along the coast, we investigated the release of CDOM reported in the literature from other potential sources, i.e. resuspended sediments, seagrass meadows and mangroves.

The literature on the release of DOC from coastal sediments and plant litter is extensive, but published data on the specific emission factors (EFs) for CDOM are much more limited. We were unable to find EFs for resuspended sediments, having to rely on estimates for DOC release (Komada and Reimers, 2001; Kieber et al., 2006; Shank et al., 2011). CDOM release from seagrasses has only been investigated in one study (Stabenau et al., 2004), while the literature for mangroves is currently restricted to two papers (Shank et al. 2010a; Shank et al., 2010b).

For the estimation of CDOM release from sediments, we compiled local papers that report on the content of both OC and <63 μm (resuspendable) sediments (Jenkins, 2005; Fernandes et al., 2006; Bone et al., 2006; Fernandes et al., 2010). We then assumed that all OC was contained in the fine fraction, and calculated an average OC in resuspendable sediments of 5% (range 2-15%). The release of DOC from these sediments was estimated at 15% (range 3-33%) of the total OC pool adsorbed to particles (Kieber et al., 2006; Shank et al., 2011). The amount of DOC desorbed was further converted to UV-abs by using the ratio between UV-abs and DOC for Adelaide's coastal waters. This ratio was on average 6 in the coastal monitoring data collected off Bolivar and Grange to calibrate AREM (Chapter 3), varying between 3.5 in summer and 10 in winter at shallow sites (≤ 5 m) where resuspension is likely to occur. The average value calculated for CDOM release from resuspended sediments using these average estimates was 0.00045 cm^{-1} g DW m^{-3}.

The release of CDOM from seagrass detritus was estimated from a CDOM production of 0.08 m^{-1} L g^{-1} h^{-1} at 254 nm during detritus breakdown as recorded for the seagrass *Thalassia testudinum* (Stabenau et al., 2004). Estimates for the detritus pool in seagrass meadows in Adelaide's coastal waters are lacking, but various sources report that the detritus pool in seagrass meadows is of the same order or larger than the above-ground biomass (B) (Mateo and Romero, 1997; Paling and McComb, 2000; Romero et al., 1992). Using an average above-ground biomass (B) of 100 g DW m^{-2} for seagrass meadows in Adelaide's coastal waters (Bryars et al., 2006) and assuming that the detritus pool is the same, a conservative CDOM EF for seagrasses was estimated as 0.0019 cm^{-1} m^3 m^{-2} d^{-1}.

CDOM release from mangrove litter was estimated from a CDOM production of 1 m^{-1} L g^{-1} h^{-1} at 254 nm based on an average for yellow, orange and brown leaves of Rhizophora mangle (Shank et al., 2010b). Using a standing stock of leaf litter of 9.75 g DW m^{-2} for Adelaide's

mangroves (Imgraben and Dittmann, 2008), the CDOM EF for mangroves was calculated as 0.0023 cm^{-1} m^3 m^{-2} d^{-1}.

A numerical experiment using AREM was carried out to calculate the resulting concentrations of UV-abs as a result of each of the sources above. The sediment source was made variable in space and in time, in agreement with the simulated resuspension flux. The seagrass source was introduced according to the NatureMaps habitat map (EnvirodataSA, 2015), where the source was set to 100% of the theoretical value in cells covered with Dense Continuous seagrass, to 50% in cells covered with Continuous Medium or Patchy Dense seagrass and to 17% in cells covered with Continuous Sparse or Patchy Medium seagrass. The mangrove source was introduced according to the NatureMaps habitat map in all cells where mangroves are present. UV-abs was modelled as a conservative tracer, and mean annual concentrations have been calculated in every cell of the model domain. The results were evaluated at 3 stations along transects off Bolivar and off Grange, and compared to observed data. We used the Solver function in Excel in order to optimize EF factors, and calculate the contribution from a gulf-wide marine background, by maximising the coefficient of determination between measured and simulated UV-abs (max r^2), while constraining the slope to values ≤1. This exercise produced optimised EFs for mangrove (0.0015 cm^{-1} m^3 m^{-2} d^{-1}), seagrass (0.0013 cm^{-1} m^3 m^{-2} d^{-1}) and sediment (0.0003 cm^{-1} g DW m^{-3}), with a background value of 0.015 cm^{-1}. The correlation between measured and calculated UV-abs using these optimised values had a slope of 1 and r^2 of 0.91.

Considering the average CDOM production rates reported in the literature, these EFs would correspond to 10% of the OC pool in sediments being desorbed during resuspension, and a detritus biomass of 6 g DW m^{-2} for mangroves and 68 g DW m^{-2} for seagrasses. The fraction of OC desorbed during resuspension has been reported to vary between 3 and 33% (Kieber et al., 2006; Shank et al., 2011). The standing stock of 9.75 g DW m^{-2} of leaf litter reported for Adelaide's mangrove systems was measured during the dry summer months when leaf fall peaks (Imgraben and Dittmann, 2008) and therefore is likely to be lower as an average throughout the year. For seagrasses, above-ground biomass can vary between 10 g DW m^{-2} in local degraded systems up to 250 g DW m^{-2} in dense meadows (Bryars et al., 2006). The calculated background value of 0.015 cm^{-1} also matches the lowest UV-abs measured at the offshore stations B12 and G15 (Chapter 3).

4.2.11 Epiphytes

Seagrasses in South Australian waters always have a certain degree of epiphyte growth on their above-ground plant parts. Under normal nutrient-poor conditions, most epiphytes are found on the distal parts of older seagrass leaves (photosynthetically not so active) and on the stems of some seagrass species (e.g. *Amphibolis*), while the younger leaves and lower (fresher) parts of the leaves tend to be free from epiphyte growth (Trautman and Borowitzka, 1999; Borowitzka et al., 2006). The epiphyte community under such conditions is made up primarily of calcareous, encrusting (red) algae. These have characteristics of 'K-selected' organisms, such as slow growth, great structural strength and a high degree of resistance to herbivory. The growth of these 'healthy' (mostly calcareous) epiphytes does not appear to hamper seagrass growth or cause mortality in the seagrasses (see Fong and Harwell, 1994). In contrast, when nutrient loading is significantly increased (eutrophication), there is a gradual shift in species composition of the epiphyte community (Cambridge et al., 2007). Fast-growing filamentous algae (including brown, red and green algae) take over, covering nearly all the surfaces of all above-ground seagrass plant parts, including the young and fresh (photosynthetically active) parts of the seagrass leaves. These filamentous algae are opportunistic and show characteristics of 'r-selected' organisms, such as rapid nutrient uptake

and high growth rates that confer an advantage during periods/events of higher (pulsed) nutrient availability, as well as low structural development and high vulnerability to herbivory (Littler and Littler, 1980). When nutrient availability is increased significantly, the rapid growth and biomass of these “nuisance” epiphytes can result in severe attenuation of light reaching the seagrasses, and may cause mortality of the seagrass plants if sustained.

The AREM focuses on the growth of the “nuisance” epiphytes. We consciously ignore the “healthy”, calcareous epiphytes, in the understanding that these do not hamper seagrass growth. A comparable approach was followed with success by Fong and Harwell (1994) in their modelling study of seagrass communities in tropical and subtropical bays and estuaries in Florida. Any effect of “healthy” epiphytes on the amount of light reaching the seagrass leaves is considered to be implicitly included in the habitat suitability thresholds for light availability. In view of the dependency of “nuisance” epiphytes on external nutrient supply, we included them in the biogeochemical model as phytoplankton attached to seagrass, which competes with pelagic algae for nutrients. The parameter settings for representing “nuisance” epiphytes have been tuned to reflect the main algal species that constitute these “nuisance” epiphytes on seagrasses in South Australian and West Australian waters. These include filamentous brown and red algae, as well as some filamentous green algae. This was based on a literature review. More details are provided in Appendix E. In particular, the nutrient requirements and the mortality rate were found to be lower than common values for pelagic algae.

4.2.12 Model validation

The model validation targets the capability of the model to predict the impact of coastal discharges on the light reaching the seagrass leaves. Key elements are the validation of the simulated concentrations of water quality variables affecting underwater light, the evaluation of the simulated nuisance epiphytes loads, and the validation of key physical parameters such as currents and water levels. Relevant data sets are available from various sources, see Table 4.4, Figure 4.14 and Figure D.6.

Table 4.4 Overview of relevant data for model validation

Description (source)	Period / frequency	Location(s)	Variables
seagrass cover map (DEWNR)	2013	area with depth < 20m, north of Pt Gawler to Hallet Cove	1x1 m grid of seagrass presence
coastal water quality data (EPA)	up to and including 2008, monthly samples	9 coastal stations, 8 stations in Port River and Barker Inlet	total N and N species, total P, dissolved oxygen, chlorophyll-a
marine water quality data (EPA)	second half of 2009 – first half of 2011, four surveys	28 stations in coastal waters	total N and N species, total P and filterable reactive P, chlorophyll-a, suspended solids
marine water quality data (SA Water)	Nov 2014 – Sep 2015, biweekly to monthly	2 transects of 3 stations, off Bolivar and off Grange	total N and N species, total P and filterable reactive P, chlorophyll-a, suspended solids and particle size distribution, downward light attenuation, UV-absorption
Gulf wide data (SA Water)	April-September 2015, continuous, every 15 minutes	6 stations, near surface and near bottom	temperature and salinity
marine habitat monitoring (EPA)	2009-2011, up to 5 surveys	28 stations in coastal waters	epiphytes index (1-5) in 2009 (1 survey); epiphyte cover (%) in 2010-2011 (up to 4 surveys)
light data (ACWS, SARDI)	March 2005-February 2006, continuous	transect off Grange	monthly statistics of downward light attenuation
suspended solids (ACWS)	1997 to 2004 remote sensing	11 stations off-shore, 1 station in central Gulf	summary statistics of suspended solids
ADCP Pt Stanvac (SA Water)	2011, reliable continuous data for about 6 months	Pt Stanvac	current
water level data (BoM)	2011 continuous	Outer Harbour, Port Giles	water levels
Salinity and temperature data (SA Water)	2011, monthly data	3 reference stations off Pt Stanvac	salinity, temperature

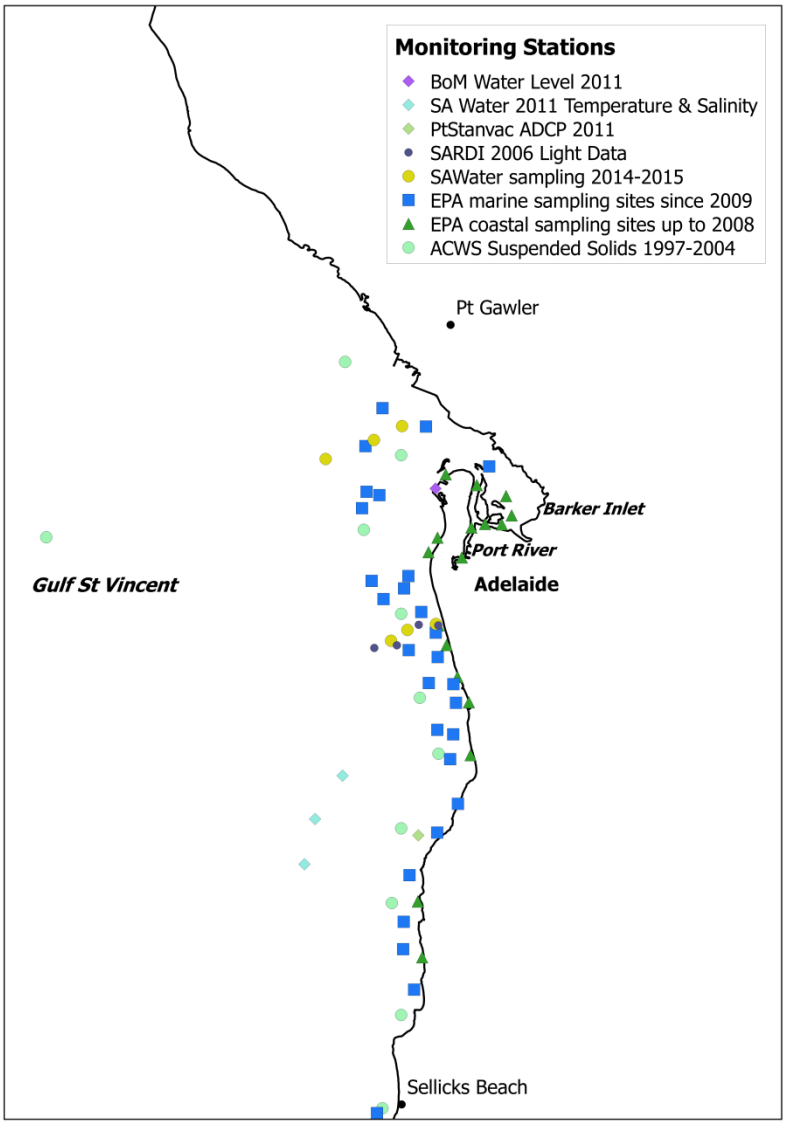

Figure 4.14 Sampling locations of various data sets relevant for model validation

The available data cover different periods and different locations. This presents a sub-optimal situation: there is no complete data set that allows the evaluation of all aspects of model performance at all relevant locations in one consistent effort. We chose to validate the model based on a simulation for one selected year. The simulation results are compared to datasets from different years. Differences between these years are subsequently accounted for by discussion and interpretation. The alternative approach of carrying out a long, multi-year simulation in order to compare simulation results from the correct year with the individual data sets, would have been extremely time consuming and would not have solved the basic issue. All validation runs have been carried out for 2011. At the start of the development of AREM in 2013, this year was selected as the simulation period representative for normal conditions. It represents the most recent year with complete forcing data, and is considered to be a more or less average year following a period of drought in the study area that lasted until 2010.

4.2.12.1 *BGC and sediment model validation*

While selecting data sets for model validation, we looked for data sets:

- providing relevant variables that can be compared to model output,
- covering relevant spatial gradients,
- with sufficient temporal resolution to avoid a too strong dependency on the results from individual data points.

The EPA coastal data satisfy these criteria. These data have been considered from 2005-2008. During these years, the WWTP discharges of total nitrogen deviated less than 10% from the 2011 discharges (Zijl et al., 2014). The 2005-2008 data are therefore considered relevant for 2011. In terms of rainfall (BoM data from Adelaide Airport), the total precipitation in 2011 of 444 mm exceeds the mean annual precipitation in 2005-2008 of 347 mm. However, the largest part of that difference is connected to higher than usual precipitation in the autumn months February and March. Due to the general dryness of soils in this period, the 2011 autumn rains lead to relatively small runoff and probably did not cause large differences between runoff volumes in 2005-2008 and 2011.

The EPA marine data have been considered for 2009-2011, a period with similar loads and similar precipitation as the simulation year 2011. These data concern a series of stations off-shore. This dataset contains 4 surveys in 2009-2011, with each survey spread out over a period of weeks or months (the 2009 survey for instance, spans a period of 83 days). We found that the spatial patterns emerging from this dataset were hard to understand. This is probably an artefact caused by the low number of samples and the survey duration. For example, the first survey in 2010 resulted in very high concentrations of suspended solids (> 20 mg/L) at a sequence of stations between Semaphore and Grange. These samples were taken on 10 March 2010, probably on a windy day. All other samples from the first survey in 2010 were from other dates and showed much lower concentrations. This caused an unrealistic spatial pattern. For this reason we decided not to use this dataset for model validation.

The SA Water data from 2014-2015 are not fully comparable to 2011 because the Penrice discharge was stopped in 2013 (see Chapter 2). This means that the load of suspended solids and nitrogen from Port River was substantially smaller in 2014-2015 than it was in 2011. Also, the year 2015 was a relatively dry year. Despite these drawbacks, this dataset is indispensable, because of its wide range of parameters, its high frequency and its relevant spatial gradients. As shown in Figure 4.14, it spans the gradients between inshore waters covered by the EPA coastal data and the offshore waters covered by EPA marine data. As such it partly compensates for not using the EPA marine data.

In addition, we make use of the 2005-2006 ACWS light data provided by SARDI (Collings et al., 2006) since this dataset provides field values of downward light attenuation, and 1997-2004 ACWS offshore suspended solids data (Petrusevics, 2005) since this dataset provides a valuable spatial gradient at some distance from shore. Both datasets are older, but they reflect phenomena strongly affected by wave-induced resuspension. It is unlikely that this has changed significantly over the past period, and therefore we consider these datasets useful also for the present period.

The 2005-2008 EPA coastal data do not show distinct seasonal patterns that can be used to evaluate the performance of the model (validation). We therefore carried out a validation using annually mean concentrations and their spatial gradients. We used the target diagrams method (Los and Blaas, 2010 and references therein). We evaluate the bias $B = \overline{M} - \overline{D}$ of the station averages, where M denotes a modelled annual mean value at one station and D denotes the average of all observations at one station and the overbar denotes an average

over all stations. This bias is normalised with the standard deviation of observed station means σ_D to obtain $B^* = B / \sigma_D$. Next, the unbiased root-mean square error is calculated as $RMSD' = \left[\overline{(M' - D')^2}\right]^{1/2}$, where the prime denotes the difference between the station mean and the mean of all stations, e.g. $M' = M - \bar{M}$. This quantity is attributed a sign and again normalised with the standard deviation of observed station means to obtain $RMSD'^* = sign(\sigma_M - \sigma_D)\, RMSD' / \sigma_D$. The value of B^* quantifies the mean error, with values > 0 indicating an overestimation and values < 0 indicating an underestimation. The value of $RMSD'^*$ evaluates the spatial variability, with values > 0 indicating an overestimation and values < 0 indicating an underestimation. For every parameter, a point ($RMSD'^*$, B^*) is plotted in the target diagram. Values within the unit circle $\sqrt{((B^*)^2 + (RMSD'^*)^2)} < 1$ are considered to represent an adequate model performance, and therefore the area within this circle represents the target for the goodness of fit. This same method is also used to evaluate the goodness of fit between the model results and the 2014-2015 SA Water dataset.

4.2.12.2 *Epiphytes data*

Table 4.5 shows an overview of data collected from the literature about observed epiphyte biomasses, expressed in mass per area units. All references relate to South Australia, though not all of them to the Adelaide waters. One reference reports values under influence of fertiliser treatment. Such data still serve to show a realistic range of epiphyte biomass values under conditions of higher nutrient availability. The values collected in Table 4.5 allow direct comparison with the modelled epiphyte cover expressed in gC m^{-2}. Assuming a carbon to dry weight ratio of 0.36 (see Section 5.2.4), this translates to values of 0.18 to 166 gC m^{-2}.

Table 4.5 Observed epiphytes biomass on relevant seagrass species

seagrass species	epiphyte biomass	region	reference
Posidonia spp.	19 - 44 g DW m^{-2} (1)	Spencer Gulf, SA (4 sites)	Keuskamp, 2004
Amphibolis sp.	20 - 460 g DW m^{-2}	Gulf St Vincent, SA	Bryars et al., 2009 (2)
Amphibolis sp.	84 - 440 g DW m^{-2}	Gulf St Vincent, SA	Bryars et al., 2011 (3)
Posidonia sp.	45 - 168 g DW m^{-2}	Gulf St Vincent, SA	Bryars et al., 2011 (3)
Posidonia spp.	24 - 90 g DW m^{-2}	Gulf St Vincent, SA	Neverauskas, 1987
Posidonia sp.	43 - 65 g DW m^{-2}	Gulf St Vincent, SA	Lill, 2005
Amphibolis sp.	105 - 144 g DW m^{-2}	Gulf St Vincent, SA	Lill, 2005
various sp.	up to 200 g DW m^{-2} (1)	Gulf St Vincent, SA	EWS, 1975; 1985

(1) Converted from wet weight, assuming 10% dry weight.
(2) High values refer to the Western part of the Gulf of St Vincent.
(3) High values refer to a situation with fertiliser treatment.

EPA (1998) examined epiphyte growth on artificial substrates placed at a range of locations along the Adelaide coast and one reference site at Port Hughes, during two experiments in April and October 1996. This was intended as a comparative assessment of potential epiphyte loads on seagrass leaves. The highest loads (expressed along a relative scale only) were encountered in the Port River / Barker Inlet area, with smaller but still markedly elevated loads near Glenelg, Henley and to a lesser extent near Largs Bay. Elsewhere the loads were slightly elevated as compared to the reference site.

4.2.12.3 *Hydrodynamics model validation*

SA Water deployed a bottom-mounted Teledyne Workhorse Sentinel ADCP in 15 m deep water in the direct vicinity of the Port Stanvac desalination plant outfall to measure current

direction and velocity with a 10 minute interval during most of 2011. The ADCP readings have been converted to depth averaged velocity components from west to east (U) and from south to north (V). Periods with reliable data are 13 January – 1 April, 6 April – 11 May, 21 July – 13 September and 15 September – 13 October. For these periods, simulated currents are compared to observed currents at the location of the ADCP. A direct comparison of the simulated and observed velocities would mostly show tide-induced fluctuation. Such a comparison however only provides limited insight in the transport of substances. A more meaningful comparison is obtained after filtering out the tide-induced fluctuation, which leaves the residual current. The tide has a mixed diurnal / semi-diurnal character, but the largest component is K1. This constituent has a period of 23.934 hours, so we used an averaging period of 24 hours. Consequently, both the observed and simulated currents were converted by applying a 24-hours moving average filter.

The validation of predicted water levels was carried out using data from BoM for the stations of Outer Harbour and Port Giles (Figure 4.2). The root mean square error (RMSE) of the water level signal is determined for the entire year of 2011. The error is separately assessed for the tidal and for the non-tidal (surge) parts. In addition, the amplitude and phase errors of the tidal components are quantified. The salinity and temperature are validated using three stations off Port Stanvac with monthly data in 2011. Continuous readings of temperature and salinity in the winter of 2015 at 6 stations around Gulf St Vincent are used to evaluate gradients at the scale of the Gulf St Vincent as simulated by the overall model.

In addition to the above quantitative assessments, we also evaluate the coupled flow-wave model by the model's representation of the characteristic gyre in front of the Port River outlet and the impact of waves on residual currents.

4.3 Results

4.3.1 BGC model validation

The degree of agreement between the simulation results and the various datasets discussed above is presented here. Table 4.6 provides the mean and standard deviation of the EPA coastal data for 2005-2008 and the simulated 2011 annually-averaged concentrations. It also shows the normalized bias (B*) and signed, normalized, unbiased root-mean square difference (RMSD'*) of the model results with respect to the observations. Figure 4.15 shows the associated target diagram, a graphical representation of B* against RMSD'*. For illustrative purposes, Figure 4.16 shows the simulated and observed annual means at individual stations for the parameter total N.

Table 4.6 Skill assessment results: AREM 2011 results vs EPA coastal data 2005-2008, evaluated on spatial gradients for various water quality parameters.

Parameter	EPA Data (2005-2008)		Model (2011)		Goodness of Fit	
	Mean	SD	Mean	SD	B*	RMSD'*
Total N	0.37	0.24	0.34	0.15	-0.13	-0.51
Ammonia	0.10	0.13	0.04	0.08	-0.44	-0.56
Oxidised N	0.06	0.06	0.02	0.05	-0.51	-0.54
Kjeldahl N	0.31	0.17	0.32	0.10	0.05	-0.52
Total P	0.037	0.010	0.029	0.013	-0.74	0.89
Dissolved Oxygen	7.43	0.27	7.80	0.29	1.36	1.21
Chlorophyll-a	3.80	3.75	3.11	2.06	-0.18	-0.78

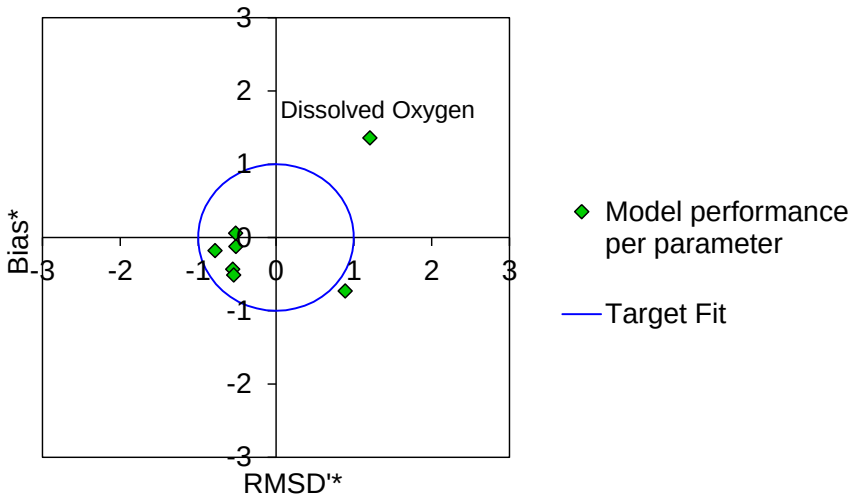

Figure 4.15 Assessment of model performance: AREM 2011 results vs EPA coastal data 2005-2008, evaluated on spatial gradients for various parameters. Dots represent goodness of fit for individual parameters. The area within the circle represents target model performance.

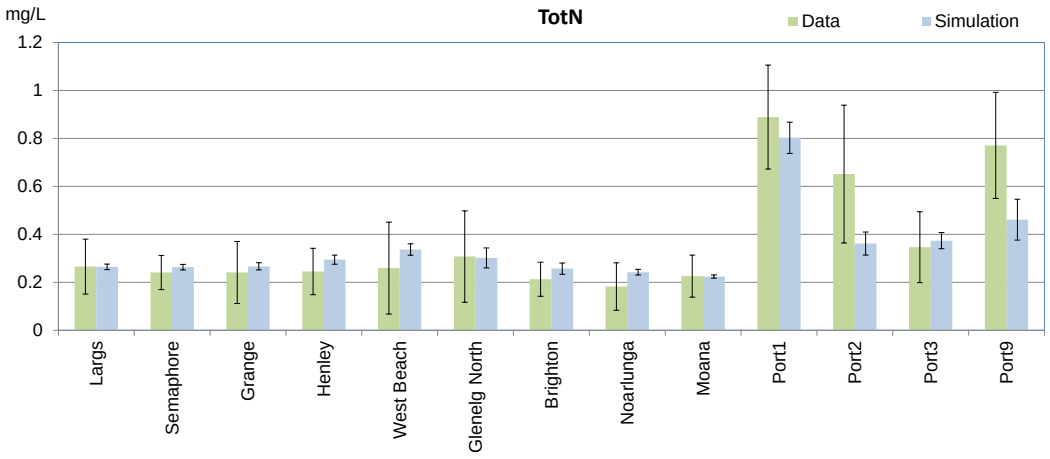

Figure 4.16 Annually averaged observed concentrations of total N derived from EPA coastal stations in 2005-2008, plotted against annually averaged simulated concentrations of total N at the same stations. Error bars represent the standard deviation obtained from the 12 monthly means.

The comparison to 2005-2008 EPA coastal data shows that the model performance is within target for most of the parameters assessed (total N, ammonia, oxidised N, Kjeldahl N, Chlorophyll-a) except total P and dissolved oxygen. The former is only slightly out of the target and this is caused by the simulated P that is too low at stations Port1-2-3-9. Since these stations are outside the prime area of interest, we consider this performance acceptable. The off target model performance for dissolved oxygen is obviously not caused by organic loads being too low (Chapter 2) or phytoplankton production being too high (good fit for chlorophyll-a). Since dissolved oxygen neither plays a role in the habitat model (Chapter 5) nor is a reason for concern otherwise, we did not pay further attention to the dissolved oxygen results.

Table 4.7 provides the mean and standard deviation of the SA Water marine data for 2014-2015 and the simulated 2011 annually averaged concentrations. It also shows the normalized bias (B*) and signed, normalized, unbiased root-mean square difference (RMSD'*) of the

model results with respect to the observations. Figure 4.17 shows the associated target diagram, a graphical representation of B* against RMSD'*. For illustrative purposes, Figure 4.18 shows the simulated and observed annual means at individual stations for the parameter total N.

Table 4.7 Skill assessment results: AREM 2011 results vs SA Water marine data 2014-2015, evaluated on spatial gradients for various water quality parameters.

Parameter	SA Water Data (2014-2015)		Model (2011)		Goodness of Fit	
	Mean	SD	Mean	SD	B*	RMSD'*
Total N	0.19	0.02	0.22	0.05	1.55	1.97
Total ammonia	0.01	0.00	0.01	0.00	-0.85	0.79
Oxidised N	0.003	0.001	0.000	0.000	-2.72	-0.83
Total P	0.02	0.02	0.02	0.01	-0.03	-0.62
Filterable Reactive P	0.006	0.003	0.006	0.004	0.00	0.47
CDOM	0.0203	0.0038	0.0203	0.0039	0.00	0.29
SS <63 µm	4.47	1.79	4.61	4.42	0.47	1.40
Chlorophyll-a	0.68	0.36	1.04	1.24	1.01	2.73
K_d	0.35	0.14	0.37	0.20	0.13	0.40

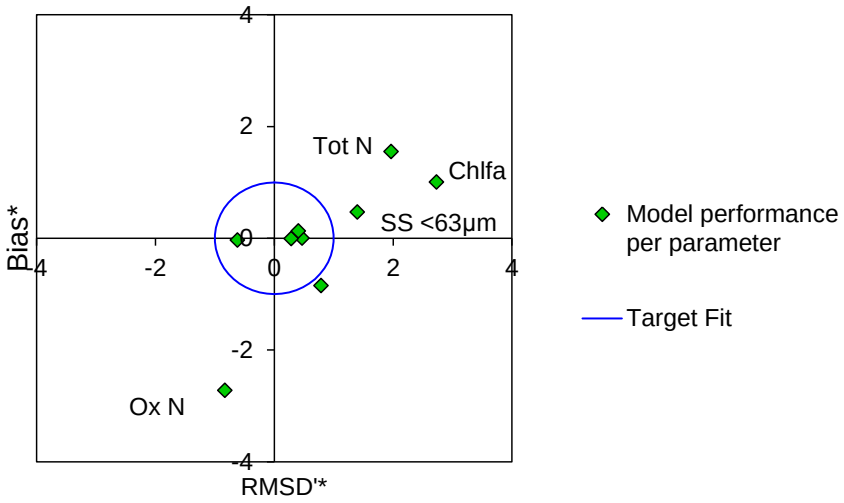

Figure 4.17 Assessment of model performance: AREM 2011 results vs SA Water marine data 2014-2015, evaluated on spatial gradients for various parameters. Dots represent goodness of fit for individual parameters. The area within the circle represents target model performance.

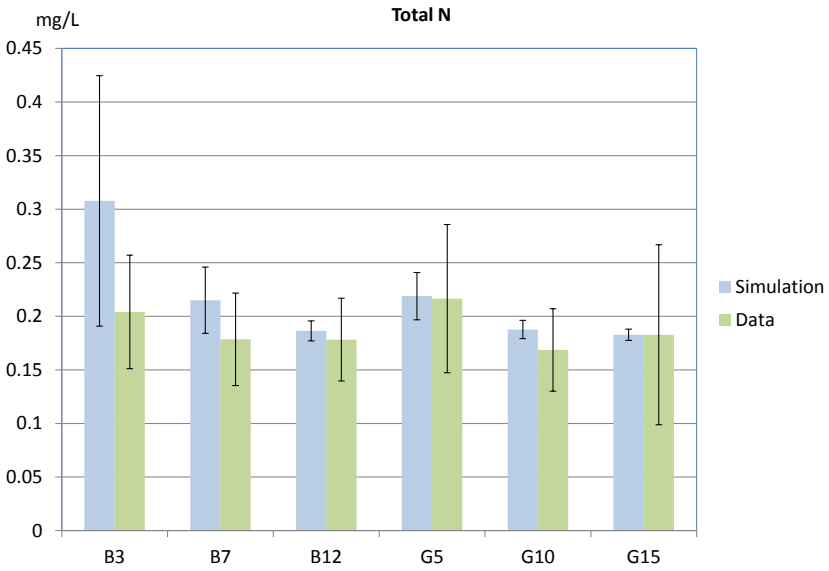

Figure 4.18 Annually averaged observed concentrations of total N derived from SA Water sampling in 2014-2015, plotted against annually averaged simulated concentrations of total N at the same stations.

The comparison to 2014-2015 data from the Bolivar and Grange transects reveals that the model performance is within target or very close to target for ammonia, total P, filterable reactive phosphorus, CDOM and total downward attenuation of PAR. The concentrations of total N and chlorophyll-*a* are overestimated and also their spatial variability is overestimated. This is a consequence of the Penrice discharge which is present in the simulation, but which had stopped when the data were collected. The average concentrations of SS <63 µm are reproduced well, but the gradients are overestimated. This could partly be due to the Penrice discharge, which affects the Bolivar transect, but at the Grange transect it seems that the resuspension intensity might be overestimated. We chose not to change this on the basis of the comparison to the 2005-2006 light data in the same transect (see below). The off target model performance for oxidised N is the result of very small (0.003 mgN/L) measured concentrations, with a small standard deviation, while the simulated concentrations are effectively zero because of the model assumption that all oxidised N is available for uptake by phytoplankton in combination with a strong nitrogen limitation. Because this concerns very small concentrations that do not significantly affect the other parameters, we did not pay further attention to these results.

Figure 4.19 shows the comparison of monthly averages of the measured downward attenuation in 2005-2006 along a transect consisting of 4 stations off Grange (Collings, et al., 2006) and simulated downward attenuation at the same stations in 2011. The presentation format is such that it allows direct comparison. The results show very similar spatial gradients and very similar differences over the year, while evidently the variation over the months is different in both cases because of the difference in meteorological conditions.

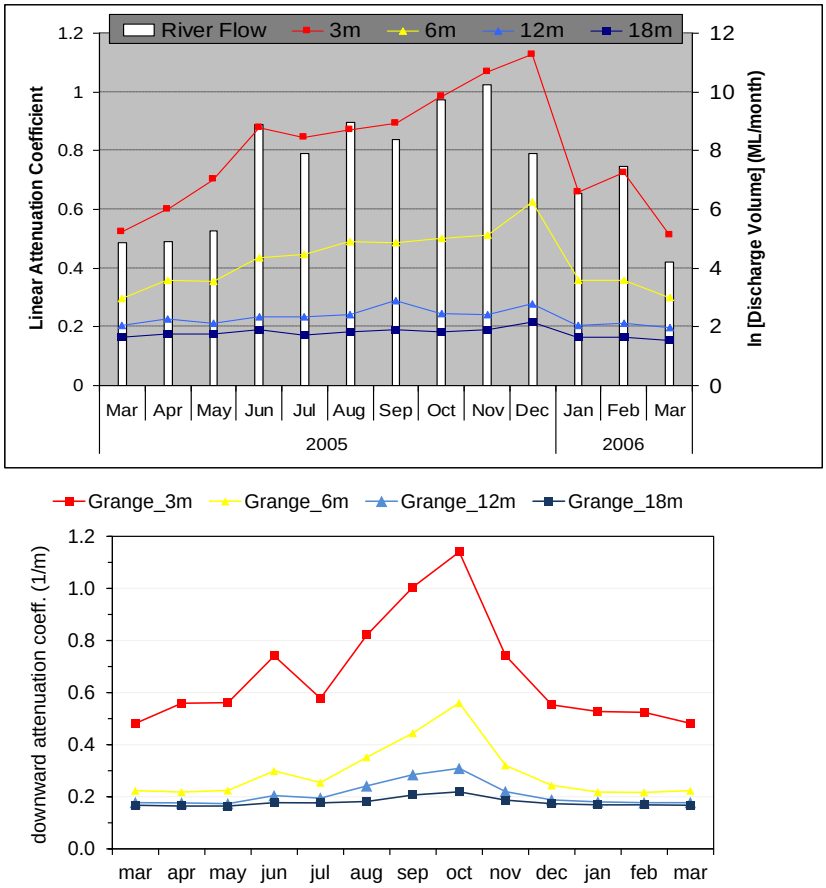

Figure 4.19 Monthly averages of total downward attenuation of PAR, measured in 2005-2006 (top, copied from Collings, et al. 2006) and simulated in 2011, at four stations along a transect of Grange.

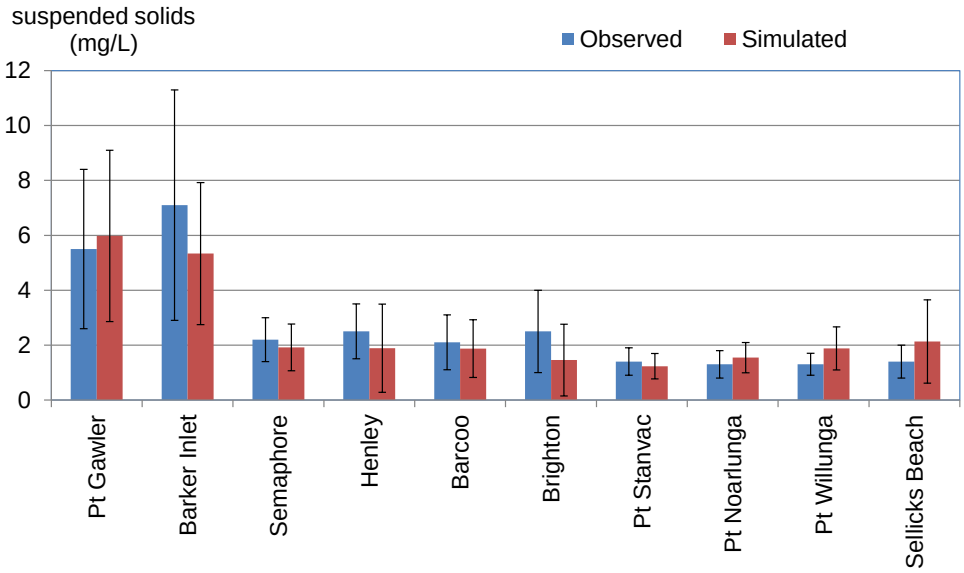

Figure 4.20 Simulated annual averages of suspended solids, simulated at eleven stations corresponding to stations of 1997-2004 ACWS SeaWifs data.

Figure 4.20 shows mean concentrations of suspended solids observed in 1997-2004 at a chain of “ACWS suspended solids” stations off-shore (Petrusevics, 2005) and mean simulated concentrations in 2011 at the same locations. The comparison shows that there is agreement between the mean values and the spatial gradient.

4.3.2 Epiphytes biomass

A contour plot of the simulated potential (i.e. independent of the presence of seagrass substrate) mean nuisance epiphytes biomass (gC m^{-2}) in 2011 is shown in Figure 4.21. The plot shows three spots with high nuisance epiphytes biomass, near the WWTP discharge points, which are the main sources of nitrogen. The biomass at some distance from these sources is low (2-3 gC m^{-2}), while values close to these sources reach values over 50 gC m^{-2}, with a peak exceeding 100 gC m^{-2} under the Bolivar discharge point. The spatial gradients show remarkable resemblance to the spatial gradients observed in epiphyte growth rates on artificial substrates at a sequence of sites along the Adelaide coast in 1996 (EPA 1998).

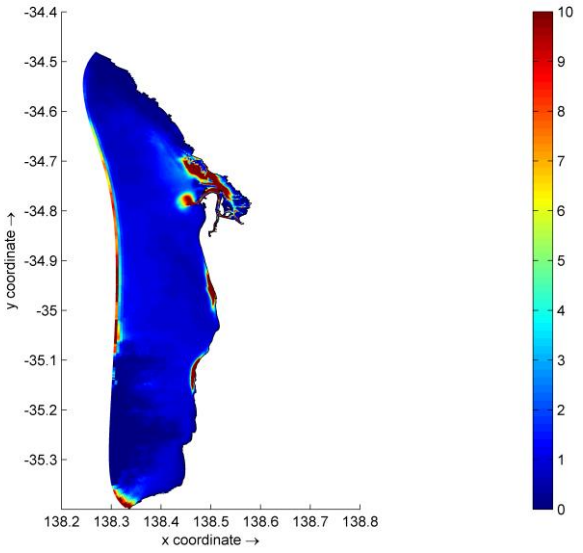

Figure 4.21 Simulated mean nuisance epiphytes biomass (gC m^{-2}) in 2011

The simulated nuisance epiphytes biomass of 2-50 gC m^{-2} is in the same range but somewhat lower than the 7-166 gC m^{-2} of observed total epiphytes biomass (Table 4.5). In view of the fact that the model accounts for only the nuisance epiphytes this is within expectations, and therefore we consider the results from the epiphyte modelling consistent with the sparse available data.

4.3.3 Wave model results

The output of the wave model runs include two-dimensional maps over the entire computational area, showing various wave parameters like significant wave height H_s, spectral wave period $T_{m-1,0}$, mean wave direction, directional spreading and the root mean square value of the maxima of the orbital motion near the bottom (U_{bot}). The wave spectra are provided at a number of selected output locations. As an example, Figure 4.22 shows the simulated significant wave height and mean wave direction fields at 17:00h on 1/4/2011. In the figure, the dissipation of wave energy and wave refraction as waves propagate to the coast can be seen clearly. Figure 4.23 and Figure 4.24 show the wave roses at two nearshore observation locations: Bolivar 12 (138.38264°E and 34.75342°S) and Bolivar 3 (138.45081°E and 34.72404°S). As the figures show, there is quite a lot of wave dissipation

occurring from the deeper (Bolivar 12, at a depth of about 12m) to the shallower location (Bolivar 3, at a depth of about 3m) as well as a further alignment in a direction that is perpendicular to the depth contours.

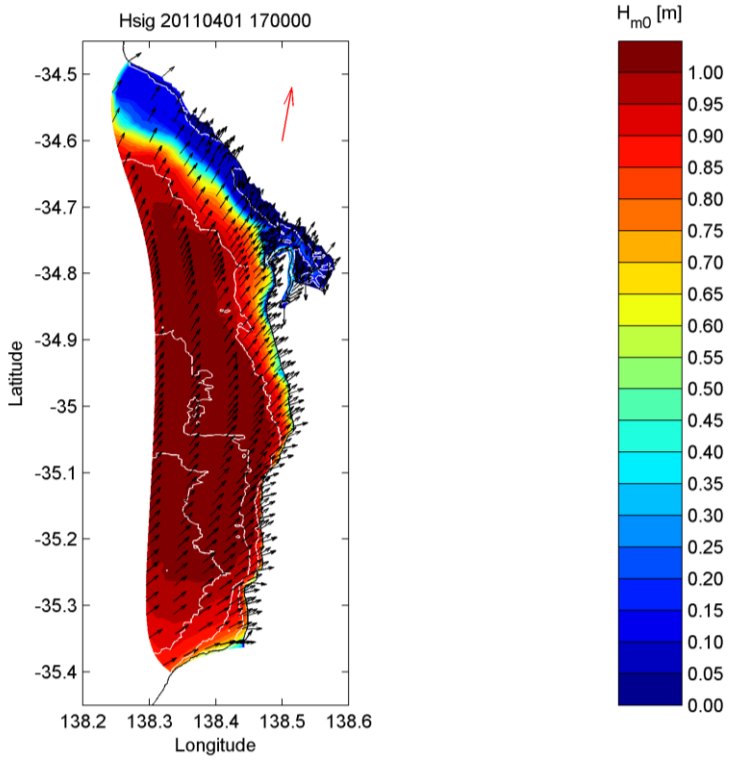

Figure 4.22 Simulated significant wave height (colour) and mean wave direction (arrows) fields at 17:00 1/4/2011.

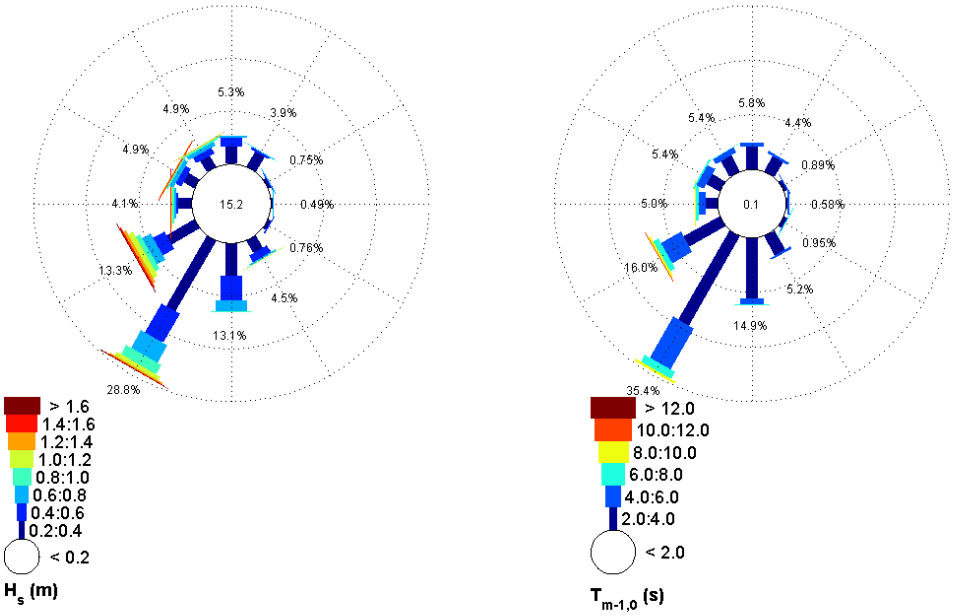

Figure 4.23 Simulated significant wave height (left) and mean wave period (right) roses for 2011 at Bolivar 12 (138.38264°E and 34.75342°S).

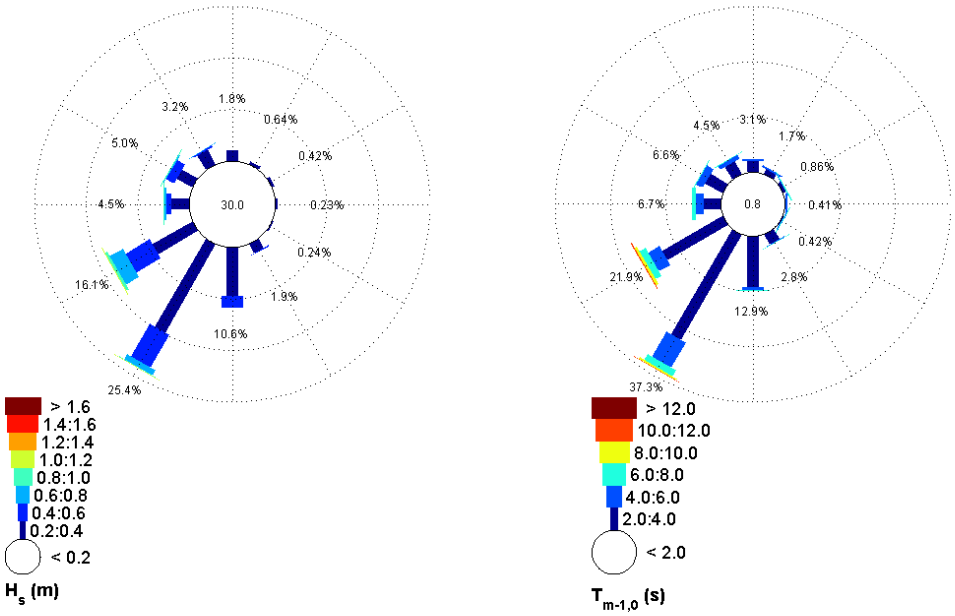

Figure 4.24 Simulated significant wave height (left) and mean wave period (right) roses for 2011 at Bolivar 3 (138.45081°E and 34.72404°S).

4.3.4 Currents

Simulated depth and tidally averaged U and V velocity components for 2011 have been compared to time series of observed depth and tidally averaged U and V velocity components measured by the ADCP. The results are shown in Figure 4.25 to Figure 4.28 for the periods with reliable data. We note that the results show small oscillations, typically of the order of 0.01 m/s, due to the fact that the 24 hours moving average we applied does not properly account for all tidal components with their different periodicities.

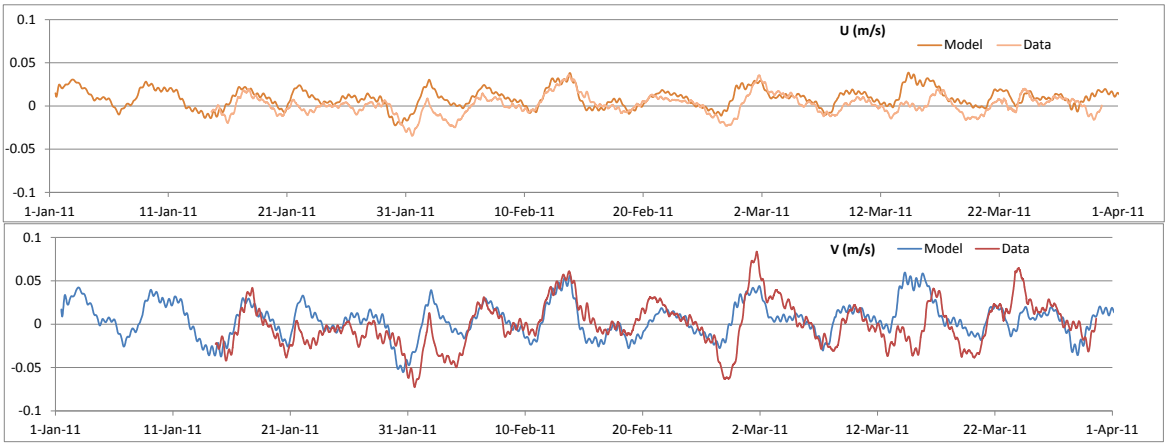

Figure 4.25 Comparison of depth averaged simulated and observed currents after applying 24h moving average filter in west-east (U; top) and south-north (V; bottom) direction; 13 January – 1 April.

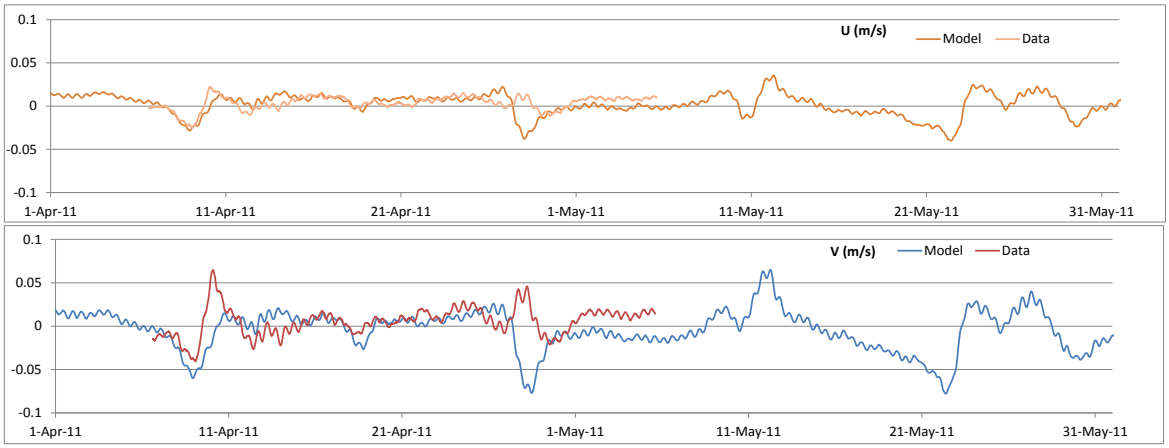

Figure 4.26 Comparison of depth averaged simulated and observed currents after applying 24h moving average filter in west-east (U; top) and south-north (V; bottom) direction; 6 April – 11 May.

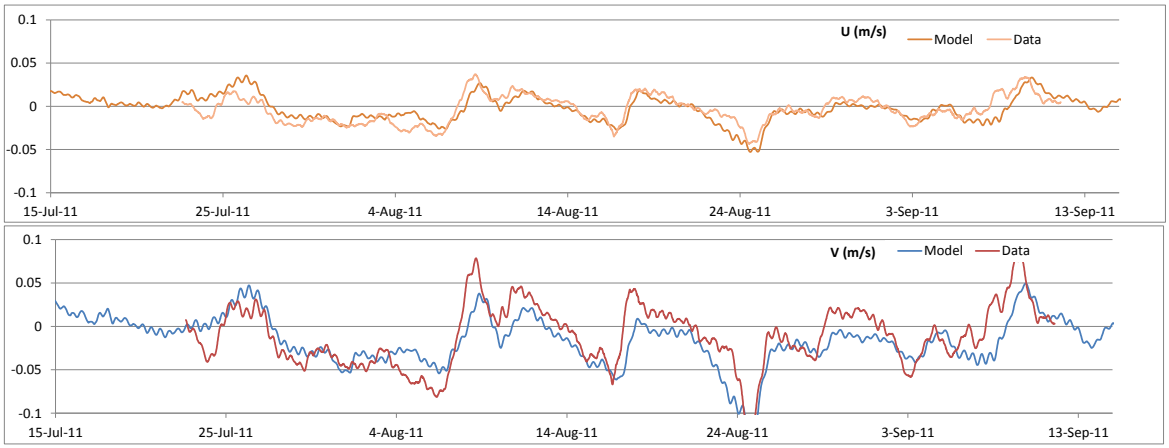

Figure 4.27 Comparison of depth averaged simulated and observed currents after applying 24h moving average filter in west-east (U; top) and south-north (V; bottom) direction; 21 July – 13 September.

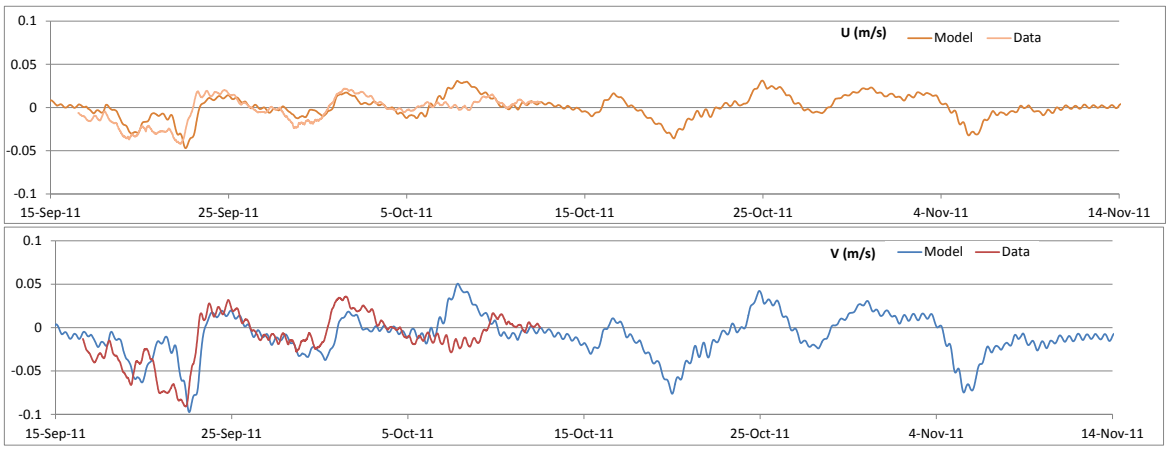

Figure 4.28 Comparison of depth averaged simulated and observed currents after applying 24h moving average filter in west-east (U; top) and south-north (V; bottom) direction; 15 September - 13 October.

The results presented show that there is a good resemblance between the simulated and the observed magnitude and variability of the residual currents. The south-to-north (V) components of the residual currents are larger than the west-to-east (U) components, both in

the model results and in the observations. This is due to the orientation of the local coastline from south-southwest to north-northeast. The pattern of variability of the residual currents is strongly linked to wind variability. There is a strong resemblance between the south-to-north observed residual velocity component at Port Stanvac and the daily mean of the south-to-north wind velocity component observed at Adelaide Airport.

There are episodes, where the model results and the ADCP data show distinct differences. An example is a period around 1 March (see Figure 4.25). A remarkable event is around 28 April (Figure 4.26), when the temporal trend of the simulated and observed residuals is very different. One possible explanation of such events is the impact from shelf waves hitting the Gulf from outside. The timing of the shelf waves in 2011 however does not correlate with high discrepancies between simulated and observed residual currents in Gulf St Vincent (Deltares & Jacobs, 2015). Another possible explanation is the use of homogeneous wind forcing. Due to the relatively slow movement of frontal systems, wind changes are in reality not simultaneous everywhere, but will move over the model domain. Inhomogeneous wind patterns would in fact have the effect of introducing additional circulation patterns in the flows. In view of the relation between wind forcing and residual currents, we expect this to be a main reason for differences between the simulated and observed residual currents.

As illustrated by Figure 4.29, the model shows the characteristic gyre in front of the Port River outlet. These results have been obtained by simulating a continuous release of a decaying tracer (decay rate 1 d^{-1}) right in the mouth of Port River during January 2011.

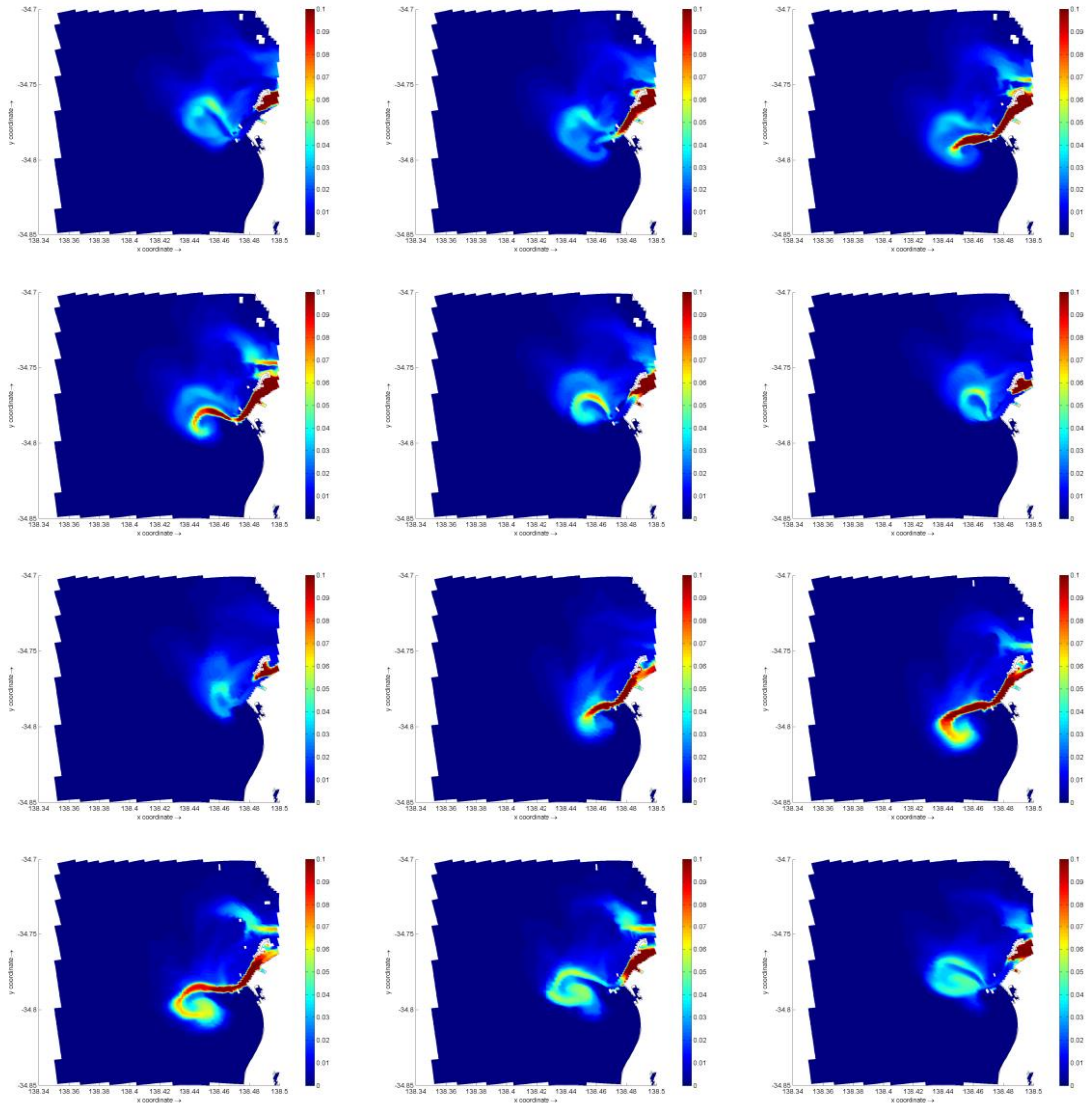

Figure 4.29 Snap shots of the simulated concentration as a result of a continuous release of a decayable tracer in the mouth of Port River, on 17 January 2011 with 2 hour intervals (00.00h to 22.00h), showing the gyre in front of the Port River outlet.

4.3.5 Effect of waves on residual currents

By means of a numerical experiment, we investigated the effect of waves on the residual currents. A conservative tracer was released at a constant rate from the mouth of Torrens River. The simulated tracer flux was recorded during the year 2011 through two transects: one north of the release point and one south of the release point. Without the effect of waves included, 36% of the released material went north and 57% south, while the remaining 6% went west and did not pass any of the two transects. With the effect of waves included, 43% of the released material went north and 44% south, while the remaining 13% went west. The increasing share of tracer going west in a simulation with waves could be explained as follows. During a period without a residual current the discharged tracer material accumulates and a strong concentration gradient builds up perpendicular to the coast. Independent of the degree of mixing in this direction, the stronger concentration gradient causes a larger transport flux to the west. In the simulation without waves, the westward transport is small (6%) while southbound transport (57%) was dominating northbound transport (36%) in 2011.

The presence of waves coming in from the southwest (Figure 4.22, Figure 4.23, Figure 4.24) is expected to cause a northbound wave generated current along the coast. This increases the northbound transport (43%), decreases the southbound transport (44%) and apparently increases the frequency of events without a residual current, presumably cases where a southbound circulation is counteracted by a northbound wave induced current. This leads to a higher westward transport (13%) in the simulation with waves.

4.3.6 Water levels, salinity and temperature

The 3D hydrodynamic model results have been evaluated based on a hindcast simulation for the year 2011. For the overall model, the water level representation is good with an average Root-Mean-Square Error (RMSE) at two stations on opposite sides of the Gulf St Vincent equal to 7.7 and 8.8 cm respectively. The tide representation is excellent with an average RMSE of 4.4 and 4.5 cm respectively. Most amplitude errors of the tidal constituents' representation do not exceed 1 cm, whereas most phase errors are less than 1°. There is a good representation of the water temperature in the study area, with an average RMSE of 1°C 1 m below surface and 1 m above bottom. There is an acceptable representation of the salinity in the study area, with an average RMSE of 0.5 psu at 1 m below surface and 1 m above bottom. Based on a comparison with Gulf-wide observations made in June-August 2015, it appears that the model produces realistic monthly averaged spatial and temporal gradients.

For the detail model, the water level representation is good with a Root-Mean-Square Error (RMSE) at Outer Harbour equal to 10.5 cm respectively. The tide representation is good with an average RMSE of 7.3 cm. Most amplitude errors of the tidal constituents' representation do not exceed 1 cm, whereas most phase errors are less than 5°. The water level representation of the detail model is not as good as in the overall model. Since all forcing is the same in both models, we suspect that the different grid and possibly the more detailed bathymetry are the cause. In particular, the area inside the Port River entrance where the tide gauge is located is represented by 2-3 cells while the cells are not aligned with the breakwaters. This is expected to cause an extra (unrealistic) resistance that disturbs the tide propagation. In addition, the more detailed bathymetry may result in extra resistance. We note that the overall model is too coarse to resolve any of the Port River mouth features and does not contain the breakwaters. Hence, there are no schematisation elements that cause extra resistance. In the detail model there is a good representation of the water temperature, with an average RMSE of 1°C at 1 m below surface and 1 m above bottom. There is an acceptable representation of the salinity, with an average RMSE of 0.5 psu and 0.4 psu at 1 m below surface and 1 m above bottom, respectively.

For detailed information we refer to Appendix D.

4.4 Discussion

The model validation results show the capability of the model to predict the impact of coastal discharges on the light reaching the seagrass leaves. The validation exercise was sub-optimal, because we had to test different aspects of model performance and different spatial gradients using a variety of datasets stemming from different years. The additional data collected as a part of the present study (Chapter 3) were essential, because this dataset includes all parameters that contribute to the downward attenuation of light and the attenuation itself. This enabled us to validate the parameters of the light model. The additional data were furthermore useful because they had a high enough frequency to make the results independent of the timing of sampling relative to individual weather events.

The AREM has no explicit seagrass compartment: we do not model the growth, mortality and decomposition of seagrass and the effect those processes have on the marine nutrient

cycles. This was a choice we made for different reasons. First, seagrass meadows in natural conditions can live in areas without significant nutrient supplies and rely mostly on internal nutrient cycling. This implies that the net effect on marine nutrient cycles can be expected to be limited. It is possible that there is a seasonal effect of seagrass on nutrient cycling, with seagrass being a net sink of nutrients in the growth season and a net source outside the growth season. We analysed the only available longer term dataset with seasonal resolution, the EPA coastal monitoring data, but found no seasonal trends whatsoever. It is also possible that seagrass is a net sink of nutrients since it slowly builds up mats of organic matter in the seabed. If this would have been a significant flux within the near-shore areas, we would have noticed it by simulated nutrients concentrations being larger than observed nutrient concentrations. Adding a seagrass compartment adds complexity and a series of additional parameters to the model. Because data to calibrate such parameters were lacking, and because there was no obvious necessity to include the seagrass compartment in AREM, we omitted it. Instead, we implemented sinks and sources from seagrass meadows as forcing a function in AREM whenever the data showed there was the need to do so (e.g. seagrass as a source of CDOM), and benchmarked the magnitude of this forcing on relevant scientific literature. In addition, the effect of seagrass on particle dynamics by the effect it has on waves, currents and the stabilisation of the seabed was included in the model.

The validated model allows us to investigate how various water quality parameters affect the downward attenuation of light and the amount of light reaching the seagrass canopy. Figure 4.30 shows the breakdown of the total light attenuation into four contributing parts: the background from clean sea water and the contributions by CDOM, inorganic particles and organic particles including phytoplankton.

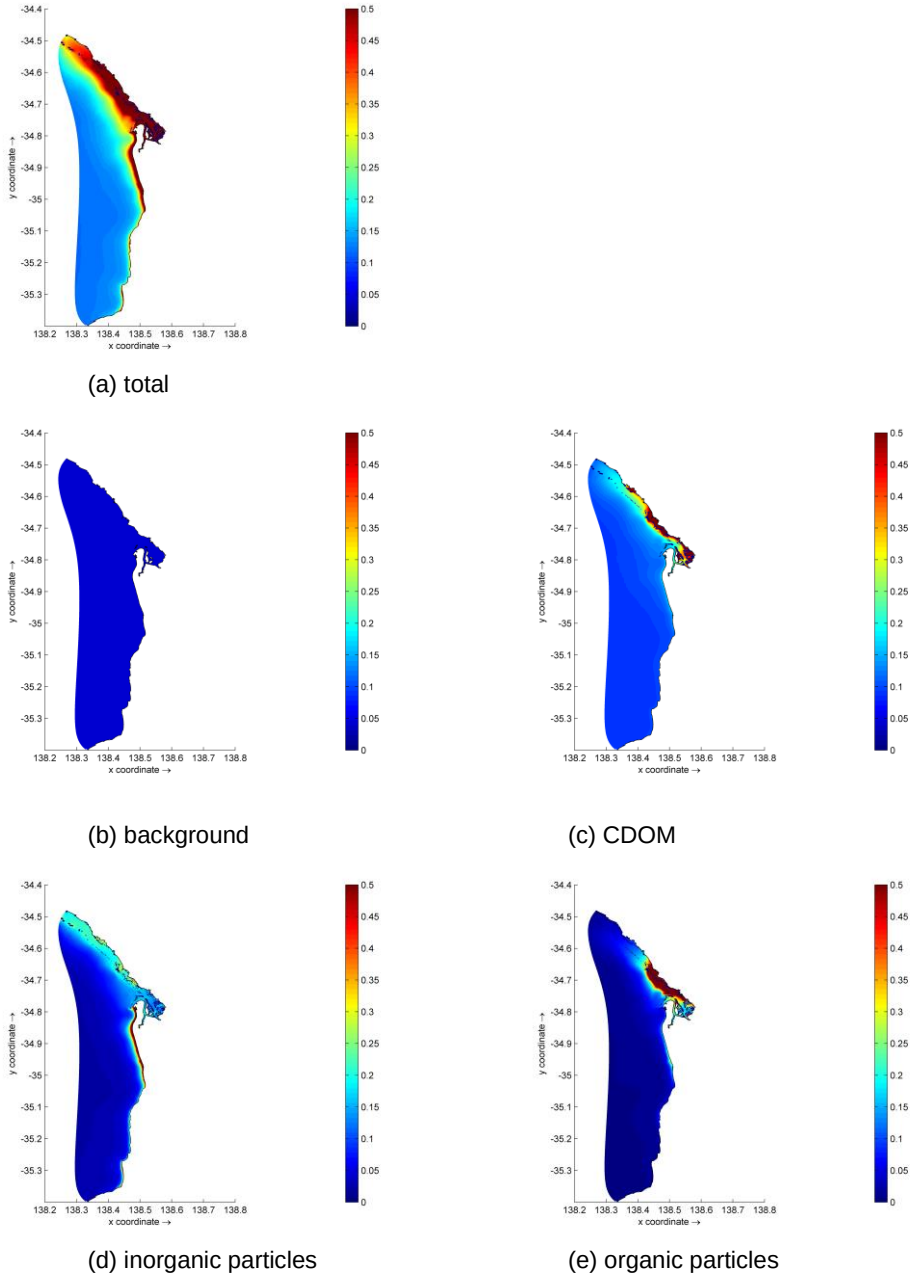

(a) total

(b) background

(c) CDOM

(d) inorganic particles

(e) organic particles

Figure 4.30 Mean simulated total downward light attenuation K_d (m^{-1}) in 2011, and components thereof: background (b), CDOM (c), inorganic particles (d) and organic particles including phytoplankton (e).

Figure 4.31 shows the relative contribution of these four components of downward light attenuation and of nuisance epiphytes to the total light reduction (light entering the water column minus light reaching seagrass leaves).

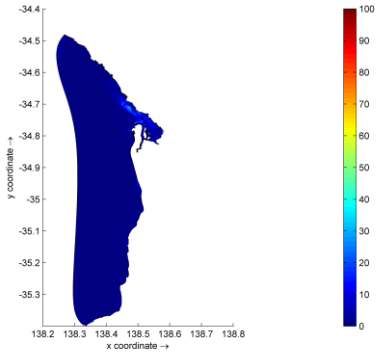

(a) nuisance epiphytes

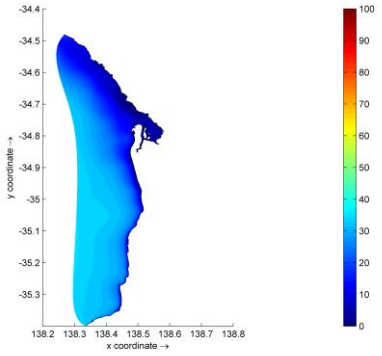

(b) background

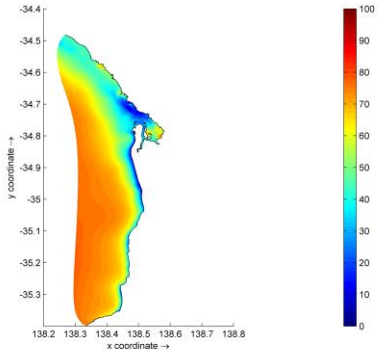

(c) CDOM

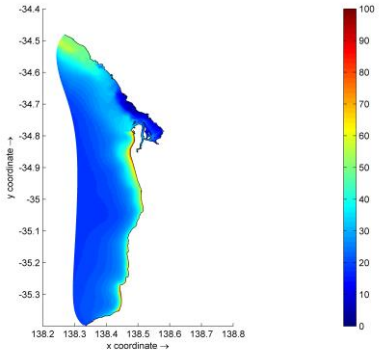

(d) inorganic particles

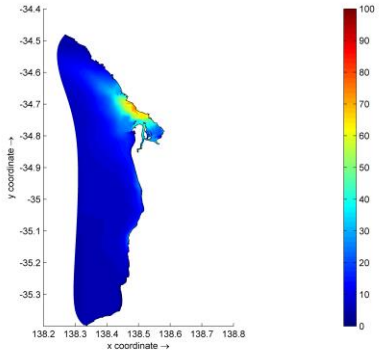

(e) organic particles

Figure 4.31 Mean simulated share of local light reduction (in %) by nuisance epiphytes (a) and by water column attenuation due to 4 different constituents ((b) to (e)).

These results show that off-shore, the light reduction is dominated by CDOM water column attenuation, and that the background of clean sea water is the second most relevant component. Close to shore, CDOM is still a relevant component, but water column attenuation by inorganic and organic particles is also relevant. Organic particles dominate in front of the Port River outlet and north of that outlet, while inorganic particles dominate along the metropolitan coast. This conclusion justifies in retrospect the selection of the two transects in the 2014-2015 surveys, with the Bolivar transect north of Port River and the Grange transect to the south. The light reduction by nuisance epiphytes is noticeable close to the Bolivar discharge and is of limited relevance elsewhere.

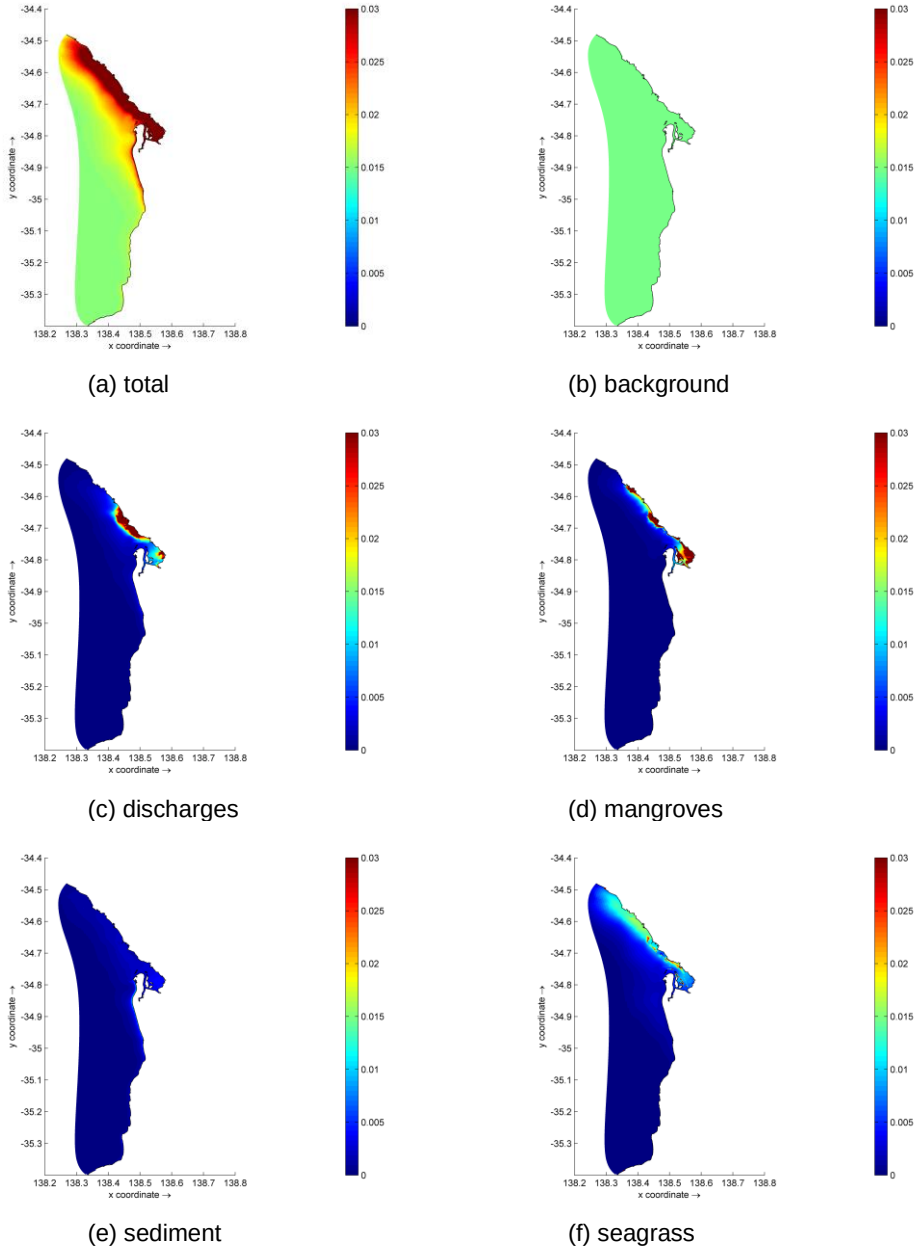

Figure 4.32 Average simulated concentration of CDOM (cm^{-1}) in 2011 (a), broken down in contributions from the background (b), from coastal discharges (c), from mangrove releases (d), sediment releases (e) and seagrass releases (f). Contributions (c) to (f) stem from releases within the model domain.

Figure 4.32 shows the simulated annually averaged concentrations of CDOM, and how this concentration breaks down into contributions from outside the model domain ("background") and from various sources within the model domain. Away from the coast, the background dominates, but towards the coast, the concentration of CDOM increases, due to a blend of other sources. In the 2011 simulation, accumulated over the total domain, coastal discharges make up 16% of the emissions, mangroves 7%, sediment (resuspension) 23% and seagrass 54%.

Figure 4.33 shows the simulated average and maximum concentrations of total inorganic (suspended) matter, with and without resuspension. The average concentrations are dominated by resuspension, which has the strongest effect in a narrow band along the Metropolitan coast. The maximum concentrations are also dominated by resuspension, though locally some river plumes contribute significantly (e.g. Gawler River). At the SA Water sampling stations along the Grange and Bolivar transects, the contribution by resuspension is one order of magnitude larger than the contribution by coastal discharges.

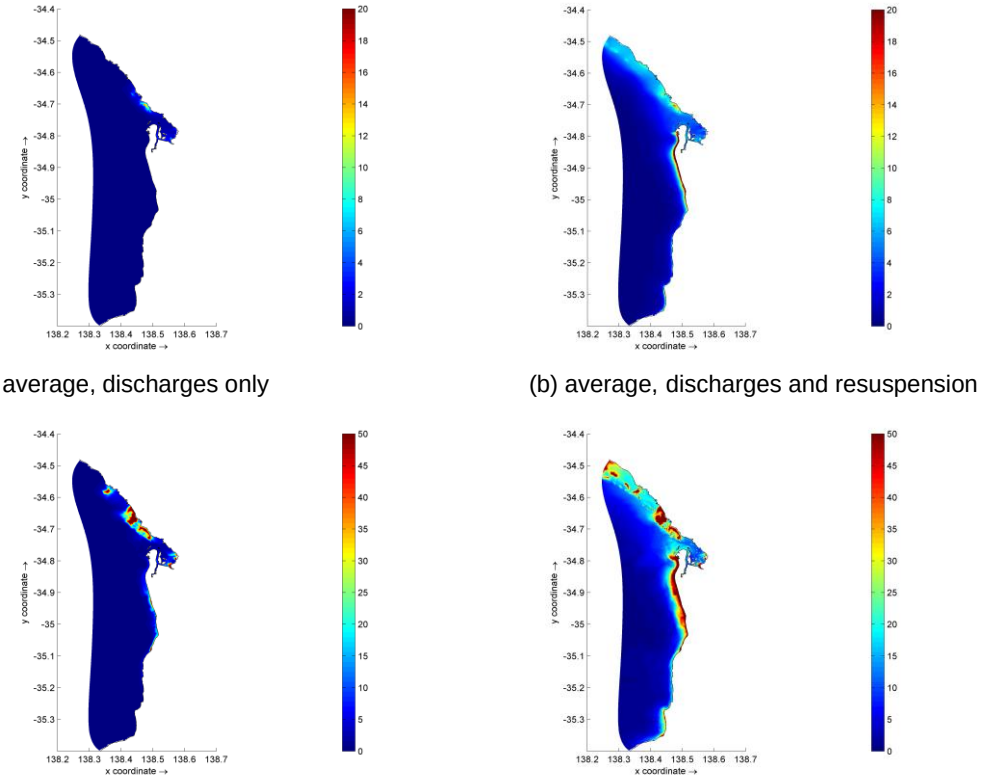

(a) average, discharges only

(b) average, discharges and resuspension

(c) maximum, discharges only

(d) maximum, discharges and resuspension

Figure 4.33 Average (top) and maximum (bottom) simulated concentration of inorganic suspended particles (g m^{-3}) in 2011, without resuspension (left) and with resuspension (right).

This study established for the first time a complete and quantitative relation between coastal discharges and downward light attenuation. We found that the concentrations of suspended matter are not just the result of coastal discharges, but are in fact predominantly determined by resuspension, especially along the Metropolitan coast. Similarly, this study also quantitatively established that the concentrations of CDOM are not just the result of coastal discharges, but are in fact dominated by a marine water background and to a lesser extent by releases from sediments, mangroves and seagrass. This all implies that the relation between the coastal discharges and the concentrations of water quality parameters affecting downward light attenuation is not direct and linear, under the influence of these background contributions.

The reliability of the AREM is highest in a band along the coast, at some distance of the seaward edge of the detail model. Farther away, water quality is controlled by discharges and processes at the scale of the whole Gulf St Vincent and by exchange with the open ocean, which have not been the prime focus of this study.

We have not studied whether the background concentration of CDOM and the releases from sediment, seagrass and mangroves are natural or anthropogenic. We see no direct link to human activities, except the fact that seagrass die-off due to anthropogenic pressures is likely to temporally lead to extra releases of CDOM. For management purposes, a worst-case assumption dictates that the background and natural sources of CDOM should be assumed permanent, until proven otherwise by marine water quality monitoring.

We have not studied whether the presence and quantity of fines in the seabed are natural or anthropogenic. There probably is a relation to stormwater, wastewater and sludge discharges from the past. It is likely that the response time to changes of such inputs is in the order of decades (Section 4.2.8). The inputs have been higher in the past than they are today. This reduction will probably at least locally reduce the quantity of fines in the seabed, but we do not know by how much and we do not know when. For management purposes, a worst-case assumption dictates that the quantity of fines in the seabed should be assumed constant, until proven otherwise by marine sediment monitoring.

4.5 Conclusions

The pilot version of the AREM has been successfully upgraded and calibrated. The AREM contains interconnected models describing the hydrodynamics, waves, fine sediment dynamics and biogeochemistry of the Adelaide Coastal waters. These models have the objective of quantifying relevant environmental conditions for seagrass habitat suitability evaluation, as affected by local river discharges and discharges of treated wastewater and stormwater, taking into account the morphology, meteorology and oceanography of the study area.
The upgrade of these models encompassed:

- the implementation of a local high resolution grid and bathymetry;
- the incorporation of the effects of waves on shear stresses and currents in the study area by an on-line coupling between the waves and hydrodynamics models;
- the incorporation of the effect of the presence of seagrasses on currents, waves and sediment stability;
- the implementation of a spatially variable pool of fine particles in the top sediment;
- the improvement of the nuisance epiphyte cover sub-model supported by a literature survey to determine key model parameters;
- the implementation of the load data discussed in Chapter 2;
- the implementation of the empirical light model discussed in Chapter 3.

An extensive validation has been conducted using a wide variety of data sets. The model validation results show the capability of the model to predict the impact of coastal discharges on the light reaching the seagrass leaves. The validation exercise was sub-optimal, because we had to test different aspects of model performance and different spatial gradients using a variety of datasets stemming from different years. The additional data collected as a part of the present study (Chapter 3) were essential, because this dataset includes all parameters that contribute to the downward attenuation of light and because they had a high enough frequency to make the results independent of the timing of sampling relative to individual weather events. In this sense, the new datasets are unique, and this enabled us to validate AREM beyond the achievable level thus far.

This study established for the first time a complete and quantitative relation between coastal discharges and downward light attenuation in the Adelaide coastal waters. On an annually

averaged basis, CDOM is the most relevant component over large parts of the study area. Close to the metropolitan coast, inorganic suspended matter is the most relevant, while phytoplankton and organic particles are the most relevant close to the shore north of the Port River outlet.

The concentrations of inorganic particles, important close to the metropolitan coast, cannot be directly linked to coastal discharges alone. Wave-induced resuspension events stir up the sediments and release fine particles which stay in suspension for some days to cause “darkness events”. The contribution by resuspension is simulated to be one order of magnitude larger than the direct contribution by coastal discharges. The presence of fines in the seabed could be natural or anthropogenic. There probably is a relation to stormwater, wastewater and sludge discharges from the past. It is likely that the marine sediments “buffer” such inputs over a period in the order of decades. Since discharges have been higher in the past than they are today, the situation may well improve because previously discharged particles that were stored in the sediments are gradually washed out to open sea. A worst-case assumption dictates that the quantity of fines in the seabed should be assumed constant, until proven otherwise by marine sediment monitoring.

The newly available data allowed us to establish that the concentrations of CDOM cannot be directly linked to coastal discharges alone either. Away from the coast, sources from elsewhere dominate. Only towards the coast, the concentration of CDOM increases, due to a blend of local sources. In the 2011 simulation, coastal discharges make up 16% of the total emissions in the study area, CDOM release by mangroves 7%, CDOM release from sediment resuspension 23% and CDOM release by seagrass 54%.

This all implies that the relation between the coastal discharges and the concentrations of water quality parameters affecting downward light attenuation is not direct and linear, under the influence of these background contributions.

5 The relation between coastal discharges and seagrass habitat suitability for the Adelaide Coastal Waters

Seagrass meadow of Amphibolis and Posidonia spp - Photo by Kingsley Griffin

5.1 Introduction

Habitat Suitability Index (HSI) models are commonly used to predict habitat quality and species distributions based on known relationships between environmental conditions and the tolerances/requirements of plant or animal species (Guisan and Zimmermann, 2000). The reliable prediction of the spatial distribution of habitats or species is central to various applications in ecology, conservation and management (Guisan and Thuiller, 2005; Elith et al., 2006). Originally developed for application in the management of selected fish and wildlife species (U.S. Fish and Wildlife Services, 1980, 1981; Thomasma et al., 1991), the use of habitat suitability index models was initially criticised because of unreliable model performance due to inadequate consideration of input parameter variability, inappropriate spatial scaling and timeframes, and a lack of validation (Brooks, 1997; Roloff and Kernohan, 1999). Following methodological improvements and innovations (e.g. Guisan and Thuiller, 2005; Elith et al., 2006), along with the rise of new powerful statistical techniques and GIS tools (Pearce and Ferrier, 2000; Hirzel et al., 2006), habitat suitability modelling has now become an effective and widely used spatial decision-support tool for natural resource management and ecosystem restoration (Guisan and Zimmerman, 2000; Burgman et al., 2001; Guisan and Thuiller, 2005; Detenbeck and Rego, 2015; Zajac et al., 2015).

Successful applications of habitat suitability modelling to predict seagrass distribution include ecological studies (Greve and Krause-Jensen, 2005; Van der Heide et al., 2009; Valle et al., 2013), environmental impact and risk assessments (Kemp et al., 2004; Meyer, 2013; Shafer et al., 2016), selection of cost-effective approaches for habitat mapping of large or inaccessible areas (Kelly et al., 2001; Lathrop et al., 2001; Fonseca et al., 2002; Holmes et al., 2007; Bekkby et al., 2008; Grech and Coles, 2010), assessment of the effectiveness of management measures (Adams et al., 2015; Detenbeck and Rego, 2015; Zajac et al., 2015), evaluation of investment scenarios to comply with water quality threshold criteria or ecosystem health targets (Carruthers and Wazniak, 2004; Erftemeijer and Van de Wolfshaar, 2006; Erftemeijer and Van de Wolfshaar, 2008; Santos and Lirman, 2012), and site-selection for restoration projects (Valle et al., 2011; Thom et al., 2014; Zhou et al., 2016). These modelling applications proved useful in directing localised management actions (to reduce stressors, halt decline and promote recovery of seagrasses), saving costs in large-area mapping of seagrass distribution, informing the selection of water quality criteria, predicting the effects of sea level rise and changing water management practices, curbing the spread of invasive species and selecting the most suitable sites for seagrass transplantation.

Seagrasses in South Australian waters have suffered significant declines due to natural and anthropogenic causes (Westphalen et al., 2004; Seddon et al., 2000). Since the 1940s, some 6,000 ha of seagrass meadows have been lost from the coastal waters around Adelaide (Westphalen et al., 2004; Bryars and Rowling, 2009; Tanner et al., 2014), which has been attributed to high nutrient loads from wastewater discharges (peaking in the late 70s/early 80s) and high sediment loads from stormwater (Collings et al., 2006; Fox et al., 2007; Fernandes et al., 2015). This loss prompted management agencies to agree on aspirational load reductions for both nitrogen (by 75% to 600t) and suspended solids (by 50% to 4,200t) (Fox et al., 2007; McDowell and Pfennig, 2013). A significant reduction in effluents from wastewater treatment plants (WWTP) has already been realised to date, resulting in considerable water quality improvements along the Adelaide coast over the past three decades (Fernandes et al., 2015). Despite these efforts, signs of seagrass recovery have been slow to appear (Bryars and Neverauskas, 2004). Further nutrient load reductions would involve significant investments. Meanwhile, the population of Adelaide is expected to grow by up to 45-50% between 2006 and 2036, resulting in higher volumes of wastewater to treat and a larger urbanised drainage area.

To guide investments into further nutrient reduction initiatives, the Adelaide Receiving Environment Model (AREM) was developed, a coastal modelling suite consisting of hydrodynamic, wave, biogeochemical and seagrass habitat suitability modules. The overall aim of AREM is to enable reliable prediction of the outcome of different nutrient reduction strategies and investment scenarios and to evaluate their potential effectiveness in halting further loss and promoting recovery of seagrasses in Adelaide's coastal waters.

5.2 Materials and Methods

5.2.1 Habitat Suitability Model Set-Up

The seagrass habitat suitability module of AREM was supported by an inventory of objective, quantitative habitat suitability thresholds for each of the seagrass species occurring in the study area. The selection of appropriate predictor variables was guided by the level of scientific understanding of the quantitative relationship between environmental conditions and the occurrence and health of seagrasses, derived from a thorough review of available literature (Erftemeijer, 2014). In this study, habitat suitability for seagrasses was predicted as

a function of eight different environmental variables: light reaching the canopy (as a function of water column light attenuation and water depth), light reaching the leaves (as a function of attenuation by epiphyte cover, modelled dynamically within the biogeochemical module), salinity, water temperature, substrate, wave exposure, flow velocity and tidal exposure.

Other environmental parameters (e.g. pH, sediment biogeochemistry, e.g. composition, nutrients, redox conditions, sulphides, toxic substances), biological processes (bioturbation, herbivory, detritivory, diseases) and anthropogenic activities (such as dredging, trawling, outfall decommissioning) were not included as predictors in the model. Either they were not considered a major driver of seagrass distribution in the study area, or they operate at a spatial scale finer than the output habitat suitability maps, or their effect on seagrass health is poorly understood, or there was a lack of spatial data on these variables.

Habitat suitability modelling followed a two-step approach:

1 calculating suitability indices (values between 0 and 1) for each individual variable (based on species-specific response curves describing the relationship between seagrass health and that variable, derived from literature review),
2 combining all individual suitability indices (SI's) to obtain one overall HSI (the lowest value for each grid cell).

This process was repeated for each of the nine seagrass species separately to obtain individual species distribution maps. An overall seagrass distribution map was obtained for all species combined by merging the maps of all species together, taking the highest HSI value of any species for each grid cell.

No weighting was applied to the variables, as there is no conclusive evidence to suggest that the effects of some variables are greater than others in determining seagrass health and survival. While synergistic effects may occur between some of the variables, these interactions are not understood well enough to be incorporated in the model.

5.2.2 Seagrass species

There are an estimated 15,000 km^2 of seagrass beds in southern Australia (Greenwood and Gum, 1986) with 9,620 km^2 in South Australia; 3,700 km^2 in Spencer Gulf and 1,530 km^2 in Gulf St Vincent (Shepherd and Robertson, 1989; Eddyvane, 1999). Adelaide's Coastal Waters support nine seagrass species: *Posidonia australis, Posidonia sinuosa, Posidonia coriacea, Posidonia angustifolia, Amphibolis antarctica, Amphibolis griffithii, Heterozostera tasmanica* (formerly also known as *Zostera tasmanica*), *Zostera muellerii* (formerly also known as *Zostera capricornii* or *Zostera mucronata*) and *Halophila australis*. This diversity encompasses a wide array of morphologies and life histories and thus a range of responses to disturbance.

In addition, there are three additional species of submerged angiosperms in South Australia (i.e. *Lepilaena marina*, *Ruppia megacarpa* and *Ruppia tuberosa*) that were not considered for the present model, as they primarily occur in saltmarsh areas and hypersaline lakes up to ten times the salinity of seawater (Robertson, 1984). They are often not considered true seagrasses and were reportedly not among the species affected by the widespread seagrass losses in South Australia.

5.2.3 Review of thresholds

5.2.3.1 Light

Light is one of the key environmental resources imperative for the growth and survival of seagrasses (Hemminga and Duarte, 2000). The degree of water transparency (which determines the depth-penetration of photosynthetically active radiation of sunlight) is the primary factor determining the maximum depth at which seagrasses can occur. Reduction in light due to turbidity has been identified as a major cause of the loss of seagrasses worldwide (Shepherd et al., 1989; Green and Short, 2003). The amount of light that reaches a seagrass leaf is determined by water depth and quality, including the concentration of coloured dissolved organic matter, the concentration of suspended solids (incl. fine sediment particles and dead organic matter) and phytoplankton in the water, and the epiphyte cover of the leaf. There are various reports of sub-lethal and lethal effects on seagrass meadows due to prolonged exposure to high turbidity (Caldwell, 1985; Gaby et al., 1986; Onuf, 1994; Gordon et al., 1994; Cheshire et al., 2002). Laboratory experiments have shown that some seagrasses can survive in light intensities below their minimum requirements for periods ranging from 4 weeks to several months (Backman and Barilotti, 1976; Bulthuis, 1983; Gordon et al., 1994; Czerny and Dunton, 1995; Longstaff et al., 1999). The minimum light requirements specific to the nine seagrass species in the study area, as reported in the literature, are summarised in Table 5.1.

5.2.3.2 Salinity

Tolerance to salinity is an essential requirement for seagrasses and they may encounter a wide range in the shallow coastal environments in which they occur (Walker and McComb, 1990). The optimum and range of salinities that can be tolerated varies among seagrass species (Lirman and Cropper, 2003). There are species that can tolerate a wide range of salinities, usually demonstrated by their role of occupying shallow coastal areas subject to extreme salinity changes. Others tolerate just a narrow range. In general, experimentation shows that a wide range may be tolerated by several seagrass species for very short periods, but their long-term tolerances are narrower (Hillman et al., 1989). Low salinities have also been shown to have lethal effects on seagrasses. Many nearshore environments, where seagrasses occur, are subject to rapid changes in salinity from freshwater run-off. Some field studies on seagrasses suggest increased sensitivity to low salinities at high temperatures, but as yet no laboratory experiments on salinity/temperature interactions, or salinity interactions with most other environmental variables, have been carried out (Hillman et al., 1989). The salinity tolerance thresholds specific to the nine seagrass species in the study area, as reported in the literature, are summarised in Table 5.1.

5.2.3.3 Water Temperature

The temperature tolerance of seagrasses varies with geographical latitude. The range of thermal tolerance of tropical seagrass species is about half that of temperate seagrass species, whereas their upper tolerance limit is similar. Tropical and subtropical species do not tolerate low temperatures and are only slightly more tolerant of extended periods of high temperatures than temperate species (Hillman et al., 1989). Intertidal seagrass populations, which are likely to be exposed to air at low tides, show greater tolerance of high temperatures than those which occur in deeper sites and remain submerged (McMillan, 1984). Temperatures above or below optimum limits might not necessarily destroy a meadow, but they might inhibit metabolism and thus decrease the plant's productivity (Bulthuis, 1987). Temperatures above the upper tolerance limits of seagrasses may cause substantial leaf mortality while their roots and rhizomes often remain unaffected, protected by the overlying

sediments (Zieman, 1982). The temperature tolerance thresholds specific to the nine seagrass species in the study area, as reported in the literature, are summarised in Table 5.1.

5.2.3.4 *Substrate*

Where space is available, seagrass populations can only develop if the substrate (bed composition) is suitable. Most seagrass species are confined to sandy and muddy sediments, which are easily penetrated by seagrass roots, although some species can grow on rubble and over rock (Hemminga and Duarte, 2000). Areas with a high mobility of sediments (causing successive burial and erosion) and areas with very fine sediments rich in organic matter contents (causing high redox and sulphide levels) tend to be unsuitable for seagrass growth. Seagrass habitat suitability was modelled as a function of substrate (represented by a hard/soft substrate map for the Gulf of St Vincent) in a simple way: hard substrate was denoted as unsuitable (HSI=0) and soft substrate as suitable (HSI = 1) for all species except *Amphibolis antarctica*, for which all substrate was denoted suitable (HSI = 1) as this species is known to occupy also rocky substrate. In the absence of a more detailed map of sediment grain-size distribution, no distinction was made between the nine seagrass species for this variable (see Table 5.1), although it is known that some species (e.g. *Amphibolis spp*. and some *Posidonia spp*.) prefer coarser sediments, while some other species prefer fine muddy substrates (e.g. *Zostera muelleri*). Indirectly, however, this variability is captured in the hydrodynamic variables (flow velocity and wave exposure).

5.2.3.5 *Wave exposure*

Although often overlooked, hydrodynamic parameters are crucial in determining the habitat suitability of an area for seagrasses (Koch, 2001). In their natural environment, seagrasses are exposed to wind-driven currents, tides, waves and wave-driven currents. While these hydrodynamic processes affect seagrasses, seagrasses in turn also affect these hydrodynamic processes through the attenuation of currents and waves (Koch et al., 2006a). In areas with high wave exposure and strong currents, seagrass may be uprooted or damaged due to excessive sediment transport, which does not allow seeds to become established, or by eroding/burying existing seagrass beds. As a result, wave-exposed areas tend to have patchy seagrasses or are unvegetated (Koch et al. 2006b). The temporal statistics of waves relevant to seagrass loss are described by maxima during events with a relevant return period. How long this relevant return period is, depends on how long it takes the seagrass to grow back in areas where it was affected by waves, under otherwise suitable conditions. Not all seagrass species are equally susceptible to the impacts of waves (i.e. their intensity and frequency) (Infantes et al., 2009; De Jong et al., 2005). *Amphibolis antarctica* is adapted to hydrodynamically active environments and appears to be the only species capable of occupying high intensity disturbance sites (Clarke and Kirkman, 1989). *Amphibolis griffithii* and *Posidonia coreacea* are also wave-tolerant species. *Heterozostera tasmanica* and *Zostera muellerii* appear to be quite sensitive to exposure to wave energy and are primarily found in sheltered areas characterised by fine sediments. *Halophila australis*, a species with limited root penetration, which limits its anchoring strength (Kiswara et al., 2009) is also relatively sensitive to wave energy. This qualitative information was translated into approximate, species-specific tolerance thresholds to wave exposure for the various seagrass species in the study area, expressed as a critical near-bottom orbital velocity (m s^{-1}) with a return period of once per six months, as summarised in Table 5.1. The six month return period used in our model corresponds to a higher frequency of return of extreme wave conditions (reflecting local hydrodynamic conditions) than what was used in other recent modelling studies by Infantes et al. (2009) and Vacchi et al. (2012; 2014), who adopted an extreme wave return period of one year as relevant when describing hydrodynamic

constraints to meadow expansion of *Posidonia oceanica* and modelling the upper limits of *P. oceanica* seagrass distribution in the (generally calmer) Mediterranean Sea.

5.2.3.6 *Flow velocity*

Forces generated by water motion originating from tides and wind can have a measurable effect on growth and distribution of seagrasses. Increasing flow can enhance nutrient uptake in seagrasses by reducing the boundary layer around the leaves. Studies on eelgrass (Fonseca and Kenworthy, 1987; Koch, 2001) suggest that there may be an optimum current speed below which metabolism is limited by diffusion and above which growth may decline as a result of physical disruption of the plants. Seagrass beds themselves reduce current velocity by dissipating momentum from the moving water. The magnitude of this process depends on the density of the seagrass bed (Koch, 2001). Excessively weak currents may adversely affect seagrass growth through detrimentally high sediment organic contents, high levels of sedimentation, or by limiting leaf diffusive boundary layer conditions. Highly elevated current flows, on the other hand, may result in erosion of sediments and potentially destroy the meadow. There is very limited species-specific information available on the tolerance limits to flow velocity for each of the species occurring in Adelaide's coastal waters. We therefore adopted a more general set of flow velocity tolerance thresholds (same for all species, see Table 5.1) based on available seagrass literature (Van Keulen and Borowitzka, 2002; Fonseca et al., 1983).

5.2.3.7 *Tidal exposure*

The degree to which seagrasses can withstand low tide exposure differs between species. In the intertidal zone, seagrasses and seaweeds are periodically exposed to air where they experience a variety of potentially stressful environmental conditions, including desiccation, high light and UV radiation, nutrient limitation, high and low temperature, and osmotic stress (Davison and Pearson, 1996; Dawson and Dennison, 1996). The period during which a seagrass plant is exposed at low tide is essentially a function of the tidal amplitude and the depth at which the seagrass plant occurs. Wind stress on shallow nearshore waters may often aggravate the situation. Nevertheless, intertidal seagrass plants are not always entirely exposed because a thin lens of water may often be retained due to micro-variations in bottom-topography. The duration of the exposure period fluctuates over the tidal (spring-neap) cycle. Low tide exposure in this study is defined and expressed as the average percentage of the time that the plants are exposed to water levels less than 10 cm. A threshold of 10 cm was chosen for tidal exposure, as for most seagrass species in the study area this is well below half their mean canopy height (especially for *Posidonia* spp. and *Amphibolis* spp.). At water levels below 10 cm, most seagrasses will definitely start to feel the effect of desiccation, as a significant proportion of the plants will be sticking out or float on the water surface. The tolerance thresholds for tidal exposure specific to the nine seagrass species in the study area, as reported in the literature, are summarised in Table 5.1.

Table 5.1 Summary[*] of key environmental variables defining habitat suitability for seagrasses in South Australian waters, representing critical thresholds that describe species-response relationships as used in the model

	Light (% of surface irradiance)	Salinity (ppt)	Temperature (^{0}C)	Flow Velocity (m s^{-1})	Low tide exposure (duration, hrs)	Substrate (type)	Wave exposure (bottom orbital vel., m s^{-1})
Amphibolis antarctica							
unsuitable	<5	0	0 - 10	0			
suboptimal	5 - 12	0 - 20	10-23	0 - 0.05			
optimal	>12	20 - 42.5	23 - 26	0.05 - 1.5	0	all	<0.6
suboptimal		42.5 - 65	26 - 30	1.5 - 1.6			
unsuitable		>65	>30	>1.6	>0		>0.6
Amphibolis griffitthii							
unsuitable	<8	0	0 - 10	0		hard	
suboptimal	8 - 20	0 - 20	10 - 20	0 - 0.05			
optimal	>20	20 - 42.5	20 - 23	0.05 - 1.5	0	soft	<0.5
suboptimal		42.5 - 65	23 - 30	1.5 - 1.6			
unsuitable		>65	>30	>1.6	>0		>0.5
Posidonia australis							
unsuitable	<5	0	0 - 13	0		hard	
suboptimal	5 - 10	0 - 20	13 - 19	0 - 0.05			
optimal	>10	20 - 40	19 - 23	0.05 - 1.5	0	soft	<0.4
suboptimal		40 - 57	23 - 30	1.5 - 1.6			
unsuitable		>57	>30	>1.6	>0		>0.4
Posidonia sinuosa							
unsuitable	<4	0	0 - 13	0		hard	
suboptimal	4 - 20	0 - 20	13 - 18	0 - 0.05			
optimal	>20	20 - 40	18 - 23	0.05 - 1.5	0	soft	<0.4
suboptimal		40 - 57	23 - 24.1	1.5 - 1.6			
unsuitable		>57	>24.1	>1.6	>0		>0.4
Posidonia coriacea							
unsuitable	<5	0	0 - 13	0		hard	
suboptimal	5 - 12	0 - 20	13 - 19	0 - 0.05			
optimal	>12	20 - 50	19 - 23	0.05 - 1.5	0	soft	<0.5
suboptimal		50 - 51	23 - 30	1.5 - 1.6			
unsuitable		>51	>30	>1.6	>0		>0.5
Posidonia angustifolia							
unsuitable	<4	0	0 - 13	0		hard	
suboptimal	4 - 12	0 - 20	13 - 19	0 - 0.05			
optimal	>12	20 - 34	19 - 23	0.05 - 1.5	0	soft	<0.4
suboptimal		34 - 57	23 - 30	1.5 - 1.6			
unsuitable		>57	>30	>1.6	>0		>0.4
Heterozostera tasmanica							
unsuitable	<2	0	0 - 5	0		hard	
suboptimal	2 - 20	0 - 20	5 - 30	0 - 0.05			
optimal	>20	20 - 38	30	0.05 - 1.5	0 - 1	soft	<0.3
suboptimal		38 - 40	30 - 41	1.5 - 1.6	1 - 2		
unsuitable		>40	>41	>1.6	>2		>0.3
Zostera muellerii							
unsuitable	<5	0	0 - 9	0	<1	hard	
suboptimal	5 - 40	0 - 10	9 - 30	0 - 0.05	1 - 2		
optimal	>40	10 - 32	30	0.05 - 1.5	2 - 5	soft	<0.3
suboptimal		32 - 40	30 - 36	1.5 - 1.6	5 - 6		
unsuitable		>40	>36	>1.6	>6		>0.3
Halophila australis							
unsuitable	<2.5	0	0 - 9	0		hard	
suboptimal	2.5 - 16	0 - 15	9 - 10	0 - 0.05			
optimal	>16	15 - 58	10 - 30	0.05 - 1.5	0 - 1	soft	<0.3
suboptimal		58 - 59	30 - 38	1.5 - 1.6	1 - 2		
unsuitable		>59	>38	>1.6	>2		>0.3

[*]This summary is based on an in-depth literature review published previously (Erftemeijer, 2014)

5.2.4 Determination of relevant environmental conditions

The overall approach for quantifying the selected relevant environmental conditions for the study area is shown in Figure 5.1.

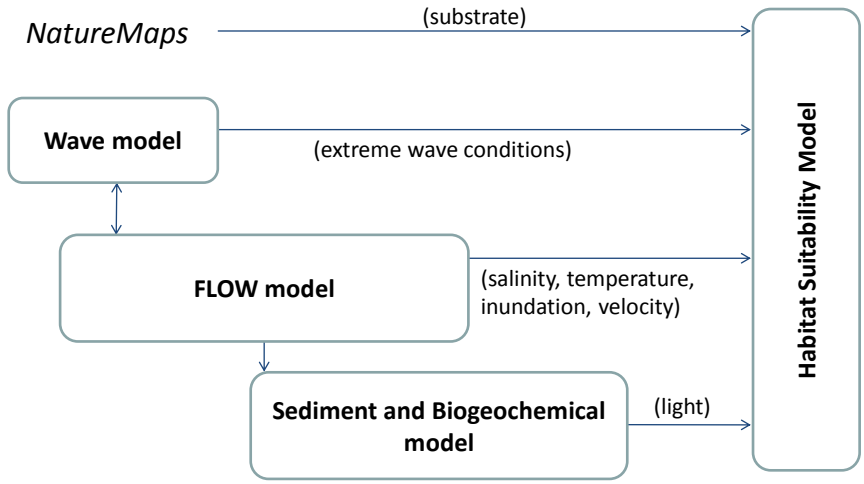

Figure 5.1 Schematic overview of AREM modules and their relations

The substrate in the study area is predominantly sandy, with localised patches of hard substrate including reefs. A map characterising the substrate in the study area has been derived from the NatureMaps database (EnviroDataSA 2015). In particular, the areas mapped as 'Low Profile Reef', 'Medium Profile Reef', 'High Profile Reef' and 'Cobble' have been classified as hard, all the others as soft.

Extreme wave conditions have been established during Phase 1 of the AREM development (Zijl et al., 2014). Available data included 31 years of ocean wind data derived from the Climate Forecast System Reanalysis (CFSR) (Saha et al., 2010) and wave data from the third generation wind wave model WAVEWATCH III (Chawla et al., 2013). A transformation of the offshore to nearshore wave climate has been carried out using the model SWAN (Booij et al., 1999). The results have been post-processed as maps of the extreme wave exposure expressed as discussed in Section 5.2.3.5.

For flow velocity, we used the maximum value of hourly averages predicted to occur during one year of simulation to assess the habitat suitability for seagrasses. For salinity, water temperature and tidal exposure, the simulated annual averages were used to assess the habitat suitability for seagrasses, recognizing that seagrasses are able to tolerate a certain degree of (short-term) natural variability in these parameters (Hemminga and Duarte, 2000). For light conditions, we adopted an approach using rolling averages that took into consideration the duration for which seagrasses are able to tolerate sustained periods of low light. There is a growing body of scientific evidence that shows that the various seagrass species differ in the length of time (duration) they can endure low light conditions below their minimum light requirements (Bulthuis, 1983; Neverauskas, 1988; Gordon et al., 1994;

Fitzpatrick and Kirkman, 1995; Longstaff et al., 1999; Collier, 2006; Mackey et al., 2007; Bryars and Collins, 2008; Collier et al., 2009; Lavery et al., 2009; McMahon et al., 2011; Serrano et al., 2011; Kirkman et al., 2012; Yaakub et al., 2013). To accommodate these species-specific differences, we applied the following time-averaging assumptions when interrogating model output of modelled light (%SI) reaching the plants for an estimation of habitat suitability for the different seagrass species (see also Appendix F):

- a 30-day rolling mean of modelled light (%SI) for *Zostera muelleri* and *Halophila australis*;
- a 60-day rolling mean of modelled light (%SI) for *Amphibolis griffithii*, *A. antarctica* and *Heterozostera tasmanica*;
- a 180-day rolling mean of modelled light (%SI) for *Posidonia australis*, *P. sinuosa*, *P. angustifolia* and *P. coriacea*.

In particular, the rolling means are applied to the following quantities:

$$\%SI = \frac{I_{bot}}{SI} \times 100\%$$

$$\%SI_{Epi} = \frac{I_{bot}}{SI} \times \left(100 - 92.4 \times \frac{EpiCov}{2.2 + EpiCov}\right)\% \quad with\ EpiCov = C_{Epi} \times (S_{leaves})^{-1} \times 0.278$$

where *%SI* is the percentage of incident PAR reaching the seagrass canopy, $\%SI_{Epi}$ is the percentage of incident PAR reaching the seagrass leaves as affected by nuisance epiphytes cover, *SI* is the daily averaged incident PAR in W m^{-2}, I_{bot} is the daily averaged PAR reaching the seagrass canopy after downward attenuation in the water column in W m^{-2}, *EpiCov* is the epiphytes load on seagrass leaves in mgDW per cm^2 of leaf area, C_{Epi} is the simulated nuisance epiphytes biomass in gC m^{-2} of seabed, S_{leaves} is the ratio between seagrass leaves area and seabed area and 0.278 is a scale factor converting gC m^{-2} to mgDW cm^{-2}, which includes a dry weight to carbon ratio of 1/0.36 gDW gC^{-1}, as well as the conversion of area and mass units. The empirical expression used for the effect of nuisance epiphytes cover on the PAR reaching the seagrass leaves is derived from Brush and Nixon (2002) and quantifies the transmission *T* of light through the epiphytes layer in % as:

$$T = \left(100 - 92.4 \times \frac{EpiCov}{2.2 + EpiCov}\right)\%$$

The estimated carbon to dry weight in epiphytes of 0.36 is based on various sources (Den Hartog and Nienhuis, 1987; Taylor et al., 1997; Boyd, 2002; Lefevre et al., 2003). The ratio between seagrass leaves area and seabed area was chosen as 5 (Deltares & Jacobs, 2015, section 2.3). Rolling means over periods of 30, 60 and 180 days are calculated as a function of space and time, for the quantities *%SI* and $\%SI_{Epi}$. For every location, the minimum value of these rolling means at any time is calculated and mapped. The calculation of the habitat suitability makes use of these mapped quantities.

The final environmental conditions maps that go into the habitat suitability model are collected in Figure 5.2 for the 2011 simulation.

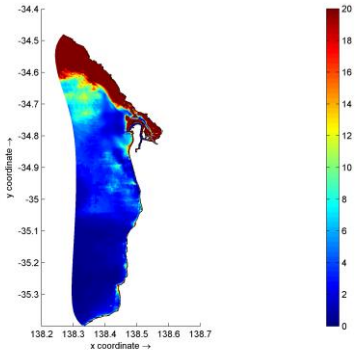

(a) Light (%SI, 30d rolling average)

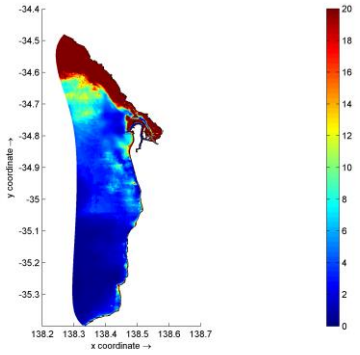

(b) Light (%SI, 60d rolling average)

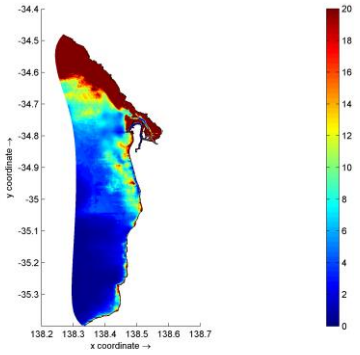

(c) Light (%SI, 180d rolling average)

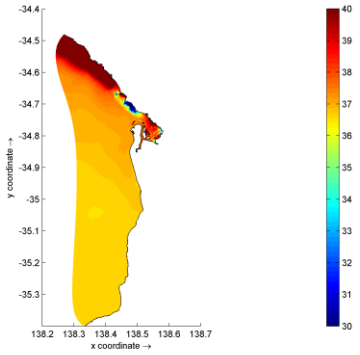

(d) Mean Salinity (ppt)

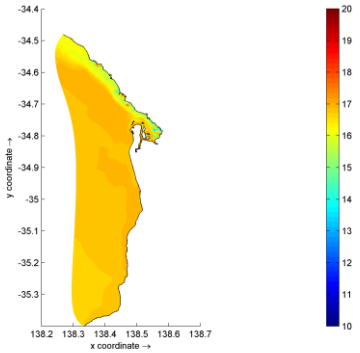

(e) Mean Temperature (°C)

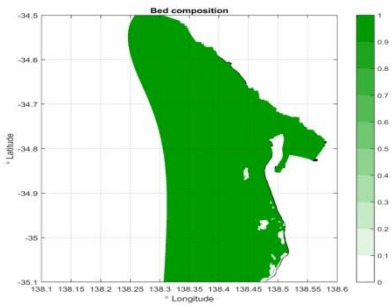

(f) Soft (1) / Hard (0) substrate

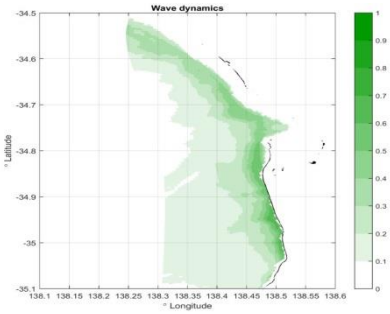

(g) Max Orbital Velocity (m/s)

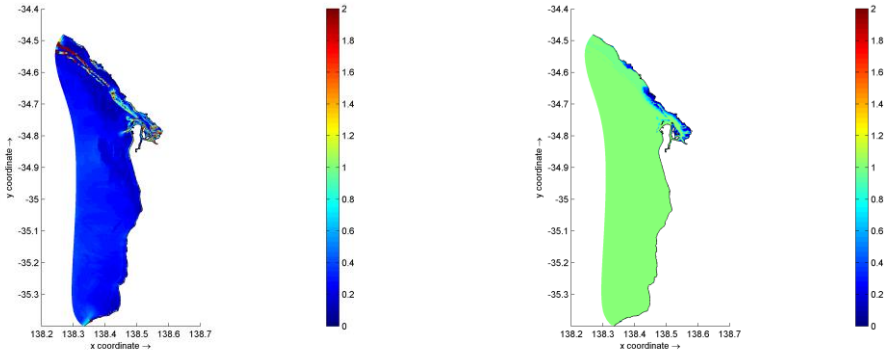

(h) Max velocity (m/s) (i) Rel. frequency depth > 10cm (-)

Figure 5.2 Simulated environmental conditions maps for the year 2011 that feed into the HSI calculation: (a) minimum of 30d rolling average of % of SI reaching the seagrass leaves; (b) idem for 60d; (c) idem for 180d; (d) mean annual salinity (ppt); (e) mean annual temperature (°C); (f) substrate; (g) maximum orbital velocity (m/s) with a 6 month return period, (h) maximum flow velocity (m/s); (i) mean tidal exposure, expressed as the relative frequency that a depth of 10 cm is exceeded.

5.2.5 Model evaluation

5.2.5.1 Comparison to 2013 observed seagrass cover

For evaluation of the seagrass habitat suitability model, the predicted habitat suitability for 2011 was compared to the Adelaide coastal waters seagrass presence/absence cover map for 2013 (Hart, 2013). This map (itself based on interpretation of aerial photography) was available at a 1x1m spatial resolution in areas with depth < 20m, north of Pt Gawler to Hallet Cove. These data were converted to a fraction of seagrass cover in all AREM grid cells. This provided a number *C* [0,1] in every grid cell. We compared this number to the simulated *HSI* for all species, which is also a number [0,1]. In every grid cell we calculated a goodness of fit (GOF) indicator, and mapped it. We also compiled a two-dimensional histogram showing the number of grid cells having a certain combination of values of *HSI* and *C* (subdivided in 10 equidistant classes each). The GOF indicator used is provided in Table 5.2. This GOF indicator expresses whether there is agreement between the values of *HSI* and *C*. Since both quantities have a range [0:1], we defined agreement, “true positives” and “true negatives” together, as a difference less than 0.5 and disagreement, “false positives” and “false negatives”, as a difference more than 0.5 or less than -0.5 respectively.

Table 5.2 Definition of habitat model goodness of fit indicator

GOF Indicator	Definition
true positive	$-0.5 < HSI - C < 0.5$
true negative	$-0.5 < HSI - C < 0.5$
false positive	$HSI - C > 0.5$
false negative	$HSI - C < -0.5$

5.2.5.2 1940 and 1975 scenarios

A further assessment of model credibility was carried out by running AREM with historical pollution loads equal to the estimated loads in the years 1940 and 1975. The year 1940 represents the situation preceding major seagrass losses, while the year 1975 represents a period of high coastal discharges with a significant seagrass loss observed along the central Adelaide coast between the 1971 and 1977 surveys.

The 1940 and 1975 loads have been reconstructed using reconstructed, simulated river flows derived from Wilkinson (2005). Concentrations of particles and nutrients for the year 1975 were derived from observations compiled by Wilkinson et al. (2005). For CDOM, the same values as in 2011 were used, in the absence of field data for 1975. Observations of river water concentrations were not available for any of the relevant substances for the year 1940. They were estimated on the basis of a compilation of estimated event mean concentrations associated with classes of land use and observed event mean concentrations from data collected by the Adelaide and Mount Lofty Ranges Natural Resources Management Board water quality monitoring network in Adelaide's rivers (Rouse et al., 2016). The results are shown in Figure 5.3 for total suspended solids, total nitrogen and total phosphorus. This figure shows the values for two specific land uses "forestry" and "open space" that we expect are most relevant for the 1940s situation. In all cases, these land uses produced low concentrations as compared to other land uses, which were in the low end of the range of values observed today. On the basis of this information, we adopted estimated concentrations for Adelaide's rivers in 1940 of 50 mg/L of total suspended solids, 1 mg/L of total nitrogen and 0.1 mg/L of total phosphorus. For UV-absorption representing CDOM we adopted a value of 0.15 cm^{-1}, which is a value in the low end of the range of values observed today. Concentrations and flows are then multiplied and the resulting loads are applied as modifications to the year 2011 simulation by scaling the loads.

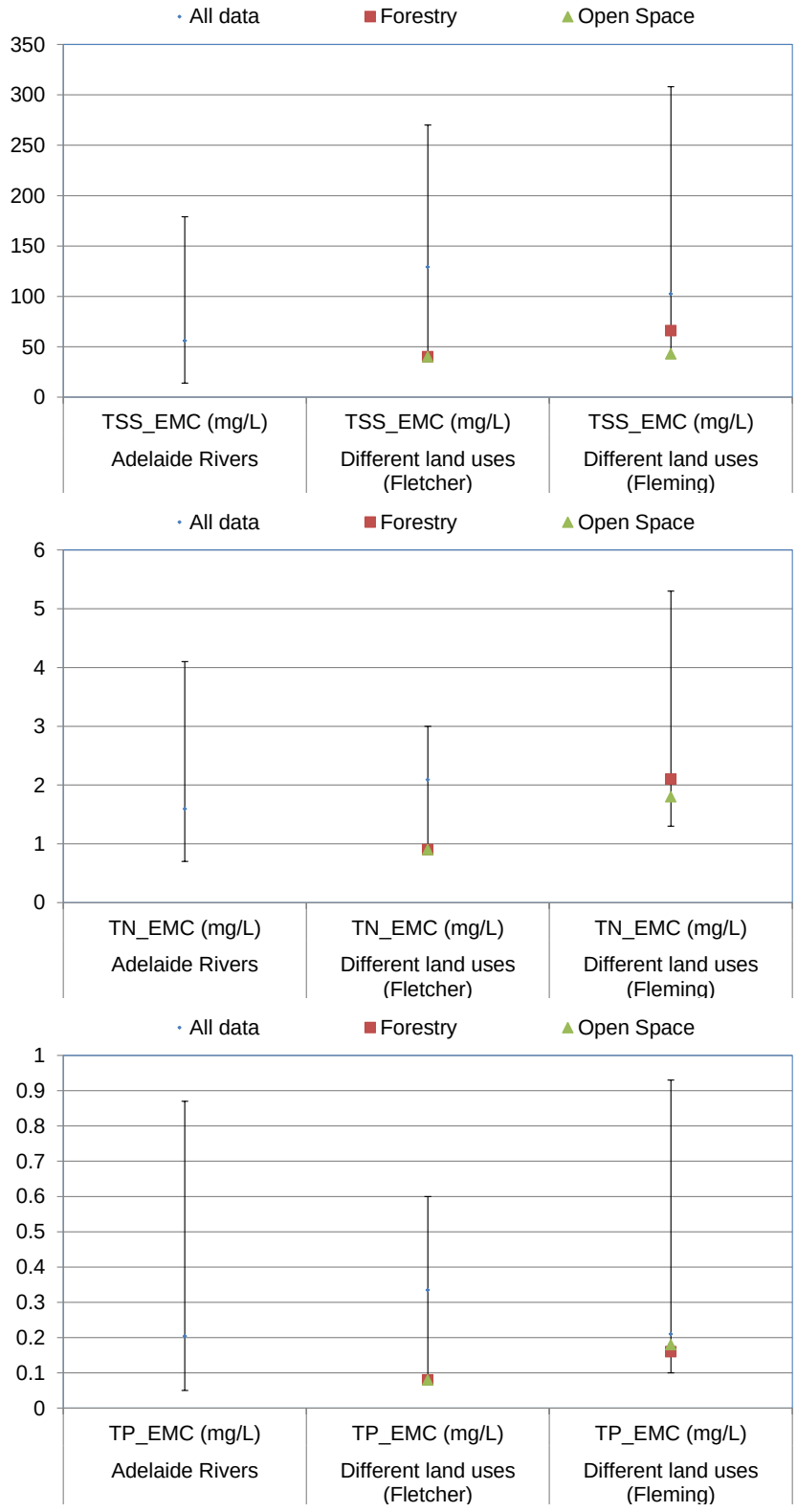

Figure 5.3 Overview of ranges of estimated Event Mean Concentrations (EMC) for different land uses (with Forestry and Open Space highlighted) according to Fletcher et al. (2004) and Fleming et al. (2010); range of observed EMCs in Adelaide's rivers (Rouse et al., 2016), for total suspended solids (TSS; top), total nitrogen (TN; middle) and total phosphorus (TP; bottom).

For the evaluation of the 1940 and 1975 scenario results, we made use of historical seagrass cover data from DEWNR (Hart, 1997), for the period 1949-1996. These data are available for a limited area in front of the Metropolitan coast (see Figure 5.4). The area covered by this map was divided into area without seagrass cover during 1949-1996 ("sand"), area with seagrass cover during 1949-1996, area where seagrass was lost in 1949-1977, area where seagrass was lost in 1977-1996 and area classified as rock. The map was sampled on a raster with 2m resolution and afterwards projected on the detailed model grid, to obtain fractions of each grid cell classified in the above way.

5.2.5.3 Load reduction scenarios

The sensitivity of the simulated HSI to various load reductions was explored. Firstly, a scenario equal to 2011 but without the Penrice loads was evaluated. This reflects a situation that currently exists, since the Penrice operation was actually stopped in 2013. Next, two scenarios were evaluated relative to the scenario without Penrice: one where all wastewater discharges are stopped and one where all stormwater and river water discharges are stopped. These are purely hypothetical scenarios, but they provide an understanding of sensitivity and indicate maximum achievable improvements by measures directed towards wastewater and stormwater management respectively.

The load reduction scenarios have been assessed graphically and in terms of tabulated spatial statistics. The area suitable for seagrass has been calculated in the study area, between Sellicks Beach in the south and 20 km north of Port Gawler (Figure 5.4). The assessment domain is limited to the inner part of the detailed model grid; it stays away from the model boundaries where the accuracy is expected to be reduced. The assessment domain is distributed in a north, middle and south part. The middle part encompasses the domain of the 1949-1996 seagrass change map. The north and middle parts are almost completely covered by the 2013 seagrass mapping. In these two parts, the spatial statistics distinguish between area not covered by the 2013 seagrass map, area with seagrass cover in 2013 and area without seagrass cover in 2013.

The area suitable for seagrass is calculated by scaling the surface area of a model cell by a weighing factor. This factor considers a threshold of HSI = 0.5 to separate unsuitable area from suitable area, and adopts a linear transition in the HSI range [0.25;0.75]. Therefore, areas with a HSI below 0.25 have a weighing factor equal to 0, areas with a HSI over 0.75 have a weighing factor of 1, and linear interpolation is applied in the HSI range [0.25;0.75].

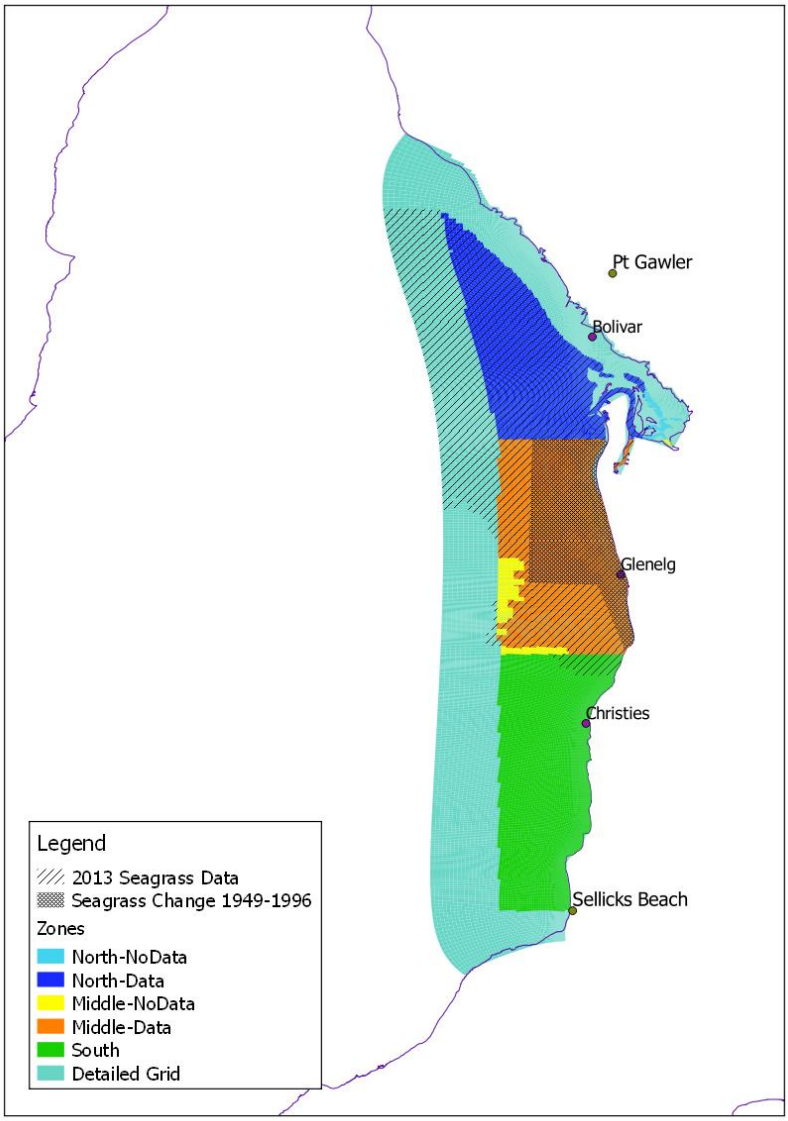

The North and Middle zones are subdivided in areas covered ("Data") and not covered ("NoData") by the 2013 seagrass mapping by Hart (2013).

Figure 5.4 Map showing North, Middle and South study area zones and areas covered by the 2013 seagrass mapping (Hart, 2013) and 1949-1996 seagrass change mapping (Hart,1997).

5.2.5.4 *Resuspension and seagrass cover*

The sensitivity of the HSI under present conditions (with and without Penrice discharges) was analysed under the assumption that resuspension does not occur in areas where seagrass cover was present in 1949. Historical seagrass maps are available for a limited geographical extent only. The baseline resuspension critical shear stress map (Figure 4.12) was adapted in grid cells where the historical map indicated that seagrass was present in 1949 but was subsequently lost. Depending on the fraction of the grid cell covered, the critical shear stress was given a value between 1 N m^{-2} (bare sand) and 10 N m^{-2} (100% seagrass cover). The change implemented in the baseline resuspension critical shear stress map is shown in Figure 5.5.

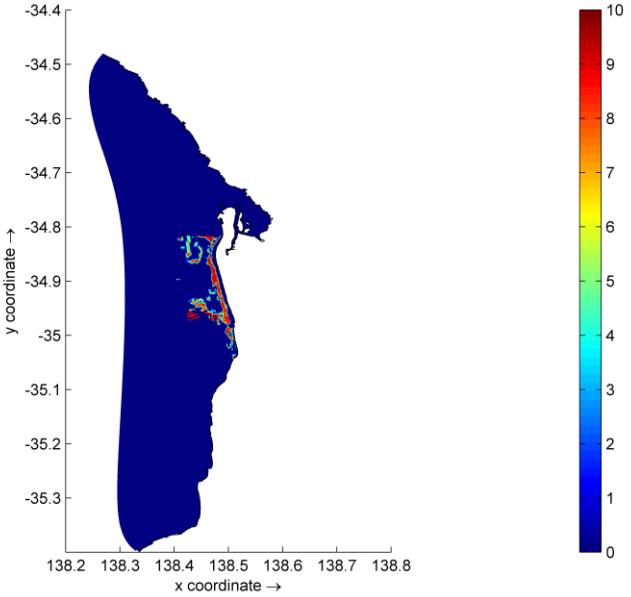

Figure 5.5 Change of critical shear stress for resuspension (N m^{-2}) in 1949 relative to 2011.

5.3 Results

5.3.1 2011 baseline scenario

The simulated habitat suitability map for 2011 is shown in Figure 5.6. This map is the overall result of an evaluation of the HSI for nine individual species, and shows the maximum HSI for any of the species in any grid cell. Figure 5.7 shows a map of the “most suitable species” (i.e. the species with the highest calculated HSI), while Figure 5.8 shows the most limiting environmental factor for the most suitable species in 2011. We note that in cells where two or more species are the most suitable, the first one is shown in the most suitable species map. This occurs typically in cells where two or more species have a HSI equal to 1. The map of the most limiting environmental factor for the most suitable species shows a result also in cases where the HSI is close to 1 and there is not really any environmental factor limiting the HSI. This results in temperature often being the limiting environmental factor in area with high HSI. In cells where two or more environmental factors are the most limiting for the most suitable species, the first one is shown in the map. The definition of the “first” species or “first” environmental factor is coincidental and is determined by the order of the species and the environmental factors in the input file of the HSI model.

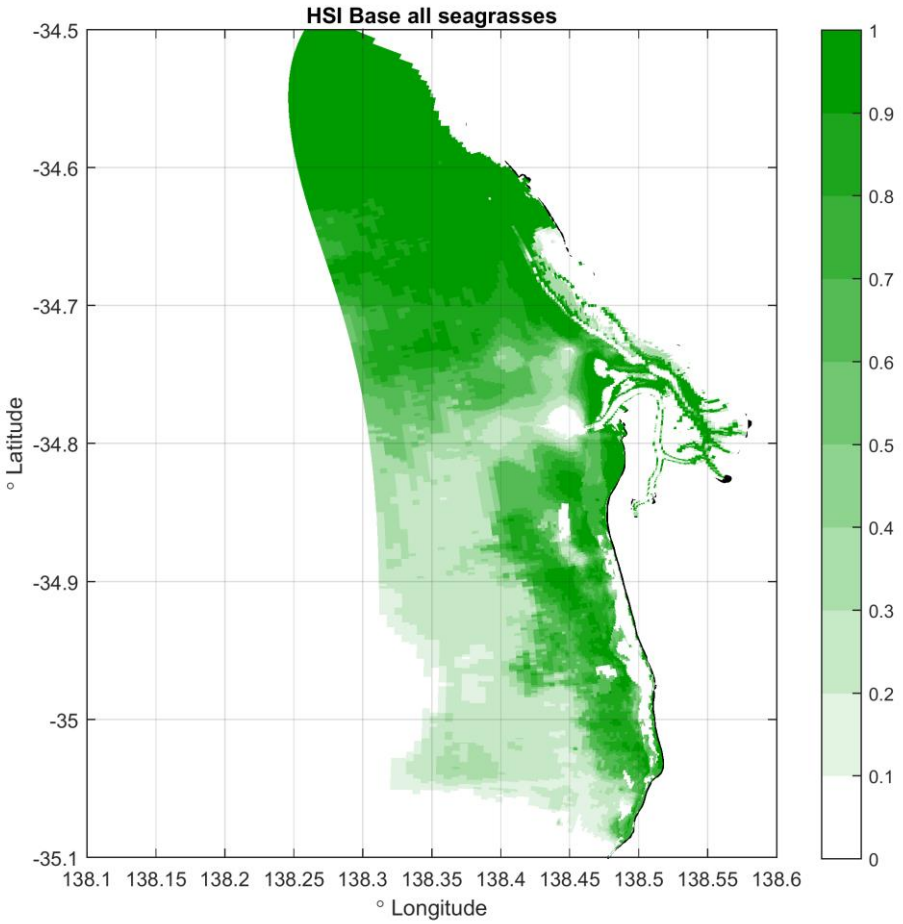

Figure 5.6 Simulated habitat suitability index in 2011

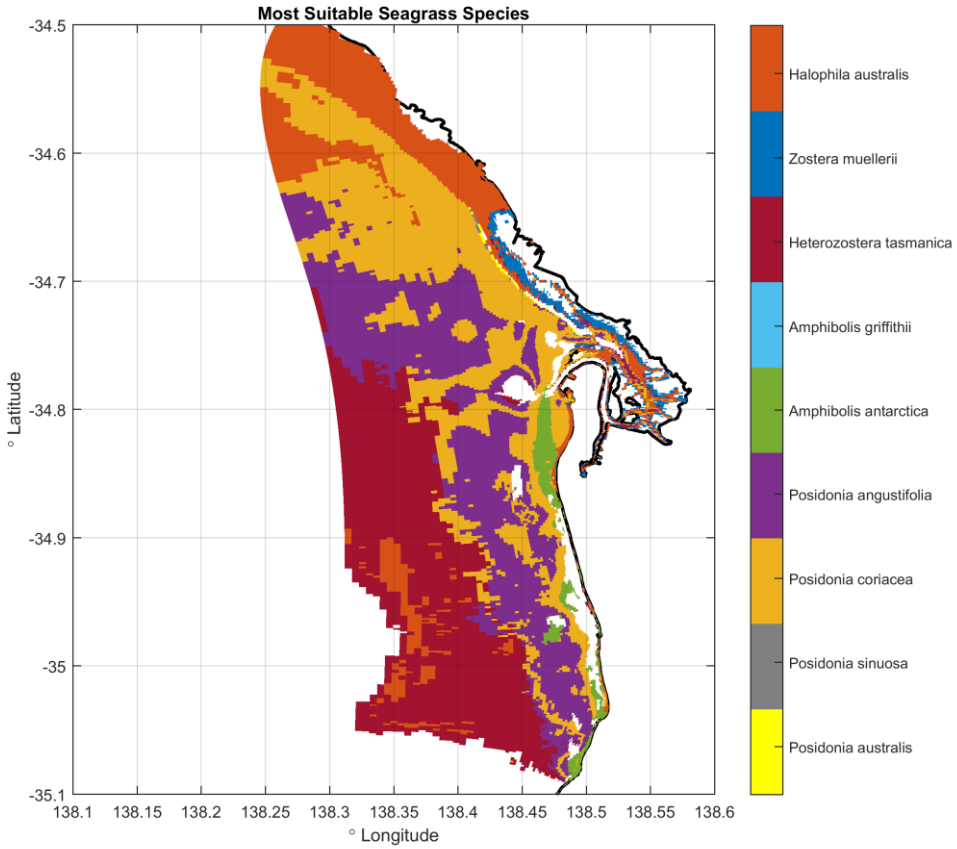

Figure 5.7 Simulated most suitable species (species with highest HSI) in 2011

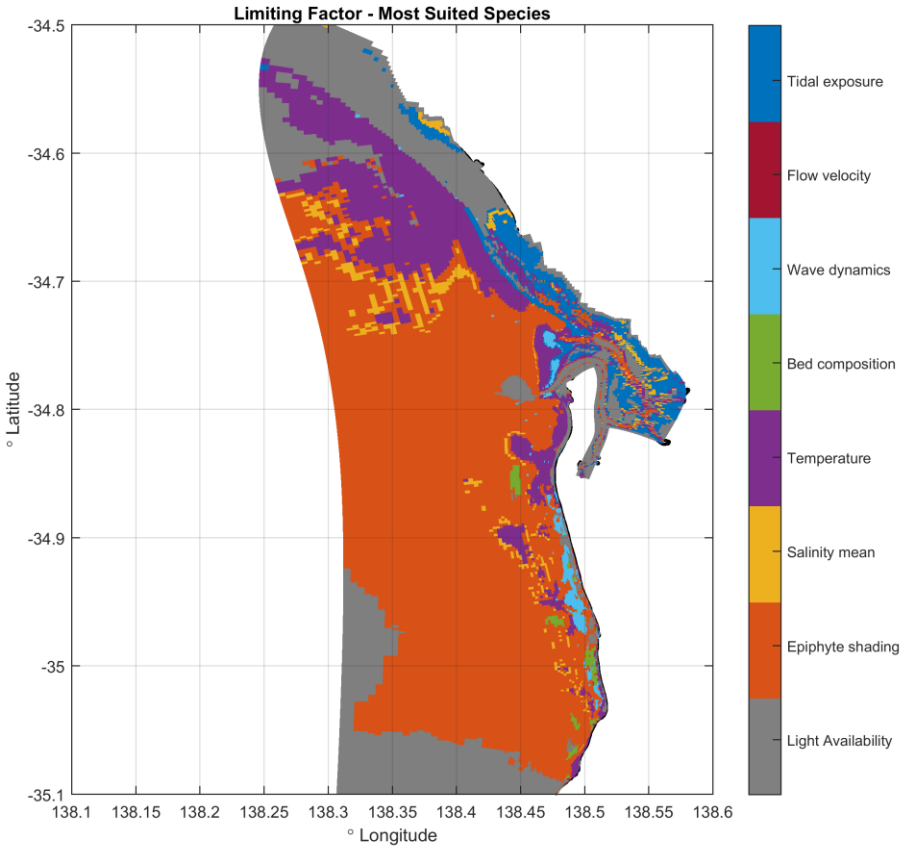

Figure 5.8 Limiting environmental factor for most suitable species (species with highest HSI) in 2011

The HSI shows areas with clearly reduced habitat suitability, both close to shore and in deep waters (Figure 5.6). In the deeper parts, light availability is limiting habitat suitability (Figure 5.8). In the intertidal areas, tidal exposure is a limiting factor. There are also areas close to shore where light availability is a limiting factor, due to local turbidity. This concerns in particular the area in front of the mouth of Port River, and parts of the Metropolitan coast. Along the Metropolitan coast, extreme waves also limit habitat suitability in certain areas. The presence of hard substrate locally reduces habitat suitability as compared to the surrounding sandy substrate. In general, *Posidonia* spp. appear to be the best suited species in the largest part of the domain (Figure 5.7). Close to the Metropolitan coast, there are some places where A*mphibolis antarctica* is the most suitable species.

A further interpretation of the model results in terms of the limiting environmental conditions can be done taking into account the results for the individual species. Plots of the calculated HSI per species as well as the most limiting environmental parameter per species are collected in Appendix G. *Amphibolis antarctica* has a low suitability along most of the Metropolitan coast. It is limited by light and by tidal exposure in shallow areas, but not limited by substrate and does not appear to be sensitive to extreme wave action. *Amphibolis griffithii* has a lower HSI because of the higher light requirements, but shows a similar pattern of limitations. *Halophila australis* shows a zero HSI close to shore because of extreme waves limitation. In deeper waters, it shows a moderate HSI because of the very favourable lower light limit of only 2%. *Heterozostera tasmanica* shows a very similar picture, also with a

favourable lower light limit of 2.5%, while it is limited by salinity along the coast in the north part of the model domain. The latter two species are adapted to some tidal exposure and this limitation is therefore less relevant. The *Posidonia* species are all limited by light, but the limitation appears to be less restrictive than for the previously discussed species because they respond to the 180 days rolling average and are therefore not affected by shorter scale light fluctuations. All *Posidonia* are limited by tidal exposure in shallow areas, and by wave action close to shore. *Posidonia angustifolia* and *Posidonia australis* show very similar results. *Posidonia coriacea* is less sensitive to extreme waves and therefore has a higher HSI close to shore. *Posidonia sinuosa* has stricter light requirements than the other *Posidonia* and therefore generally has a lower HSI. Finally, *Zostera muellerii* is limited by light, wave action and salinity, and has a high HSI only in areas which are exposed during low tides.

5.3.2 2011 baseline scenario vs. 2013 observed seagrass cover

Figure 5.9 shows an overlay of the observed seagrass cover in 2013 (1m resolution data projected on model grid) in shades of green and simulated HSI in shading patterns. The agreement between simulated HSI and observed seagrass cover is quantified by maps of the goodness of fit (GOF) indicator in Figure 5.10. The statistics of the agreement between simulated HSI (2011) and observed seagrass cover (2013) are collected in Table 5.3. Table 5.4 tabulates a two-dimensional histogram of simulated HSI (2011) and observed seagrass cover (2013). This table also illustrates how the GOF indicator is defined by using different cell shading.

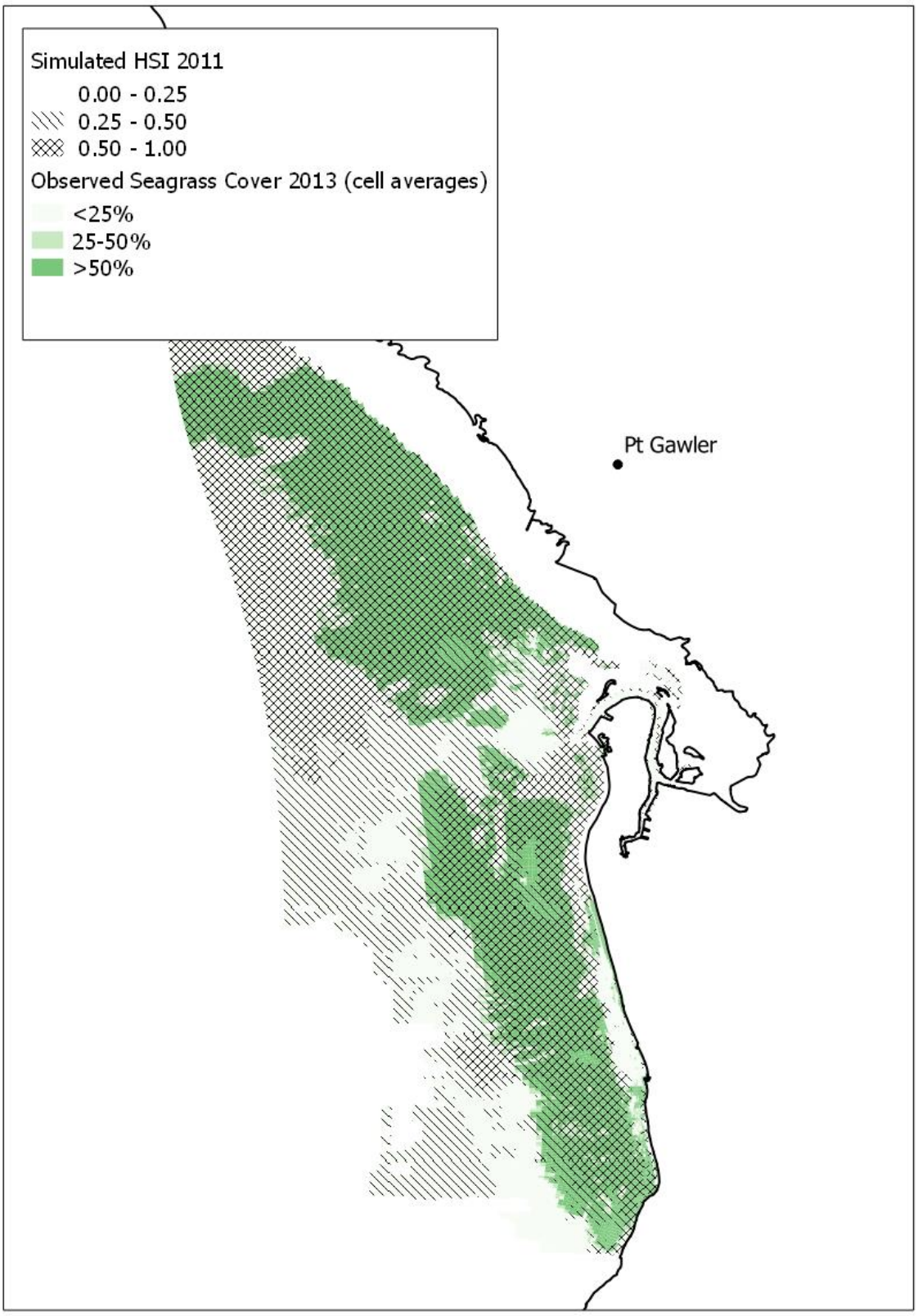

Figure 5.9 Overlay of observed seagrass cover in 2013 (1m resolution data projected on model grid) in shades of green and simulated HSI in shading patterns.

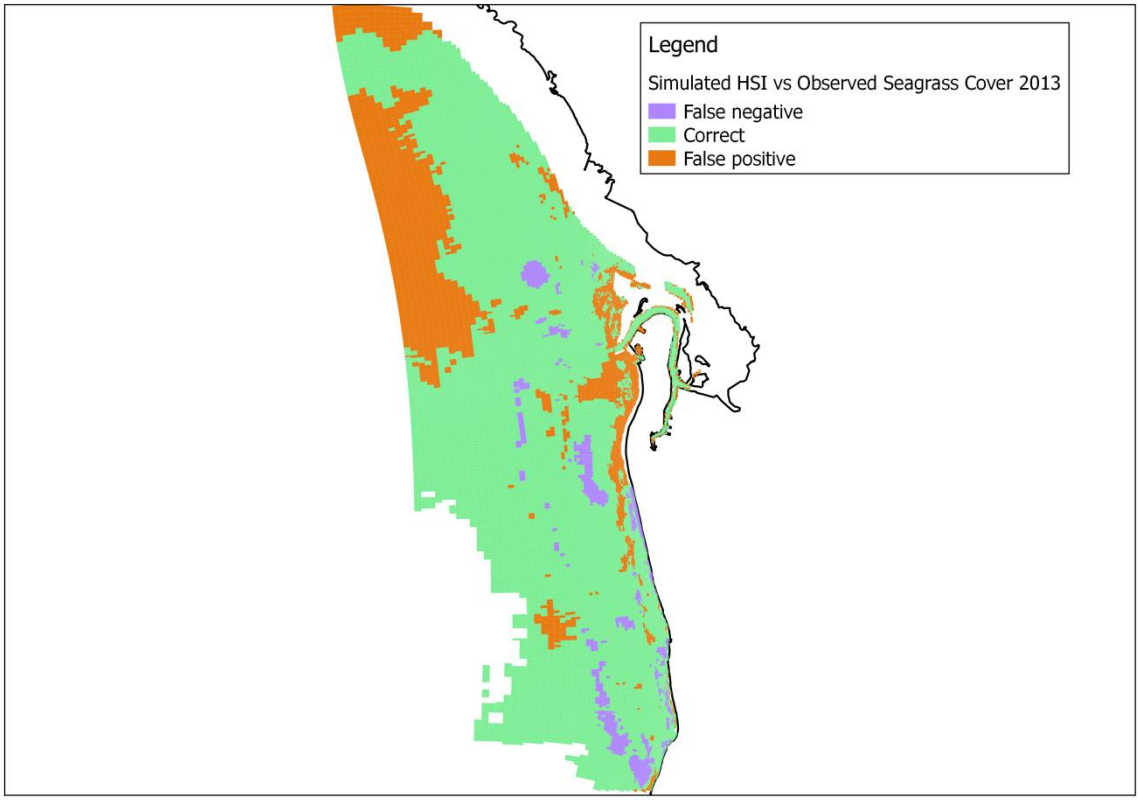

Figure 5.10 Goodness of fit indicator showing the agreement / disagreement between observed seagrass cover and simulated HSI.

Table 5.3 Statistics of agreement between simulated HSI (2011) and observed seagrass cover (2013).

	Cell count GOF	
Correct (true positive and negative)	13811	72%
False Positive	4157	22%
False Negative	1180	6%
Total	19148	100%

Table 5.4 Two-dimensional histogram (cell count) of simulated HSI (2011) and observed seagrass cover (2013)

	Observed seagrass cover in 2013									
HSI 2011	<10%	<20%	<30%	<40%	<50%	<60%	<70%	<80%	<90%	>90%
<0.1	1442	95	83	53	46	68	59	59	64	307
<0.2	306	13	6	1	3	1	4	3	5	16
<0.3	1909	61	38	34	23	26	33	29	38	159
<0.4	1079	78	49	34	56	48	54	61	60	157
<0.5	387	53	55	46	46	43	44	45	64	248
<0.6	472	24	18	18	20	21	27	34	54	133
<0.7	660	91	84	81	71	73	105	129	212	724
<0.8	637	85	58	74	82	72	103	128	176	663
<0.9	542	94	62	74	62	82	110	105	218	1090
>0.9	1039	154	143	115	159	158	134	139	244	1604

shading of cells illustrates GOF indicator: blue = false negative, orange = false positive, no colour = correct

The comparison between observed seagrass cover and simulated HSI in terms of the GOF indicator shows a wide band of cells along the coast where the presence or absence of seagrass coincides with a corresponding high or low simulated HSI (green colour in Figure 5.10). Close to shore, along the northern part of the Metropolitan coast, there are areas where a high HSI coincides with no or limited seagrass cover (orange colour in Figure 5.10). Also close to shore, but mostly along the southern part of the Metropolitan coast, there are areas where a low HSI coincides with the presence of seagrass (purple colour in Figure 5.10). Further offshore, in the north, there are areas where a higher HSI coincides with no or limited seagrass cover (orange colour in Figure 5.10). The cell counts show 72% of green cells, 22% of orange cells and 6% of purple cells.

In general, differences between the simulated HSI and the actual seagrass distribution may indicate:

1 model errors or inaccuracies;
2 model omissions (i.e. due to another factor or a localised perturbation not captured in the present model set-up);
3 seagrass mapping errors;
4 areas likely to decline (false negatives) or recover (false positives) over the next few years.

The false negatives (purple areas) are often areas where substrate or extreme waves are limiting the HSI. It is possible that these environmental conditions have not been quantified accurately enough or that the sensitivity of seagrass has been overestimated. This does not affect the fitness for use of the model, since it does not concern the relation between coastal discharges and seagrass habitat suitability.

The false positives far from shore could have been caused by modelling inaccuracies. This occurs in the shallower parts up north. This area is actually far away from Adelaide's discharges and close to the detail model boundary. The water quality there is governed by larger scale phenomena, which we did not include in the modelling. This could be fixed by applying a different boundary condition. It does not affect the fitness for use of the model, since it does not concern the inshore areas where seagrass has been lost.

The false positives close to shore could indicate areas without seagrass cover due to losses in the past, which are now again suitable for seagrasses recolonisation due to load reductions. They could also indicate losses due to other (anthropogenic) causes that were not taken into consideration in the model (e.g. impacts from dredging, damage from bottom trawling etc.). Of course, they may also indicate model or mapping inaccuracies.

5.3.3 1940 and 1975 scenarios

The estimated loads of suspended solids (SS) and nitrogen (N) in 1940 and 1975 are shown and compared to the 2011 load inventory data in Figure 5.11. The 1975 loads are more than double the 2011 loads for both SS and N. The 1940 loads are 2.5 times smaller than the 2011 loads for SS and 20 times lower for N. The latter is mostly due to the fact that no wastewater was discharged in 1940.

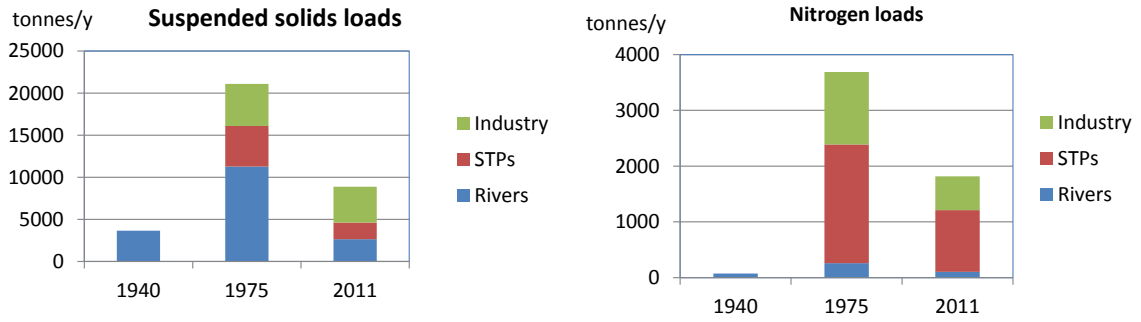

Figure 5.11 Overview of total loads of suspended solids (left) and nitrogen (right) for rivers, wastewater treatments plants and industry for the 2011 baseline, 1940 and 1975 scenarios.

The simulated habitat suitability map for the 1940 scenario is shown in Figure 5.12, the map of the "most suitable species" in Figure 5.13 and the map of the limiting stressor for the most suitable species in Figure 5.14. The simulated habitat suitability map for the 1975 scenario and the map of the "most suitable species" and the limiting stressor for that scenario are shown in Figure 5.15, Figure 5.16 and Figure 5.17 respectively.

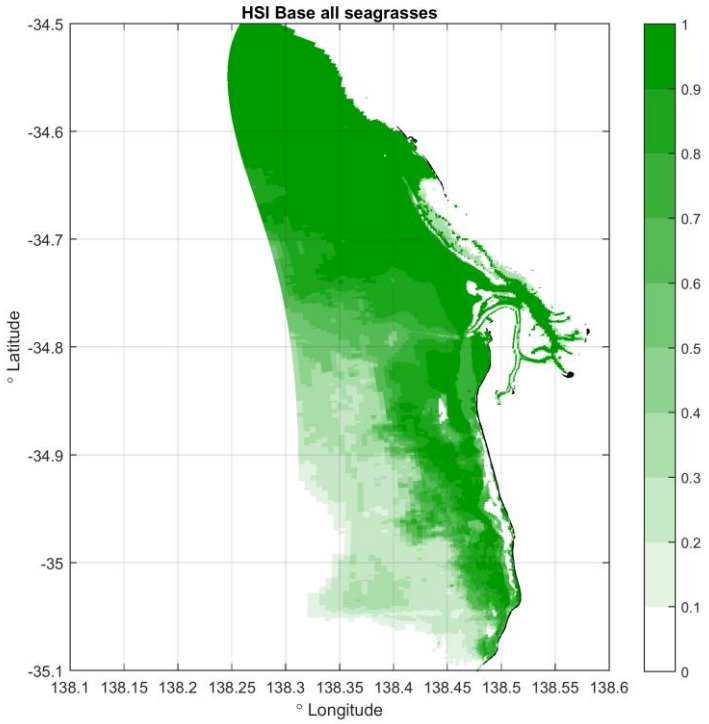

Figure 5.12 Simulated habitat suitability index for the 1940 scenario

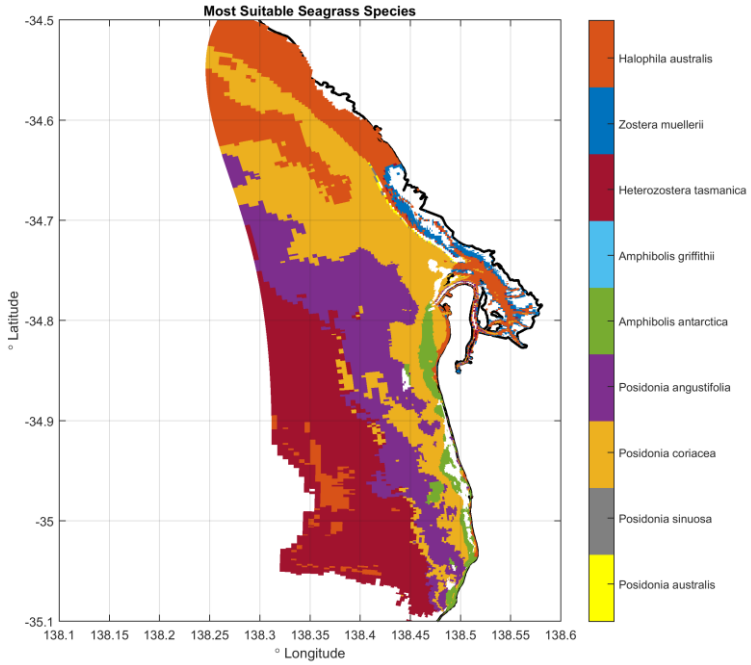

Figure 5.13 Simulated most suitable species (species with highest HSI) in the 1940 scenario

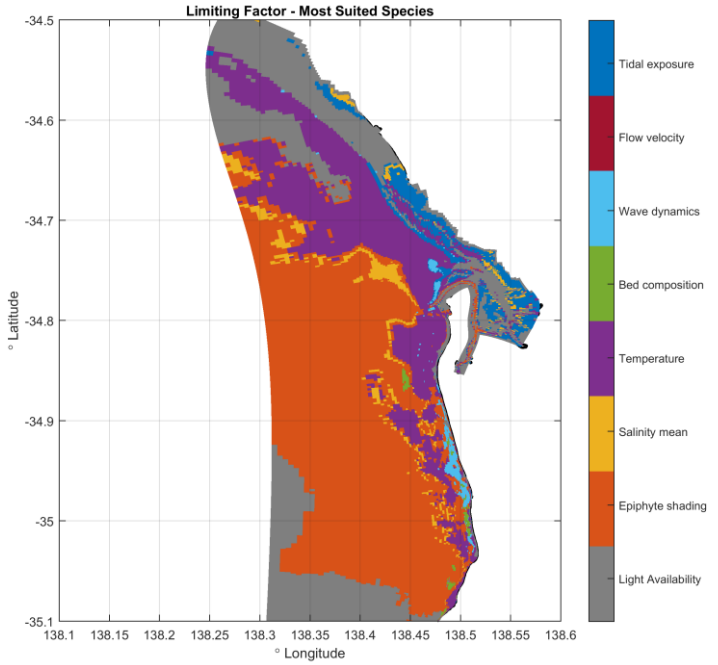

Figure 5.14 Limiting environmental factor for most suitable species (species with highest HSI) in the 1940 scenario

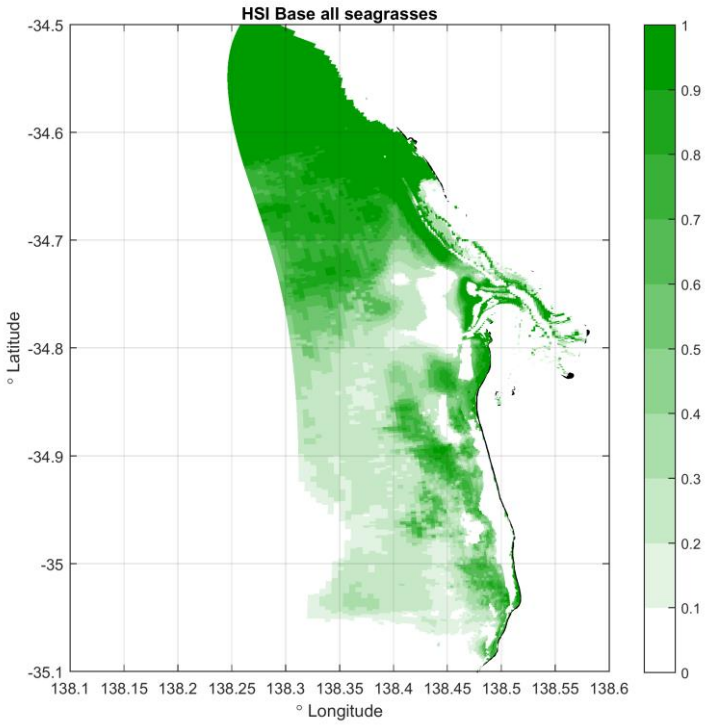

Figure 5.15 Simulated habitat suitability index for the 1975 scenario

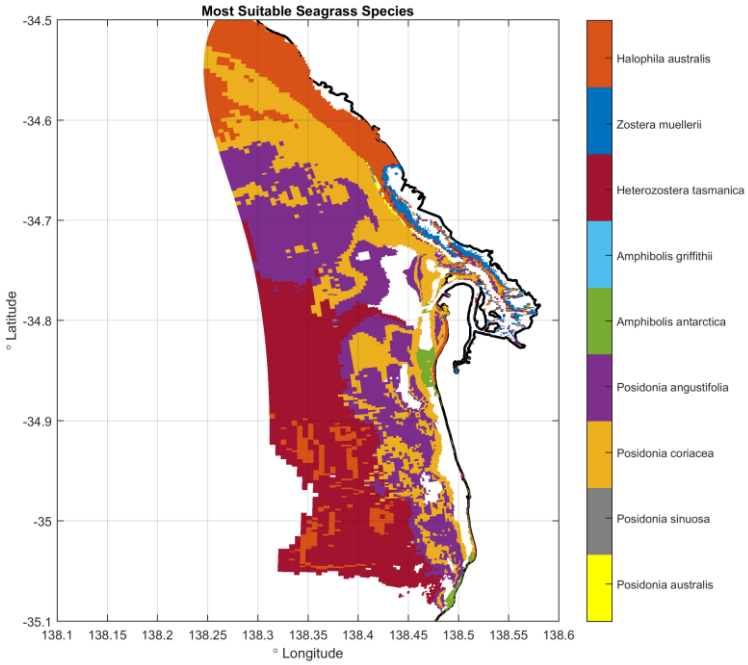

Figure 5.16 Simulated most suitable species (species with highest HSI) in the 1975 scenario

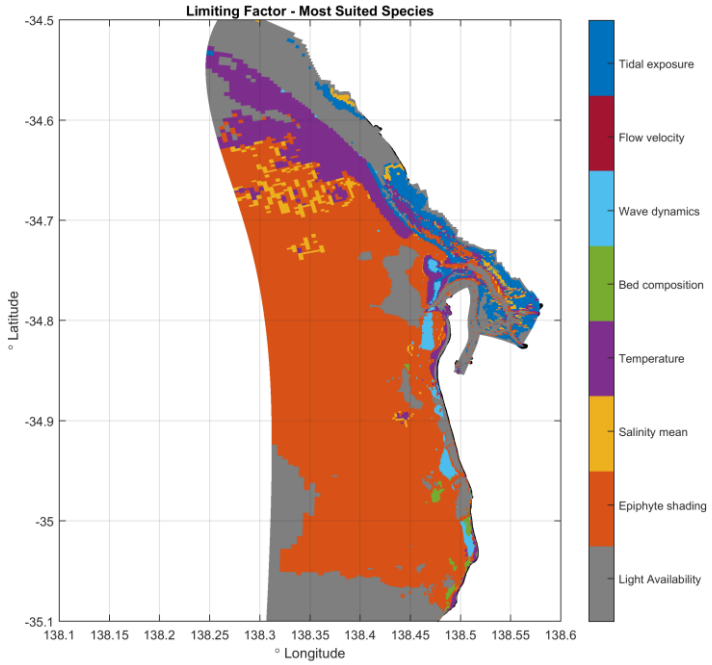

Figure 5.17 Limiting environmental factor for most suitable species (species with highest HSI) in the 1975 scenario

The simulated HSI from the 1940 and 1975 scenarios has been compared to historical seagrass cover data from DEWNR (Hart, 1997). In particular, we plotted the earliest observed seagrass cover along the Metropolitan coast from a 1949 survey, and coloured brown those areas which were observed to be lost in subsequent surveys up to 1977. The result is shown in Figure 5.18 and Figure 5.19.

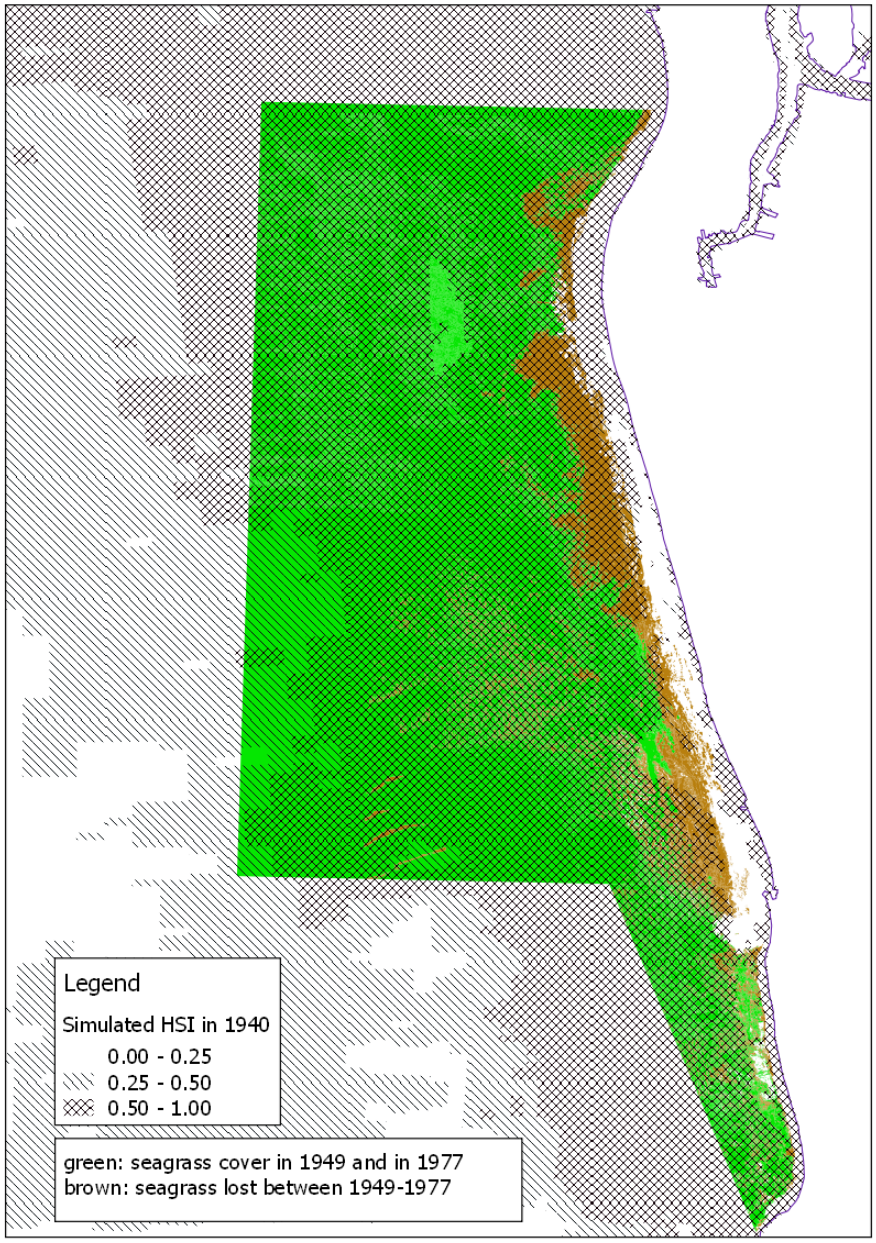

Figure 5.18 Simulated HSI for the 1940 scenario compared to observed seagrass cover in 1949 and seagrass area lost between 1949 and 1977 along the Metropolitan coast.

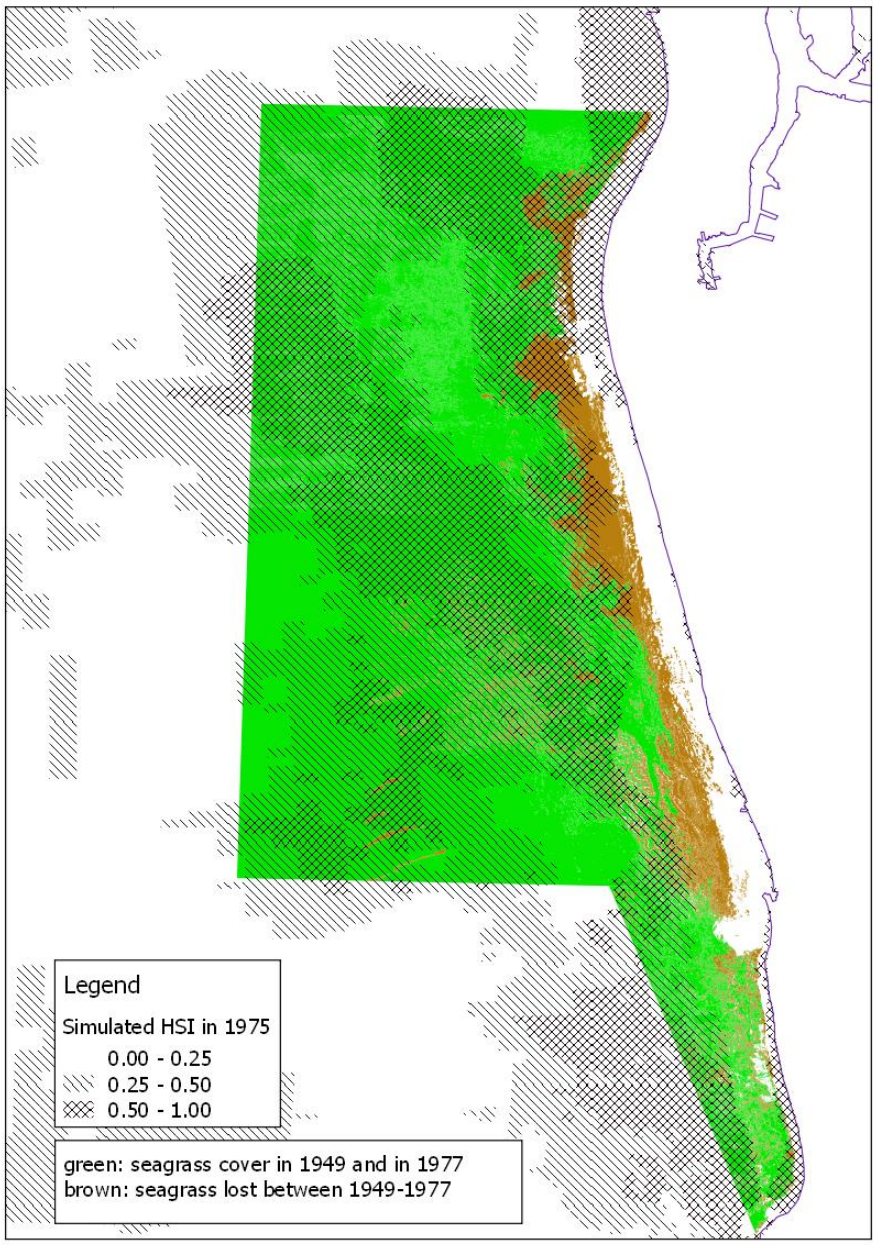

Figure 5.19 Simulated HSI for the 1975 scenario compared to observed seagrass cover in 1977 and seagrass area lost between 1949 and 1977 along the Metropolitan coast.

In Table 5.5 we show the predicted area suitable for seagrass for the present, 1940 and 1975 time horizons in the area covered by the 1949-1996 seagrass change map (as shown in Figure 5.18). We refer to section 5.2.5.3 for an explanation how these numbers are calculated.

Table 5.5 Predicted area suitable for seagrass for the present, 1940 and 1975 time horizons in the area covered by the 1949-1996 seagrass change map (as shown in Figure 5.18).

Class	**Total**	**2011**		**1940**		**1975**	
1949-1996 change	Area (ha)	Suitable (ha)	%	Suitable (ha)	%	Suitable (ha)	%
Sand always	1232	558	45%	704	57%	419	34%
Seagrass always	9901	7473	75%	8645	87%	4459	45%
Seagrass lost 1949-1977	1698	1054	62%	1316	78%	590	35%
Seagrass lost 1977-1996	2104	1675	80%	1949	93%	869	41%
Rock	87	11	12%	26	30%	1	1%
Total	15022	10769	72%	12641	84%	6338	42%

The 1940 scenario shows smaller areas with low HSI close to shore than the 2011 scenario. In particular, the area suitable for seagrass in the area where seagrass was lost between 1949 and 1977 (brown colour in Figure 5.18) increases from 62% to 78% (Table 5.5). In the total 1949-1996 seagrass change map extent this percentage is 72% in 2011 and 84% in 1940. This is due to the smaller discharges in 1940, which have a smaller negative impact on the light available for seagrasses, as illustrated by the limiting stressor map. Again, *Posidonia* spp. come out as the best suited species in the largest part of the domain. In this case, there is a more or less continuous strip with A*mphibolis antarctica* as the most suitable species close to and along the Metropolitan coast. The areas with low HSI have mostly waves or substrate as the limiting environmental condition.

The simulated HSI in the 1975 scenario is low over larger areas than in 2011. The simulated area suitable for seagrass in the 1949-1996 seagrass change map extent is 72% in 2011 and 42% in 1975 (Table 5.5). In the area where seagrass was lost between 1949 and 1977, this percentage is 62% in 2011 and 35% in 1975. This is due to the much higher discharges in 1975, which have a negative impact on the availability of light for seagrasses, as illustrated by the limiting stressor map.

According to the 1940 scenario results, 78% of the seagrass area lost between 1949 and 1977 (brown colour) is suitable for seagrass (Table 5.5). According to the 1975 scenario results, this percentage drops to 35% (Figure 5.19).

However, the 1940 simulated HSI and the 1949 observed seagrass cover show some differences (Figure 5.18). In some places the simulated HSI is high right up to the beach. In other places, areas that are covered with seagrass have low HSI. This is caused by inaccuracies in the predicted extreme waves and the sensitivity of seagrass to these waves and by mapping inaccuracies. In addition, this simulation uses 2013 seagrass cover to model resuspension and thus overestimates resuspension locally.

The 1975 simulated HSI and the 1977 observed seagrass cover show some differences (Figure 5.19). In particular, there are some seagrass covered areas with low simulated HSI. It is unlikely that seagrasses would not yet have responded to low habitat suitability over quite large areas after a period of more than 2 years. Apparently, the response of the model to the 1975 estimated discharges is stronger than the actual response of the real system was to the actual discharges. This could be caused either by inaccurate estimates of the 1975 loads, or by inaccuracies in the AREM sediment, biogeochemical and habitat models, or by a combination of both, possibly worsened by the inherent inaccuracies in the mapping data. The simulated amount of resuspended sediment in 1975 could for example be wrong,

because a 1975 seagrass cover map covering the whole model domain is lacking and we had to use the 2013 map. A complicating factor for model evaluation is the non-linear response of the habitat suitability model to changes in the environmental factors (so-called “tipping points”). This implies that a relatively small inaccuracy in one of the predicted environmental factors can lead to a large error in the predicted HSI if the value of the environmental factor in question is close to such a tipping point.

5.3.4 Load scenario sensitivity assessments

Figure 5.20 and Figure 5.21 show the simulated HSI and the limiting stressor for a situation equal to 2011, but with the Penrice load stopped. Figure 5.22 shows the difference between the simulated HSI with and without the Penrice discharges, overlain with the 2013 seagrass map.

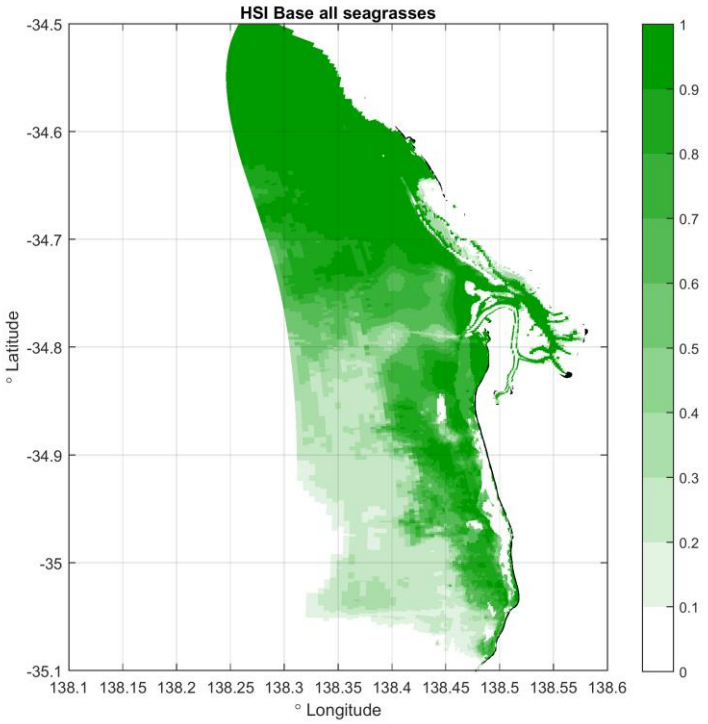

Figure 5.20 Simulated habitat suitability index for the 2011 scenario without the Penrice loadings

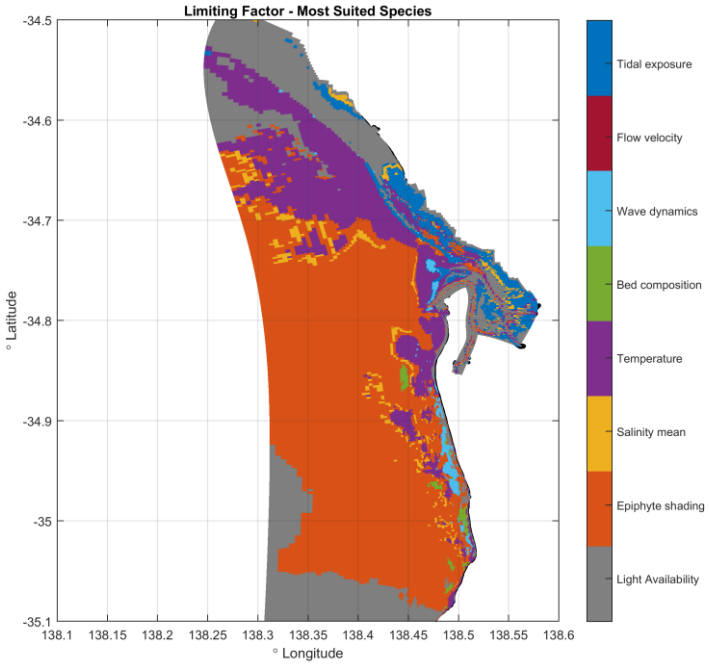

Figure 5.21 Limiting environmental factor for most suitable species (species with highest HSI) for the 2011 scenario without the Penrice loadings

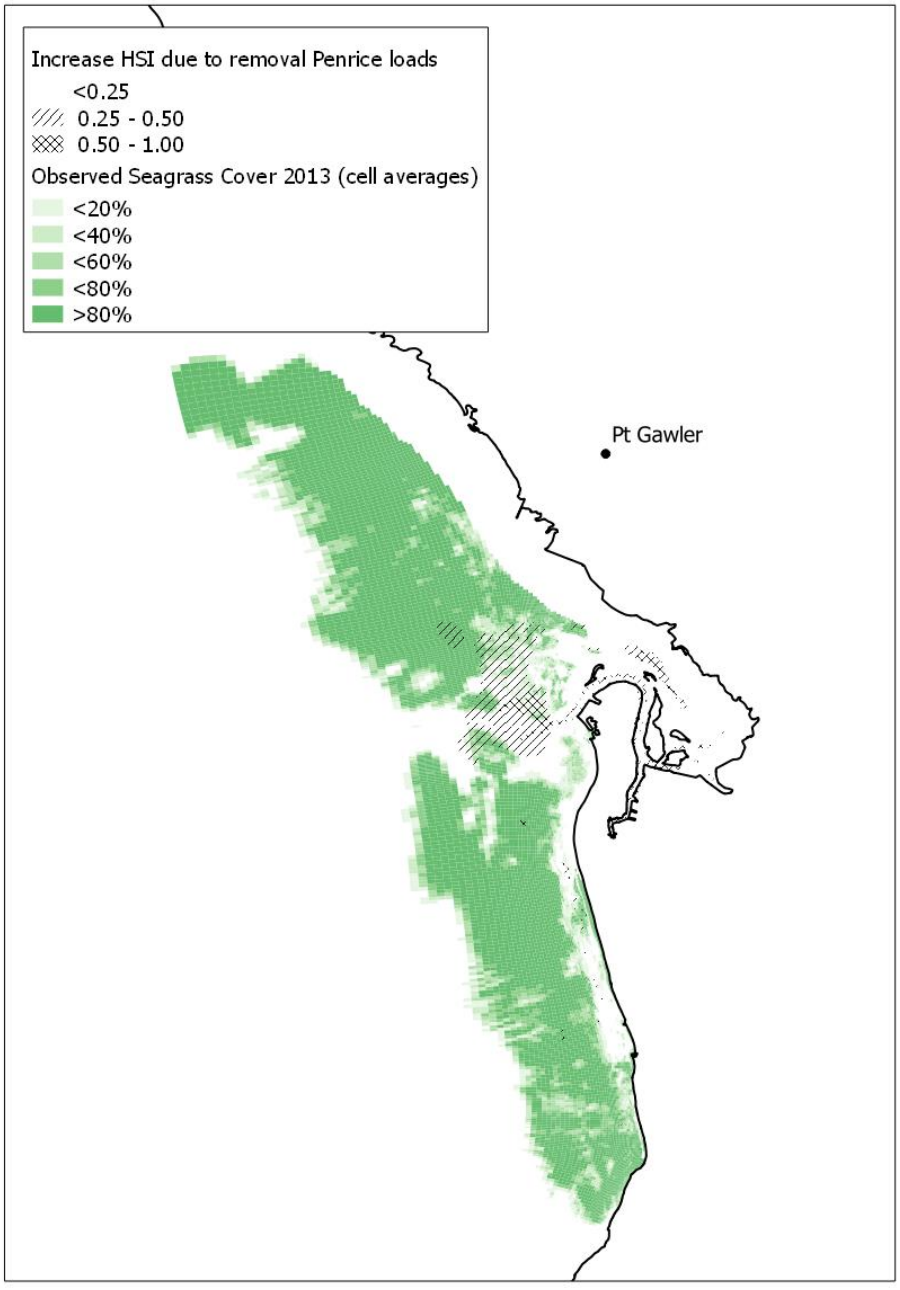

Figure 5.22 Overlay of observed seagrass cover in 2013 (1m resolution data projected on model grid) in shades of green and increase of simulated HSI after removal of Penrice loads in shading patterns.

Figure 5.23 and Figure 5.26 show the overall HSI maps for the scenarios without wastewater loads and without river loads respectively. Figure 5.24 and Figure 5.27 show the limiting stressor maps for these scenarios. Figure 5.25 and Figure 5.28 show the differences relative to the scenario where the Penrice load has been removed.

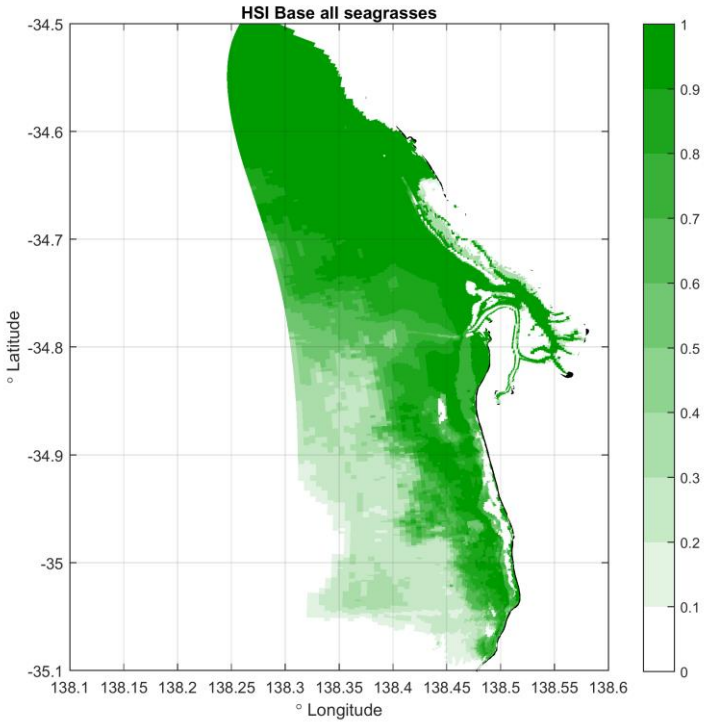

Figure 5.23 Simulated habitat suitability index for the 2011 scenario without the Penrice loadings and all wastewater discharges

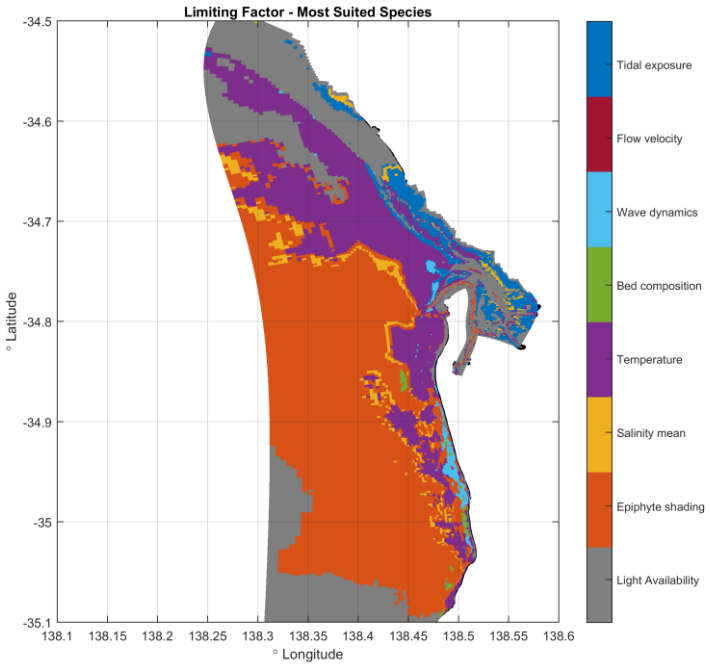

Figure 5.24 Limiting environmental factor for most suitable species (species with highest HSI) for the 2011 scenario without the Penrice loadings and all wastewater discharges

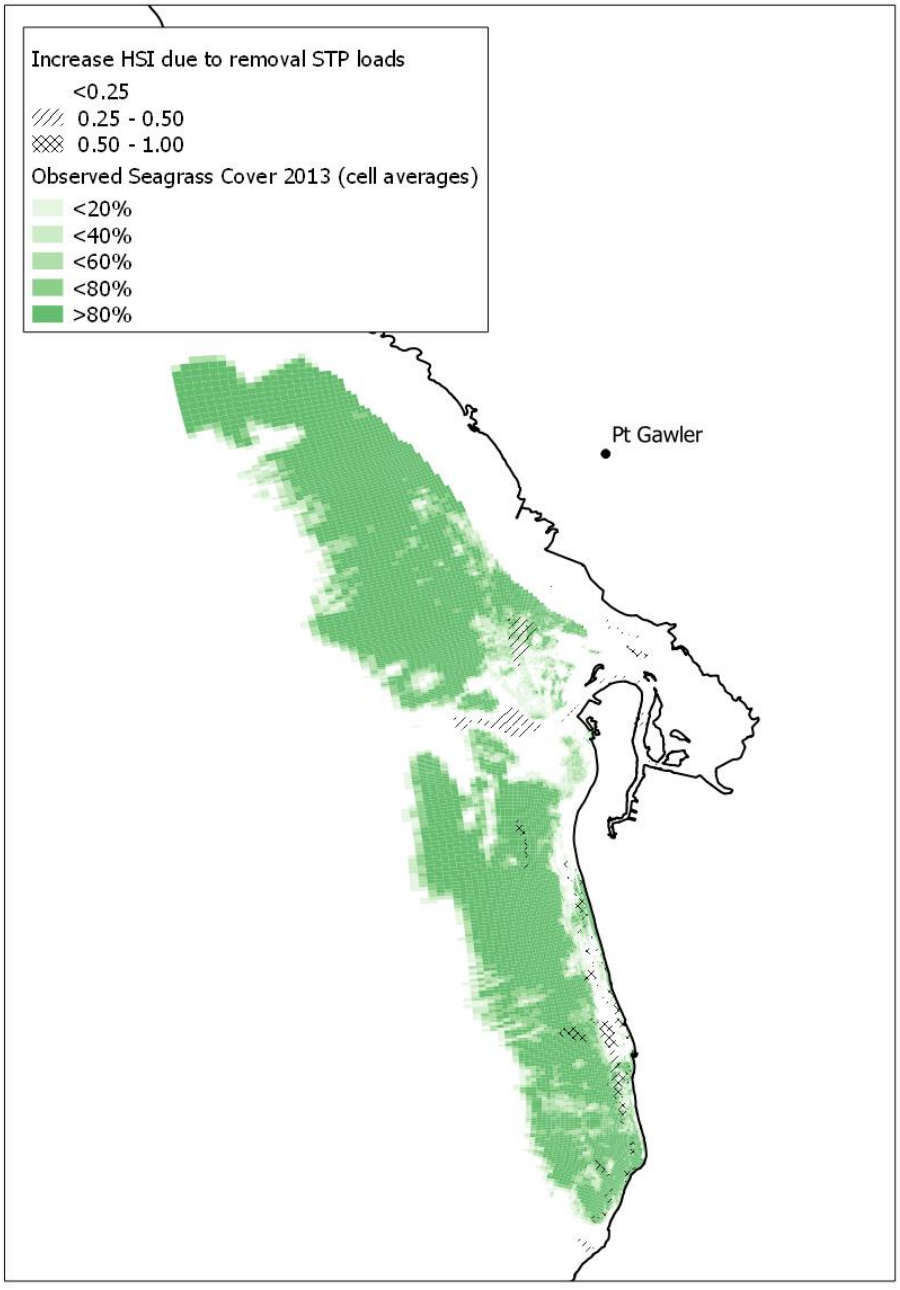

Figure 5.25 Overlay of observed seagrass cover in 2013 (1m resolution data projected on model grid) in shades of green and increase of simulated HSI after removal of wastewater loads relative to a situation without Penrice loads in shading patterns.

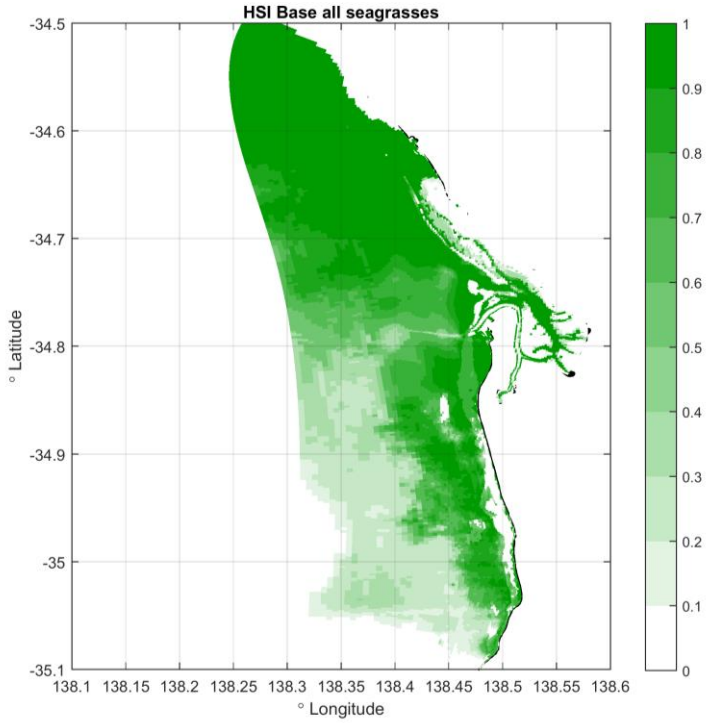

Figure 5.26 Simulated habitat suitability index for the 2011 scenario without the Penrice loadings and all river and stormwater discharges

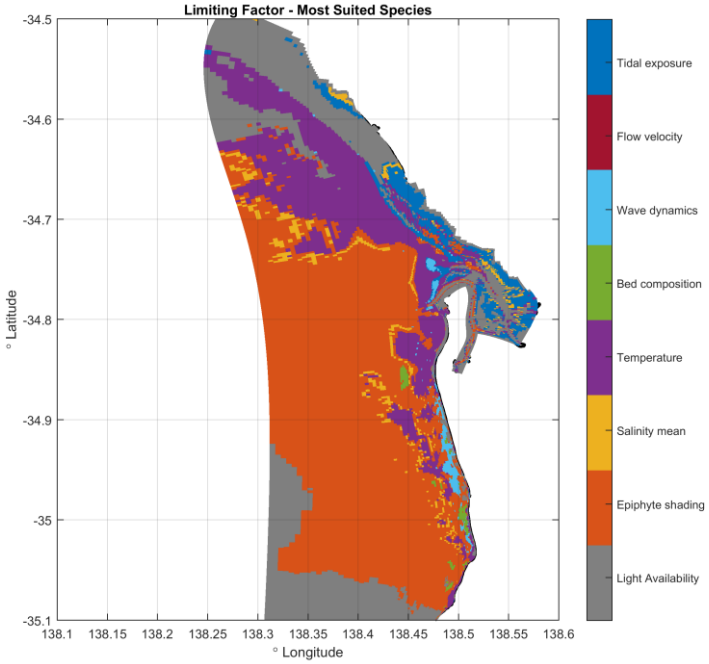

Figure 5.27 Limiting environmental factor for most suitable species (species with highest HSI) for the 2011 scenario without the Penrice loadings and all river and stormwater discharges

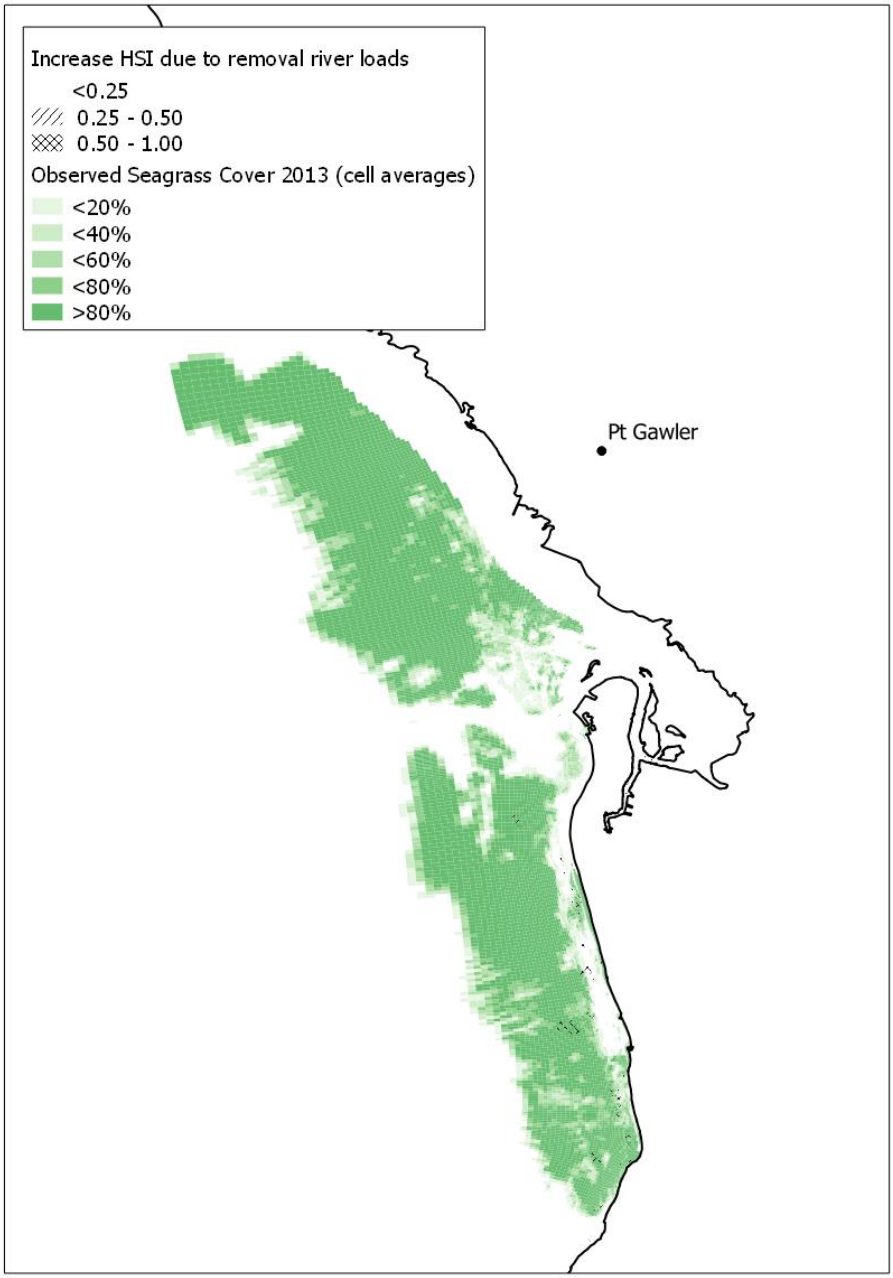

Figure 5.28 Overlay of observed seagrass cover in 2013 (1m resolution data projected on model grid) in shades of green and increase of simulated HSI after removal of river loads relative to a situation without Penrice loads in shading patterns.

Table 5.6 lists the simulated area suitable for seagrass for the present time horizon and for the three load reduction scenarios in the study area, subdivided in the north, middle and south parts (Figure 5.4), and, where possible, subdivided over areas with and without seagrass cover in 2013.

Table 5.6 Predicted area suitable for seagrass for the present time horizon and for three load reduction scenarios in the study area, separated in north, middle and south zones, and in areas with and without seagrass cover (where possible).

Class	Total	2011		Penrice removed		Penrice and WWTPs removed		Penrice and rivers removed	
Study Area	Area (ha)	Suitable (ha)	%	Suitable (ha)	%	Suitable (ha)	%	Suitable (ha)	%
North-NoData	497	387	78%	451	91%	451	91%	451	91%
North-Seagrass	14071	12729	90%	13736	98%	14026	100%	13902	99%
North-Sand	8434	4127	49%	6348	75%	7552	90%	6865	81%
Middle-NoData	2187	42	2%	51	2%	61	3%	58	3%
Middle-Seagrass	13299	10065	76%	10705	80%	11652	88%	11084	83%
Middle-Sand	14852	3925	26%	4497	30%	5483	37%	4927	33%
South	27733	1481	5%	1494	5%	2055	7%	1574	6%
Total	81073	32756	40%	37283	46%	41280	51%	38862	48%
North+Middle-Sand	23286	8052	35%	10845	47%	13035	56%	11792	51%
North+Middle-Seagrass	27370	22794	83%	24441	89%	25678	94%	24987	91%

The removal of the Penrice discharge results in significant improvements in habitat suitability for seagrass, concentrated in an area in front of the Port River outflow where there was little or no seagrass in 2013 (Figure 5.22). This is caused by a decreasing negative impact of coastal discharges on light limitation for seagrasses. The area suitable for seagrass in places where there is no seagrass in 2013 increases by 2221 ha in the north zone and by 572 ha in the middle zone. In the south zone, the suitable area increase is negligible.
The removal of all WWTP discharges causes a marked change of the simulated HSI, especially in front of Port River, presumably due to the removal of the Bolivar discharges, and near the Glenelg and Christies Beach plants along the Metropolitan coast (Figure 5.25), due to a further reduction of light limitation for seagrasses. Relative to the scenario without Penrice, the area suitable for seagrass in places where there is no seagrass in 2013 increases by 1204 ha in the north zone and by 985 ha in the middle zone (Table 5.6). In the south zone, the suitable area increase is 561 ha (in areas with and without seagrass in 2013).
The removal of all river and stormwater discharges causes a limited change of the simulated HSI in some areas close to the Metropolitan coast and in front of the Port River outlet (Figure 5.28). Relative to the scenario without Penrice, the area suitable for seagrass in places where there is no seagrass in 2013 increases by 517 ha in the north zone and by 430 ha in the middle zone (Table 5.6). In the south zone, the suitable area increase is 80 ha (in areas with and without seagrass in 2013).

Of all scenarios investigated, the removal of Penrice and the subsequent removal of all WWTP discharges have a positive impact of comparable magnitude. The removal of all river discharges has a smaller positive impact.

5.3.5 Resuspension and seagrass cover sensitivity assessment

Figure 5.29 and Figure 5.30 show the simulated HSI and the limiting stressor for a situation equal to 2011 (including Penrice discharges) assuming that resuspension would not be occurring in areas where seagrass cover was present in 1949. Figure 5.31 shows the difference between the simulated HSI with reduced resuspension and in the 2011 simulation, overlain with the 2013 seagrass map.

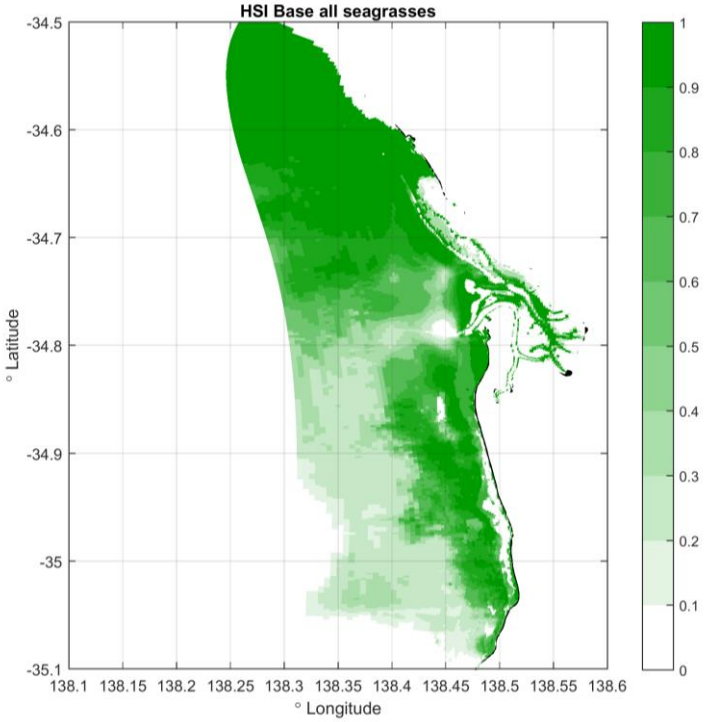

Figure 5.29 Simulated habitat suitability index for the 2011 scenario (including Penrice discharges) without resuspension in areas along the Metropolitan coast where seagrass was present in 1949.

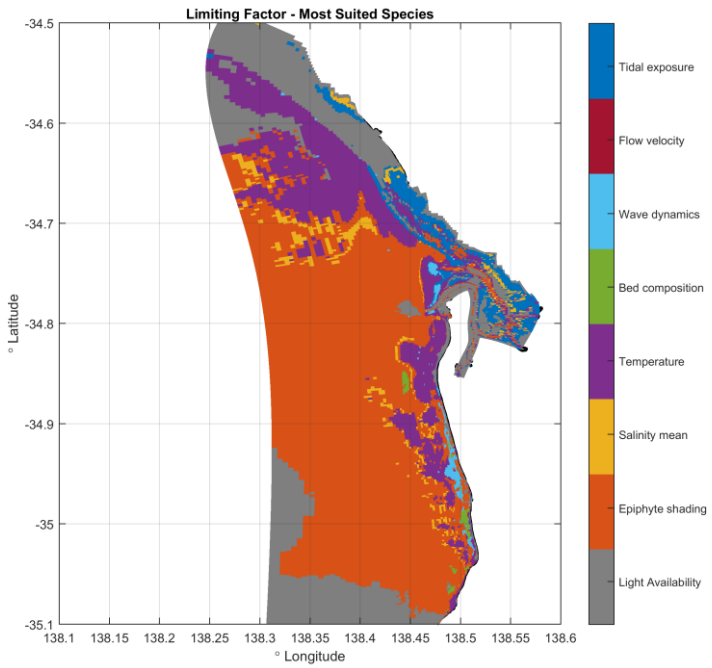

Figure 5.30 Limiting environmental factor for most suitable species (species with highest HSI) for the 2011 scenario (including Penrice discharges) without resuspension in areas along the Metropolitan coast where seagrass was present in 1949.

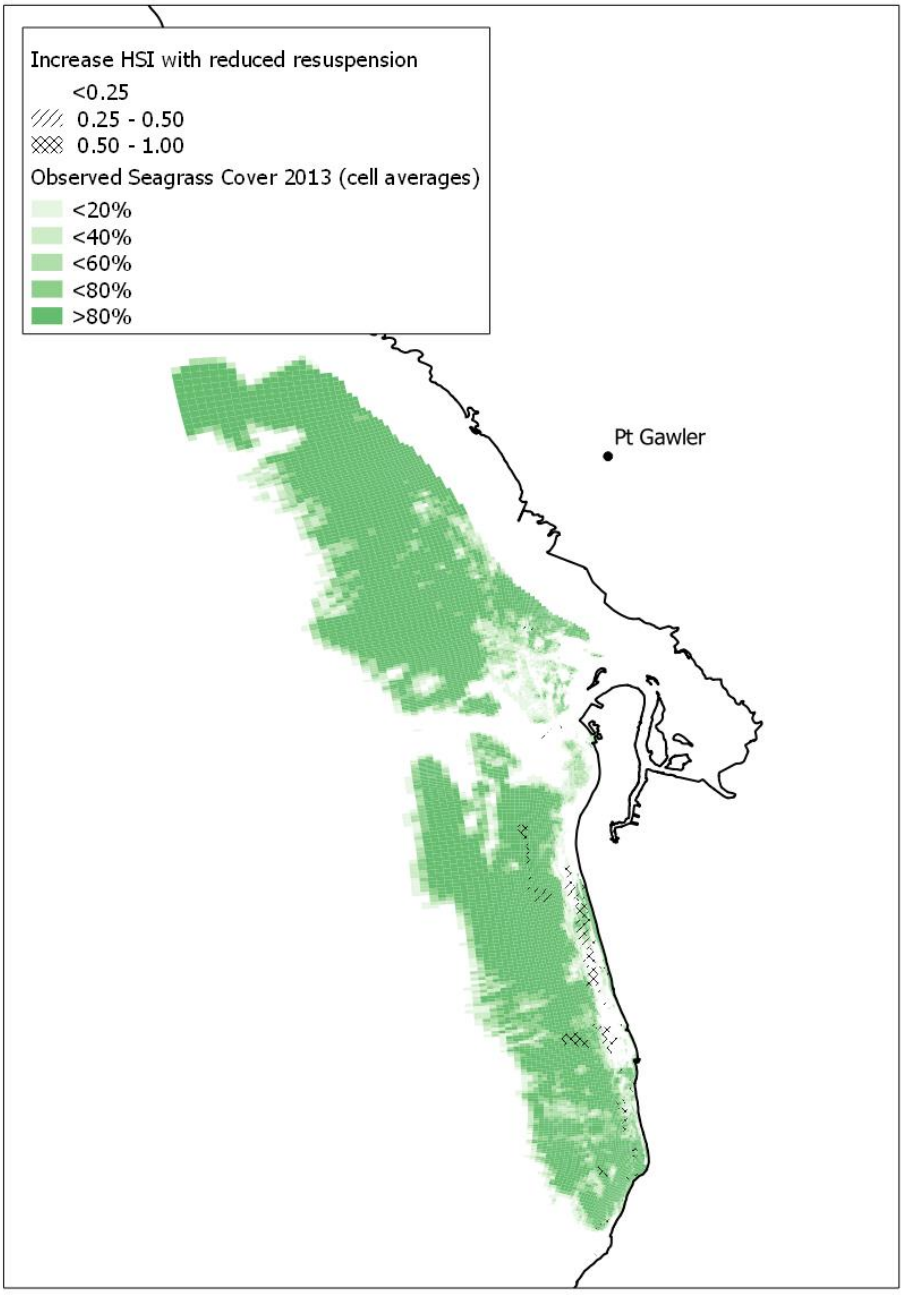

Figure 5.31 Overlay of observed seagrass cover in 2013 (1m resolution data projected on model grid) in shades of green and increase of simulated HSI due to 1949 seagrass cover controlled resuspension relative to a situation with 2013 seagrass cover controlled resuspension in shading patterns (including Penrice).

Table 5.7 Predicted area suitable for seagrass for the 2011 scenario (including Penrice discharges) with 2013 seagrass cover controlled resuspension and 1949 seagrass cover controlled resuspension in the study area, separated in north, middle and south zones, and in areas with and without seagrass cover (where possible).

Class	**Total**	**2011 (2013 seagrass cover resuspension)**		**2011 (1949 seagrass cover resuspension)**	
Study Area	Area (ha)	Suitable (ha)	%	Suitable (ha)	%
North-NoData	497	387	78%	392	79%
North-Seagrass	14071	12729	90%	13137	93%
North-Sand	8434	4127	49%	4676	55%
Middle-NoData	2187	42	2%	51	2%
Middle-Seagrass	13299	10065	76%	11135	84%
Middle-Sand	14852	3925	26%	4809	32%
South	27733	1481	5%	1583	6%
Total	81073	32756	40%	35782	44%
North+Middle-Sand	23286	8052	35%	9485	41%
North+Middle-Seagrass	27370	22794	83%	24271	89%

Table 5.8 Predicted area suitable for seagrass for the 2013 scenario (2011 excluding Penrice discharges) with 2013 seagrass cover controlled resuspension and 1949 seagrass cover controlled resuspension in the study area, separated in north, middle and south zones, and in areas with and without seagrass cover (where possible).

Class	**Total**	**2013 (2013 seagrass cover resuspension)**		**2013 (1949 seagrass cover resuspension)**	
Study Area	Area (ha)	Suitable (ha)	%	Suitable (ha)	%
North-NoData	497	451	91%	451	91%
North-Seagrass	14071	13736	98%	13868	99%
North-Sand	8434	6348	75%	6739	80%
Middle-NoData	2187	51	2%	64	3%
Middle-Seagrass	13299	10705	80%	11623	87%
Middle-Sand	14852	4497	30%	5383	36%
South	27733	1494	5%	1739	6%
Total	81073	37283	46%	39867	49%
North+Middle-Sand	23286	10845	47%	12121	52%
North+Middle-Seagrass	27370	24441	89%	25491	93%

The reduced resuspension leads to significant improvements in habitat suitability along the Metropolitan coast. This is caused by a decreasing negative impact of resuspended fines on light limitation for seagrasses. Relative to the 2011 scenario, the area suitable for seagrass in places where there is no seagrass in 2013 increases by 549 ha in the north zone and by 884 ha in the middle zone (Table 5.7). In the south zone, the suitable area increase is 102 ha (in areas with and without seagrass in 2013). Relative to the 2013 scenario, the area suitable for seagrass in places where there is no seagrass in 2013 increases by 391 ha in the north zone and by 886 ha in the middle zone. In the south zone, the suitable area increase is 102 ha (Table 5.8). The reduction of resuspension from areas where seagrass was lost has a positive impact comparable to the impact of the removal of all WWTP discharges in the middle zone. In the north and south zones, the impact is less relevant.

5.4 Discussion

We quantified the current (2011) suitability of Adelaide's coastal waters for seagrass by a habitat suitability index (HSI). Taking into account eight different environmental conditions, we found that the final result was dominated over large areas by light penetration to the seagrass leaves, with extreme wave conditions and tidal exposure locally limiting habitat suitability. This is in agreement with previous studies that found that the presence/absence of seagrasses is often determined by only a few main environmental drivers (Grech and Coles, 2010; Van der Heide et al., 2009).

Though the method is based on HSI maps for 9 individual species, we present our results for "seagrass" by taking the highest HSI value for any of the 9 species. Species interactions (competition, succession, and dynamics) have not been included in the model, because there is hardly any literature on such interactions. In this respect, the model is a simplification of reality.

Temporal dynamics, e.g. seasonality and inter-annual variability of seagrass occurrence, has not been explicitly included in the habitat modelling. The model was set up to produce a representative annually-averaged result that incorporates most of the normal seasonal and other within-year temporal variability. To this end, we derived information regarding environmental factors from hydrodynamics and biogeochemical models run for a full year (2011) by a suitable aggregation method (e.g. the use of the minimum value of rolling averages over defined periods in the calculation of a representative quantity of light reaching the seagrass canopy). Inter-annual variability would be caused by differences in WWTP and industry loads and differences in meteorological conditions, which have an impact on river and stormwater discharges, on wave-induced resuspension and on the circulation patterns in the study area and in the Gulf St Vincent. The impact of differences in WWTP and industry loads will be discussed below. The impact of differences in meteorological conditions has not been addressed in this study, but has been investigated by (Rouse et al., 2016) on the basis of an older version of the model. The contrast of a wet year (2005) and a dry year (2006) versus 2011 showed similar outputs. The wet year showed a small loss of suitability at the deep seagrass edge.

We evaluated the model results by comparison to observed seagrass cover. We note that large scale seagrass mapping has some inherent errors and uncertainties. Literature on this subject indicates that older maps probably have an accuracy that rarely exceeds 70% (Mumby and Green, 2000; Mumby and Edwards 2002), while the latest high resolution mapping methodology typically has an accuracy in the order of 85% (Uhrin and Townsend, 2016). The 2013 seagrass map we used has a 30 cm resolution. This implies it resolves patchiness up to a significant degree. Because we aggregated this map to the coarser AREM grid, patchiness will show as a fraction of observed seagrass cover < 100% in a grid cell. By comparing seagrass cover and HSI, we implicitly assume that a lower HSI is correlated to patchy seagrass cover. The observed seagrass map does not account for variable density. This is a factor complicating the comparison with the simulated HSI, since we would expect seagrass density to be correlated to habitat suitability.

Taking all this into account, we compared the 2011 simulated HSI to the observed 2013 seagrass. We found that 72% of the grid cells in the domain where a comparison was possible showed an agreement between HSI and observed seagrass cover, while about 22% of cells showed high HSI and no seagrass cover ("false positives") and 6% showed low HSI in areas with seagrass cover ("false negatives"). Many of the false positives are far off-shore, outside the direct impact zone of the coastal discharges. These false positives could well be

the result of model inaccuracies, which could be resolved by making small changes in the biogeochemical model or refinement of thresholds for individual species for the local situation, but they do not affect the fitness for use of the model in the area of concern for this study. Close to shore, the calculation of the available light for seagrass is expected to be accurate in view of the effort made to accurately quantify the discharges (Chapter 2), the relation between the water quality and the penetration of light in the water column (Chapter 3) and the water quality in the coastal waters as a result of coastal discharges (Chapter 4). We therefore consider these false positives either areas affected by factors not included in the present model set-up, or areas previously unsuitable and now suitable. The false negatives are mostly connected to the substrate and extreme waves environmental factors. This does not concern the relation between coastal discharges and seagrass habitat suitability, and therefore does not affect the fitness for use for this study. In summary, the comparison between the 2011 simulated HSI and the observed 2013 seagrass cover, supported by a quantitative goodness of fit analysis, confirms a good match.

The available seagrass map does not distinguish between seagrass species. The model has the ability to predict which species is more likely to dominate certain areas. Comparison with some limited data on the distribution patterns of individual species, as presented by Bryars and Rowling (2009) shows our species-specific model results match well with mapped distribution (revealing similar spatial distribution patterns for most species) and according to what would be expected from what is known about the general ecology of those species.

As expected, the historical 1940 scenario shows much larger areas of high suitability for seagrass than the 1975 scenario (due to different coastal discharges). The 1940 scenario also shows a considerable difference to the present scenario (due to higher discharges and slow recovery). When comparing to older seagrass data, we need to apply caution because older seagrass mapping efforts were less accurate, and there may be inconsistencies in mapping methodology over historic timescales. Looking at areas where the older mapping data indicate that seagrass was lost between 1949 and 1977, the model results show a high HSI in the 1940 scenario and a low HSI in the 1975 scenario. This is fully consistent. On the other hand, the 1975 HSI is unrealistically low in some areas which were reported to have seagrass cover in 1977. It is not possible to establish whether this is the result of inaccuracies in model input data (loads), model formulation and parameters, or field data.

Habitat suitability modelling can help to better understand what is the most influential predictor or the most limiting factor to seagrass (which can be spatially variable). It can also help to detect the areas with highest/lowest suitability, or to find out what would be the most suitable species (in certain areas) for restoration programs. The current results show how light penetrating to the seagrass canopy is affected by coastal discharges and where this is limiting the suitability for seagrass cover. By carrying out sensitivity simulations we showed that the closure of the Penrice discharge has improved seagrass habitat suitability, in particular in front of the Port River mouth, with an estimated gain in area suitable for seagrass where seagrass is presently absent of 2,793 ha (north and middle zone). Reduction of WWTP discharges may locally improve seagrass habitat suitability along the Metropolitan coast, in areas where seagrass is currently absent, and the estimated additional gain in area suitable for seagrass where seagrass is presently absent is 2,190 ha (north and middle zone). Future seagrass recolonisation is most likely to occur in areas with predicted high HSI and absence of seagrass cover.

A high HSI does not automatically imply the recovery of seagrass cover. Successful recruitment and seedling establishment of seagrasses at a site depend on several factors,

which are essentially a function of seed supply and (micro-)site habitat suitability (Inglish, 2000; Orth et al., 2006; Rivers et al., 2011; Tanner et al., 2014). The probability of uprooting of seedlings is much higher than for mature plants, because seedlings are not as well-established and anchored as mature plants. For most other environmental variables, the habitat requirements of seedlings appear to be similar to those of mature plants (Appendix F). Thus, recovery is primarily a matter of "windows of opportunity", i.e. seedlings will manage to successfully establish if offered a window of time with sufficiently suitable conditions without major perturbations (Cambridge et al., 2002). Seedlings of the dominant seagrasses off Adelaide typically become established during winter (*Amphibolis* spp.) or early summer (*Posidonia* spp.), after which the seedlings need approximately 4-6 months of relatively calm conditions to develop and anchor themselves sufficiently before the onset of the rougher winter season, with the first storms arriving around May. Most seedling mortality appears to occur during the onset of winter storms through uprooting and dislodgement of the seedlings and increased sediment instability (Chisholm, 2009; Rivers et al., 2011; Verduin et al., 2013). During the first 4-9 months (especially the first 4 months), *Posidonia* seedlings are less sensitive to low light conditions, as they are able to grow and develop from the nutrition and energy reserves stored in the seed (Hocking et al., 1981) but after that period they become increasingly dependent on their own ability to photosynthesise and thus on water clarity. The still limited extent of the root systems of young plants at this time represents both an advantage (lower light requirements due to the limited oxygen demand) and a disadvantage (lack of carbohydrate reserves to make it through low light periods).

In view of the fact that Adelaide's coast has been colonised by seagrasses before the onset of anthropogenic pressure, it could be expected that it will return by itself in areas where it has been lost at some point in time once the pressures (low light and/or physical distortion) are relieved. The AREM can now be used as a management tool to investigate what needs to be done to return to conditions with sufficient light for seagrasses.

5.5 Area specific loads as an indicator for pressure from coastal discharges

The ACWS Final Report (Fox et al., 2007) discussed the pressure by coastal discharges on the Adelaide Coastal Waters as expressed by an overall area specific load (ASL) of nitrogen in tN km^{-2} (equal to gN m^{-2}, integrated over the residence time). The authors quantified the ASL integrated over the total surface area of the Adelaide Coastal Waters and over the residence time of this area as an indicator of pressure by coastal discharges that has ecological relevance. Here we used the Adelaide Receiving Environment Model (AREM) to calculate the pressure by coastal discharges expressed as an ASL, including its spatial and estimated temporal variability in the Adelaide Coastal Waters. The time dependency of the ASLs is expressed by calculating annual mean values and maximum values of the rolling average of the ASL over periods of 6 months, 3 months and 1 month. This approach parallels our approach to quantify representative minimum light conditions for various seagrass species as explained in Section 5.2.4. As well as for nitrogen, we calculated ASLs also for suspended solids and we quantified separately the relative contributions from rivers and stormwater, domestic wastewater and industrial wastewater. The method to derive these ASLs as well as contour plots of the results from the simulations for the 1975 and 2011 time horizons, with and without the Penrice discharges, are compiled in Appendix A.

The results obtained show some overall patterns. Firstly, 1975 ASLs are generally higher than 2011 ASLs because of the higher loads. A distinctive feature of the 1975 scenario is the Glenelg sludge discharge at some distance off the Metropolitan coast, which is clearly visible as a local maximum in many of the ASL plots for 1975. We note that the Port Adelaide sludge discharge had not yet been commissioned in 1975. Secondly, the plots without Penrice

evidently show lower ASLs than the plots with Penrice included. The difference is quite dramatic as the Penrice load was and is very significant for both nitrogen and suspended solids (Chapter 2). The footprint from the Penrice load is clearest in front of the Port River mouth but it reaches the shallows to the north and the Metropolitan coast. In all cases, the annually averaged ASL and the maximum value of the 6 months, 3 months and 1 month rolling averages show increasing ASLs. The shorter the averaging period gets, the more the result is affected by shorter periods of unfavourable conditions. The 3 month rolling average can be expected to represent the most unfavourable season whereas the 1 month rolling average can be expected to represent the most unfavourable month and the latter therefore presents more extreme conditions than the former.

By a comparison of the simulated 1975 ASLs to observed seagrass loss between 1949-1977 we tried to establish an empirical relation between the ASL and seagrass loss. Figure 5.32 shows an overlay of the 1975 simulated nitrogen ASL (maximum of 3 months rolling average), seagrass cover in 1949 and seagrass losses in 1949-1977. Within the area of seagrass loss in 1949-1977 the values of the ASL have been binned and plotted in a histogram. The result shows that the area of inshore continuous seagrass losses is characterised by ASL values exceeding 1.5 tN km^{-2}. The correlation is not perfect though. In the south part of the mapped area there are significant areas of (patchy) seagrass loss in zones with an ASL between 1.0 and 1.5 tN km^{-2}. There is also a large patch with ASLs exceeding 1.5 away from the coast that is connected to the Glenelg sludge discharge with limited seagrass loss. It is possible that due to the specific nature of this discharge, containing nutrients in particulate organic form, the effects on seagrass are not direct but need some time to materialise, and that the patchy seagrass loss east and north of the sludge discharge footprint is connected to this discharge.

Figure 5.33 shows similar results for suspended solids. In this case, the inshore losses occur mostly within the area with ASLs exceeding 10 t km^{-2}. The Glenelg sludge discharge footprint covers a larger part of the areas of patchy seagrass loss in the south. In the north however, there is a area with seagrass loss where the ASL is between 7 and 10 t km^{-2}.

The results described here are in line with similar results obtained from an earlier version of the AREM by Rouse et al. (2016). The threshold of 1.5 tN km^{-2} for the spatially variable ASL is close to the threshold value of 1 t km^{-2} derived by for the Adelaide coastal waters as a whole by Fox et al. (2007).

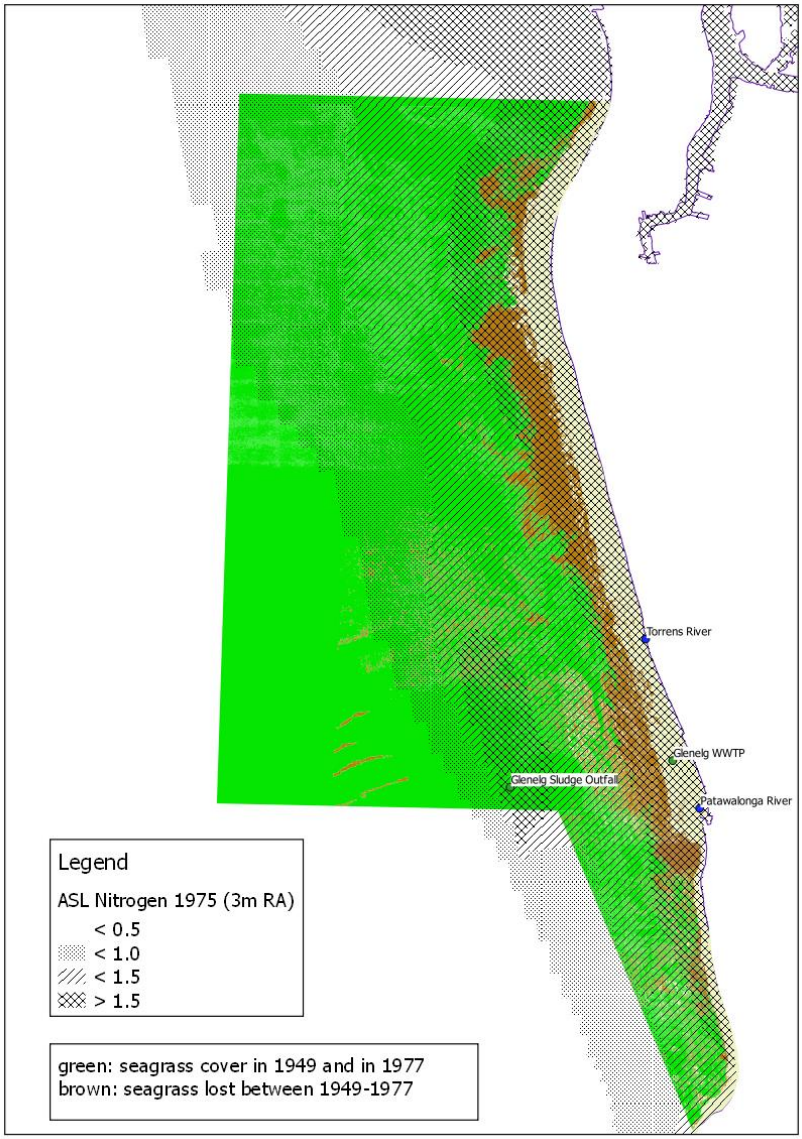

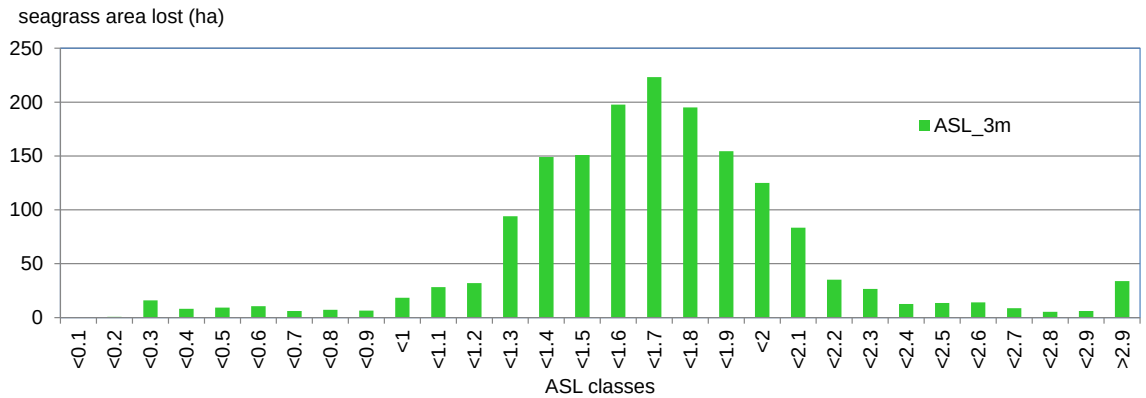

Figure 5.32 Overlay of 1975 simulated nitrogen ASL (maximum of 3 months rolling average), seagrass cover in 1949 and seagrass losses in 1949-1977 (top); statistics of ASL values in area of seagrass loss in 1949-1977 (bottom).

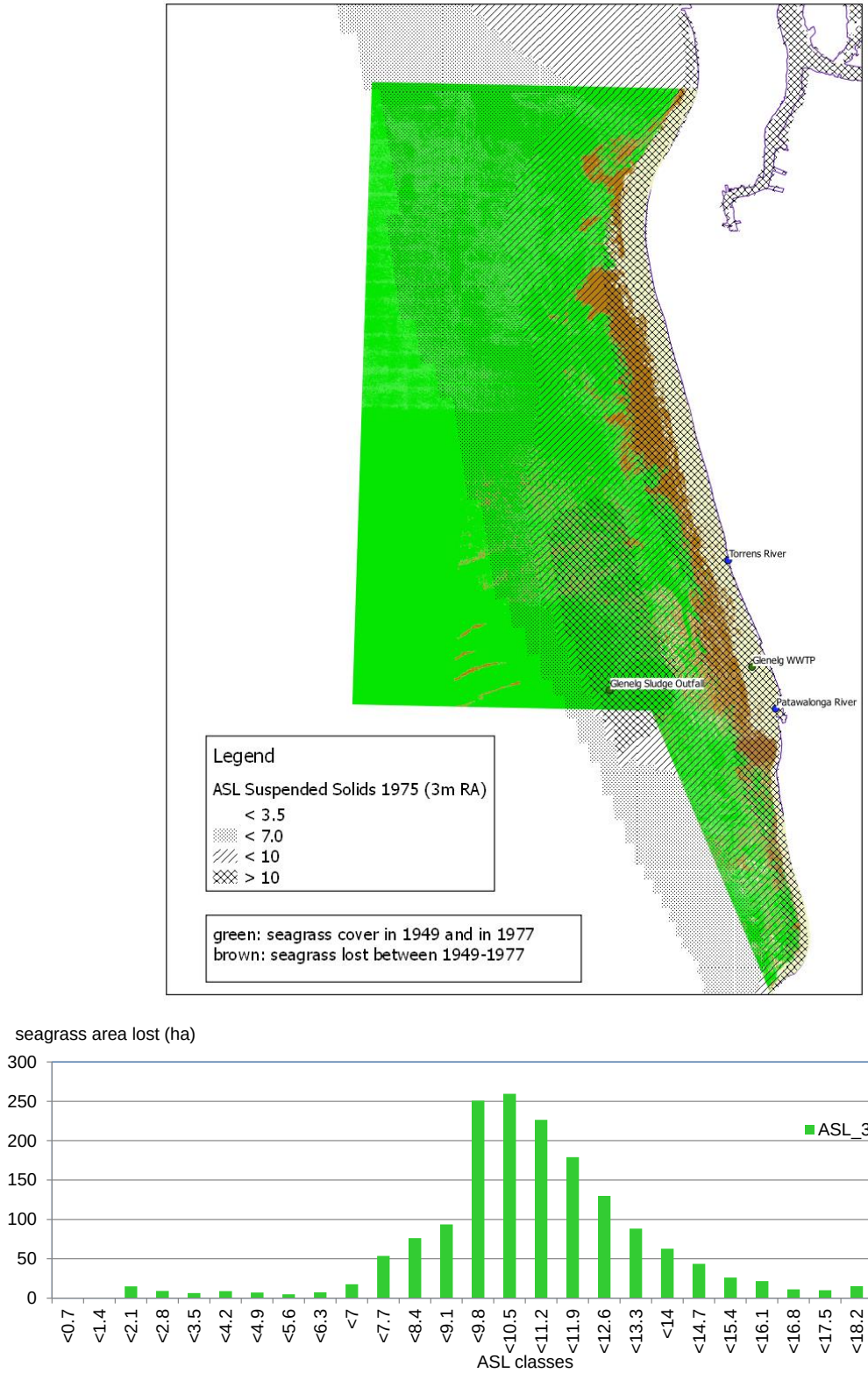

Figure 5.33 Overlay of 1975 simulated suspended solids ASL (maximum of 3 months rolling average), seagrass cover in 1949 and seagrass losses in 1949-1977 (top); statistics of ASL values in area of seagrass loss in 1949-1977 (bottom).

We note that the actual value of the thresholds obtained from this analysis depends on the time factor. We used the maximum of the 3 months rolling average of the ASL. This period of averaging is in between the time scales for characterizing representative light conditions for *Amphibolis* spp (60 days) and *Posidonia* spp (180 days). Using another averaging period leads to different ASL values and different threshold values. Furthermore, the calculation of ASLs does not take into account loss processes (settling of particulates, denitrification, etc.). This is expected to cause an overestimation of the ASLs, which is probably stronger for SS than it is for N. Finally, we note that the ASL based analysis completely neglects the resuspension of particles, the role of CDOM, the interaction between nutrients, and particles, etc. The analysis is elegant however, because it avoids the complexities and uncertainties of the BGC and habitat models.

Figure 5.34 shows the 2011 nitrogen ASLs around the SA Water discharge points for the 2011 situation (excluding Penrice) for the 3 months rolling average.

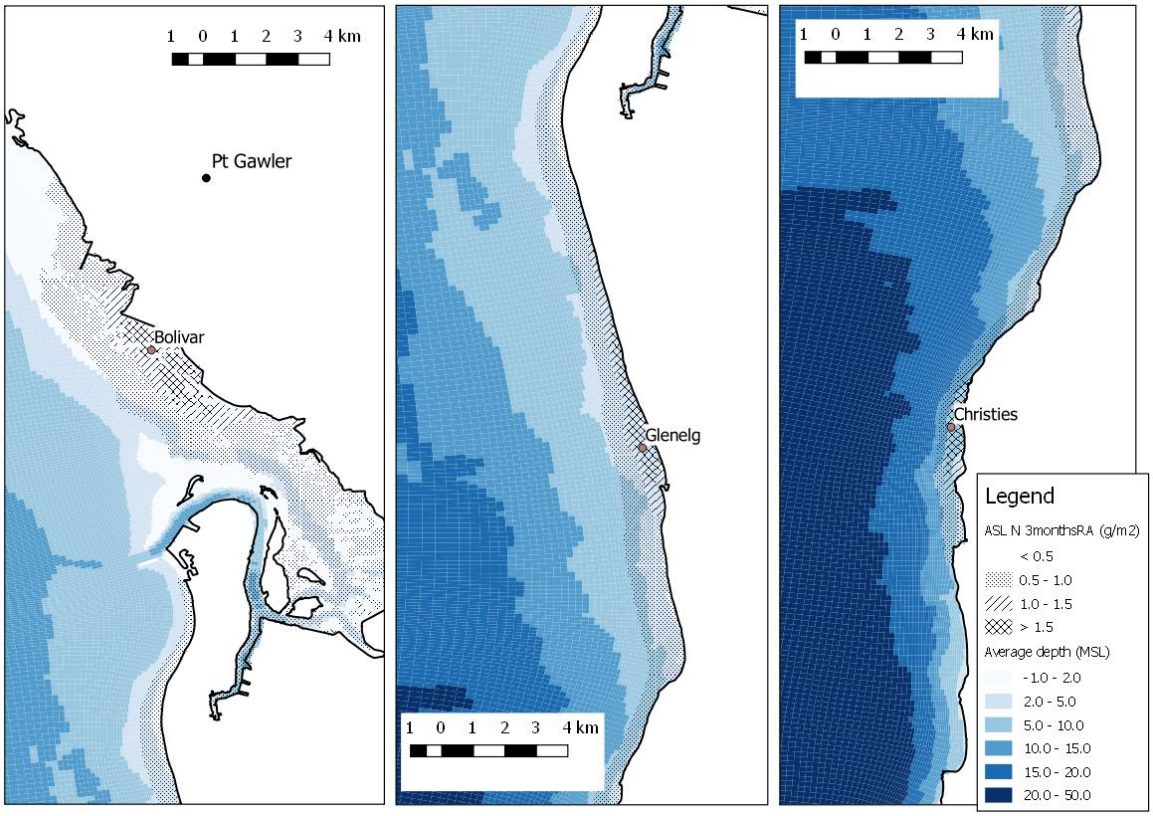

Figure 5.34 Simulated nitrogen ASL (maximum value of 3 months rolling average) in the vicinity of SA Water discharges in 2011 (without Penrice loads).

Figure 5.34 clearly shows that the 1.0 or 1.5 tN km^{-2} thresholds for the spatially variable ASL (3 months rolling average) are exceeded today in fairly small and narrow zones around the WWTP discharge points. In particular, the 1.0 tN km^{-2} threshold is exceeded around Bolivar outfall over 964 ha, around Glenelg outfall over 466 ha and around Christies Beach outfall over 249 ha. We note that these numbers are inclusive of shallow areas (average depth < 2m). According to the data in Table 5.6, which exclude shallow areas, the removal of all WWTP discharges leads to an increase of the area suitable for seagrass of 1204 ha in the north zone (Bolivar WWTP), 985 ha in the middle zone (Glenelg WWTP) and 561 ha in the south zone (Christies Beach WWTP). This seems inconsistent, since the AREM based

positive impacts of removing WWTP loads are larger than the areas where relevant ASL thresholds are exceeded.

This apparent inconsistency is caused by methodological differences. The ASL based approach results in a threshold that expresses which coastal discharges could kill seagrass in an otherwise “pristine” environment (without enhanced resuspension due to seagrass losses). The AREM simulations evaluate the current loads in a situation with extra resuspension in areas where seagrass was lost. Thus, the ASL based criterion neglects the seagrass-sediment-light feedback loop (Adams et al., 2016). In the middle zone, around the Glenelg outfall, where the ASL thresholds were determined, we find that the 1.0 tN km^{-2} threshold is exceeded over 466 ha. This suggests that WWTP load reduction could only have a positive impact of 466 ha. The AREM simulations reveal that removing these loads has a larger impact (+985 ha). This is because their removal compensates the extra resuspension. Table 5.7 shows that this extra resuspension indeed has a significant effect on the area suitable for seagrass in the middle zone (+884 ha). In order to be comparable to ASL derived thresholds, we would need to investigate the effect of load reduction in a situation without this extra resuspension. In that case a smaller positive effect from load reduction is expected, since the reference situation is already much more positive. This would be methodologically consistent, but practically meaningless however. The AREM results show to what degree reducing loads would have a positive effect in view of the increased turbidity caused by historical seagrass losses.

5.6 Conclusions

A Habitat Suitability Index (HSI) model has been successfully set up for the Adelaide coastal waters. The AREM quantifies the HSI for all nine different species of seagrasses known to occur in the Adelaide Coastal Waters. For each species, the suitability is quantified in relation to 7 environmental conditions, being (a) light reaching the seagrass leaves, (b) salinity, (c) water temperature, (d) substrate, (e) extreme wave exposure, (f) flow velocity and (g) tidal exposure. For all nine seagrass species, a literature survey provided their requirements and tolerance related to these conditions. The models discussed in Chapter 4 were used to quantify 6 of these 7 conditions, while a substrate map was obtained from field data. Apart from an overall seagrass habitat suitability index, the AREM also produces maps of the most suitable species (or best adapted species) and the most limiting environmental factor for that species.

Contrary to the pilot model, the upgraded AREM reproduces the inshore light minimum as it was observed in the ACWS study, which is typical for the Adelaide Coastal Waters. Light availability is the dominant environmental factor determining seagrass habitat suitability, together (locally) with substrate, extreme wave conditions and tidal exposure.

The simulated habitat suitability was found to correlate well with 2013 seagrass cover (72% of model grid cells). 6% of the grid cells have seagrass cover despite a low simulated HSI (“false negative”), while the remaining 22% have no seagrass cover but a high simulated HSI (“false positive”). False positives and negatives could indicate model shortcomings, but also seagrass mapping errors or areas likely to decline (false negatives) or recover (false positives) over the next few years. We note that a large share of the false positives is found close to the model boundary, away from the inshore areas affected by discharges where seagrass has been lost.

The validity of the AREM was further tested by simulating seagrass habitat suitability for the 1940s (prior to human impact) and the mid 1970s (maximum seagrass loss rate), and

comparing the results to seagrass maps obtained from that period. For the mapped area of seagrass loss between 1949 and 1977, the simulated habitat suitability was 78% in the 1940s and only 35% in the mid-1970s. This demonstrates that observed gradients in seagrass cover in the study area are reproduced remarkably well.

By a sensitivity assessment we provided further insights in the relation between the coastal discharges and the habitat suitability for seagrasses. The simulation results are evaluated in the Central Metropolitan Coast area ("central"), in the area north of it and in the area south of it. In the north and central zones, results are presented for the area presently without seagrass ("sand"), for the south zone this difference could not be made due to lack of data on seagrass cover.

	Effect of Penrice removal in 2013 (change of suitable area (ha), relative to 2011)	**Effect of all WWTPs removed (change of suitable area (ha), relative to 2013)**	**Effect of all rivers removed (change of suitable area (ha), relative to 2013)**	**Effect of reduced resuspension (change of suitable area (ha), relative to 2013)**
North-sand	2221	1204	517	391
Central-sand	572	985	430	886
South	13	561	80	245
Total	2806	2751	1027	1521

The results show that the removal of Penrice has already had a strong positive effect, which is concentrated in front of Port River, in the north. The (hypothetical) removal of all WWTP discharges is expected to have a similar additional positive effect, but more equally distributed. The (hypothetical) removal of all rivers would have a marked effect too, but significantly smaller. Finally, omitting resuspension from areas where seagrass cover in the 1940s still existed, would cause a significant improvement especially in the central part.

A high HSI does not automatically imply the immediate recovery of seagrass. Successful recruitment, assuming sufficient seed supply, is determined by the probability of uprooting of seedlings because seedlings are not as well-established and anchored as mature plants. Thus, recovery is primarily a matter of "windows of opportunity", when seedlings will manage to successfully establish during a window of time with sufficiently calm conditions without major perturbations.

The Adelaide Coastal Waters Study used the concept of area specific loads (ASL) for the coastal area as a whole, as an indicator for the pressure from coastal discharges on seagrasses. A method to derive spatially explicit maps of simulated ASLs has been developed and applied. The results obtained for the mid 1970s were overlayed with areas of recorded seagrass loss. A correlation was found, which indicated that the area of inshore continuous seagrass losses is characterised by ASL values exceeding 1.5 tN km^{-2}. Assuming that this value represents a historically based threshold value for coastal discharges, we evaluated current conditions against this threshold and found that it is only exceeded in small areas in the direct vicinity of the present WWTP outfalls. This would imply that current conditions would be sufficient for almost complete recovery of previous seagrass losses.

The AREM simulation results explain why this is not the case. The ASL based threshold expresses which coastal discharges could kill seagrass in an otherwise "pristine" environment (without enhanced resuspension due to seagrass losses). The AREM simulations reveal a so-called positive feedback loop: seagrass losses cause enhanced resuspension, which causes further losses if the discharges remain high and prevents recovery after discharges have

been reduced. Only after the discharges have been reduced far enough to compensate the resuspension-induced turbidity, recovery may start. This is all included in the habitat suitability maps produced by AREM. The ASL threshold neglects this positive feedback loop.

6 Epilogue

Christies Beach WWTP and receiving coastal waters – Photograph by SA Water

This report discussed how we expanded and evaluated the pilot version of the Adelaide Receiving Environment Model (AREM) in a way that enables clearer communication with local stakeholders and provides a means to create consensus on the results. The effort relied to a large extent on additional data collected by SA Water, in particular about the discharges of particles, nutrients and Coloured Dissolved Organic Matter (CDOM) to Adelaide's coastal waters (Chapter 2). The data collected related to the water quality in the study area (Chapter 3) had the specific aim to validate the relation between water quality and Photosynthetically Active Radiation (PAR) downward attenuation in the Adelaide Coastal Waters. The AREM is based on a habitat suitability assessment approach (Chapter 5) and is supported by state-of-the-art wave, hydrodynamic, sediment and biogeochemical models (Chapter 4).

The AREM results show that light penetration to the seafloor is the dominating environmental condition determining habitat suitability for seagrasses. Light penetration to the seafloor is determined by the water depth and the water transparency. Based on the results compiled in this report, both organic and inorganic particles significantly affect the water transparency close to shore, with organic particles dominating north of Port River and inorganic particles dominating south of Port River. CDOM is relevant close to shore as well, and is the dominating factor away from shore.

The concentrations of inorganic particles in Adelaide's coastal waters are not the sole result of direct discharges of stormwater and wastewater, but are actually dominated by wave induced resuspension. The concentrations of CDOM in Adelaide's coastal waters are

primarily caused by a background contribution from open sea water and releases from sediment, seagrass and mangroves, and only to a lesser extent by coastal discharges. This implied that the relation between coastal discharges and the water transparency is affected by partly natural phenomena.

It is clear that Adelaide's coastal waters are a complex system and that there are many interactions between natural and anthropogenic processes that determine the water transparency, the amount of light reaching the seafloor and thus the habitat suitability for seagrasses. The AREM for the first time offers a model system that encompasses this complexity in a state-of-the-art fashion, which allows local stakeholders to investigate the impact of changes and measures. Validation of the model system indicates that it is not 100% perfect, while the material collected in this report demonstrates that it captures the relevant phenomena and spatial gradients therein to a large degree. The model system can therefore contribute to the development of well-considered interventions by SA Water and possibly also by other stakeholders.

The AREM can now be used to identify the nearshore areas still experiencing sub-optimal light conditions for seagrass, and to investigate to what degree discharges reductions will promote conditions for recolonisation. The results presented in this report indicate that the removal of the Penrice discharge has already contributed to improved conditions for seagrasses in front of the Port River outlet. The results also indicate that the positive effects on seagrass habitat suitability to be expected from reducing WWTP discharges are larger than those to be expected from reducing stormwater discharges. Our sensitivity analysis further revealed that resuspended fine particles from areas of seagrass loss since 1949 have a negative effect on seagrass habitat suitability, which is similar in magnitude to the current effect of all WWTP discharges.

Finally, the authors hope that the findings of this report may be a stimulus for all stakeholders to jointly design an integrated monitoring programme that can support environmental management effectively and efficiently.

7 References

Adams, M. P., R. K. Hovey, M. R. Hipsey, L. C. Bruce, M. Ghisalberti, R. J. Lowe, R. K. Gruber, L. Ruiz-Montoya, P. S. Maxwell, D. P. Callaghan, G. A. Kendrick, and K. R. O'Brien. 2016. Feedback between sediment and light for seagrass: Where is it important? Limnology and Oceanography:doi:10.1002/lno.10319.

Adams, M.P., M.I. Saunders, P.S. Maxwell, D. Tuazon, C.M. Roelfsema, D.P. Callaghan, J. Leon, A.R. Grinham and K.R. O'Brian, 2015. Prioritizing localized management actions for seagrass conservation and restoration using a species distribution model. Aquatic Conservation: Marine and Freshwater Ecosystems, published online July 2015, DOI: 10.1002/aqc.2573.

APHA-AWWA-WEF (1995). Method 5310 A, C. In: Standard Methods for the Examination of Water and Wastewater (eds. Eaton AD, Clesceri LS & Greenberg AE). American Public Health Association Washington.

APHA-AWWA-WEF (2012a). Method 2540 D and E. In: Standard methods for the examination of water and wastewater (eds. Rice EW, Baird RB, Eaton AD & Clesceri LS). American Public Health Association Washington.

APHA-AWWA-WEF (2012b). Method 4500-N org A. In: Standard methods for the examination of water and wastewater (eds. Rice EW, Baird RB, Eaton AD & Clesceri LS). American Public Health Association Washington.

APHA-AWWA-WEF (2012c). Method 4500-NH3 G. In: Standard methods for the examination of water and wastewater (eds. Rice EW, Baird RB, Eaton AD & Clesceri LS). American Public Health Association Washington.

APHA-AWWA-WEF (2012d). Method 4500-NO3 I. In: Standard methods for the examination of water and wastewater (eds. Rice EW, Baird RB, Eaton AD & Clesceri LS). American Public Health Association Washington.

APHA-AWWA-WEF (2012e). Method 4500-P F. In: Standard methods for the examination of water and wastewater (eds. Rice EW, Baird RB, Eaton AD & Clesceri LS). American Public Health Association Washington.

APHA-AWWA-WEF (2012f). Method 4500-P G. In: Standard methods for the examination of water and wastewater (eds. Rice EW, Baird RB, Eaton AD & Clesceri LS). American Public Health Association Washington.

Atlas, D. and T. T. Bannister. 1980. Dependence of mean spectral extinction coefficient of phytoplankton on depth, water color, and species. Limnology and Oceanography **25**:157-159.

Babin, M., A. Morel, V. Fournier-Sicre, F. Fell, and D. Stramski. 2003. Light scattering properties of marine particles in coastal and open ocean waters as related to the particle mass concentration. Limnology and Oceanography **48**:843-859.

Backman, T.W. and D.C. Barilotti, 1976. Irradiance reduction: effects on standing crop of eelgrass *Zostera marina*. Marine Biology 34: 33-40.

Baker, E. T. and J. W. Lavelle. 1984. The effect of particle size on the light attenuation coefficient of natural suspensions. Journal of Geophysical Research: Oceans **89.C5**:8197-8203.

Baptist, M. J., V. Babovic, J. Rogriguez Uthurburu, M. Keijzer, R.E. Uittenbogaard, A. Mynett and A. Verwey, 2007. On inducing equations for vegetation resistance. Journal of Hydraulic Research 45(4): 435–450.

Barma D. & Varley I. (2012). Hydrological modelling practices for estimating low flows - guidelines. In. Australian Government, National Water Commission Canberra, Australia, p. 53.

Batiuk, R.A., P. Bergstrom, M. Kemp and E. Koch, 2000. Chesapeake Bay Submerged Aquatic Vegetation Water Quality and Habitat based Requirements and Restoration Targets: A Second Technical Synthesis. Annapolis, Maryland: EPA Chesapeake Program.

Battjes, J.A., and J.P.F.M. Jansen, 1978. Energy loss and set-up due to breaking of random waves. Coastal Engineering 1978: 569–588.

Bekkby, T., E. Rinde, L. Erikstad, V. Bakkestuen, O. Longva, O. Christensen, M. Isæus and P.E. Isachsen, 2008. Spatial probability modelling of eelgrass (*Zostera marina*) distribution on the west coast of Norway. ICES Journal of Marine Science 65: 1093-1101.

Blauw, A.N., H.F.J. Los, M. Bokhorst and P.L.A. Erftemeijer, 2009. GEM: a Generic Ecological Model for estuaries and coastal waters. Hydrobiologia 618: 175-198.

Bone, Y., L. Deer, S.A. Edwards and E. Campbell, 2006. Adelaide Coastal Waters Study – Sediment Budget. ACWS Technical Report No. 16, Adelaide: Adelaide University, Department of Geology, 2006.

Booij, N., R.C. Ris and L.H. Holthuijsen, 2009. "A third generation wave model for coastal regions: 1. Model description and validation." J. Geophys. Res. 104(C4): 7649-7666.

Borowitzka, M.A., P.S. Lavery and M. van Keulen, 2006. Epiphytes of Seagrasses. Chapter 19 in: A.W.D. Larkum et al. (eds.), 'Seagrasses: Biology, Ecology and Conservation', Springer, pp. 441-461.

Bowers, D. G. and C. E. Binding. 2006. The optical properties of mineral suspended particles: A review and synthesis. Estuarine Coastal and Shelf Science **67**:219-230.

Boyd, P.W., 2002. The role of iron in the biogeochemistry of the Southern Ocean and equatorial Pacific: a comparison of in situ iron enrichments. Deep-Sea Research II 49(9-10): 1803–1821.

Branco, A. B. and J. N. Kremer. 2005. The relative importance of chlorophyll and colored dissolved organic matter (CDOM) to the prediction of the diffuse attenuation coefficient in shallow estuaries. Estuaries **28**:643-652.

Brooks, R.P., 1997. Improving habitat suitability index models. Wildlife Society Bulletin 25(1): 163-167.

Brush, M.J. and S.W. Nixon, 2002. Direct measurements of light attenuation by epiphytes on eelgrass *Zostera marina*. Mar. Ecol. Prog. Ser. 238: 73-79.

Bryars, S. and G. Collins, 2008. Causes of Adelaide's seagrass loss. In: S. Murray-Jones (Ed.) 'Proceedings of the Second Seagrass Restoration Workshop, Adelaide, April 2008'. Department for Environment and Heritage, Adelaide, pp. 18-37.

Bryars, S. and K. Rowling, 2009. Benthic habitats of Eastern Gulf St Vincent: major changes in benthic cover and composition following European settlement of Adelaide. Transactions of the Royal Society of South Australia 133(2): 318–338.

Bryars, S. and V. Neverauskas, 2004. Natural recolonisation of seagrasses at a disused sewage sludge outfall. Aquatic Botany 80: 283-289.

Bryars, S., D. Miller, G. Collings, M. Fernandes, G. Mount, and R. Wear. 2006. Field surveys 2003-2005: Assessment of the quality of Adelaide's coastal waters, sediments and seagrasses. Adelaide Coastal Waters Study Technical Report No. 14, July 2006. SARDI Aquatic Sciences Publication No. RD01/0208-15. Adelaide, South Australia.

Bryars, S., G. Collings and D. Miller, 2011. Nutrient exposure causes epiphytic changes and coincident declines in two temperate Australian seagrasses. Marine Ecology Progress Series 441: 89-103.

Bulthuis, D.A., 1983. Effects of in situ light reduction on density and growth of the seagrass *Heterozostera tasmanica* (Martens ex Aschers.) den Hartog in Western Port, Victoria, Australia. Journal of Experimental Marine Biology and Ecology 67: 91-103.

Bulthuis, D.A., 1987. Effects of temperature on photosynthesis and growth of seagrasses. Aquatic Botany 27: 27-40.

Burgman, M.A., D.R. Breininger, B.W. Duncan and S. Ferson, 2001. Setting reliability bounds on habitat suitability indices. Ecological Applications 11: 70-78.

Burkholder, J. M., D. A. Tomasko, and B. W. Touchette. 2007. Seagrasses and eutrophication. Journal of Experimental Marine Biology and Ecology **350**:46-72.

Caldwell, J.W., 1985. Effects of elevated turbidity and nutrients on the net production of a tropical seagrass community. Ph.D thesis, University of Florida, Gainesville FL, USA, 146 pp.

Cambridge, M.L., G.R. Bastyan and D.I. Walker, 2002. Recovery of *Posidonia* meadows in Oyster Harbour, Southwestern Australia. Bulletin of Marine Science 71(3): 1279-1289.

Cambridge, M.L., J.R. How, P.S. Lavery and M.A. Vanderklift, 2007. Retrospective analysis of epiphyte assemblages in relation to seagrass loss in a eutrophic coastal embayment. Marine Ecology Progress Series 346: 97−107.

Campbell, D. E. and R. W. Spinrad. 1987. The relationship between light attenuation and particle characteristics in a turbid estuary. Estuarine, Coastal and Shelf Science **25**:53-65.

Carruthers, T. and C. Wazniak, 2004. Development of a Seagrass Habitat Suitability Index for the Maryland Coastal Bays. Chapter 6.2 in: Maryland's Coastal Bays: Ecosystem Health Assessment. Maryland Department of Natural Resources, Document Number DNR-12-1202-009, pp. 6-18 to 6-22.

Chapra, S.C., 1996. Surface Water Quality Modeling. New York: McGraw-Hill Science / Engineering / Math.

Chawla, A, DM Spindler, and HL Tolman, 2013. Validation of a thirty year wave hindcast using the climate forecast system reanalysis winds. Ocean Modelling 70: 189-206.

Cheshire, A.C., D.J. Miller, S. Murray-Jones, L. Scriven and R. Sandercock, 2002. The Section Bank: ecological communities and strategies for the minimization of dredging impacts. A report to the Office for Coast and Marine National Parks and Wildlife, South Australia, Department for Environment and Heritage. SARDI Aquatic Sciences, West Beach.

Chisholm, W.J., 2009. The stability of shallow coastal sediments with and without seagrasses. PhD thesis, Murdoch University, Perth (Australia).

Christian, D. and Y. P. Sheng. 2003. Relative influence of various water quality parameters on light attenuation in Indian River Lagoon. Estuarine Coastal and Shelf Science **57**:961-971.

Clark, C. D., J. Jimenez-Morais, G. Jones, E. Zanardi-Lamardo, C. A. Moore, and R. G. Zika. 2002. A time-resolved fluorescence study of dissolved organic matter in a riverine to marine transition zone. Marine Chemistry **78**:121-135.

Clarke S.M. and Kirkman H., 1989. Seagrass dynamics. In: A.W.D. Larkum, A.J. McComb and S.A. Shepherd (Eds.), Biology of Seagrasses. Elsevier, Amsterdam, pp. 304-345.

Clementson, L. A., J. S. Parslow, A. R. Turnbull, and P. I. Bonham. 2004. Properties of light absorption in a highly coloured estuarine system in south-east Australia which is prone to blooms of the toxic dinoflagellate Gymnodinium catenatum. Estuarine, Coastal and Shelf Science **60**:101-112.

Coble, P.G., 2007. Marine Optical Biogeochemistry: The Chemistry of Ocean Color. Chem. Rev. 107(2): 402-418.

Collier, C.J., 2006. Characterising responses of the seagrass *Posidonia sinuosa* to changes in light availability. Ph.D. thesis, Faculty of Computing, Health and Science. Perth, Edith Cowan University.

Collier, C.J., P.S. Lavery, R.J. Masini and P.J. Ralph, 2009. Shade-induced response and recovery of the seagrass *Posidonia sinuosa*. Journal of Experimental Marine Biology and Ecology 370: 89-103.

Collings, G., D. Miller, E. O'Loughlin, A. Cheshire and S. Bryars, 2006. Turbidity and reduced light responses of the meadow forming seagrasses, *Amphibolis* and *Posidonia*, from the Adelaide Metropolitan Coastline. ACWS Technical Report No. 12 prepared for the Adelaide Coastal Waters Study Steering Committee. SARDI Aquatic Sciences Publication No. RD01/0208e17. South Australian Research and Development Institute (Aquatic Sciences), Adelaide, South Australia.

Cox, D, J Kaempf, and M Fernandes, 2013. Dispersion and connectivity of land-based discharges near the mouth of a coastal inlet. Journal of Coastal Research 29(6): 100-109.

Czerny, A.B. and K.H. Dunton, 1995. The effects of in situ light reduction on the growth of two subtropical seagrasses, *Thalassia testudinum* and *Halodule wrightii*. Estuaries 18: 418-427.

Davison, I.R. and G.A. Pearson, 1996. Stress tolerance in intertidal seaweeds. Journal of Phycology 32: 197-211.

Dawson, S.P. and W.C. Dennison, 1996. Effects of ultraviolet and photosynthetically active radiation on five seagrass species. Marine Biology 125(4): 629-638.

de Boer, W. F. 2007. Seagrass-sediment interactions, positive feedbacks and critical thresholds for occurrence: a review. Hydrobiologia **591**:5-24.

De Jong, D.J., M.M. van Katwijk and A.G. Brinkman, 2005. Kansenkaart Zeegras Waddenzee. Potentiele groeimogelijkheden voor zeegras in de Waddenzee. Rijksinstituut voor Kust en Zee / RIKZ, Rapport RIKZ/2005.013, Augustus 2005, 51 pp. (in Dutch)

Deltares & Jacobs, 2015. Adelaide Receiving Environment, Phase 2 Inception Report, 1210877-000-ZKS-0006. Delft, The Netherlands.

Deltares, 2014. "Processes Library Description." Version: 5.01 Revision 34078, Delft, The Netherlands.

Den Hartog, C., and P.H. Nienhuis, 1987. Capita Selecta – Estuarine Ecology. Syllabus, Delta Institute for Hydrobiological Research (Yerseke) and University of Nijmegen.

Detenbeck, N.E. and S. Rego, 2015. Predictive Seagrass Habitat Model. US Environmental Protection Agency (EPA), Technical Report EPA/600/R-15/003, September 2015, 163 pp.

Devlin, M. J., J. Barry, D. K. Mills, R. J. Gowen, J. Foden, D. Sivyer, N. Greenwood, D. Pearce, and P. Tett. 2009. Estimating the diffuse attenuation coefficient from optically active constituents in UK marine waters. Estuarine Coastal and Shelf Science **82**:73-83.

Dijkstra, J.T., and R.E. Uittenbogaard, 2010. Modeling the interaction between flow and vegetation. Water Resources Research 46(12), 14 pp. doi:10.1029/2010WR009246.

Dijkstra, J.T., 2012. Macrophytes in estuarine gradients - Flow through flexible vegetation. , PhD Thesis, Delft University of Technology, Delft, The Netherlands.

Duarte, C. M. 1991. Seagrass depth limits. Aquatic Botany **40**:363-377.

Duarte, C. M., N. Marbà, D. Krause-Jensen, and M. Sánchez-Camacho. 2007. Testing the predictive power of seagrass depth limit models. Estuaries and Coasts **30**:652-656.

Eddyvane, K.S., 1999. Conserving Marine Biodiversity in South Australia – Part 2 – Identification of Areas of High Conservation Value in South Australia, Adelaide. South Australian Research and Development Institute (SARDI), Technical Report No. 39, August 1999, 328 pp.

Elith, J., C.H. Graham, R.P. Anderson, M. Dudik, S. Ferrier, A. Guisan, R.J. Hijmans, F. Huettmann, J.R. Leathwick, A. Lehmann, J. Li, L.G. Lohmann, B.A. Loiselle, G. Manion, C. Moritz, M. Nakamura, Y. Nakazawa, J. McC. Overton, A.T. Peterson, S.J. Phillips, K.S. Richardson, R. Scachetti-Pereira, R.E. Schapire, J. Soberon, S. Williams, M.S. Wisz and N.E. Zimmermann, 2006. Novel methods improve prediction of species' distributions from occurrence data. Ecography 29: 129-151.

EnviroDataSA. NatureMaps. 2015. https://data.environment.sa.gov.au/NatureMaps/Pages/default.aspx (accessed Sep 16, 2015).

EPA, 1998. Changes in Seagrass Coverage. ISBN 0-7308-0243-4, Adelaide: EPA South Australia.

Erftemeijer, P.L.A. and K.E. van de Wolfshaar, 2006. Ecological model of the Lagoon of Venice. Part III: Seagrass Habitat Model. WL | Delft Hydraulics, Technical Report Z3733.60, prepared for Technital S.p.A., 142 pp.

Erftemeijer, P.L.A. and K.E. van de Wolfshaar, 2008. Predicting seagrass distribution based on habitat characteristics: a validated model for Venice Lagoon. Paper presented at the 8th International Seagrass Biology Workshop (ISBW8), Vancouver Island, Bamfield, Canada, 31 August - 6 September 2008 (Book of Abstracts).

Erftemeijer, P.L.A., 2014. Seagrass Habitat Model – Adelaide's Coastal Waters. Literature review of habitat requirements of seagrasses in Adelaide's coastal waters. Sinclair Knight Merz (SKM), Technical Report Rev 2, prepared for Deltares and SA Water, February 2014, 44 pp.

Erftemeijer, P.L.A., 2015. Seagrass-Wave Interactions: A Review. Technical Memo, Jacobs Group (Australia), Perth.

EWS, 1975. Gulf St Vincent Water Pollution Studies 1972-1975. Adelaide, SA: Engineering and Water Supply Department, 1975.

EWS, 1985. Gulf St Vincent Water Pollution Studies 1976-1983. Adelaide, SA: Engineering and Water Supply Department, 1985.

Eyre, B. D., A. J. P. Ferguson, A. Webb, D. Maher, and J. M. Oakes. 2011. Denitrification, N-fixation and nitrogen and phosphorus fluxes in different benthic habitats and their contribution to the nitrogen and phosphorus budgets of a shallow oligotrophic sub-tropical coastal system (southern Moreton Bay, Australia). Biogeochemistry **102**:111-133.

Fernandes, M., A. Cheshire, and A. Doonan. 2006. Sediment geochemistry in lower Spencer Gulf: Implications for southern bluefin tuna farming. Australian Journal of Earth Sciences 53:421-432.

Fernandes, M., A. Shareef, R. Kookana, S. Gaylard, S. Hoare, and T. Kildea, 2010. Estrogens, triclosan and derivatives in sediments of Barker Inlet, South Australia: a reported prepared for the Adelaide and Mount Lofty Ranges Natural Resources Management Board and the South Australian Environment Protection Authority. SARDI Aquatic Sciences Publication No. F2010/000385-1. SARDI Research Report Series No. 448. Adelaide, South Australia.

Fernandes, M.B., S. Benger, H. Stuart-Williams, S. Gaylard and S. Bryars, 2015. Coastal nitrogen plumes and their relationship with seagrass distribution. Estuarine, Coastal and Shelf Science 167: 390-403.

Fitzpatrick, J. and H. Kirkman, 1995. Effects of prolonged shading stress on growth and survival of seagrass *Posidonia australis* in Jervis Bay, New South Wales, Australia. Marine Ecology Progress Series 127: 279-289.

Fleming, N.K., J.W. Cox, Y. He, S. Thomas, and J. Frizenschaf, 2010. Analysis of constituent concentrations in the Mount Lofty Ranges for modelling purposes. eWater Cooperative Research Centre, Technical Report, June 2010, 42 pp.

Fletcher, T., Duncan, H., Poelsma, P., & Lloyd, L., 2004. Stormwater flow and quality, and the effectiveness of non-proprietary stormwater treatment measures — a review & gap analysis. Cooperative Research Centre for Catchment Hydrology, Technical Report 04/8, Melbourne.

Folkard, A. M., 2005. Hydrodynamics of model *Posidonia oceanica* patches in shallow water." Limnology and Oceanography 50(5): 1592–1600.

Fong, P. and M.A. Harwell, 1994. Modelling seagrass communities in tropical and subtropical bays and estuaries: a mathematical model synthesis of current hypotheses. Bulletin of Marine Science 54(3): 757-781.

Fonseca, M., P.E. Whitfield, N.M. Kelly and S.S. Bell, 2002. Modeling seagrass landscape pattern and associated ecological attributes. Ecological Applications 12(1): 218-237.

Fonseca, M.S. and W.J. Kenworthy, 1987. Effects of current on photosynthesis and distribution of seagrasses. Aquatic Botany 27: 59-78.

Fonseca, M.S., J.C. Zieman, G.W. Thayer and J.S. Fisher, 1983. The role of current velocity in structuring eelgrass (*Zostera marina* L.) meadows. Estuarine and Coastal Shelf Science 17: 367-380.

Fox, D.R., G.E. Batley, D. Blackburn, Y. Bone, S. Bryars, A. Cheshire, G. Collings, D. Ellis, P. Fairweather, H. Fallowfield, G. Harris, B. Henderson, J. Kämpf, S. Nayar, C. Pattiaratchi, P. Petrusevics, M. Townsend, G. Westphalen and J. Wilkinson, 2007. The Adelaide Coastal Waters Study, Final Report, Volume 1: Summary of Study Findings. CSIRO, November 2007, 68 pp.

Gaby, R., S. Langley and R.F. Keough, 1986. Port of Miami seagrass restoration: analysis of management and economics of a large scale dredge mitigation project. In: J.H. Volbeda, V.L. van Dam and N. Oosterbaan (Eds.), Proceedings of the XIth World Dredging Congress, Brighton, UK, 4–7 March 1986, Central Dredging Association, Delft, pp. 550–561.

Gallegos, C. L. 2001. Calculating optical water quality targets to restore and protect submersed aquatic vegetation: overcoming problems in partitioning the diffuse attenuation coefficient for photosynthetically active radiation. Estuaries **24**:381-397.

Gaylard, S. 2004. Ambient water quality monitoring of the Gulf St Vincent metropolitan coastal waters. Report no 2: 1995-2002. E. P. Authority, Adelaide, South Australia.

Gill, A.E., 1982. Atmosphere-Ocean dynamics. Vol. 30 of International Geophysics Series. Academic Press, New York, 1982.

Gordon, D.M., K.A. Grey, S.C. Chase and C.J. Simpson, 1994. Changes to the structure and productivity of a *Posidonia sinuosa* meadow during and after imposed shading. Aquatic Botany 47: 265-275.

Gordon, H. R. 1989. Can the Lambert-Beer law be applied to the diffuse attenuation coefficient of ocean water? Limnology and Oceanography **34**:1389-1409.

Grech, A, and R.G. Coles, 2010. An ecosystem-scale predictive model of coastal seagrass distribution. Aquatic Conservation: Marine and Freshwater Ecosystems 20: 437-444.

Green E.P. and F.T. Short, 2003. World Atlas of Seagrasses. University of California Press, 298 pp.

Greenwood, G. and E. Gum, 1986. The State of Environmental Resources in South Australia. A Contribution towards Improving our Understanding of the South Australian Environment. Conservations Project Branch, Department of Environment and Planning, 253 pp.

Greve, T.M. and D. Krause-Jensen, 2005. Predictive modelling of eelgrass (*Zostera marina*) depth limits. Marine Biology 146: 849-858.

Guisan, A. and N.E. Zimmerman, 2000. Predictive habitat distribution models in ecology. Ecological Modelling 135: 147-186.

Guisan, A. and W. Thuiller, 2005. Predicting species distribution: offering more than simple habitat models. Ecology Letters 8: 993-1009.

Hart, D., 2013. Seagrass extent change 2007-2013 - Adelaide coastal waters. Technical note 2013/07, Adelaide: DEWNR, 2013.

Hart, D., 1997. Near-shore seagrass change between 1949 and 1996 mapped using digital aerial orthophotography, metropolitan Adelaide area, Largs Bay-Aldinga, South Australia. A report prepared for the South Australian EPA. Department of Environment and Natural Resources, Adelaide, South Australia, p. 12.

Hasselmann, S., K. Hasselmann, J.A. Allender and T.P. Barnett, 1985. Computations and parameterizations of the nonlinear energy transfer in a gravity-wave spectrum. Part 2: Parameterization of the nonlinear transfer for application in wave models. J. Phys. Oceanogr. 15(11): 1378-1391.

Hemminga, M.A. and C.M. Duarte, 2000. Seagrass Ecology. Springer, Cambridge (UK), 298 pp.

Hendriks, I. E., T. Sintes, T. J. Bouma, and C. M. Duarte. 2008. Experimental assessment and modeling evaluation of the effects of the seagrass Posidonia oceanica on flow and particle trapping. Marine Ecology Progress Series **356**:163-173.

Hillman, K., D.I. Walker, A.W.D. Larkum and A.J. McComb, 1989. Productivity and nutrient limitation. In: A.W.D. Larkum, A.J. McComb and S.A. Shepherd (Eds.), Biology of seagrasses: A treatise on the biology of seagrasses with special reference to the Australian region. Elsevier, Amsterdam, pp. 635-685.

Hirzel, A.H., G. Le Lay, V. Helfer, C. Randin and A. Guisan, 2006. Evaluating the ability of habitat suitability models to predict species presence. Ecological Modelling 199: 142-152.

Hocking, P.J., M.I. Cambridge and A.J. McComb, 1981. The nitrogen and phosphorus nutrition of developing plants of two seagrasses, *Posidonia australis* and *Posidonia sinuosa*. Aquatic Botany 11: 245-261.

Holmes, K.W., K.P. van Niel, G.A. Kendrick and B. Radford, 2007. Probabilistic large-area mapping of seagrass species distribution. Aquatic Conservation: Marine and Freshwater Ecosystems 17: 385-407.

Hu C., Muller-Karger F.E. & Zepp R.G. (2002). Absorbance, absorption coefficient, and apparent quantum yield: A comment on common ambiguity in the use of these optical concepts. Limnol. Oceanogr., 47, 1261-1267.

Imgraben, S. and S. Dittmann. 2008. Leaf litter dynamics and litter consumption in two temperate South Australian mangrove forests. Journal of Sea Research 59:83-93.

Infantes, E., J. Terrados, A. Orfila, B. Caňellas and A. Alvarez-Ellacuria, 2009. Wave energy and the upper depth limit distribution of *Posidonia oceanica*. Botanica Marina 52: 419-427.

Inglis, G.J., 2000. Variation in the recruitment behaviour of seagrass seeds: implications for population dynamics and resource management. Pacific Conservation Biology 5(4): 251-259.

Jenkins, C.,2005. Nutrient flux assessment in the Port waterways. Adelaide, South Australia.

Jones, E. M., J. Kämpf, and M. Fernandes. 2012. Characterisation of the wave field and associated risk of sediment resuspension in a coastal aquaculture zone. Ocean & Coastal Management **69**:16-26.

Jones, R. 2015. Adelaide Coastal Waters Study: stormwater data audit report 2015 draft. A report prepared for the EPA. Adelaide, South Australia.

Jonsson, I. G. 1966. Wave boundary layers and friction factors. Pages 127-148 Proceedings 10th International Conference of Coastal Engineering. ASCE.

Kelble, C. R., P. B. Ortner, G. L. Hitchcock, and J. N. Boyer. 2005. Attenuation of photosynthetically available radiation (PAR) in Florida Bay: Potential for light limitation of primary producers. Estuaries **28**:560-571.

Kelly, N.M., M. Fonseca and P. Whitfield, 2001. Predictive mapping for management and conservation of seagrass beds in North Carolina. Aquatic Conservation: Marine and Freshwater Ecosystems 11: 437-451.

Kemp, W.M., R. Batiuk, R. Bartleson, P. Bergstrom, V. Carter, C.I. Gallegos, W. Hunley, L. Karrh, E.W. Koch, J.M. Landwehr, K.A. Moore, L. Murray, M. Naylor, N.B. Rybicki, J.C. Stevenson and D.J. Wilcox, 2004. Habitat requirements for submerged aquatic vegetation in Chesapeake Bay: water quality, light regime, and physical-chemical factors. Estuaries 27(3): 363-377.

Kieber, R. J., R. F. Whitehead and S. A. Skrabal, 2006. Photochemical production of dissolved organic carbon from resuspended sediments. Limnology and Oceanography 51: 2187-2195.

Kirk, J. T. O. 1983. Light and Photosynthesis in Aquatic Ecosystems. Cambridge University Press.

Kirkman, H., A. Cohen and H. Houridis, 2012. A seagrass shading experiment to determine the effects of a dredge plume. Victorian Naturalist 129(3): 97-108.

Keuskamp, D., 2004. Limited effects of grazer exclusion on the epiphytes of *Posidonia sinuosa* in South Australia. Aquatic Botany, 78: 3-14.

Kiswara, W., P. van Avezaath, A.H.L. Huiskes, P.L.A. Erftemeijer and T.J. Bouma, 2009. Root architecture of six oligotrophic seagrass species growing in three contrasting habitats. Aquatic Botany 90: 235-245.

Koch E.W. et al., 2006a. Fluid dynamics in seagrass ecology – from molecules to ecosystems. Chapter 8 in: A.W.D. Larkum et al. (Eds.) Seagrasses: Biology, Ecology and Conservation, pp. 193-225.

Koch E.W. et al., 2006b. Waves in Seagrass Systems: Review and Technical Recommendations. US Army Corps of Engineers, Engineer Research and Development Center, Technical Report ERDC TR-06-15, 92 pp.

Koch, E.W., 2001. Beyond light: physical, geological and geochemical parameters as possible submerged aquatic vegetation habitat requirements. Estuaries 24(1): 117.

Koftis, T., P. Prinos, and V. Stratigaki. 2013. Wave damping over artificial Posidonia oceanica meadow: A large-scale experimental study. Coastal Engineering **73**:71-83.

Komada, T. and C. E. Reimers. 2001. Resuspension-induced partitioning of organic carbon between solid and solution phases from a river-ocean transition. Marine Chemistry 76:155-174.

Kostoglidis, A., C. B. Pattiaratchi, and D. P. Hamilton. 2005. CDOM and its contribution to the underwater light climate of a shallow, microtidal estuary in south-western Australia. Estuarine, Coastal and Shelf Science **63**:469-477.

Krone, R., 1962. Flume studies of transport of sediment in estuarial shoaling processes. Berkeley, USA: University of California, Hydraulics Engineering and Sanitary.

Lane, A., 1989. The heat balance of the North Sea. Tech. Rep. 8, Proudman Oceanographic Laboratory.

Lathrop, R.G., R.M. Styles, S.P. Seitzinger and J.A. Bognar, 2001. Use of GIS mapping and modeling approaches to examine the spatial distribution of seagrasses in Barnegat Bay, New Jersey. Estuaries 24(6A): 904-916.

Lavery, P.S., K. McMahon, M. Mulligan, A. Tennyson, 2009. Interactive effects of timing, intensity and duration of experimental shading on *Amphibolis griffithii*. Marine Ecology Progress Series 394: 21–33.

Le, C., C. Hu, D. English, J. Cannizzaro, Z. Chen, C. Kovach, C. J. Anastasiou, J. Zhao, and K. L. Carder. 2013. Inherent and apparent optical properties of the complex estuarine waters of Tampa Bay: what controls light? Estuarine, Coastal and Shelf Science **117**:54-69.

Lee, ZP, KP Du, and R Arnone, 2005. A model for the diffuse attenuation coefficient of down-welling irradiance. Journal of Geophysical Research 110, C02016, doi:10.1029/2004JC002275, 2005.

Leendertse, J.J., 1987. A three-dimensional alternating direction implicit model with iterative fourth-order dissipative non-linear advection terms. WD-3333-NETH, Rijkswaterstaat.

Lefevre, N., A.H. Taylor, F.J. Gilbert and R.J. Geider, 2003. Modelling carbon to nitrogen and carbon to chlorophyll a ratios in the ocean at low latitudes: evaluation of the role of physiological plasticity. Limnology and Oceanography 48(5): 1796–1807.

Lesser G.R., J.A. Roelvink, J.A.T.M. Van Kester and G.S. Stelling, 2004. Development and validation of a three-dimensional morphological model. Coastal Engineering 51: 883-915.

Lewis, S. A. 1975. Gulf St Vincent water pollution studies 1972-1975. Report EWS 3876/70. Engineering and Water Supply Department, Adelaide, South Australia.

Lill, J., 2005. The effect of nutrients on the morphology of two seagrass species: *Posidonia sinuosa* and *Amphibolis antarctica*. SARDI Aquatic Sciences Summer Scholarship Project 2004-05/4. (quoted in ACWS Report No. 13)

Lirman, D. and W.P. Cropper, 2003. The influence of salinity on seagrass growth, survivorship and distribution within Biscayne Bay, Florida: Field, experimental and modeling studies. Estuaries 26(1): 131-141.

Littler, M.M. and D.S. Littler. 1980. The evolution of thallus form and survival strategies in benthic marine macroalgae: field and laboratory tests of a functional form model. Am. Nat. 116: 25-44.

Longstaff, B.J., N.R. Loneragan, M.J. O'Donohue and W.C. Dennison, 1999. Effects of light deprivation on the survival and recovery of the seagrass *Halophila ovalis* (R.Br.) Hook. Journal of Experimental Marine Biology and Ecology 234: 1-27.

Lorenzen, C. J. 1972. Extinction of light in the ocean by phytoplankton. Journal du Conseil **34**:262-267.

Los, F.J., 2009. Eco-hydrodynamic modelling of primary production in coastal waters and lakes using BLOOM. Ph.D. Thesis, Wageningen University, 2009.

Los F.J. and M. Blaas, 2010. Complexity, accuracy and practical applicability of different biogeochemical model versions. Journal of Marine Systems 81: 44–74.

Mackey, P., C.J. Collier and P.S. Lavery, 2007. Effects of experimental reduction of light availability on the seagrass *Amphibolis griffithii*. Marine Ecology Progress Series 342: 117–126.

Madsen, O.S., Y.K. Poon and H.C. Graber, 1988. Spectra wave attenuation by bottom friction: theory. Proceedings of the 21st International Conference on Coastal Engineering, 1998, New York, pp. 492-504.

Mateo, M.A. and J. Romero, 1997. Detritus dynamics in the seagrass *Posidonia oceanica*: Elements for an ecosystem carbon and nutrient budget. Marine Ecology Progress Series 151(1-3): 43-53.

McDowell, L.M. and P. Pfennig, 2013. Adelaide Coastal Water Quality Improvement Plan (ACWQIP). Environmental Protection Authority, South Australia, July 2013.

McMahon, K., P.S. Lavery and M. Mulligan, 2011. Recovery from the impact of light reduction on the seagrass *Amphibolis griffithii*, insights for dredging management. Marine Pollution Bulletin 62: 270–283.

McMillan, C., 1984. The distribution of tropical seagrasses with relation to their tolerance of high temperatures. Aquatic Botany 19: 369-379.

Meybeck, M. and R. Helmer, 1989. The quality of rivers: from pristine stage to gloval pollution. Palaeogeography, Palaeoclimatology, Palaeoecology 75 (1989): 283-309.

Meybeck (1982). Carbon, nitrogen, and phosphorus transport by world rivers. American Journal of Science, 282, 401-450.

Meyer, C.A., 2013. Evaluating habitat vulnerability and sustainability of urban seagrass resources to sea level rise. PhD thesis, University of South Florida, January 2013, 163 pp.

Middelburg, J. J. and P. M. J. Herman. 2007. Organic matter processing in tidal estuaries. Marine Chemistry **106**:127-147.

Moate, B. D., D. G. Bowers, and D. N. Thomas. 2012. Measurements of mineral particle optical absorption properties in turbid estuaries: Intercomparison of methods and implications for optical inversions. Estuarine Coastal and Shelf Science **99**:95-107.

Moore, K. A., R. L. Wetzel, and R. J. Orth. 1997. Seasonal pulses of turbidity and their relations to eelgrass (Zostera marina L.) survival in an estuary. Journal of Experimental Marine Biology and Ecology **215**:115-134.

Mumby, P.J. and A.J. Edwards, 2002. Mapping marine environments with IKONOS imagery: enhanced spatial resolution can deliver greater thematic accuracy. Remote Sensing of Environment 82(2-3): 248-257.

Mumby, P.J. and E.P. Green, 2000. Mapping seagrass beds. Chapter 12 in: E.P. Green et al. (Eds.) Remote Sensing Handbook for Tropical Coastal Management. Coastal Management Sourcebooks 3. Unesco, pp. 175-181.

Neverauskas, V.P. 1987. Accumulation of periphyton biomass on artificial substrates deployed near a sewage sludge outfall in South Australia. Estuarine Coastal and Shelf Science 25: 509-517.

Neverauskas, V., 1988. Response of a *Posidonia* community to prolonged reduction in light. Aquatic Botany 31: 361-366.

Obrador, B. and J. L. Pretus. 2008. Light regime and components of turbidity in a Mediterranean coastal lagoon. Estuarine, Coastal and Shelf Science **77**:123-133.

Onuf, C.P., 1994. Seagrasses, dredging and light in Laguna Madre, Texas, USA. Estuarine Coastal and Shelf Science 39: 75-91.

Orth, R.J., M.C. Harwell and G.J. Inglis, 2006. Ecology of seagrass seeds and seagrass dispersal processes. Chapter 5 in: A.W.D. Larkum et al. (Eds), Seagrasses: Biology, Ecology and Conservation, Springer, pp. 111-133.

Paling, E.I. and A.J. McComb, 2000. Autumn biomass, below-ground productivity, rhizome growth at bed edge and nitrogen content in seagrasses from Western Australia. Aquatic Botany 67: 207-219.

Parsons, T. R., M. Takahashi, and B. Hargrave. 1984. Biological oceanographic processes, 3rd edition. Pergamon Press, New York.

Partheniades, E., 1962. A study of erosion and deposition of cohesive soils in salt water. Ph.D. thesis, Berkeley, USA: University of California, 1962.

Pattiaratchi, C., J. Newgard and B. Hollings, 2007. Physical oceanographic studies of Adelaide coastal waters using high resolution modelling, in-situ observations and satellite techniques. ACWS Technical Report No. 20, School of Environmental Systems Engineering, University of Western Australia, 2007.

Pearce, J. and S. Ferrier, 2000. Evaluating the predictive performance of habitat models developed using logistic regression. Ecological Modelling 133: 225-245.

Pedersen, T. M., C. L. Gallegos, and S. L. Nielsen. 2012. Influence of near-bottom re-suspended sediment on benthic light availability. Estuarine Coastal and Shelf Science **106**:93-101.

Petrusevics, P., 2005. Distribution of Suspended Matter Using SeaWiFS Data. ACWS Technical Report No. 5, Adelaide: Oceanique Perspectives, 2005.

Pfannkuche, J. 2002. Optical properties of Otago shelf waters: south island New Zealand. Estuarine, Coastal and Shelf Science **55**:613-627.

Ralph, P. J., M. J. Durako, S. Enriquez, C. J. Collier, and M. A. Doblin. 2007. Impact of light limitation on seagrasses. Journal of Experimental Marine Biology and Ecology **350**:176-193.

Rivers, D., Kendrick, G., Walker, D.I., 2011. Microsites play an important role for seedling survival in the seagrass *Amphibolis antarctica*. J. Exp. Mar. Biol. Ecol. 401(1): 29–35.

Robertson, E.L., 1984. Seagrasses. In: H.B.S. Womersley (Ed.), The Marine Benthic Flora of Southern Australia - Part 1. Adelaide, S.A. Government Printer.

Robson Barbara J., Vincent Dourdet, 2015. Prediction of sediment, particulate nutrient and dissolved nutrient concentrations in a dry tropical river to provide input to a mechanistic coastal water quality model. Environmental Modelling & Software 63 (2015) 97-108.

Roelvink, J.A. and G.K.F.M. Van Banning, 1994. Design and development of Delft3D and application to coastal morphodynamics. In: A. Verwey, A.W. Minns and V. Babovic (Eds.), Proceedings Hydroinformatics 1994. Balkema, Rotterdam, pp. 451-456.

Roloff, G.J. and B.J. Kernohan, 1999. Evaluating reliability of habitat suitability index models. Wildlife Society Bulletin 27(4): 973-985.

Romero J, Pergent G, Pergent-Martini C, Mateo MA and Regnier C, 1992. The detritic compartment in a *Posidonia oceanica* meadow: litter features, decomposition rates and mineral stocks. PSZN I: Mar Ecol 13(1):69-83.

Rouse K, Gonzalez D, Fernandes M, Daly R, Maheepala S, Mirza F, van Gils J, He Y, Cuddy SM (2016) New modelling capability to target stormwater interventions that support seagrass health along Adelaide's coast, Goyder Institute for Water Research Technical Report Series No. 16, Adelaide, South Australia.

Saha, S., S. Moorthi, and H.L. Pan, 2010. The NCEP Climate Forecast System Reanalysis. Bulletin of the American Meteorological Society 91(8): 1015-1057.

Samarasinghe, J. R. D., L. Bode, and L. B. Mason. 2003. Modelled response of Gulf St Vincent (South Australia) to evaporation, heating and winds. Continental Shelf Research **23**:1285-1313.

Santos, R.O. and D. Lirman, 2012. Using habitat suitability models to predict changes in seagrass distribution caused by water management practices. Canadian Journal of Fisheries and Aquatic Sciences 69: 1380-1388.

Seddon, S., R.M. Connolly and K.S. Edyvane, 2000. Large-scale seagrass dieback in northern Spencer Gulf, South Australia. Aquatic Botany 66: 297-310.

Serrano, O., M.A. Mateo and P. Renom, 2011. Seasonal response of *Posidonia oceanica* to light disturbances. Marine Ecology Progress Series 423: 29-38.

Servais et al. (1999). Supply of organic matter and bacteria to aquatic systems through waste water effluents, 33(16), 3521-3531.

Shafer, D.J., T.M. Swannack, C. Saltus, J.E. Kaldy and A. Davis, 2016. Development and validation of a habitat suitability model for the non-indigenous seagrass *Zostera japonica* in North America. Management of Biological Invasions 7 (2): 141-155.

Shank, G. C., A. Evans, Y. Yamashita, and R. Jaffe, 2011. Solar radiation-enhanced dissolution of particulate organic matter from coastal marine sediments. Limnology and Oceanography 56: 577-588.

Shank, G. C., R. Lee, A. Vahatalo, R. G. Zepp, and E. Bartels, 2010a. Production of chromophoric dissolved organic matter from mangrove leaf litter and floating *Sargassum* colonies. Marine Chemistry 119: 172-181.

Shank, G. C., R. G. Zepp, A. Vahatalo, R. Lee, and E. Bartels, 2010b. Photobleaching kinetics of chromophoric dissolved organic matter derived from mangrove leaf litter and floating *Sargassum* colonies. Marine Chemistry 119: 162-171.

Shepherd, S.A. and E.L. Robertson, 1989. Regional studies - Seagrasses of South Australia, Victoria and Bass Strait. In: A.W.D. Larkum, A.J. McComb and S.A. Shepherd (Eds.), Biology of Seagrasses. Elsevier, Amsterdam, pp. 211-229.

Shepherd, S.A., A.J. McComb, D.A. Bulthuis, V. Neverauskas, D.A. Steffensen and R. West, 1989. Decline of seagrasses. In: Larkum, A.W.D., McComb, A.J., Shepherd, S.A. (Eds.), Seagrasses: A Treatise on the Biology of Seagrasses with Special Reference to the Australian Region. Elsevier, North Holland, pp. 346–387.

Short, F., T. Carruthers, W. Dennison, and M. Waycott. 2007. Global seagrass distribution and diversity: A bioregional model. Journal of Experimental Marine Biology and Ecology **350**:3-20.

Smith, S.D. and E.G. Banke, 1975. Variation of Sea Surface Drag Coefficient with Wind Speed. Quart. J. R. Met. Society 101(429): 665-673.

Smits, J.G.C. and J.K.L. van Beek, 2013. ECO: A Generic Eutrophication Model Including Comprehensive Sediment-Water Interaction. PLoS ONE 8(7), 2013: e68104.

Stabenau, E.R., R.G. Zepp, E. Bartels, and R.G. Zika, 2004. Role of the seagrass *Thalassia testudinum* as a source of chromophoric dissolved organic matter in coastal south Florida. Marine Ecology Progress Series 282: 59-72.

Standards Australia (1990). Australian Standard AS3753 - 1990. Recommended Practice for Chemical Analysis by Ultraviolet/Visible Spectrophotometry – 1990 edition. In. Standards Australia Homebush, NSW, Australia.

Steffensen, D. A. 1985. Gulf St Vincent water pollution studies phase II 1976-1983. Part 1 Southern and Central metropolitan zones. Report EWS 142/84. Engineering and Water Supply Department, Adelaide, South Australia.

Stelling, G.S., 1983. On the construction of computational methods for shallow water flow problems. PhD thesis, Delft University of Technology.

Stramski, D., M. Babin, and S. B. Wozniak. 2007. Variations in the optical properties of terrigenous mineral-rich particulate matter suspended in seawater. Limnology and Oceanography **52**:2418-2433.

Strickland, J. D. H. 1958. Solar radiation penetrating the ocean. A review of requirements, data and methods of measurement, with particular reference to photosynthetic productivity. Journal of the Fisheries Board of Canada **15**:453-493.

Sverdrup, H. U. 1953. On conditions for the vernal blooming of phytoplankton. Journal du Conseil **18.3**:287-295.

Syvitski J.P.M., Morehead M.D., Bahr D.B. & Mulder T. (2000). Estimating fluvial sediment transport: the rating parameters. Water Resources Research, 36, 2747-2760.

Tanner, J.E., Irving, A.D., Fernandes, M., Fotheringham, D., McArdle, A. and S. Murray-Jones, 2014. Seagrass rehabilitation off metropolitan Adelaide: a case study of loss, action, failure, and success. Ecological Management & Restoration 15: 168-179.

Taylor, A.H., R.J. Geider and F.J.H. Gilbert, 1997. Seasonal and latitudinal dependencies of phytoplankton carbon-to-chlorophyll a ratios: results of a modelling study. Marine Ecology Progress Series 152: 51-66.

Thom, R.M., J.L. Gaeckle, K.E. Buenau, A.B. Borde, J. Vavrinec, L. Aston and D.L. Woodruff, 2014. Eelgrass (*Zostera marina* L.) Restoration in Puget Sound: Development and Testing of Tools for Optimizing Site Selection. Pacific Northwest National Laboratory, Technical Report PNNL-23635, prepared for the U.S. Department of Energy, September 2014, 62 pp.

Thomann, R.V. and J.A. Mueller, 1987. Principles of Surface Water Quality Modelling and Control. New York: Harper & Row Publ., 1987.

Thomasma, L.E., T. Drummer and R.O. Peterson, 1991. Testing the habitat suitability index for the fisher. Wildlife Society Bulletin 19: 291-297.

Trautman, D.A. and M.A. Borowitzka, 1999. Distribution of epiphytic organisms on *Posidonia australis* and *P. sinuosa*, two seagrasses with differing leaf morphology. Mar Ecol Prog Ser 179: 215-229.

Twigt, D, E de Goede, F Zijl, D Schwanenberg and A Chiu, 2009. Coupled 1D–3D hydrodynamic modelling, with application to the Pearl River Delta. Ocean Dynamics 59(6): 1077-1093.

U.S. Fish and Wildlife Services, 1980. Habitat Evaluation Procedures (HEP). Ecol. Serv. Man. 101, Div. Ecol. Serv., U.S. Dep. Inter. Fish Wildl. Serv., Washington D.C.

U.S. Fish and Wildlife Services, 1981. Standards for the development of habitat suitability index models. United States Fish and Wildlife Service, Release No. 1-81, 103 ESM.

Uhrin, A.V. and P.A. Townsend, 2016. Improved seagrass mapping using linear spectral un-mixing of aerial photographs. Estuarine, Coastal and Shelf Science 171: 11-22.

Vacchi, M., Montefalcone, M., Bianchi, C.N., Morri, C., Ferrari, M., 2012. Hydrodynamic constraints to the seaward development of *Posidonia oceanica* meadows. Estuarine, Coastal and Shelf Science 97: 58–65.

Vacchi, M., M. Montefalcone, C.F. Schiaffino, V. Parravicini, C.N. Bianchi, C. Morri and M. Ferrari, 2014. Towards a predictive model to assess the natural position of the *Posidonia oceanica* seagrass meadows upper limit. Marine Pollution Bulletin 83: 458–466.

Valle, M., A. Borja, G. Chust, I. Galparsoro and J.M. Garmendia, 2011. Modelling suitable estuarine habitats for *Zostera noltii*, using Ecological Niche Factor Analysis and Bathymetric LiDAR. Estuarine and Coastal Shelf Science 94: 144-154.

Valle, M., M.M. van Katwijk, D.J. de Jong, T.J. Bouma, A.M. Schipper, G. Chust, B.M. Benito, J.M. Garmendia and A. Borja, 2013. Comparing the performance of species distribution models of *Zostera marina*: implications for conservation. Journal of Sea Research 83: 56-64.

Van der Heide, T., E.T.H.M. Peeters, D.C.R. Hermus, M.M. van Katwijk, J.G.M. Rolofs and A.J.P. Smolders, 2009. Predicting habitat suitability in temperate seagrass ecosystems. Limnology and Oceanography 54(6): 2018-2024.

van der Heide, T., E. H. van Nes, M. M. van Katwijk, H. Olff, and A. J. P. Smolders. 2011. Positive Feedbacks in Seagrass Ecosystems - Evidence from Large-Scale Empirical Data. PLoS ONE **6**.

Van der Westhuysen, AJ, M Zijlema and JA Battjes, 2007. Nonlinear saturation-based white-capping dissipation in SWAN for deep and shallow water. Coastal Engineering 54: 151-170.

Van Gils, J., Tatman, S., 2003. Light penetration in the water column. MARE Report, WL2003001 Z3379. WL | Delft Hydraulics, Delft, The Netherlands, 38p.

Van Gils, J, K van Heeringen, D Schwanenberg, E de Goede and F Zijl, 2007. Pearl River Delta Water Quality Model. Final Study Report, Delft: Delft Hydraulics, 2007.

Van Gils, J. and G. Barbara, 2014. Adelaide Receiving Environment Model Field Data Collection Programme. Delft: Deltares and SKM, 2014.

Van Keulen, M. and M.A. Borowitzka, 2002. Comparison of water velocity profiles through morphologically dissimilar seagrasses measured with a simple and inexpensive current meter. Bulletin of Marine Science 71(3): 1257–1267.

Van Rijn, L., 1993. Principles of sediment transport. Aqua publications.

van Ruth, P. D. 2010. Adelaide Desalination Project Plankton Characterisation Study, prepared for Adelaide Aqua. SARDI Publication No. F2010/000378-1. SARDI Research Report Series No. 487. Adelaide, South Australia.

van Ruth, P. D. 2012. Adelaide Desalination Project Plankton Characterisation Study, Phase 2. Prepared for Adelaide Aqua. SARDI Publication No. F2010/000378-2. SARDI Research Report Series No. 606. Adelaide, South Australia.

Vant, W. N. 1990. Causes of light attenuation in nine New Zealand estuaries. Estuarine, Coastal and Shelf Science **31**:125-137.

Verduin, J.J., A. Seidlitz, M. van Keulen and EI. Paling, 2013. Maximising establishment success of *Amphibolis antarctica* seedlings. Journal of Experimental Marine Biology and Ecology 449: 57-60.

Walker, D.I. and A.J. McComb, 1990. Salinity response of the seagrass *Amphibolis antarctica* (Labill.) Sonder et Aschers.: an experimental validation of field results. Aquatic Botany 36: 359-366.

Walling D.E., Owens P.N., Waterfall B.D., Leeks G.J.L. & Wass P.D. (2000). The particle size characteristics of fluvial suspended sediment in the Humber and Tweed catchments, UK. Sci. Total Environ., 251, 205-222.

Walsby, A. E. 1997. Numerical integration of phytoplankton photosynthesis through time and depth in a water column. New Phytologist **136**:189-209.

Westphalen, G., G. Collings, R. Wear, M. Fernandes, S. Bryars and A. Cheshire, 2004. A review of seagrass loss on the Adelaide metropolitan coastline. ACWS Technical Report No. 2, prepared for the Adelaide Coastal

Waters Study Steering Committee. South Australian Research and Development Institute (Aquatic Sciences) Publication No. RD04/0073, Adelaide.

Whiteway, TG., 2009. Australian Bathymetry and Topography Grid. Record 2009/21, Canberra: Geoscience Australia.

Wilkinson, J., N. White, L. Smythe, J. Hutson, E. Bestland, C. Simmons, S. Lamontagne and H. Fallowfield, 2005. Volumes of inputs, their concentrations and loads received by Adelaide metropolitan coastal waters. ACWS Technical Report No. 18, Adelaide: Flinders Centre for Coastal and Catchment Environments, Flinders University of SA, 2005.

Wilkinson, J., 2005. Reconstruction of historical stormwater flows in the Adelaide metropolitan area. ACWS Technical Report No. 10, Adelaide: Department of Environmental Health, Flinders University of SA.

Wilkinson, J., J. Hutson, E. Bestland, and H. Fallowfield. 2005a. Audit of contemporary and historical quality and quantity data of stormwater discharging into the marine environment, and field work programme. ACWS Technical Report No. 3 prepared for the Adelaide Coastal Waters Study Steering Committee. Adelaide, South Australia.

Wintermans, J. F. G. M. and A. D. Mots. 1965. Spectrophotometric characteristics of chlorophylls a and b and their phenophytins in ethanol. Biochimica et Biophysica Acta (BBA)-Biophysics including Photosynthesis **109**:448-453.

Woźniak, S. B., D. Stramski, M. Stramska, R. A. Reynolds, V. M. Wright, E. Y. Miksic, M. Cichocka, and A. M. Cieplak. 2010. Optical variability of seawater in relation to particle concentration, composition, and size distribution in the nearshore marine environment at Imperial Beach, California. Journal of Geophysical Research: Oceans **115**.

Xu, J. T., R. R. Hood, and S. Y. Chao. 2005. A simple empirical optical model for simulating light attenuation variability in a partially mixed estuary. Estuaries **28**:572-580.

Yaakub, S.M., E. Chen, T.J. Bouma, P.L.A. Erftemeijer and P.A. Todd, 2013. Chronic light reduction reduces overall resilience to further shading stress in the seagrass *Halophila ovalis*. Marine Pollution Bulletin 83: 467-474.

Yamaguchi, H., R. Katahira, K. Ichimi, and K. Tada. 2013. Optically active components and light attenuation in an offshore station of Harima Sound, eastern Seto Inland Sea, Japan. Hydrobiologia **714**:49-59.

Zajac, Z., B. Stith, A.C. Bowling, C.A. Langtimm and E.D. Swain, 2015. Evaluation of habitat suitability index models by global sensitivity and uncertainty analyses: a case study for submerged vegetation. Ecology and Evolution 5(13): 2503-2517.

Zawilski & Brzezinska (2009). Variability of COD and TKN fractions of combined wastewater. Polish Journal of Environmental Studies, 18(3), 501-505.

Zhou, J., Q. Wang, W. Zhao, D. Yu and S. Guan, 2016. Habitat suitability analysis of eelgrass *Zostera marina* L. in the subtidal zone of Xiaoheishan Island. Chinese Journal of Oceanology and Limnology 34(1): 69-78.

Zieman, J.C., 1982. The ecology of seagrasses of South Florida: a community profile. U.S. Fish and Wildl. Serv., FWS/OBS82/25. Washington D.C.

Zijl F., Rego J.d.L., Groeneweg J., Dijkstra J., Chatelain M., de Kluijver A. & van Gils J. (2014). Adelaide Receiving Environment Model. Pilot Model set-up and evaluation. Deltares report 1207457-000. In: Delft, the Netherlands, p. 164.

A The derivation of spatially and temporally explicit Area Specific Loads (ASL) for coastal waters using mathematical models

A.1 Method to calculate ASLs

The computation of area specific loads (ASL) was based on the assessment of a tracer simulation. We released one conservative tracer and one decaying tracer from all individual discharge points in the AREM (rivers and stormwater discharges, Penrice industrial wastewater discharge, treated domestic wastewater discharges from Bolivar, Christies and Glenelg). At all discharge points, the associated conservative and decaying tracers were released at a rate equal to the release rate of the parameter under investigation (nitrogen, suspended solids).

The results from the tracer simulation were postprocessed to obtain ASLs. For every discharge point, we first calculated annual and depth averaged concentrations of the associated conservative tracer. Next, we established a series of relevant equal concentration contour lines. For every individual contour line with concentration C (g m^{-3}), we calculated the area within the contour S (m^2). We calculated the mean concentration of the conservative (C_{mc}) and the decaying (C_{md}) tracers inside that contour. The ratio of these values, together with the known decay rate k (d^{-1}) of the decaying tracer provided the residence time T (d) of the tracer over the area inside the contour:

$$T = \frac{-ln\left(\frac{C_{md}}{C_{mc}}\right)}{k}$$

The ASL (g m^{-2}) for that contour was calculated from the load discharged W (g d^{-1}), the surface area S (m^2) and the residence time T (d):

$$ASL = \frac{WT}{S}$$

These ASLs were computed for individual discharge points, and then combined to obtain totals per sector and overall totals.

This approach provided annually mean ASL values, but did not allow assessing the temporal variability of the ASL. For reasons explained in section 5.2.4, we consider the extreme values of rolling averages over a defined period (30 days, 90 days, 180 days) as being representative for impacts on seagrasses at any location. To assess these quantities, we assumed that the temporal variability of the concentrations is proportional to the temporal variability of the ASL. For practical reasons, the temporal variability of the concentrations was characterised by tidally averaged concentrations calculated by the AREM and stored in an output file. The within-tide variation of the concentrations was thus neglected, as seagrass impacts are evidently not an issue of minutes to hours. This procedure maintained differences between springs and neaps, because these are relevant for the residual transport time scales.

Thus, we estimated the maximum ASL for a rolling average over N days ($ASL_{raN,max}$) as follows:

$$ASL_{raN,max} = ASL \times \frac{C_{raN,max}}{C_m}$$

where *ASL* is the annually averaged ASL, C_m is the annual average of the daily mean concentrations, and $C_{raN,max}$ is the maximum of the N days rolling average of the daily mean concentrations. While calculating rolling averages, we made the annual simulation period circular, meaning that the average over 16-31 December and 1-15 January is also a valid 30 days rolling average. In a similar way the 3 months and 6 months values are determined.

A.2 Results

Below we show the simulated ASLs for nitrogen and suspended solids as an annual mean and as a maximum value for moving averages for different periods. The Adelaide Coastal Waters Study (ACWS) suggested a nitrogen ASL threshold of 1 gN m^{-2}. We plotted the simulated ASLs for nitrogen on a scale from 0-1.5 gN m^{-2} to allow evaluation of this threshold. The ACWS specified an allowable load to the Adelaide coastal waters of 600 tN/y. For suspended solids, an allowable load of 4,200 t/y is suggested. Based on these numbers, and by analogy between nitrogen and suspended solids, we adopt a suspended solids ASL threshold of 7 g m^{-2}. We plotted the simulated ASLs for suspended solids on a scale from 0-10 g m^{-2} to allow evaluation of this threshold.

Below we present the simulated ASLs for all sources together, with and without the discharge from Penrice. The results are provided as four figures per parameter, showing:

- annual mean ASL in g m^{-2};
- maximum value of a 6 month rolling average of the ASL in g m^{-2} (ASL_6m);
- maximum value of a 3 month rolling average of the ASL in g m^{-2} (ASL_3m);
- maximum value of a 1 month rolling average of the ASL in g m^{-2} (ASL_1m).

The results are shown for two time horizons: for the year 2011 (representing current conditions) and for the year 1975. The loads of nitrogen and suspended solids in these scenarios are shown in Figure 5.11.

A.2.1 Nitrogen in 2011

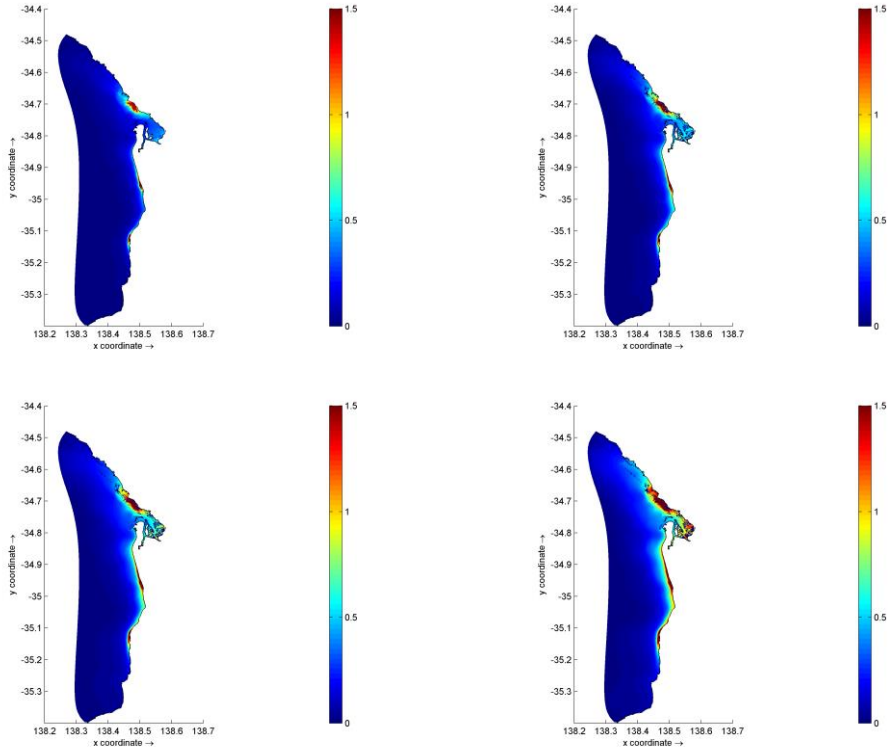

Figure A.1 Simulated nitrogen ASLs (g/m^2) in 2011 from all rivers and WWTPs; mean values (top left), 6 month RA values (top right), 3 month RA values (bottom left) and 1 month RA values (bottom right).

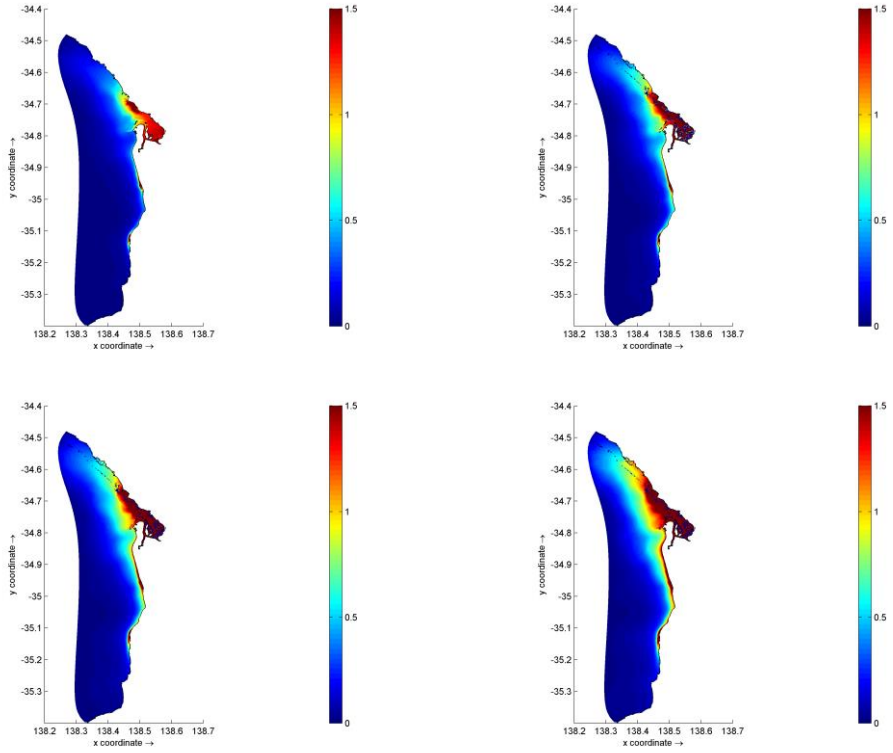

Figure A.2 Simulated nitrogen ASLs (g/m^2) in 2011 from all rivers and WWTPs and Penrice; mean values (top left), 6 month RA values (top right), 3 month RA values (bottom left) and 1 month RA values (bottom right).

A.2.2 Suspended solids in 2011

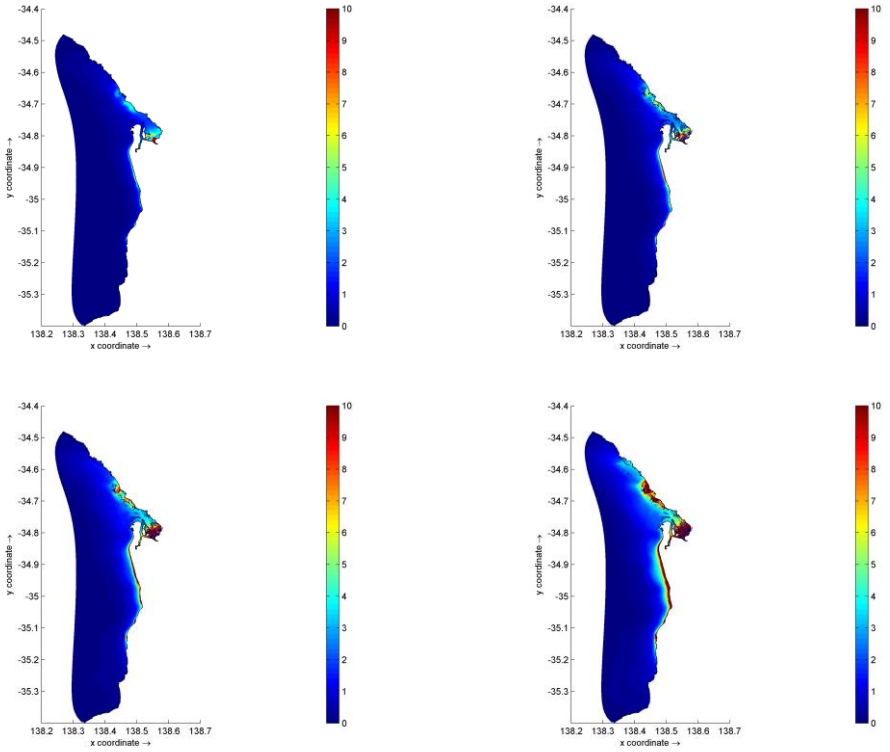

Figure A.3 Simulated suspended solids ASLs (g/m^2) in 2011 from all rivers and WWTPs; mean values (top left), 6 month RA values (top right), 3 month RA values (bottom left) and 1 month RA values (bottom right).

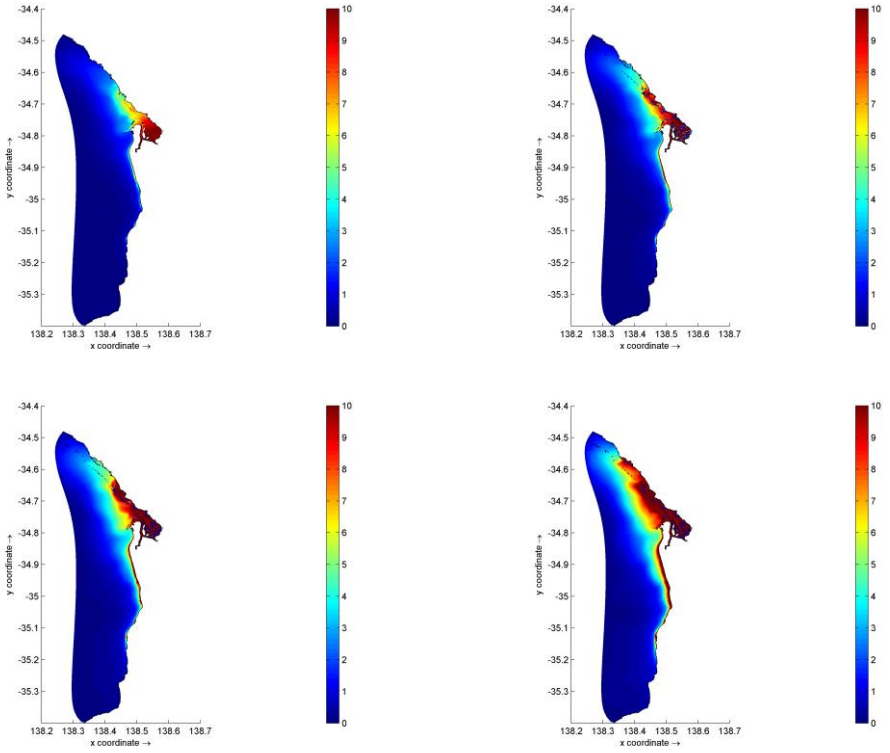

Figure A.4 Simulated susp. solids ASLs (g/m^2) in 2011 from all rivers and WWTPs and Penrice; mean values (top left), 6 month RA values (top right), 3 month RA values (bottom left) and 1 month RA values (bottom right).

A.2.3 Nitrogen in 1975

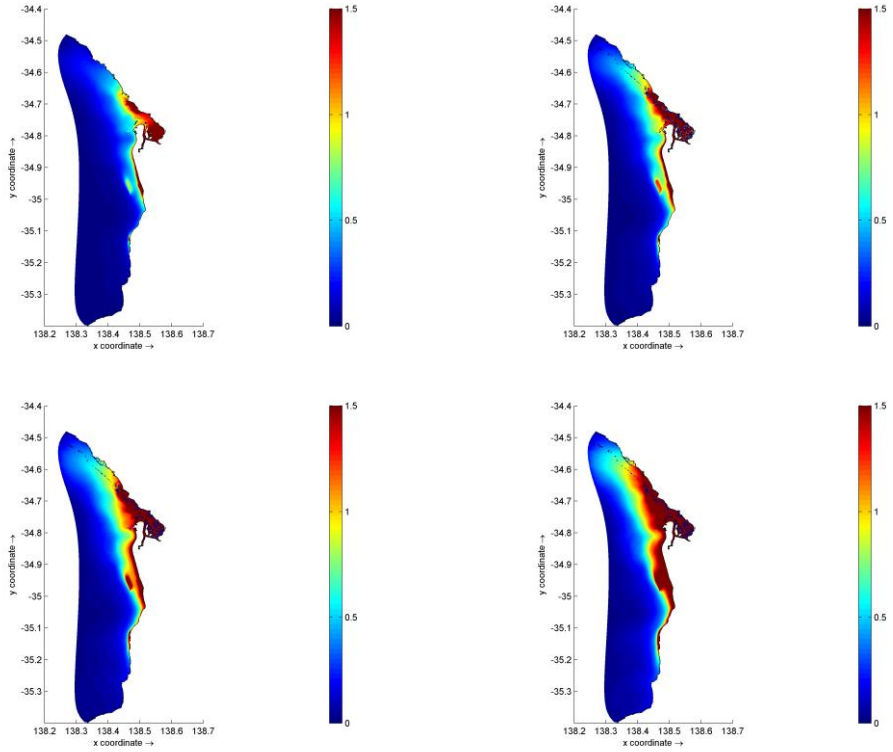

Figure A.5 Simulated nitrogen ASLs (g/m^2) in 1975 from all rivers and WWTPs; mean values (top left), 6 month RA values (top right), 3 month RA values (bottom left) and 1 month RA values (bottom right).

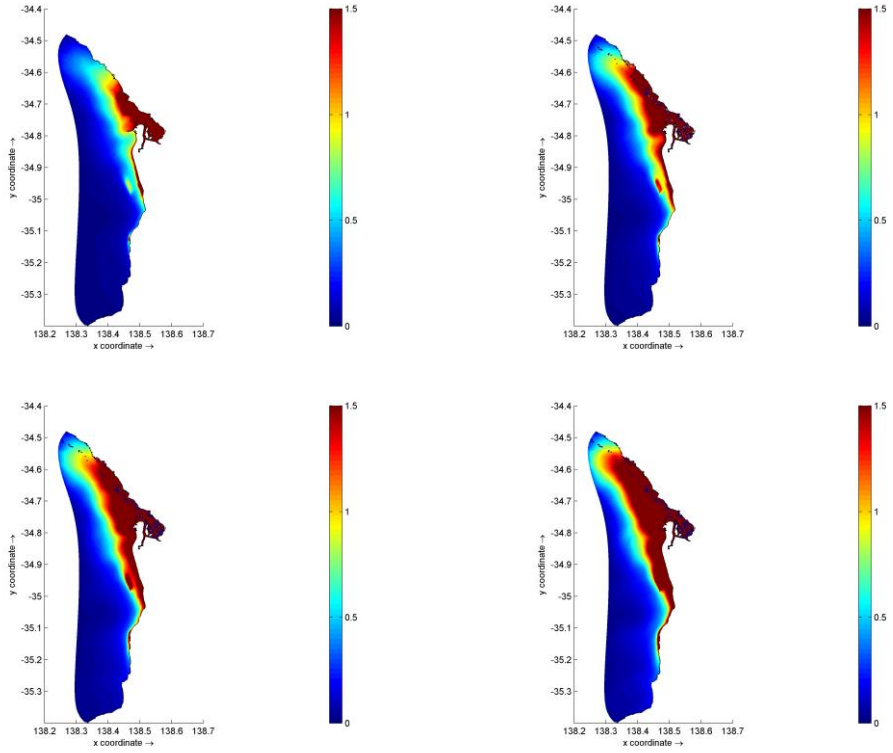

Figure A.6 Simulated nitrogen ASLs (g/m^2) in 1975 from all rivers and WWTPs and Penrice; mean values (top left), 6 month RA values (top right), 3 month RA values (bottom left) and 1 month RA values (bottom right).

A.2.4 Suspended solids in 1975

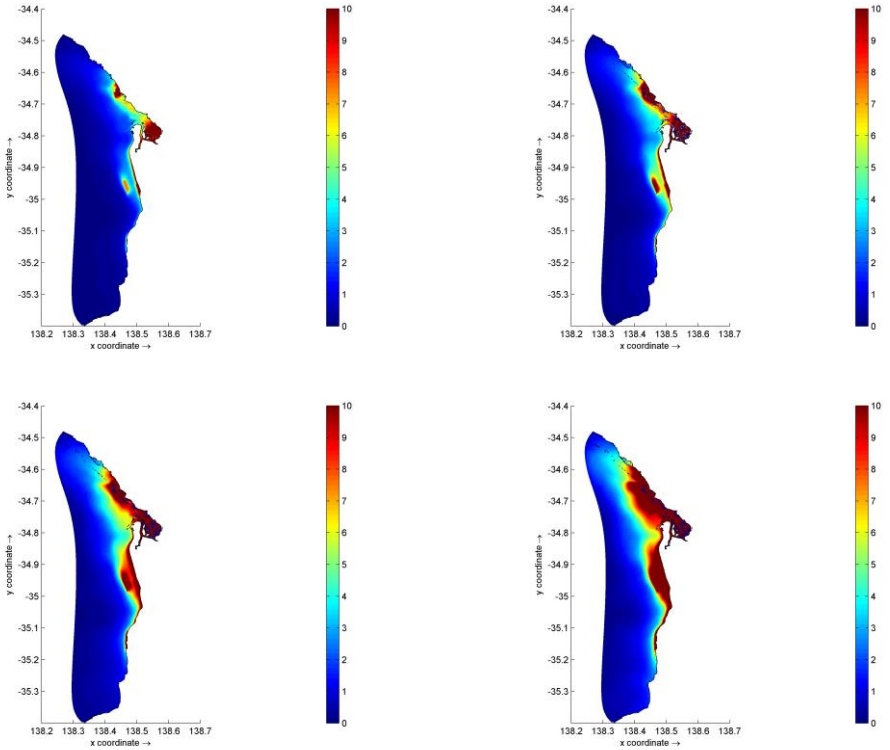

Figure A.7 Simulated suspended solids ASLs (g/m^2) in 1975 from all rivers and WWTPs; mean values (top left), 6 month RA values (top right), 3 month RA values (bottom left) and 1 month RA values (bottom right).

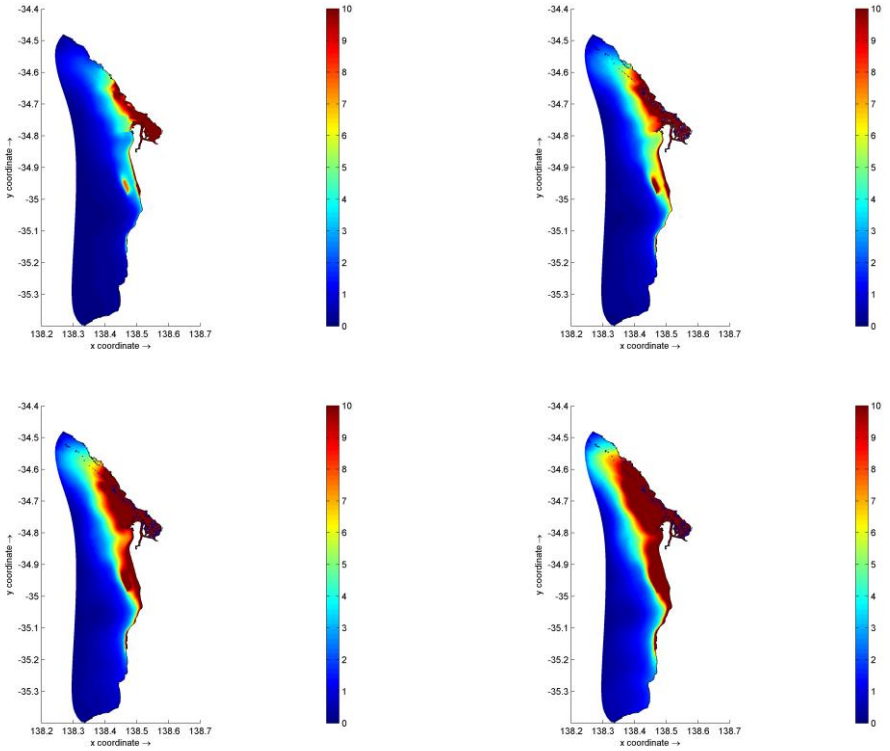

Figure A.8 Simulated susp. solids ASLs (g/m^2) in 1975 from all rivers and WWTPs and Penrice; mean values (top left), 6 month RA values (top right), 3 month RA values (bottom left) and 1 month RA values (bottom right).

B BGC model processes and parameters

B.1 Balance equations for state variables

The balance equations for state variables are as reported by Blauw et al. (2008), with the following notes:

- all processes related to grazing are not activated;
- the pool of dead organic matter is separated in two parts, POX_1/POX_2 in the water column and $POX_{1,s}$/$POX_{2,s}$ in the top sediment layer.

The fraction of dying algae released to POX_1 is indicated as f_{det}, while the remaining part is released to POX_2.

B.2 Phytoplankton processes and parameters

Phytoplankton processes are as reported by Blauw et al. (2008). The parameters used are listed in Table B.1.

Table B.1 Phytoplankton related model parameters

(1)	Parameter	Unit	Diatoms	Flagelates	Epiphytes
f_{aut}	fraction of dead algae biomass released as dissolved nutrients	(-)	0.3	0.3	0.3
f_{det}	fraction of dead algae biomass released as POC1, PON1, POP1	(-)	0.7	0.7	0.55
e_{ALG}	specific extinction coefficient for visible light	(m2/gC)	0.21-0.24	0.225-0.25	0.0
S_N	nitrogen to carbon ratio	(gN/gC)	0.125-0.225	0.14-0.2	0.1
S_P	phosphorus to carbon ratio	(gP/gC)	0.01125-0.0315	0.01125-0.02	0.0
S_{Si}	silica to carbon ratio	(gSi/gC)	0.283-0.447	0	0.0
S_{Chl}	chlorophyll-a to carbon ratio	(gChla/gC)	0.015-0.0533	0.01-0.0228	0.0
p_0	maximum growth rate at 0ºC	(1/d)	0.054-0.07	0.075-0.09	0.1
kt_p	temperature coefficient for growth (2)	(-)	-4.5 - -4.17	-1	1.080
m_0	mortality rate at 0ºC	(1/d)	0.07-0.08	0.07-0.08	0.01
kt_m	temperature coefficient for mortality	(-)	1.072-1.085	1.072-1.085	1.085
r_0	maintenance respiration rate at 0ºC	(1/d)	0.06	0.06	0.06
kt_r	temperature coefficient for respiration	(-)	1.066	1.066	1.066

Notes

1 The first column shows the parameter as it is mentioned in Blauw et al. (2008).

An amount of ammonium equal to ThrAlgNH4 is not available for uptake by phytoplankton.

B.3 Extinction of light

The representation of the downward attenuation of light is discussed in Section 4.2.9. The AREM specific attenuation coefficients are based on the K_d model derived from field data (Table 3.2; scenario 4). The data-derived coefficients cannot be directly used in AREM, since AREM calculates the extinction of PAR by a linear function of three fractions of inorganic suspended matter, the biomass of six pelagic algae phenotypes, two fractions of particulate

organic non-algal carbon and CDOM (see section 4.2.9). In AREM, particulate organic non-algal carbon includes both detritus generated by phytoplankton and organic carbon from land-based sources. Thus, in the model, the contribution by non-algal POC is implicitly included in the other terms, while in AREM there is an explicit term related to non-algal POC. As a consequence, AREM has more predictive power with respect to the effect that changes in loads have on the extinction via changes in the composition of the phytoplankton community, the composition of POC and the composition of suspended matter. However, due to these different approaches a translation of the data-derived specific extinction coefficients to AREM specific extinction coefficients is required. This translation is not possible on the basis of field data alone, but requires a hybrid approach that uses data-derived and model-derived information.

In the data-driven model, the contribution of non-algal POC is implicitly included in the Chla term and the SS term. By inspection of AREM output, we observed that simulated Chla is strongly correlated to simulated algal and non-algal POC, whereas such a correlation does not exist for SS. Moreover, the specific extinction for suspended solids derived from field data is very similar to values commonly used for ash in Delft3D models (Blauw, et al. 2008) (Los 2009), while the specific extinction for Chla derived from field data is much higher than the equivalent values commonly used for phytoplankton biomass in Delft3D models. On this basis we assume that the contribution of non-algal POC to the extinction is implicitly included in the Chla term of the model. This assumption matches our understanding of the system behaviour. Phytoplankton growth is driven by nutrient availability, which causes a correlation of phytoplankton and detritus to coastal discharges. Thus, it is likely that the measured Chla reflects the coastal discharges footprint. SS however, is strongly affected by resuspension events, which makes for a poor correlation of measured SS and the coastal discharges footprint.

Thus, the translation of the specific extinction coefficients derived from data to AREM specific extinction coefficients is based on the assumption that all POC (algae, detritus, POC in coastal discharges) is implicitly included in the Chla term. First, an AREM run is done with the specific extinction for algae and non-algal POC equal to values derived from prior Delft3D model experience (0.2 $m^{-1}(gC\ m^{-3})^{-1}$). All other AREM extinction parameters are directly copied from the data-derived model. This AREM run is used to find the simulated chlorophyll-a to carbon ratio in algae (Chla/C; dimensionless) at the 6 sampling stations and the non-algal carbon to algal carbon ratio (NAC/AC; dimensionless). In addition, AREM only simulates Chla in live phytoplankton while the data are total Chla, where the average fraction in live phytoplankton equals 63% (Section 3.4; phaeophytin accounts for 37% of the measured Chla.). By these quantities, the total POC (algal and non-algal) can be expressed as $Chla \times 0.63 \times 10^{-3} / (Chla/C) \times (1 + NAC/NA)$. The data-derived specific extinction of Chla can be translated to an equivalent AREM specific extinction for algae and non-algal POC by division by this number. A repeated AREM run with these specific extinction values provides adjusted values of Chla/C and NAC/NA, which lead to adjusted specific extinction values for algae and non-algal POC. This process is repeated until convergence is reached. The resulting specific extinction values for algae and non-algal POC are 0.20 $m^{-1}(gC\ m^{-3})^{-1}$. This implies that iteration was not required, and that the Chla term in the data derived K_d model is equivalent to the algae and non-algal POC terms in the AREM K_d while using specific extinction values derived from prior Delft3D model experience.

B.4 Decomposition of organic matter

The decomposition of the rapidly decomposing fraction of organic matter is as reported by Blauw et al. (2008). The slowly decomposing fraction of organic matter decomposes according to a simple first order process, comparable to formula D.3 in Blauw et al. (2008).

B.5 Inorganic nutrients

The nitrification process is formulated just as in Blauw et al. (2008). The denitrification process is formulated in a surface specific way, reflecting the fact that most denitrification is taking place in the sediment:

$$den = \frac{k_{den}}{Z}\, NO_3\, kt_{den}^{(T-20)}$$

where *den* is the denitrification flux (g m^{-3} d^{-1}), k_{den} is the denitrification rate at 20°C (m d^{-1}), *Z* is the water depth (m), NO_3 is the concentration of nitrates (g m^{-3}), kt_{den} is the temperature coefficient (-) and *T* is the water temperature (°C).

B.6 Settling and deposition

The deposition process (transformation of a particle in suspension to a particle in the sediment) is formulated according to Krone, with a shear stress dependent term:

$$sed = \frac{v_{sed}}{Z}\left(max\left(1 - \frac{\tau}{\tau_{cr,sed}}\right)\right) C$$

where *sed* is the settling flux (g m^{-3} d^{-1}), v_{sed} is the settling velocity (m d^{-1}), *Z* is the water depth (m), *C* is the concentration of a particulate state variable (g m^{-3}), τ is the shear stress (N m^{-2}) and $\tau_{cr,sed}$ is the critical shear stress for deposition.

B.7 Remaining processes

All remaining processes, including reaeration and burial are formulated as reported by Blauw et al. (2008).

B.8 Parameter values

The additional and modified model parameters are listed in Table B.2.

Table B.2 Additional and modified model parameters, relative to Blauw et al. (2008).

(1)	Parameter	Unit	Value
n.a.	Amount of NH4 not available for uptake by phytoplankton (ThrAlgNH4)	(gN m^{-3})	0.01
$k_{dec,POC2}$	Decay rate of POC2 at 20 °C	(d^{-1})	0.015
$k_{dec,PON2}$	Decay rate of PON2 at 20 °C	(d^{-1})	0.015
$k_{dec,POP2}$	Decay rate of POP2 at 20 °C	(d^{-1})	0.015
k_{den}	Denitrification rate at 20 °C	(m d^{-1})	0.1
b	Burial rate	(d^{-1})	0.05
n.a.	Critical shear stress for deposition	(N m^{-2})	0.1

Notes

1 The first column shows the parameter as it is mentioned in Blauw et al. (2008).

C Extended Wave Model

C.1 General

This appendix describes a stand-alone SWAN-based wave model, set up to transform high quality off-shore wave hindcasts available from the Australian Bureau of Meteorology (BoM) to the boundaries of the detail model (see Figure 4.8).

C.2 Offshore wave data

Offshore wave boundary conditions, the 2D wave spectra, for the year 2011 were obtained from the Australian Bureau of Meteorology's (BoM) wave hindcast dataset (covering 34 years). This hindcast was produced by the Bureau of Meteorology in collaboration with the Commonwealth Scientific and Industrial Research Organisation (CSIRO). The hindcast was created using the WAVEWATCH III™ model forced with NCEP's Climate Forecast System Reanalysis surface winds. Around the Australian coast, the model was run on a 4 arcminutes (~7 km) grid. As the hindcast resolution is still relatively coarse to be used in the shallow water region in the area of interest, a translation of the wave conditions has been made between offshore locations and the area of interest. The locations for which hourly time series of 2D wave spectra from 2011 were obtained from BoM are shown in Table C.1.

Table C.1 Locations in the BoM hindcast with 2D wave spectral output near the area of interest.

Point	Longitude [^{o}E]	Latitude [^{o}N]
1	135.73	-35.6
2	135.73	-36.13
3	137.33	-36.67
4	138.93	-36.67
5	138.93	-36.13

Figure C.1 shows the significant wave height roses at each of the BOM locations. The bar lengths indicate the occurrence percentages. Directions are to the centre of the roses. The numbers in the centre of the roses are the percentage of occurrences in the lowest class. It can be seen that waves coming from southwest and west-southwest are the most dominant for the area. The southwest corner shows the larger waves reaching heights of up to 9 meters in the year 2011. It is also clear that wave height decreases towards the east and that the percentages of occurrence of smaller waves are higher. The wave period roses shown in Figure C.2 indicate that the very long swell waves reach the region from the Southwest.

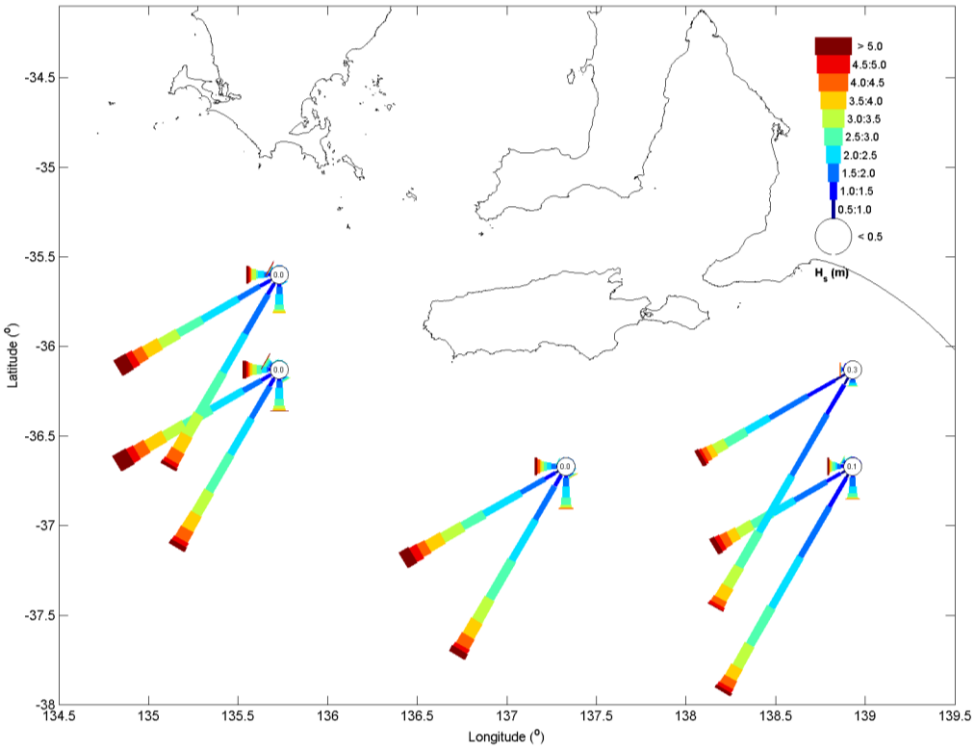

Figure C.1 Wave rose Hs at the 5 BoM locations for 2011; the bars are displaying the occurrence of Hs for 12 directional sectors. The number in the centre of the wind rose shows the occurrence of wind velocities in the lowest wind class.

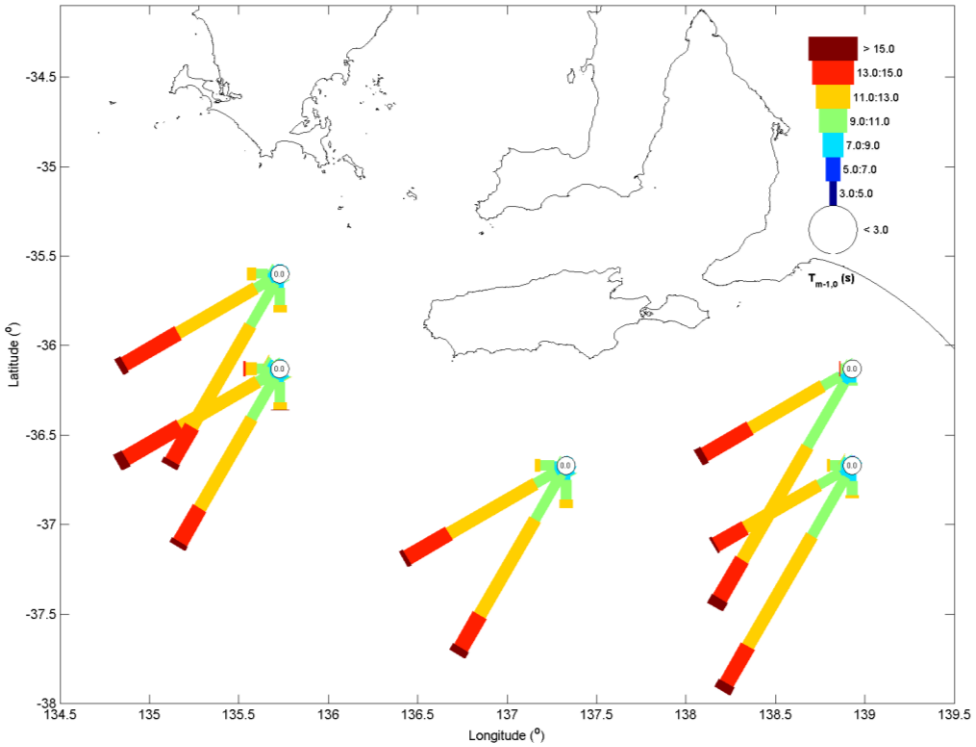

Figure C.2 Wave rose Tm-1,0 at the 5 BoM locations for 2011; the bars are displaying the occurrence of Tm-1,0 for 12 directional sectors. The number in the centre of the wind rose shows the occurrence of wind velocities in the lowest wind class.

C.3 Model grid

The purpose of the Extended Wave Model is to translate the BoM offshore conditions at the five locations to the open water boundary of the detail model. The computational grid spans an area bounded by the five locations where BoM 2D wave spectra are available, see Figure C.3. A grid resolution of 500 m was chosen, which is sufficient to resolve wave propagation in the Gulf St Vincent and the passages between the mainland and Kangaroo Island. The directional and spectral grids have been defined the same as in the detail model (section 4.2.6).

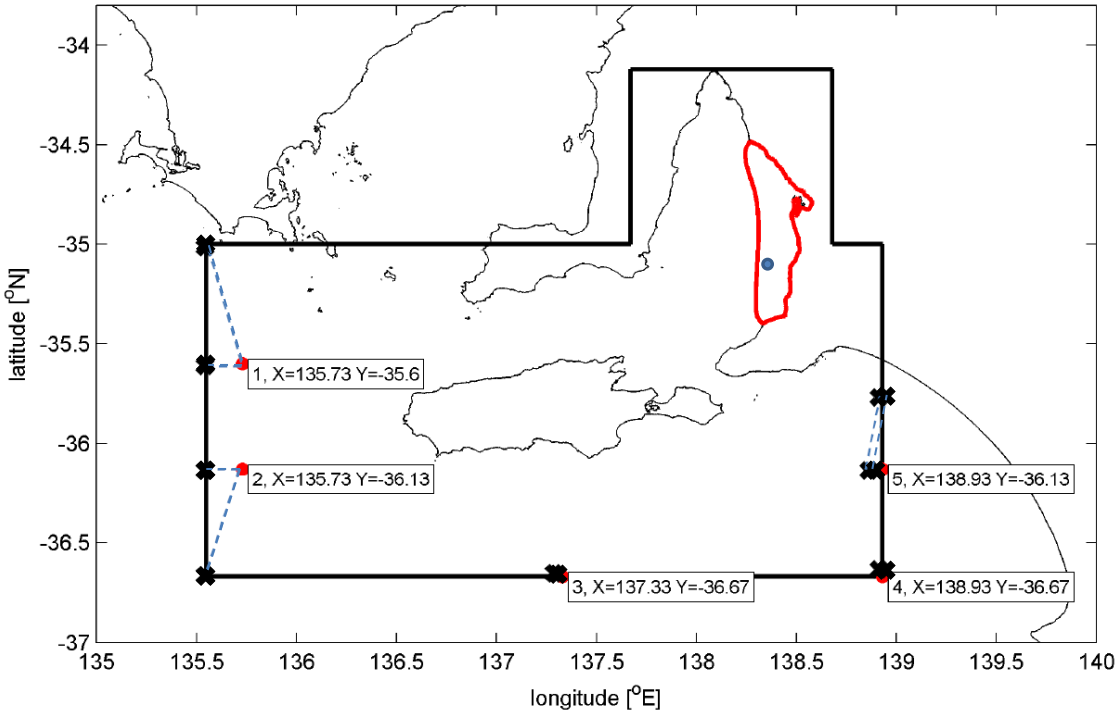

Figure C.3 Outlines of the Extended Wave Model (black lined) and the detail model (red line). The red dots indicate the locations of the BoM offshore wave data. The black crosses indicate the locations along the grid boundary were the wave data from one of the five BoM locations have been applied. The correspondence between the BoM locations and grid boundary locations is indicated by the black dashed lines. Between the crosses the wave data are linearly interpolated. The blue dot is a sample output location.

C.4 Model setup

The bathymetry was derived from the Australian Bathymetry and Topography Grid (Whiteway, 2009). The hourly 2D wave spectra provided by BoM have been applied to the model boundaries of the Extended Wave Model, as indicated in Figure C.3. Spatially uniform wind data have been used as described in section 4.2.4. No water level variations or currents have been input in the model. Physical and numerical settings are the same as in the detail model, with a uniform bottom roughness length scale (K_n) of 0.05 m.

C.5 Results

The Extended Wave Model has been run in standalone model for 2011 outputting time series of hourly 2D wave spectra along the open water boundaries of the detail model. Figure C.4 shows the computed wave rose at one of the output locations (Figure C.3). As the figure

shows, the wave energy is dissipated from offshore to nearshore (cf. Figure C.1 and Figure C.4) and the longer and more energetic wave propagate from the Southwest.

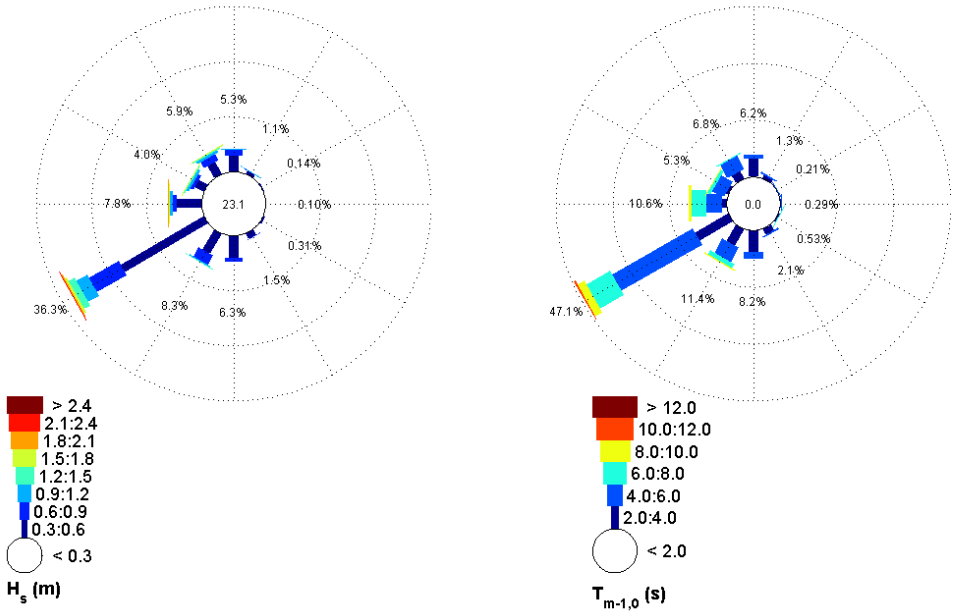

Figure C.4 Significant wave height (left) and mean wave period (right) roses for 2011 computed by the Extended Wave Model at a nearshore location (see Figure C.3) along the boundary of the detail model.

D Details of hydrodynamic model validation

D.1 Overall model: water levels

In Table D.1, the quality of the water level representation is shown. The quality is specified in terms of the RMSE of tide, surge and total water level signal. In the model area, the surge signal is generally much smaller than the tidal signal. Nonetheless, the results show that in both stations the contribution of the tide error to the total error is smaller than the contribution of the surge error. The time series of tide, surge and total water level at tide gauge locations Adelaide Outer Harbour and Port Giles are shown inFigure D.1 to Figure D.4, for the months of July and December 2011.

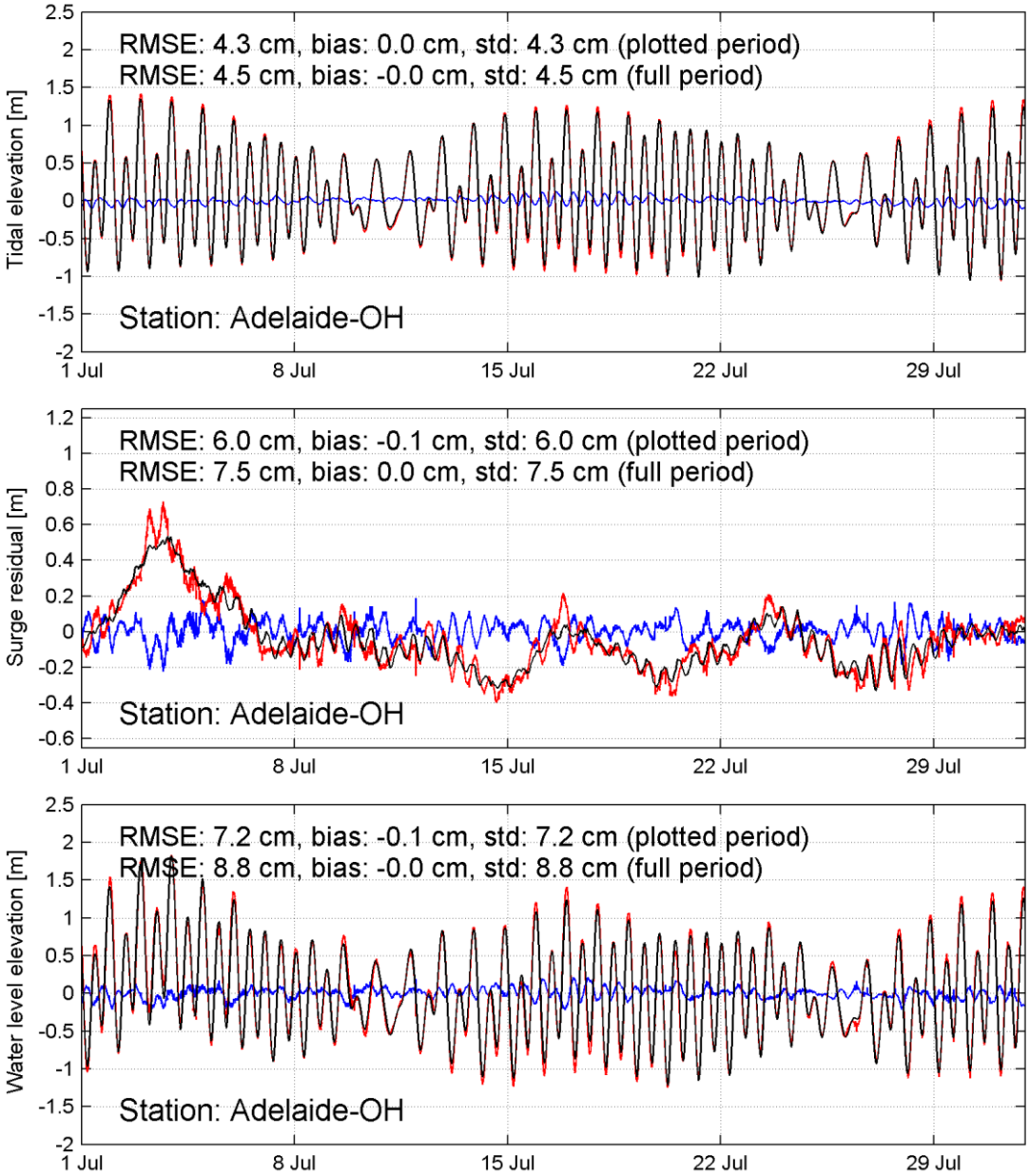

Figure D.1 Tide (upper panel), surge (middle panel) and total water level elevation (lower panel) at tide gauge station Adelaide Outer Harbour in July 2011; black: simulation; red: measurement; blue: residual.

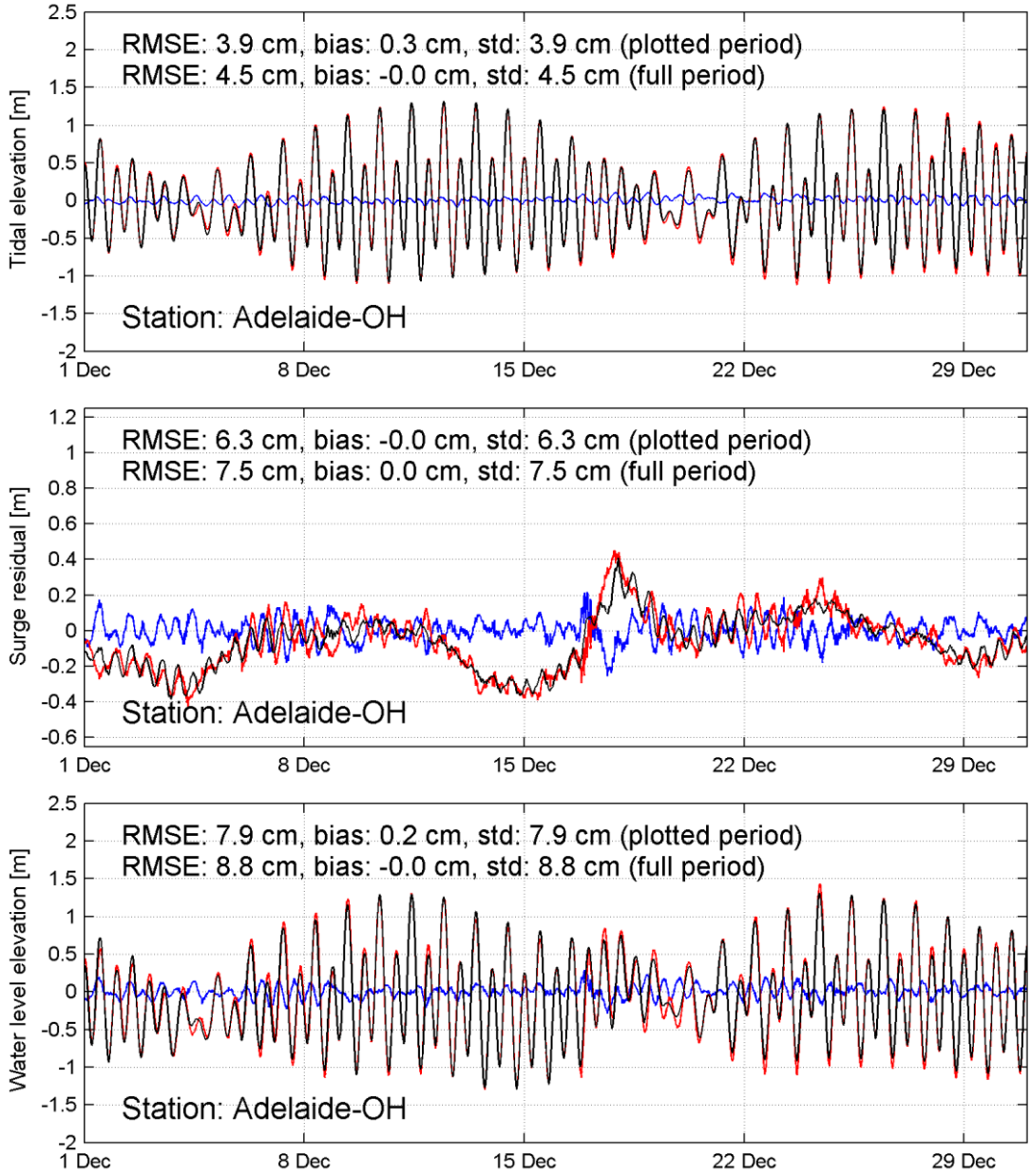

Figure D.2 Tide (upper panel), surge (middle panel) and total water level elevation (lower panel) at tide gauge station Adelaide Outer Harbour in December 2011; black: simulation; red: measurement; blue: residual.

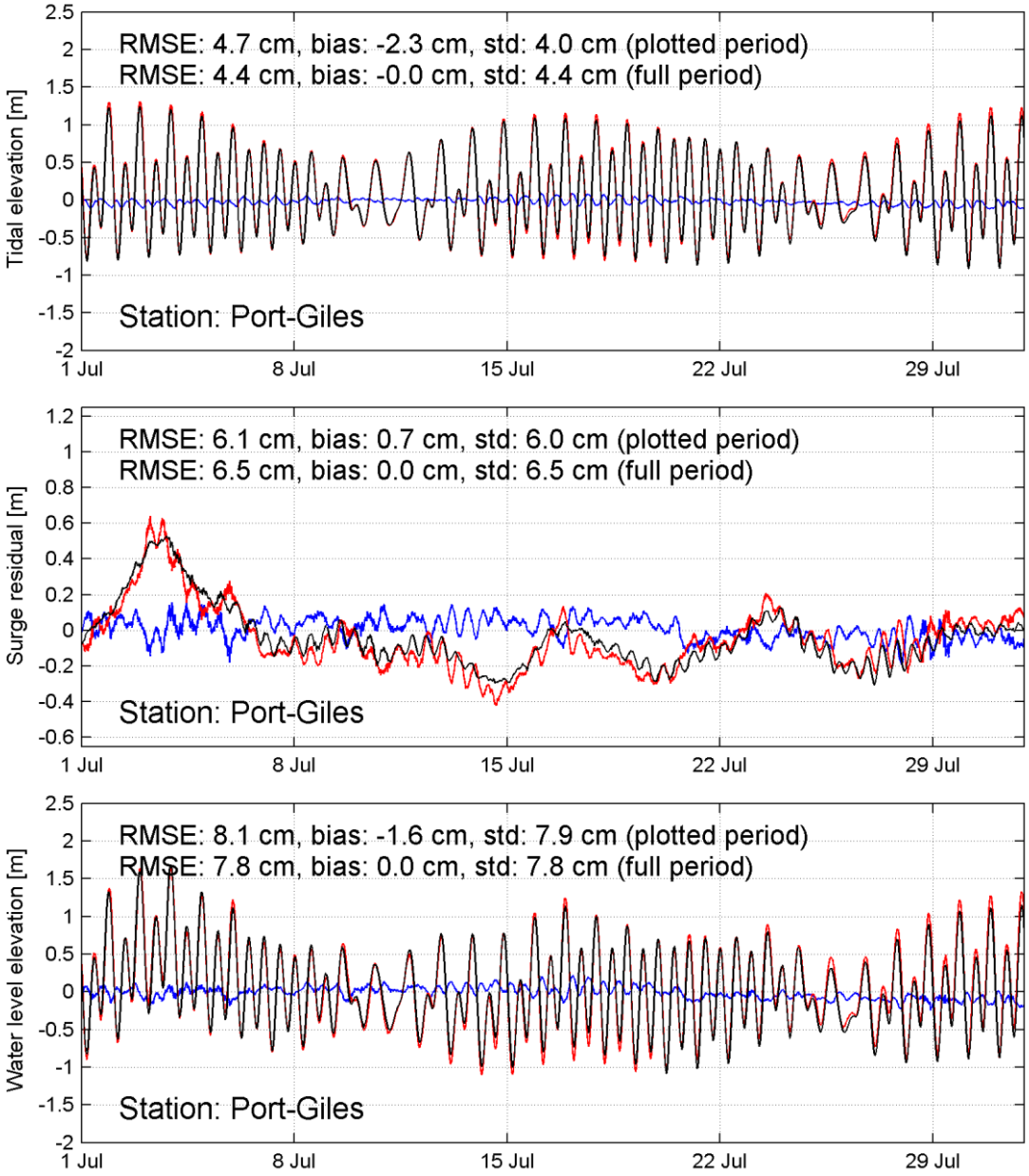

Figure D.3 Tide (upper panel), surge (middle panel) and total water level elevation (lower panel) at tide gauge station Port Giles in July 2011; black: simulation; red: measurement; blue: residual.

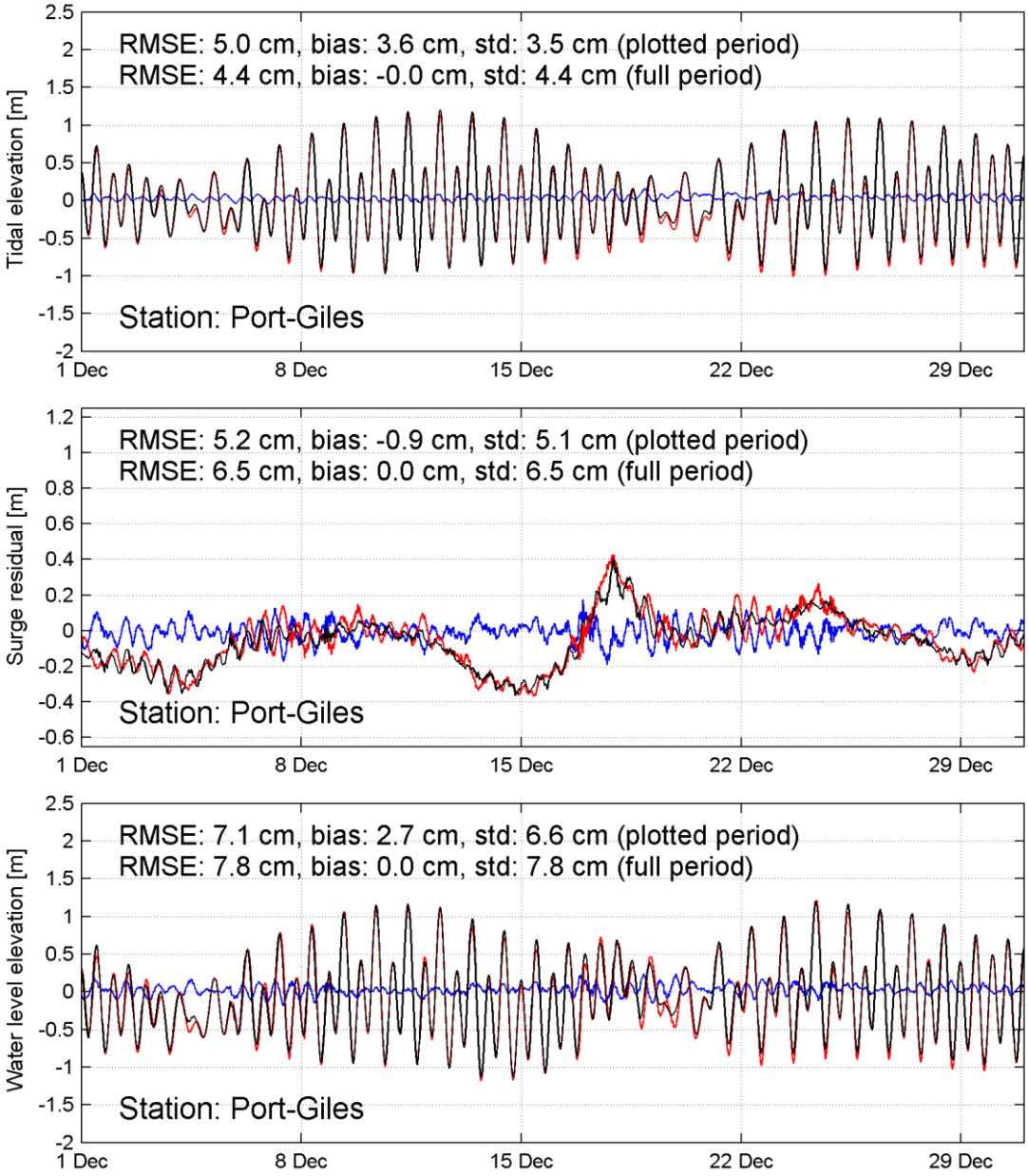

Figure D.4 Tide (upper panel), surge (middle panel) and total water level elevation (lower panel) at tide gauge station Port Giles in December 2011; black: simulation; red: measurement; blue: residual.

Table D.1 Quality of the water level representation, in terms of RMSE of tide, surge and total water level signal, determined over the entire year 2011.

Station name	RMSE tide (cm)	RMSE surge (cm)	RMSE total (cm)
Adelaide Outer Harbour	4.5	7.5	8.8
Port Giles	4.4	6.5	7.8
Average	**4.5**	**7.0**	**8.3**

Compared to other models of similar scale, the tide representation is excellent with an average RMSE of just 4.5 cm. For the assessment of tide representation, it is useful to evaluate model performance in the frequency domain as well. In addition to looking separately at amplitude and phase errors in individual tidal constituents, we use the vector

difference to assess the combined effect of these errors. The vector difference (VD) is defined as:

$$VD = \sqrt{\left[H_c \cos G_c - H_o \cos G_o\right]^2 + \left[H_c \sin G_c - H_o \sin G_o\right]^2}$$

where A_c and G_c represent the computed amplitude (in cm) and phase (in °), while A_o and G_o represent the observed amplitude and phase.

The results in Table D.2 (Port Giles) and Table D.3 (Adelaide Outer Harbour) show that, with the exception of the annual constituent S_a, the amplitude errors do not exceed 1 cm. The phase errors are less than 1 °, except for S_a and MU_2 This means that the tide representation is excellent, also compared to previous studies.

Table D.2 Representation quality in the frequency domain at location Port Giles. The harmonic constituents presented here are those with the largest amplitudes in Port Giles.

	A_o	A_c	∆A	G_o	G_c	∆G	VD
M_2	43.7	44.0	0.3	262.1	262.1	0.0	0.3
S_2	43.3	43.4	0.1	310.3	310.1	-0.2	0.2
K_1	24.5	24.3	-0.2	117.8	117.2	-0.6	0.3
O_1	16.5	16.5	-0.1	110.7	110.3	-0.4	0.1
K_2	12.5	12.5	0.0	309.2	309.5	0.4	0.1
S_a	7.7	5.7	-2.0	169.5	160.7	-8.8	2.2
MU_2	7.4	7.3	-0.2	27.6	29.1	1.6	0.3
P_1	6.9	7.0	0.0	113.1	112.9	-0.2	0.0
M_{sf}	5.9	5.7	-0.2	78.8	78.9	0.1	0.2
Q_1	4.1	4.2	0.0	96.7	95.9	-0.8	0.1

Table D.3 Representation quality in the frequency domain at location Adelaide Outer Harbour. The harmonic constituents presented here are those with the largest amplitudes in Port Giles.

	A_o	A_c	∆A	G_o	G_c	∆G	VD
M_2	50.9	50.9	0.1	275.3	276.0	0.7	0.6
S_2	51.4	50.6	-0.1	324.1	325.0	0.9	1.1
K_1	25.2	25.2	0.0	123.7	123.7	0.0	0.0
O_1	17.0	16.9	-0.1	116.4	116.1	-0.3	0.1
K_2	14.7	14.6	-0.2	323.5	323.9	0.4	0.2
S_a	5.7	5.6	-0.1	161.7	163.8	2.1	0.2
MU_2	8.9	8.5	-0.4	38.2	41.1	2.9	0.6
P_1	7.1	7.1	0.0	120.0	119.8	-0.2	0.0
M_{sf}	5.8	6.1	0.3	80.0	80.6	0.6	0.3
Q_1	4.3	4.2	-0.1	100.2	100.8	0.7	0.1

D.2 Overall model: temperature and salinity

In Figure D.5, computed temperature and salinity time series from the validation run at station Control-3 are plotted together with the measured values. This is done at two depth levels: 1 m below the surface and 1 m above the bottom. The results at all three stations are also shown quantitatively in Table D.4 and Table D.5. Note that the station locations are shown in Figure 4.14 as “SA Water 2011 Temperature and Salinity”.

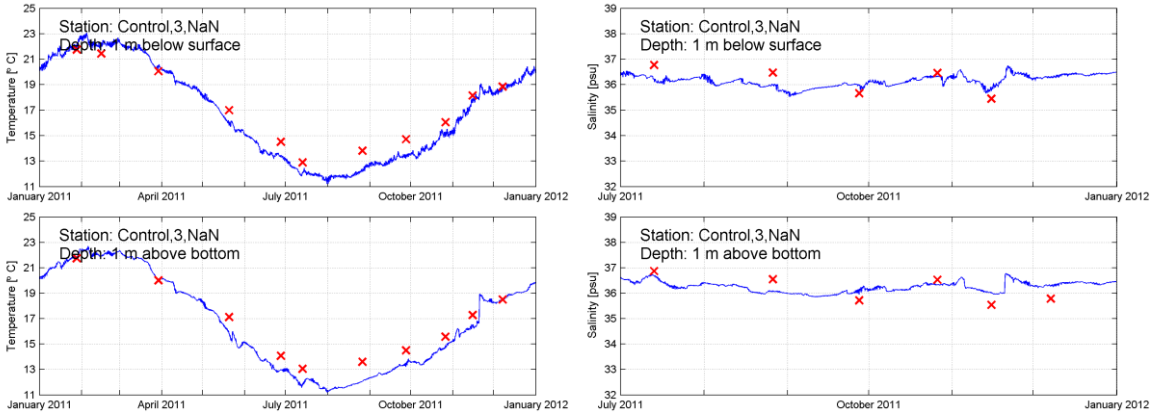

Figure D.5 Time series of computed temperature (left) and salinity (right) at 1 m below surface and 1 m above bottom for station Control-3, covering the year 2011. (blue line: model results; red crosses: measured values)

Table D.4 Overview of the quality of the temperature representation in the 3D Adelaide model at 1 m below surface and 1 m above bottom, in terms of bias, standard deviation (std) and RMSE (all in °C).

	1 m below surface			**1 m above bottom**		
station	bias	std	RMSE	bias	std	RMSE
Control-1	-0.5	0.9	1.0	-0.6	0.9	1.1
Control-2	-0.7	0.8	1.0	-0.6	0.8	1.0
Control-3	-0.6	0.7	0.9	-0.8	0.6	1.0
average	**-0.6**	**0.8**	**1.0**	**-0.7**	**0.8**	**1.0**

Table D.5 Overview of the quality of the salinity representation in the 3D Adelaide model at 1 m below surface and 1 m above bottom, in terms of bias, standard deviation (std) and RMSE (all in psu).

	1 m below surface			**1 m above bottom**		
station	bias	std	RMSE	bias	std	RMSE
Control-1	0.0	0.5	0.5	0.0	0.5	0.5
Control-2	-0.4	0.1	0.5	0.1	0.5	0.5
Control-3	-0.1	0.4	0.4	0.1	0.4	0.4
average	**-0.2**	**0.3**	**0.5**	**0.1**	**0.5**	**0.5**

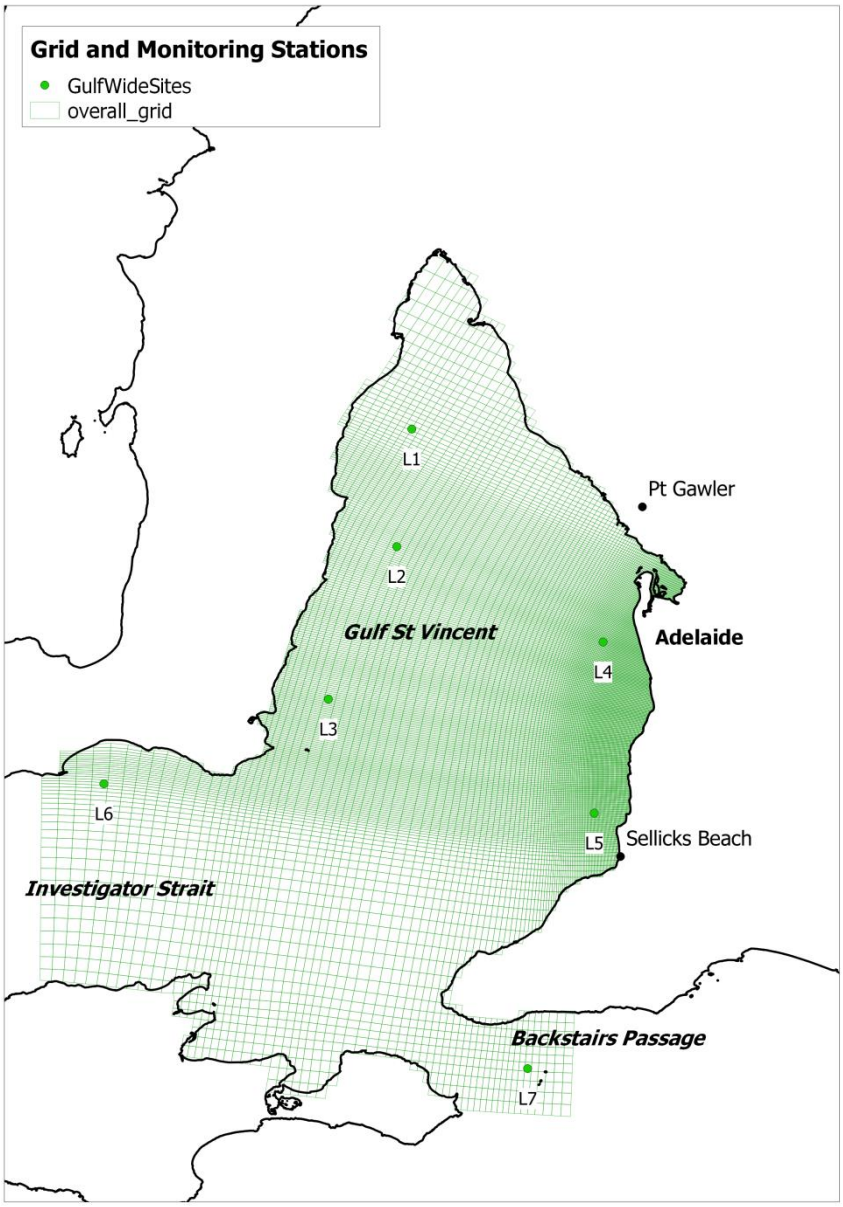

Figure D.6 Location of stations in Gulf-wide survey by SA Water in 2015, relative to overall model grid

Table D.6 and Table D.7 compare monthly averages in June, July and August of the simulated temperature and salinity in 2011 at stations around the Gulf St Vincent (Figure D.6) to observed values in 2015. We note that field data for all stations are only available in these three months, and that no data are available for station L2. The comparison has been done for the surface temperature and salinity. At none of the stations there appeared to be significant differences between the monthly-averaged observed values near the surface and near the bottom, while at some stations the near bottom data were clearly less reliable. Occasionally, vertical salinity gradients temporarily exist in both model and measurements. These vertical gradients are associated with more saline water traveling along the bottom from the coast towards the deeper parts of the Gulf.

Table D.6 Simulated monthly averaged surface water temperature (°C) in 2011 and observed monthly averaged surface water temperature (°C) in 2015 at six stations around Gulf St Vincent.

Simulated (2011)	**L1**	**L3**	**L4**	**L5**	**L6**	**L7**	**All**
Jun	12.3	12.7	13.0	14.0	13.5	14.0	13.3
Jul	10.9	11.3	11.4	12.2	12.6	12.9	11.9
Aug	11.6	12.0	11.9	12.0	13.0	13.0	12.2
Average	11.6	12.0	12.1	12.7	13.0	13.3	
Observed (2015)	**L1**	**L3**	**L4**	**L5**	**L6**	**L7**	**All**
Jun	14.0	14.1	14.3	14.9	14.1	14.9	14.4
Jul	12.6	12.8	12.8	13.4	13.6	14.0	13.2
Aug	12.4	12.5	12.4	12.6	13.3	13.3	12.7
Average	13.0	13.1	13.1	13.7	13.7	14.0	
Difference	**L1**	**L3**	**L4**	**L5**	**L6**	**L7**	**All**
Jun	-1.7	-1.5	-1.3	-0.9	-0.6	-0.8	-1.1
Jul	-1.7	-1.5	-1.3	-1.3	-1.1	-1.1	-1.3
Aug	-0.8	-0.5	-0.5	-0.6	-0.2	-0.3	-0.5
Average	-1.4	-1.1	-1.1	-0.9	-0.6	-0.7	

Table D.7 Simulated monthly averaged surface salinity (psu) in 2011 and observed monthly averaged surface salinity (psu) in 2015 at six stations around Gulf St Vincent.

Simulated (2011)	**L1**	**L3**	**L4**	**L5**	**L6**	**L7**	**All**
Jun	37.2	35.9	36.8	36.8	34.8	35.1	36.1
Jul	36.9	35.7	36.6	36.3	34.8	35.1	35.9
Aug	36.6	35.6	36.3	36.1	34.8	34.9	35.7
Average	36.9	35.7	36.6	36.4	34.8	35.0	
Observed (2015)	**L1**	**L3**	**L4**	**L5**	**L6**	**L7**	**All**
Jun	37.7	37.1	37.7	37.7	36.4	36.2	37.1
Jul	37.6	36.8	37.5	37.5	36.1	34.3	36.6
Aug	37.3	36.6	37.1	37.1	36.1	34.3	36.4
Average	37.5	36.8	37.4	37.4	36.2	34.9	
Difference	**L1**	**L3**	**L4**	**L5**	**L6**	**L7**	**All**
Jun	-0.5	-1.2	-0.9	-0.9	-1.5	-1.2	-1.0
Jul	-0.7	-1.1	-1.0	-1.2	-1.3	0.7	-0.8
Aug	-0.7	-1.0	-0.8	-0.9	-1.3	0.7	-0.7
Average	-0.6	-1.1	-0.9	-1.0	-1.4	0.1	

The temperature results (Table D.6) show differences between stations in the order of 1.5 ºC in the 2011 simulation and in the order of 1.0 ºC in the 2015 field data. Differences between months are in the order of 1.0 ºC in the 2011 simulation and in the order of 1.5 ºC in the 2015 field data. The temperature decreases towards the inner Gulf and with time in both datasets. The salinity results (Table D.7) show differences between stations in the order of 2 psu in both datasets and differences between months in the order of 0.5 psu in both datasets. The salinity increases towards the inner Gulf and decreases with time in both datasets. Based on

this comparison we conclude that the model produces realistic time-averaged spatial and temporal gradients.

The absolute values of the water temperature and salinity differ between both datasets, because of the time difference between both datasets and probably because of modelling errors. It is not possible to separate these two without setting up and running the model for 2015.

D.3 Detail model: water levels

In Table D.8, the quality of the water level, tide and surge representation at Adelaide Outer Harbour is shown for both the detailed and overall model. These results show that in the detailed model the contribution of the tide error (7.3 cm) to the total error is similar to the contribution of the surge error (7.5 cm), even though the surge signal is much smaller than the tidal signal. Furthermore, while the quality of the surge is similar in both models, the model skill with which the tide is represented has deteriorated in the detailed model. The time series of tide, surge and total water level at tide gauge locations Adelaide Outer Harbour are shown in Figure D.8, for the month of December 2011.

Table D.8 Quality of the water level representation in Adelaide Outer Harbour, in terms of RMSE of tide, surge and total water level signal, determined over the entire year 2011.

Station name	RMSE tide (cm)	RMSE surge (cm)	RMSE total (cm)
Overall model	4.5	7.5	8.8
Detailed model	7.3	7.5	10.5

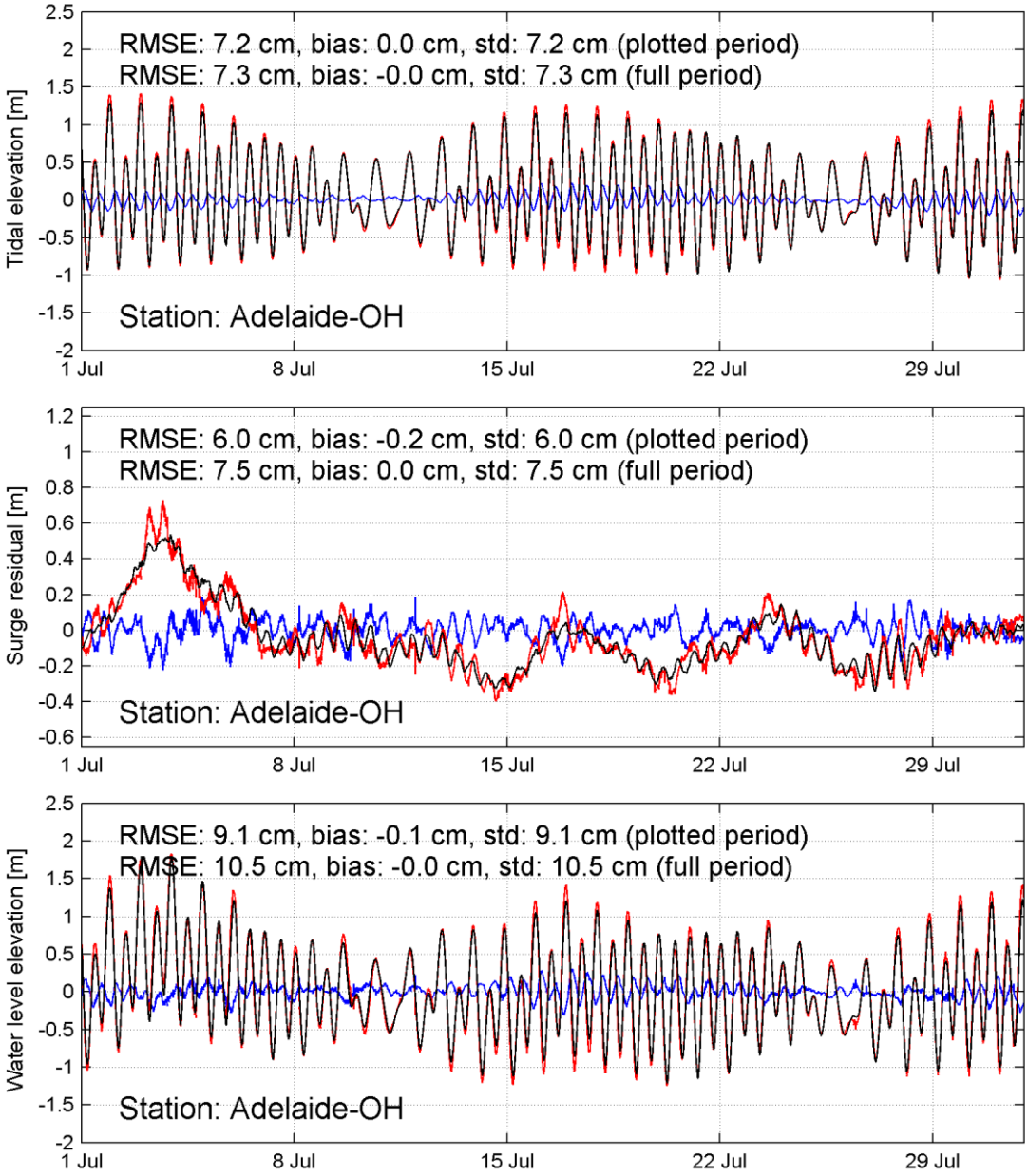

Figure D.7 Tide (upper panel), surge (middle panel) and total water level elevation (lower panel) at tide gauge station Adelaide Outer Harbour in July 2011; black: simulation (detailed model); red: measurement; blue: residual.

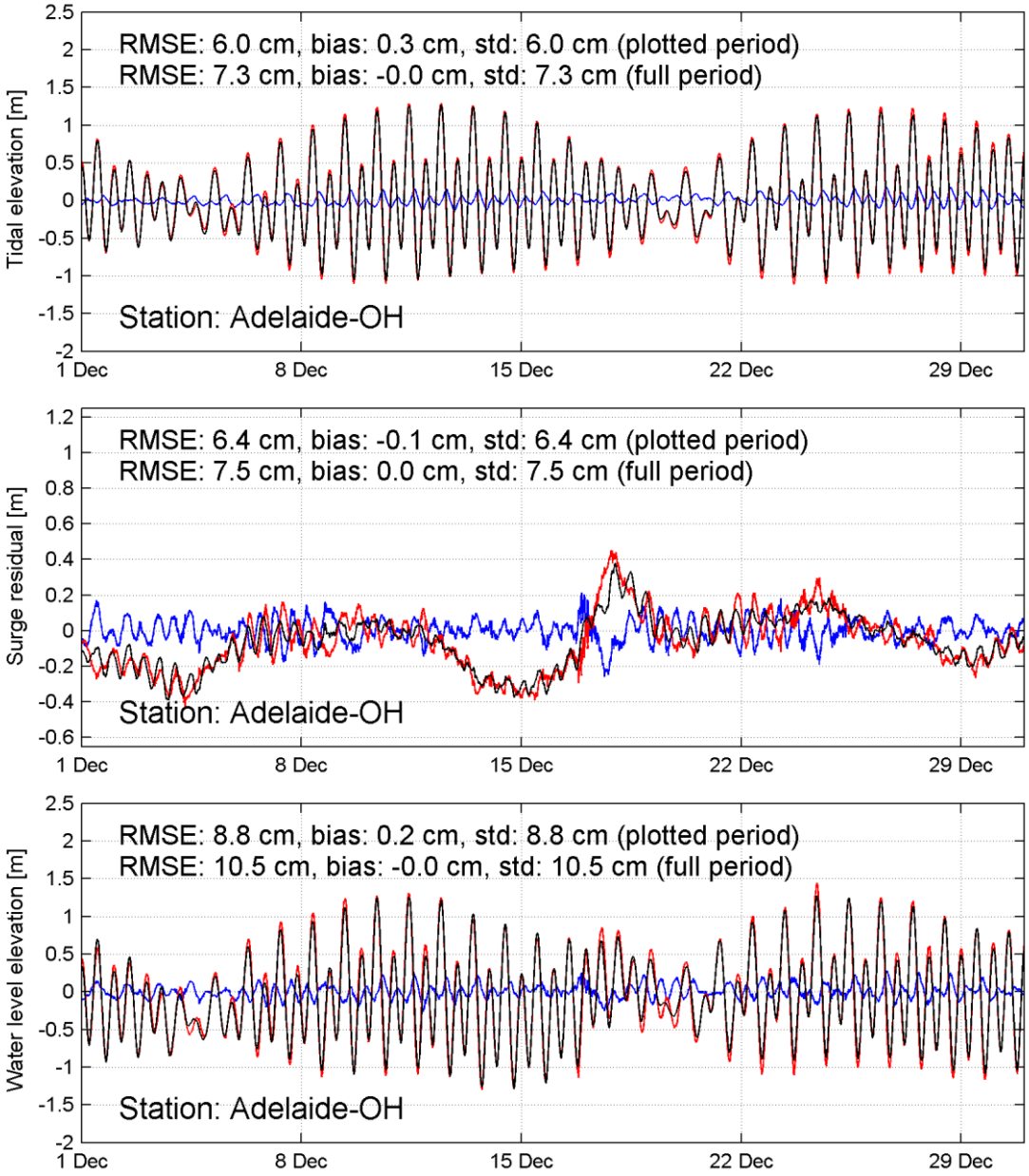

Figure D.8 Tide (upper panel), surge (middle panel) and total water level elevation (lower panel) at tide gauge station Adelaide Outer Harbour in December 2011; black: simulation (detailed model); red: measurement; blue: residual.

For the assessment of tide representation, it is useful to evaluate model performance in the frequency domain as well. Comparing the results in Table D.9 (detailed model) with those in Table D.3 (overall model), shows that, for most harmonic constituents the modelled phase had increased, while the amplitude has decreased. Both can be associated with a bottom roughness that is too high.

Table D.9 Representation quality in the frequency domain at location Adelaide Outer Harbour. The harmonic constituents presented here are those with the largest amplitudes in Port Giles.

	A_o	A_c	ΔA	G_o	G_c	ΔG	VD
M_2	50.9	49.0	-1.9	275.3	280.7	5.4	5.0
S_2	51.4	48.5	-2.9	324.1	329.7	5.5	5.6
K_1	25.2	24.6	-0.6	123.7	127.1	3.4	1.6
O_1	17.0	16.5	-0.4	116.4	119.8	3.4	0.3
K_2	14.7	13.9	-0.8	323.5	328.0	4.5	1.4
S_a	5.7	5.6	-0.1	161.7	163.8	2.1	0.2
MU_2	8.9	8.4	-0.5	38.2	42.4	4.2	0.8
P_1	7.1	6.6	-0.5	120.0	123.1	3.1	0.6
M_{sf}	5.8	6.4	0.5	80.0	79.9	-0.1	0.5
Q_1	4.3	4.1	-0.2	100.2	103.5	3.4	0.3

D.4 Detail model: temperature and salinity

In Figure D.9, computed temperature and salinity time series from the validation run at station Control-3 are plotted together with the measured values. This is done at two depth levels: 1 m below the surface and 1 m above the bottom. The results at all three stations are also shown quantitatively in Table D.10 and Table D.11.

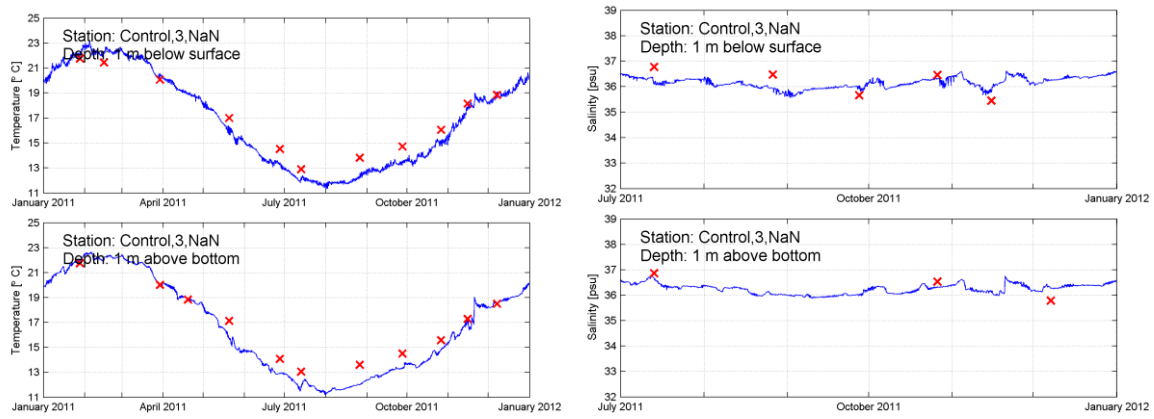

Figure D.9 Time series of computed temperature (left) and salinity (right) at 1 m below surface and 1 m above bottom for station Control-3, covering the year 2011. (blue line: model results (detailed model); red crosses: measured values)

Table D.10 Overview of the quality of the temperature representation in the detailed 3D Adelaide model at 1 m below surface and 1 m above bottom, in terms of bias, standard deviation (std) and RMSE (all in °C).

	1 m below surface			1 m above bottom		
station	bias	std	RMSE	bias	std	RMSE
Control-1	-0.5	0.9	1.0	-0.6	0.9	1.0
Control-2	-0.7	0.8	1.0	-0.6	0.8	1.0
Control-3	-0.6	0.8	0.9	-0.7	0.7	0.9
average	**-0.6**	**0.8**	**1.0**	**-0.6**	**0.8**	**1.0**

Table D.11 Overview of the quality of the salinity representation in the detailed 3D Adelaide model at 1 m below surface and 1 m above bottom, in terms of bias, standard deviation (std) and RMSE (all in psu).

	1 m below surface			**1 m above bottom**		
station	bias	std	RMSE	bias	std	RMSE
Control-1	0.0	0.5	0.5	0.0	0.5	0.5
Control-2	-0.5	0.2	0.5	0.0	0.4	0.4
Control-3	-0.1	0.4	0.4	0.0	0.3	0.3
average	**-0.2**	**0.4**	**0.5**	**0.0**	**0.4**	**0.4**

E Epiphyte Modelling – updates

Technical Memo Prepared by Paul L.A. Erftemeijer (DAMCO Consulting) Perth, 27 November 2015.

Technical Memo: EPIPHYTE MODELLING - updates

Prepared for Deltares by Paul L.A. Erftemeijer (DAMCO Consulting)
Perth, 27 November 2015 (final revision: 27 September 2016)

DAMCO CONSULTING

1. Introduction

This technical memo describes the background and justification for a number of updates and improvements to epiphyte modelling component of the Adelaide Receiving Environment Model (AREM) as part of a joint project between Deltares and DAMCO Consulting for SA Water. In a first phase of this project, a pilot model was developed, consisting of hydrodynamic, wave, biogeochemical (water quality/ecology) and seagrass habitat suitability modules (Deltares, 2014). Phase 2 of the project, for which a separate inception plan was developed (Deltares, 2015), focuses on further testing, improving and extending the model in order to make it operational and allow for the testing of scenarios. The objective of the final, operational model will be to guide investments by SA Water in nutrient reduction initiatives and other measures to prevent further degradation of seagrasses in Adelaide's coastal waters.

The present technical memo addresses updates to the way epiphyte growth on seagrass leaves is modelled. These updates include improvements to the model parameterization for epiphyte growth, based on a review of the taxonomic composition of 'nuisance' epiphytes on seagrass leaves as found in SA waters, and some additional notes on processes within the epiphyte matrix (incl. the contributing role of inorganic material trapped within the epiphyte matrix to light attenuation).

2. Epiphyte modelling – introduction

Seagrasses in SA waters always have a certain degree of epiphyte growth on their above-ground plant parts. Under normal 'nutrient-poor' conditions, most epiphytes are found on the distal parts of older seagrass leaves (photosynthetically not so active) and on the stems of some seagrass species (e.g. *Amphibolis*), while the younger leaves and lower (fresher) parts of the leaves tend to be free from epiphyte growth (Trautman and Borowitzka, 1999; Borowitzka et al., 2006). The epiphyte community under such conditions is made up primarily of calcareous, encrusting (red) algae. These have characteristics of 'K-selected' organisms, such as slow growth, great structural strength and a high degree of resistance to herbivory. The growth of these 'healthy' (calcareous) epiphytes does not appear to hamper seagrass growth or cause any mortality in the seagrasses (see Fong and Harwell, 1994). In contrast, when nutrient loading is significantly increased (eutrophication), there is a gradual shift in species composition of the epiphyte community (Cambridge et al., 2007). Fast-growing filamentous algae (including brown, red and green algae) take over, covering nearly all the surfaces of all above-ground seagrass plant parts, including the young and fresh (photosynthetically active) parts of the seagrass leaves. These filamentous algae are opportunistic and show characteristics of 'r-selected' organisms, such as rapid nutrient uptake and high growth rates that confer an advantage during periods/events of higher (pulsed) nutrient availability, as well as low structural development and high vulnerability to herbivory (Littler and Littler, 1980). When nutrient availability is increased significantly, the rapid growth and biomass of these 'nuisance' epiphytes can result in severe attenuation of light reaching the seagrasses and (if sustained) cause mortality of the seagrass plants.

In the pilot version of the model (phase 1), we opted to only focus on the growth of the 'nuisance' epiphytes (consciously 'ignoring' the healthy (calcareous) epiphytes in the understanding that these do not hamper seagrass growth, as elaborated above). A comparable approach was followed with success by Fong and Harwell (1994) in their modelling study of seagrass communities in tropical and subtropical bays and estuaries in Florida.

In our pilot model (Phase 1), we used the standard (default) parameter settings for algal growth as defined in BLOOM, the water quality module of Delft3D-WAQ, to model the growth of 'nuisance' epiphytes. These settings are in principle based on our knowledge of phytoplankton growth in Western Europe. While these parameter settings generally work well to describe algal growth in response to increased nutrient loading in most temperate waters (eutrophication), they were not specifically designed for simulating epiphyte growth. Detailed studies of epiphytic growth on seagrasses in SA and WA waters revealed that the main algal species that constitute these 'nuisance' epiphytes mainly consist of filamentous brown and red algae, as well as some filamentous green algae (see below for more detail). There is therefore scope for improvement of the parameterization of epiphyte growth in the AREM model.

3. Taxonomic composition of 'nuisance epiphytes'

Johnson (1981) studied the seasonality of algal epiphytes on *Posidonia sinuosa* in the upper Spencer Gulf (SA). His thesis included a detailed description of the taxonomic composition of the algal epiphytic community on *Posidonia* leaves over the various months of the year. He recorded 53 'erect' algal species on *Posidonia*, dominated by reds and browns, showing significant seasonality in their relative dominance. His results compare well with those of a similar study in WA by Kendrick and Burt (1997) and can be regarded as a baseline description of 'healthy' epiphytes under oligotrophic conditions.

Collings et al. (2006) investigated the response of *Posidonia* and *Amphibolis* dominated seagrass meadows in Adelaide's coastal waters to elevated nutrient availability, including the effects on epiphytes. Brown algae, principally *Hincksia* sp. generally dominated the epiphytic load, although application of nutrients also resulted in a substantial increase in green algal epiphytes. The major green epiphytes were *Cladophora* sp. and *Ulva* sp. Red algae represented a significant proportion only on the stems of *Amphibolis*. The composition of epiphytes was markedly different between the control and fertiliser treatments, with the latter dominated by (filamentous) red and green algae. The report also gives an account of the taxonomic composition of the opportunistic 'nuisance' algae:

Opportunistic 'nuisance' epiphytic algae (under nutrient enrichment) were primarily composed of:

- filamentous brown algae, especially *Hincksia* sp., *Ectocarpus* sp. and foliose *Colpomenia* sp.
- filamentous red algae *Polysiphonia* spp. and *Centroceras* sp.
- foliose green algae, such as *Enteromorpha* spp., *Cladophora* sp. and *Ulva* sp.

Such a shift in species composition of epiphytes on seagrass leaves in response to nutrient loading is also well-described in Cambridge et al. (2007):

> "In a field study, seagrass (*Posidonia* sp.) from outside Cockburn Sound was transferred to a site near the nutrient source at James Point. Within a few weeks, a predominantly encrusting calcareous epiphyte assemblage with low occurrence of larger individual macroalgae had changed to heavy epiphytic growths of filamentous brown and red algae (*Ectocarpus rhizoclonium*, *Polysiphonia* spp., *Centroceras cinnabarinum*) and foliose green algae (*Ulva* spp., *Enteromorpha* spp.). Changes in epiphyte composition occurred within a few weeks. The host seagrass plants deteriorated over ~10 weeks, with overgrowth of the leaves by epiphytes."

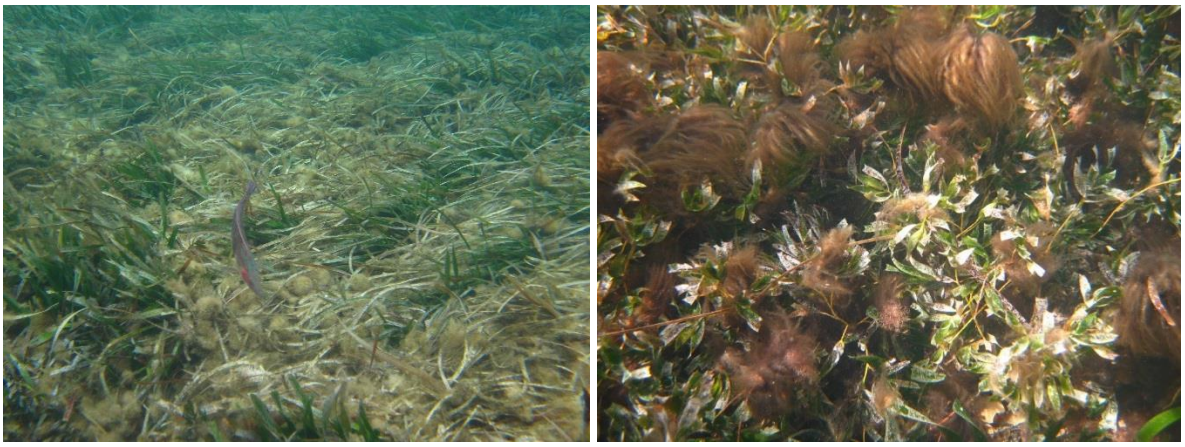

Figure 1. Growth of calcareous epiphytes on *Posidonia* (left) and nuisance epiphytes (*Lyngbia* sp.) on *Amphibolis* (right) (Photographs by Dr Marion Cambridge)

Changes in epiphyte composition in response to increasing water column nutrient concentrations was also reported by Bryars et al. (2011). Borowitzka et al. (2006) stressed that assuming a direct relationship between nutrient enrichment and epiphyte loads (and hence seagrass loss) would be an oversimplification, and that in addition to nutrients, grazing, hydrodynamics, depth and light (and interactions between all of these) all contribute to the complexity of epiphyte-mediated seagrass loss.

4. Model parameter settings for epiphyte growth

Adjustments to any of the parameter settings for epiphyte growth in the model should be based on scientific literature derived either from studies addressing ('nuisance') epiphytes on seagrass leaves (preferably in temperate Australian waters) or from species-specific studies on some of the main algal species known to dominate the epiphytes (e.g. *Hincksia* sp., *Polysiphonia* sp., *Cladophora* sp. etc., as elaborated above). Relatively little work has been done to quantify the factors controlling the distribution and abundance of epiphytic algae (Fong and Harwell, 1994).

The following Table is a summary compilation of data on some of the main parameter settings in the Delft3D-WAQ model derived from literature compared to the settings as used in the pilot model. Please note that for some parameters, no alternative data could be found in the literature. It is suggested to keep those unchanged (i.e. default settings as used in the pilot model).

Table 1. Parameterization of nuisance epiphytes

Name	Description	Unit	Default settings*	Alternative settings**	Literature reference
FrAut	fraction of dead algae biomass released as dissolved nutrients	(-)	0.3		
FrDet	fraction of dead algae biomass released as POC1, PON1, POP1	(-)	0.55		
ExtVl	specific extinction coefficient for visible light	(m^2/gC)	0.21 - 0.24		
DMCF	dry matter to carbon ratio	(gDM/gC)	3.3	2.8	Kendrick et al. (2000)
				3.4	Kendrick et al. (2000)
				8.5106	Klumpp et al. (1992)
NCR	nitrogen to carbon ratio	(gN/gC)	0.14 - 0.255	0.020	EPA (1997)
				0.059	Rutten (2007)
				0.078	Klumpp et al. (1992)
PCR	phosphorus to carbon ratio	(gP/gC)	0.018 - 0.0315	0.0012	Rutten (2007)
				0.0050	EPA (1997)
SCR	silica to carbon ratio	(gSi/gC)	0		
ChlaC	chlorophyll-a to carbon ratio	(gChla/gC)	0.025 - 0.04	0.0005	Klumpp et al. (1992)
				0.0055	Manning & Kirkman (1994)
				0.0178	Erftemeijer (1994)
PPMax	maximum growth rate at 0°C	(1/d)	0.066 - 0.083	0.0105	Paling et al. (1994)***
TcPMx	temperature coefficient for growth	(-)	1.07 - 1.08		
TFPMx	type of response to temperature (0: linear; <>0: exponential)	(-)	0	0	Fong and Harwell (1994)
Mort0	mortality rate at 0°C	(1/d)	0.07 - 0.08	0.02	Klumpp et al. (1992)****
				0.05	Kendrick et al. (2000)*****
TcMrt	temperature coefficient for mortality	(-)	1.072 - 1.085		
MResp	maintenance respiration rate at 0ºC	(1/d)	0.06		
TcRsp	temperature coefficient for respiration	(-)	1.066		

* default parameter settings of Delft3D as used in the pilot version (Phase 1) of the AREM model (showing minimum and maximum values where appropriate)
** alternative settings are based on literature review of seagrass epiphytes/nuisance algae; *** at 25°C; **** at 30°C; ***** at 20°C

Elemental constituents (C-N-P)

Literature values on Dry Matter to Carbon ratios (2.8-3.4) for seagrass epiphytes were comparable to the default settings used in the pilot model, except for one high value of 8.5 from the study of Klumpp et al. (1992), which appears due to very high ash contents (72-82%) of the samples.

Nitrogen to carbon and phosphorus to carbon ratios for epiphytes were significantly lower than the default values used in the pilot model. This indicates that these epiphytic species are likely to be more efficient in their nutrient uptake kinetics and thus able to grow faster (and accumulate more biomass) with less nutrients than what was initially assumed in the pilot model.

Chlorophyll contents

Chlorophyll to carbon ratios varied widely (in the order of 10 to 40 times) between different studies and this is therefore not probably likely a reliable model parameter to adjust. Since light attenuation by epiphytes in the Phase 2 version of the model will be calculated based on the amount of epiphytic carbon produced (using the equation by Brush and Nixon, 1993) and not on the amount of epiphytic chlorophyll (as was done in Phase 1, using the equation by Drake et al., 2003), this is probably not much of a problem.

Growth rates and temperature

The relationship between epiphyte growth and temperature is usually assumed to be linear (Fong and Harwell, 1994; Paling et al., 1994). Fong and Harwell (1994) modelled the relationship between epiphyte growth and light as 'inverse exponential', saturating at high irradiances >500 µE m^{-2} s^{-1}. Maximum growth of (sub)tropical seagrass epiphyte was estimated by Fong and Harwell (1994) to be in the order of 25% of dry weight per day at temperatures of 34-38°C, but these exact values are probably not transferable to the context of temperate seagrass epiphytes in Adelaide's coastal waters.

In a controlled experimental study of epiphyte growth on artificial seagrass (*Posidonia*) leaves, Paling et al. (1994) recorded maximum net production (P_{max}) ranging from 0.035 to 0.039 mg cm^{-2} d^{-1} at water temperatures ranging from 23 to 28°C. Saturation (I_k) values for 13 - 28°C were approximately 60 µmol m^{-2} s^{-1}. Net production/irradiance curves for summer showed a typical saturating response. This work by Paling et al. (1994) was the only study on seagrass epiphytes from which a maximum specific growth rate could be extracted, which was in the order of 0.01 day^{-1} (at ~25°C), i.e. considerably lower than the default values (0.07-0.08 day^{-1}) used in the Phase 1 pilot model.

Mortality

Loss of epiphytes (as a % of DW per day) on seagrass is controlled by both senescence of the epiphytes themselves as well as by the turnover time of seagrass blades, as epiphytes are dependent on seagrass as a physical substrate. No specific literature values could be found for mortality rates, but the values presented in Table 1 (above) were estimated indirectly from epiphyte biomass turn-over rates as follows: Turnover (in days) was calculated by dividing the measured epiphyte growth rate (g C m^{-2} d^{-1}) by the epiphyte biomass (g C m^{-2}). This turnover rate was subsequently divided by 365 to obtain an estimate of the mortality rate (d^{-1}). The values thus obtained (0.02-0.05 d^{-1}) were clearly lower than the default settings (0.07-0.08 d^{-1}) used in the Pilot model. Some studies (e.g. Paling et al., 1994) even state that the lifespan of the epiphytes appears to be determined by the turnover (lifespan) of the seagrass leaves (implying that their mortality in the model should be close to zero).

Ash contents

Though not reflected in Table 1, as it is not a parameter in the model, it was noted from several studies that the ash contents of epiphyte biomass can be very high. As noted in a review by Borowitzka et al. (2006), published data on epiphyte biomass must be interpreted with some caution; some authors determine total biomass (dry weight) that includes the $CaCO_3$ of the calcareous epiphytes rather than ash-free dry weight and this inflates the overall biomass figure. The $CaCO_3$ of the coralline algae can account for 40–60% of the total dry weight (Borowitzka et al., 1990; Bandeira, 1997).

Klumpp et al. (1992) quoted ash contents of the biomass of filamentous (mostly non-calcareous) epiphytes on tropical seagrasses in the Philippines to reach 72 to 82% of dry weight (average 78.6%). Kendrick et al. (2000) reported ash contents of epiphytes (mix of calcareous and filamentous) on seagrasses in Cockburn Sound (WA) to reach 53 to 63% of dry weight (average 58.6%) for *Posidonia coriacea* and 69 to 72% of dry weight (average 71%) for *Amphibolis griffithii.*

In some cases, this high ash contents of the epiphyte mass may have included a significant proportion of calcium carbonate (from calcareous epiphytes), but in other cases it is likely to have included inorganic components such as fine silt and inorganic debris trapped within the epiphyte matrix. The filamentous browns and reds can be quite sticky and trap all kind of stuff from the water column (see also: Drake et al., 2000). As noted by Brush and Nixon (2002), the epiphytic community found on seagrass plants is a heterogeneous and varying complex of bacteria, micro- and macroalgae, heterotrophic organisms, and organic and inorganic detritus and debris, including silt.

Some (perhaps much) attenuation through the epiphyte mass on seagrass leaves must also be due to the highly variable inorganic fraction of the epiphyte matrix (Lin, 1995). Most of the studies that report on epiphyte biomass on seagrasses have scraped off the entire intact epiphyte mass, including non-cellular organic and non-organic material in the epiphyte matrix. While this (mostly inorganic) material is not modelled, it is likely to contribute markedly to the attenuation of light reaching the seagrass leaf, and as such the model (which only calculates the biomass of the epiphytic algae) could be

underestimating the reduction of light available to the seagrasses. It may be worth considering some multiplier to compensate for this discrepancy.

The equation used in the pilot model to calculate light attenuation as a function of epiphyte biomass was derived from the paper by Drake et al. (2003). In the refined model of Phase 2, it has been decided to use a different equation (believed to be more appropriate for the present model), derived from the paper by Brush and Nixon (2002). This latter equation was, however, based on light attenuation through an intact epiphyte matrix (i.e. including the inorganic fraction). It remains unclear to what extent the amount of light attenuation as a function of dry weight would differ between a certain quantity of dry weight that is composed exclusively of living algal biomass compared to a similar quantity of epiphyte mass that is composed of a mixture of algal biomass and inorganic debris and silt fraction.

5. Cited References

Bandeira S.O., 1997. Dynamics, biomass and total rhizome length of the seagrass *Thalassodendron ciliatum* at Inhaca Island, Mozambique. Plant Ecol 130: 133–141.

Biber, P.D., M.A. Harwell and W.P. Cropper Jr., 2004. Modelling the dynamics of three functional groups of macroalgae in tropical seagrass habitats. Ecological Modelling 175: 25-54.

Borowitzka, M.A., R.C. Lethbridge and L. Charlton, 1990. Species richness, spatial distribution and colonisation pattern of algal and invertebrate epiphytes on the seagrass *Amphibolis griffithii*. Mar Ecol Prog Ser 64: 281–291.

Borowitzka, M.A., P.S. Lavery and M. van Keulen, 2006. Epiphytes of Seagrasses. Chapter 19 in: A.W.D. Larkum et al. (eds.), 'Seagrasses: Biology, Ecology and Conservation', Springer, pp. 441-461.

Brush, M.J. and S.W. Nixon, 2002. Direct measurements of light attenuation by epiphytes on eelgrass *Zostera marina*. Mar. Ecol. Prog. Ser. 238: 73–79.

Bryars, S., G. Collings and D. Miller, 2011. Nutrient exposure causes epiphytic changes and coincident declines in two temperate Australian seagrasses. Marine Ecology Progress Series 441: 89-103.

Cambridge, M.L., J.R. How, P.S. Lavery and M.A. Vanderklift, 2007. Retrospective analysis of epiphyte assemblages in relation to seagrass loss in a eutrophic coastal embayment. Marine Ecology Progress Series 346: 97−107.

Cebrian, J., J.P. Stutes and B. Christiaen, 2013. Effects of grazing and fertilization on epiphyte growth dynamics under moderately eutrophic conditions: implications for grazing rate estimates. Marine Ecology Progress Series 474: 121-133.

Collings, G., S. Bryars, S. Nayar, D. Miller, J. Lill and E. O'Loughlin, 2006. Elevated nutrient responses of the meadow forming seagrasses, *Amphibolis* and *Posidonia*, from the Adelaide metropolitan coastline. ACWS Technical Report No. 11 prepared for the Adelaide Coastal Waters Study Steering Committee. South Australian Research and Development Institute (Aquatic Sciences) Publication No. RD01/0208-16, Adelaide.

Deltares, 2014. Adelaide Receiving Environment Model – Pilot Model Set-up and Evaluation. Technical Report 1207457-000 for SA Water, Deltares, Delft (The Netherlands), version 8 (Nov. 2014), 164 pp. + appendices.

Deltares, 2015. Adelaide Receiving Environment Model – Phase 2 Inception Report. Technical Report 1210877-000-ZKS-0006 for SA Water, Deltares, Delft (The Netherlands), version 3 (June 2015), 48 pp. + appendices.

Drake, L.A., F.C. Dobbs and R.C. Zimmerman, 2003. Effects of epiphyte load on optical properties and photosynthetic potential of the seagrasses *Thalassia testudinum* Banks ex Konig and *Zostera marina* L. Limnology and Oceanography 48: 456–463.

EPA, 1997. Determination of epiphyte growth rates and seagrass health. Final report and results of October survey. Environment Protection Authority and the Patawalonga and Torrens Catchment Water Management Board, April 1997, 30 pp. + appendices.

Erftemeijer, P.L.A., 1994. Differences in nutrient nutrient concentrations and resources between seagrass communities on carbonate and terrigenous sediments in South Sulawesi, Indonesia. Bulletin of Marine Science 52(4): 403-419.

Fong, P. and M.A. Harwell, 1994. Modelling seagrass communities in tropical and subtropical bays and estuaries: a mathematical model synthesis of current hypotheses. Bulletin of Marine Science 54(3): 757-781.

Johnson, J.E., 1994. The seasonality of the algal epiphytes of *Posidonia sinuosa* in the upper Spencer Gulf. MSc thesis, University of Adelaide, March 1981.

Kendrick, G.A. and J.S. Burt, 1997. Seasonal changes in epiphytic macroalgae assemblages between offshore exposed and inshore protected *Posidonia sinuosa* Cambridge et Kuo seagrass meadows, Western Australia. Botanica Marina 40: 77-85.

Kendrick, G.A., M. Campey, P. Lavery, M. Westera and K. Wheeler, 2000. Shellsand Dredging Environmental Management Programme – Project S1: Ecological Significance of Seagrasses Primary Production. Phase 3 Report. Prepared for Cockburn Cement, November 2000.

Klumpp, D.W., J.S. Salita-Espinosa and M.D. Fortes, 1992. The role of epiphytic periphyton and macroinvertebrate grazers in the trophic flux of a tropical seagrass community. Aquatic Botany 43: 327-349.

Lavery, P.S., T. Reid, G.A. Hyndes and B.R. Van Elven, 2007. Effect of leaf movement on epiphytic algal biomass of seagrass leaves. Mar. Ecol. Prog. Ser. 338: 97–106.

Lin, H.J., 1995. Responses of epiphytes on eelgrass (*Zostera marina* L.) to nutrient enrichment. PhD thesis, University of Rhode Island, Kingston, RI (quoted in: Brush and Nixon, 2002).

Littler, M. M. and D. S. Littler. 1980. The evolution of thallus form and survival strategies in benthic marine macroalgae: field and laboratory tests of a functional form model. Am. Nat. 116: 25-44.

Manning, C. and H. Kirkman, 1994. Epiphytes – Critical Irradiances and Metabolic Rates – Data Report. Perth Coastal Waters Study, Project E3.1, CSIRO.

Paling, E.I., C.B. Slim, M.G. Pennifold and D.I. Walker, 1994. Epiphyte growth on artificial seagrass (*Posidonia*) in Perth, Western Australia. 1: The effect of light and temperature. Chapter 3 in: Walker et al. (Eds) 'Perth Coastal Waters Study – Project E3.1: Relationship between Nitrogen and Primary Production', Final Report, pp. 90-119.

Penhale, P. and W. O. Smith, Jr. 1977. Excretion of dissolved organic carbon by eelgrass (*Zostera marina*) and its epiphytes. Limnology and Oceanography 22:400-407.

Rutten, K., 2007. Studies on the biomass, diversity and nutrient relationships of macroalgae and seagrasses in Lake Illawarra, New South Wales, Australia, PhD thesis, School of Earth and Environmental Sciences, University of Wollongong, 296 pp.

Sand-Jensen, K. 1977. Effect of epiphytes on eelgrass photosynthesis. Aquatic Botany 3:55-63.

Sicko-Goad, L.M., C.L. Schelske and E.F. Stoermer, 1984. Estimation of intracellular carbon and silica content of diatoms from natural assemblages using morphometric techniques. Limnol. Oceanogr. 29(6): 1170-1178.

Trautman, D.A. and M.A. Borowitzka, 1999. Distribution of epiphytic organisms on *Posidonia australis* and *P. sinuosa*, two seagrasses with differing leaf morphology. Mar Ecol Prog Ser 179: 215-229.

Walker, D., Paling, E. I., Sim, C., Pennifold, M., Manning, C., & Kirkman, H. (1994). Perth Coastal Waters Study Project E3.1: Relatonship between Nitrogen and Primary Production. Perth: Department of Botany.

F HABITAT MODEL updates

Technical Memo: Prepared for Deltares by Paul L.A. Erftemeijer (DAMCO Consulting) Perth, 5 November 2015

Technical Memo: HABITAT MODEL updates

Prepared for Deltares by Paul L.A. Erftemeijer (DAMCO Consulting)
Perth, 5 November 2015 (final revision: 27 September 2016)

DAMCO CONSULTING

Introduction

This technical memo describes the background and justification for a number of updates and improvements to the Habitat Model for the Adelaide Receiving Environment Model (AREM) as part of a joint project between Deltares and DAMCO Consulting for SA Water. In a first phase of this project, a pilot model was developed, consisting of hydrodynamic, wave, biogeochemical (water quality/ecology) and seagrass habitat suitability modules (Deltares, 2014). Phase 2 of the project, for which a separate inception plan was developed (Deltares, 2015), focuses on further testing, improving and extending the model in order to make it operational and allow for the testing of scenarios. The objective of the final, operational model will be to guide investments by SA Water in nutrient reduction initiatives and other measures to prevent further degradation of seagrasses in Adelaide's coastal waters. The present technical memo addresses updates to the model forcing for the determination of habitat suitability for seagrasses with respect to the duration of low light periods, return periods for high wave energy events, salinity and seedling establishment (recruitment/recovery). Observations on the potential for an alternative approach to light modelling are also included.

Model Updates:

[1] Rolling means for habitat light forcing

In the pilot version of the model (phase 1), the contribution of light conditions to determining habitat suitability for seagrasses was calculated (on the basis of a literature review of their minimum light requirements) in a simplified way:

- Using the *annual mean* of modelled light for *Posidonia* species (able to withstand longer durations of poor light conditions), and
- Using the *8th-percentile* of modelled light over a year (corresponding to a cumulative total duration of poor light conditions of one month per year) for all other seagrass species.

In reality, however, it is more likely to be sustained periods of low light conditions (rather than cumulative statistics of the total number of bad days experienced throughout a year) that will impact seagrasses. In other words, if days of low light are alternating with days of sufficient (or excellent) light, seagrasses may well be able to survive, even though the annual average light statistics may suggest otherwise. If low light conditions are however sustained more or less continuously for a sufficiently long period of time, seagrasses may start dying off, even when the annual average light statistics suggest otherwise.

Moreover, there is a growing body of scientific evidence that shows that the various seagrass species differ in the length of time (duration) they can endure low light conditions (below their minimum light requirements, or MLR). Therefore, there is scope to refine this approach in the Habitat Model. The following is a summary of what has been reported in the literature:

- *Posidonia sinuosa*: In a field experiment in Western Australia, Collier et al. (2009) observed a major decline (82% loss) in shoot density of *Posidonia sinuosa* after 105 days of shading at 4-5%SI, but

with 6% of shoots still surviving after 198 days. When only moderately shaded to 12% of ambient light, individual plants managed to survive for 24 months. Collier (2006) reported 84% shoot loss within 106 days of heavy shading (at 3-4%SI). Gordon et al. (1994) observed a 32-55% reduction in shoot density in *Posidonia sinuosa* when shaded by 80-90% below ambient light levels (controls) after 148 days of shading. After 307 days, shoot density had reduced by 90% compared to controls. In an experiment off Adelaide, SA, shading of *Posidonia sinuosa* to 50% below ambient light levels caused no reduction in shoot density within the first 6 months, but after 9 months of continuous shading, shoot density had declined by 70% compared to controls (Neverauskas, 1988).

- *Posidonia australis*: Fitzpatrick and Kirkman (1995) observed a significant effect on the shoot density and growth of a *Posidonia australis* meadow after 3 months of shading to less than 10%SI. A similar (Mediterranean) species *Posidonia oceanica*, showed 54% reduction in cover and 61% drop in shoot density after 120 days of shading to ~1% of ambient light (Serrano et al., 2011).

  ➔ ***Conclusion: Posidonia spp. do not tolerate low light conditions below MLR if sustained for more than 3 to 6 months***

- *Amphibolis griffithii*: After 3 months of shading (88% reduction relative to ambient levels in control plots), declines were observed in leaf biomass (30%), leaf cluster density (50%) and the number of leaves per cluster (60%) in shaded plots in Jurian Bay, WA (Mackey et al., 2007). McMahon et al. (2011) reported 72% loss of leaf biomass after 3 months of light stress (5-18% of ambient). Lavery et al. (2009) documented 57% loss of leaf biomass at 13-19%SI after 3 months (if shaded in late summer, but no loss if shaded in late winter). If these moderately low light levels (13-19%SI) were sustained for 9 months, there was 93% leaf biomass loss, irrespective of season. At high shading intensity (5-11%SI), loss of leaf biomass after 3 months was 71% (if in late summer) and 66% (if in late winter).

- *Amphibolis antarctica:* Bryars and Collins (2008) reported 100% survival when this species was shaded to 0%SI for 6 weeks (but observed the loss of nearly all epiphytes in that period).

  ➔ ***Conclusion: Amphibolis spp. do not tolerate low light conditions below MLR if sustained for more than 2 to 3 months***

- *Heterozostera tasmanica* (=*nigricaulis*): Kirkman et al. (2012) observed the onset of a reduction in shoot density and 'paling' of leaves after ~2 months of shading to 1-3% SI, with 61% decline in shoot density after 90 days of shading and 84% decline after 134 days. Experimental shading of *H. tasmanica* by Bulthuis (1983) in Victoria revealed nearly 100% loss of leaf clusters within 2 months when irradiance was reduced to <2%SI (if in summer) and within 4 months (if in winter, with 60% loss after 2.5 months). When light was reduced to 4.7%SI, there was 65-75% shoot loss within 2 months (if in summer) with 100% shoot loss reached after 10 months. No initial decline was observed if this level of shading was imposed in winter, and shoot density only started to decline later in the following summer. Reduction of irradiance to 13-18%SI only resulted in a 25-50% decrease in leaf cluster density after 14 months of shading (after which leaf cluster density stabilised), indicating that *H. tasmanica* is able to survive such moderately low light levels. There was good survival of *Heterozostera tasmanica* plants if shaded to 9%SI for 10 months (Bulthuis, 1983).

➔ ***Conclusion: Heterozostera tasmanica does not tolerate low light conditions below MLR if sustained for more than 2 months***

- *Zostera muellerii*: Collier et al. (2012) reported a meadow-scale onset of shoot-die-off after 46 days at 1% SI, complete loss after 76 days. Grice et al. (1996) reported a maximum of 1 month survival of *Zostera capricorni* (=*muelleri*) at 5%SI.

- *Halophila* sp.: Yaakub et al. (2013) observed a major decline in shoot density (clear site) or complete shoot loss (turbid site) of *Halophila ovalis* when shaded for ~2 months below minimum light requirements. Longstaff et al. (1999) reported the onset of shoot loss in *Halophila ovalis* after ~1 month (21 days) of shading below MLR.

➔ ***Conclusion: Zostera muelleri & Halophila* spp. *do not tolerate low light conditions below MLR if sustained for more than ~1 month***

To apply these conclusions to the Habitat Model, it is suggested to use the following time-averaging assumptions when interrogating model output for an estimation of habitat suitability for the different seagrass species:

- For *Zostera muelleri* and *Halophila australis* use a ***30-day rolling mean*** of modelled light (%SI) reaching the plants (corrected for light attenuation by epiphyte cover) and compare that against their respective minimum light requirements (resulting in an estimate of habitat suitability for each individual species along a graded scale from 0 to 1, as done previously);

- For *Amphibolis griffithii, A. antarctica* and *Heterozostera tasmanica*: use a ***60-day rolling mean*** of modelled light (%SI) reaching the plants (corrected for light attenuation by epiphyte cover) and compare that against their respective minimum light requirements (resulting in an estimate of habitat suitability for each individual species along a graded scale from 0 to 1, as done previously);

- For *Posidonia australis, P. sinuosa, P. angustifolia* and *P. coriacea*: use a ***90-day rolling mean*** of modelled light (%SI) reaching the plants (corrected for light attenuation by epiphyte cover) and compare that against their respective minimum light requirements (resulting in an estimate of habitat suitability for each individual species along a graded scale from 0 to 1, as done previously).

[2] Species-specific return periods and orbital velocities for waves:

In the pilot version of the model (phase 1), the contribution of wave exposure to determining habitat suitability for seagrasses was calculated in a simplified way using a single criterion for (maximum) near-bed orbital velocity (0.5 m/s) as the critical value for all seagrass species, using the wave conditions corresponding to a once per half year event (return period). In reality, however, we know that not all seagrass species are equally susceptible to the impacts of waves (their intensity as well as their frequency). Therefore, there is scope for refinement of this approach in the Habitat Model. The following is a summary of what has been reported in the literature (see Erftemeijer, 2013):

- *Amphibolis antarctica* is adapted to hydrodynamically active environments and appears to be the only species capable of colonizing high intensity disturbance sites (Clarke and Kirkman, 1989), although particularly high hydrodynamic energy in areas off the Adelaide coast were found to prevent seedling establishment (Wear et al., 2010).

- *Amphibolis griffithii* and *Posidonia coreacea* are also known as wave-tolerant and swell-tolerant species (Shepherd and Robertson, 1989).

- *Posidonia australis* and *Posidonia sinuosa* appear to inhabit more moderately exposed or relatively sheltered areas and *Posidonia angustifolia* only inhabits deeper waters where the effects of wave energy are much less pronounced (Shepherd and Robertson, 1989).

- *Heterozostera tasmanica* and *Zostera muellerii* appear to be quite sensitive to exposure to wave energy and are primarily found in sheltered areas characterised by fine sediments (Shepherd and Robertson, 1989). *Halophila australis,* a species with limited root penetration, which limits its anchoring strength (see: Kiswara et al., 2009), is also likely to fall into this category.

This overview clearly shows that there are profound differences in how much wave energy different seagrass species can withstand (and how frequently), but this conclusion is entirely qualitative and intuitive, based on anecdotal field observations of seagrass distribution. There appear to be no published measurements or data to translate these perceived differences in wave-tolerance into more quantitative terms that would be needed for the model.

In the absence of more species-specific data on the precise tolerance thresholds for the seagrasses in (South) Australian waters, two ways can be explored to serve as a proxy for the differences in tolerance between species:

- **<u>Alternative 1</u>: Vary the return period of wave events** (i.e. the probability of such extreme events to occur) during which the critical value of 0.5 m/s for (maximum) bottom orbital velocity is exceeded, applying a more frequent return of extreme conditions for wave-tolerant species than for wave-sensitive species. Taking into consideration the findings of the literature review elaborated above, this could be adopted as follows:

- For *Amphibolis antarctica* (the most wave-tolerant of all seagrass species in SA): use a ***return period of once a month***
- For *Amphibolis griffithii* and *Posidonia coreacea* (wave-tolerant species): use a ***return period of once per 3 months***
- For *Posidonia australis, Posidonia sinuosa* and *Posidonia angustifolia* (preferring sheltered sites): use a ***return period of once per 6 months***
- For *Heterozostera tasmanica, Zostera muellerii* and *Halophila australis* (wave-sensitive species): use a ***return period of once a year***

These values are within the same range as those quoted in recent studies by Infantes et al. (2009), Vacchi et al. (2012) and Vacchi et al. (2014), who adopted an extreme wave return period of 'once a year' as relevant when describing hydrodynamic constraints to meadow expansion of *Posidonia oceanica* and modelling the upper limits of *P. oceanica* seagrass distribution in the Mediterranean.

- **<u>Alternative 2</u>: Vary the critical threshold for near-bed orbital velocity** (while keeping the return period of extreme wave events constant at once per 6 months), using lower thresholds for seagrass species that are more sensitive to wave exposure and higher thresholds for wave-tolerant species:

- For wave-sensitive species (*Heterozostera tasmanica, Zostera muelleri* and *Halophila australis*), use a critical ***bottom orbital velocity of 0.3 m/s***
- For seagrass species that prefer sheltered sites (*Posidonia australis, Posidonia sinuosa* and *Posidonia angustifolia*), use a critical ***bottom orbital velocity of 0.4 m/s***
- For wave-tolerant species (*Amphibolis griffithii* and *Posidonia coreacea*), use a critical ***bottom orbital velocity of 0.5 m/s***
- For *Amphibolis antarctica* (the most wave-tolerant of all seagrass species in SA), use a critical ***bottom orbital velocity of 0.6 m/s***

This would constitute a sensitivity assessment, as there is only limited published literature to back up any of these values (but see: De Jong et al., 2005; Infantes et al., 2009).

[3] *Zostera* salinity tolerance (update)

During the first SAG meeting, it was noted that *Zostera muelleri* is likely to tolerate a higher salinity range (as observed near the Port Augusta power station) than what was assumed in the pilot model. A recent study on the response of seagrasses to hyposalinity events (Collier et al., 2014) suggests that a 10-week exposure of *Zostera muelleri* to salinities as low as 6 ppt and 9 ppt had a positive effect on shoot density and leaf area, with no effects of 10 weeks exposure to 3 ppt compared to controls. These findings suggest that the response curve for salinity for this species should be adjusted by changing the habitat suitability (HSI) at 0 ppt to 1.

In that same study (Collier et al., 2014), the response of *Halophila ovalis* to hyposalinity was also investigated, showing an increased shoot density and leaf area of plants exposed for 10 weeks at 15 ppt compared to controls, no effects at 12 ppt, reduced shoot density and leaf area at 9 ppt, and significant mortality at 3-6 ppt. Based on their results, it is proposed to adjust the response curve for salinity for this species by adding a habitat suitability (HSI) of 1 at 15 ppt.

[4] Habitat requirements for successful seagrass recovery

In phase 1 of this project, the emphasis of the Habitat Model has always been on identifying the environmental conditions that would prevent further seagrass loss. Consequently, the selection of threshold criteria for the various environmental variables were those that relate to the tolerance of mature seagrass plants (as informed by literature review). During one of the project's stakeholder workshops and subsequent Scientific Advisory Group (SAG) meetings, it was asked: "Would the model also be able to predict the chances of successful recovery of seagrasses in areas where it was previously lost, or would that require a different set of HSI thresholds?"

While recovery can occur via two different pathways, i.e. vegetative (lateral) clonal expansion from existing meadows into un-vegetated areas (a slow process) versus sexual recruitment through seed dispersal and seedling establishment, it is believed the latter process is probably the main (large-scale)

and most rapid process (Cambridge et al., 2002; Kendrick et al., 2012). For a satisfactory answer to the question noted above, we therefore need to evaluate whether the habitat requirements of seedlings are the same or markedly different from mature plants. Below is a brief summary of the literature on this subject (supplemented with insights from helpful discussions with Gary Kendrick, John Statton and Marion Cambridge):

Successful recruitment and seedling establishment of seagrasses at a site depend on several factors, which are essentially a function of seed supply and (micro-)site suitability (Inglish, 2000; Orth et al., 2006; Rivers et al., 2011):

- Seed limitation (delivery of seeds and/or propagules to the site from existing meadows)
- Degree of seed predation, bioturbation and smothering/excessive deposition
- Hydrodynamic conditions (currents/waves) preventing initial propagule establishment (directly or through resulting sediment instability; see Irving, 2013) and/or uprooting newly established seedlings (not yet sufficiently anchored)
- Degree of seedling mortality due to unsuitable environmental (physico-chemical) conditions (light, temperature, salinity, burial, nutrient deficiency)
- Degree of seedling mortality due to biological factors (grazing and bioturbation)

Figure 1. *Posidonia* sp. meadow with mature fruits still on plants (top) and newly developing seedlings (bottom). (Photographs by Dr Marion Cambridge)

For the model, it is of particular relevance to examine the hydrodynamic and environmental (physico-chemical) conditions that determine seedling survival. As we will see, this is primarily a matter of ***"windows of opportunity"***, i.e. they will manage to successfully establish if offered a window of time with sufficiently suitable conditions without major perturbations. For example, Cambridge et al. (2002) reported significant recovery of *Posidonia australis* and *P. sinuosa* in Oyster Harbour (Southeastern Australia) following a series of drier years when less nutrients and silt were carried into the estuary, providing an important indication that catchment management and improved water quality would promote conditions favourable for seagrass recovery/regrowth.

Posidonia and *Amphibolis* have unusual reproductive strategies in that there is no real seed, but a seedling is either borne on the plant (vivipary) as is the case with *Amphibolis*, or comes from a mature fruit in *Posidonia* (Figure 1) (Kirkman, 1998; Kuo and Kirkman, 1990). In SA, seedlings of *Posidonia* spp. typically become established during early summer (~December), while *Amphibolis* spp. seedlings are released in ~September. After this, the seedlings need approximately 5-7 months of relatively calm conditions to develop and anchor themselves sufficiently before the onset of the rougher winter season, with the first storms arriving around May. During the first 4-9 months (especially the first 4 months), *Posidonia* seedlings are less sensitive to low light conditions, as they are able to grow and develop from the nutrition and energy reserves stored in the seed (Hocking et al., 1981) but after that period they become increasingly dependent on their own ability to photosynthesize and thus on water clarity. Compared to mature seagrass plants, such 6-9 month old seedlings may initially be able to do with less light, since the oxygen demand from their still poorly developed below-ground root system is lower than that of mature plants in an established meadow, but they still lack the substantial energy reserves that mature plants are able to store up in their rhizomes. Juvenile *Amphibolis antarctica* plants survive without roots and successfully depend entirely on nutrient acquisition from the water column (Paling and McComb, 1994). *Posidonia australis* seedlings in Oyster Harbour, Southwestern Australia, all had short rhizomes (<2 cm), even in 2-3 year old plants with as many as 13 shoots and over 60 leaves produced during the seedling life (Cambridge et al., 2002). In a study in southeast Australia, Meehan and West (2004) found that *Posidonia australis* seedlings only produce their second shoot after an average of 2.7 years and only begin to develop horizontal rhizomes after about 4 years.

Substantial sediment instability as a result of hydrodynamic disturbance (in areas where seagrass vegetation is absent) can also be a cause of seedling mortality. A recent study by Chisholm (2009) in Owen Anchorage (WA) on the effect of sediment instability on the survival of transplanted *Posidonia australis* seedlings, indicated a critical threshold for sediment movement of about 8 cm (maximum burial depth that can be tolerated).

Figure 2. *Amphibolis* seedlings, with characteristic 'hooks' (close-up: right) for easy initial anchoring

Most seedling mortality, however, appears to occur during the onset of winter storms through uprooting and dislodgement of the seedlings (Rivers et al., 2011; Verduin et al., 2013). *Amphibolis* seedlings are potentially at an advantage here, as they have specialised 'hooks', part of a comb-like grappling apparatus at their base to facilitate entanglement (Figure 2) with which they anchor themselves onto fibrous material (e.g. a former rhizome matte) (Wear et al., 2010; Rivers et al., 2011), but there are no published data to quantify the extent of this advantage. Infantes et al. (2011), combining flume and field observations, demonstrated how wave exposure strongly affected seedling survival in *Posidonia oceanica*, with high losses experienced when bottom orbital velocities exceeded 18 cm s^{-1} during the first autumn storms. In a similar study, Alagna et al. (2015) reported how seedling anchorage success in *Posidonia oceanica* seedlings depends primarily on substrate firmness and complexity, with firm and complex hard substrates allowing for early and strong anchorage of propagules, enhancing seedling persistence and establishment probabilities. The minimum force required to dislodge plantlets attached to rocky substrates reached 23.830 N (equivalent to 2.43 kg), which would potentially allow many plantlets to overcome winter storms in the field.

The most critical habitat requirement for *Posidonia* and *Amphibolis* seedlings appears to be a calm period without hydrodynamic disturbance during the first 4-6 months. The timing of this calm period is critical, as it should coincide with the period immediately following fruit shedding (~first week of December for *Posidonia*) or seedling release (~September for *Amphibolis*).

Sediment nutrient availability does not seem to play a critical role in determining seedling survival, at least not for *Posidonia australis* (Statton et al., 2014). Increasing nutrient availability through application of slow-release fertiliser in the sediment did not affect seedling survival, but reduced their average root length, thus compromising their anchorage and making them more susceptible to hydrodynamic disturbances.

Posidonia coriacea seedlings were able to recruit successfully on Success Bank in Western Australia (Campey et al., 2002) despite low ambient nutrient concentrations. The nutrient reserves in the seeds appear to provide a pool of nitrogen and phosphorus that seedlings draw upon to enable growth, effectively protecting them from nutrient stresses in their environment. Although nitrogen and phosphorus were depleted from seeds within the first year, the seeds provided enough nutrients to enable the seedlings to establish root systems and sustain shoots, allowing them to then assimilate nutrients from the environment (Walker et al., 2004).

The life history strategy of *Halophila* spp. means they are also well adapted for recovery once conditions become favourable as they are fast growing and rapid colonisers. *Halophila* spp. typically produce large numbers of long lived seeds. Areas with sufficient seed banks have a high capacity for *Halophila* sp. to recruit and recolonise quickly through seeds, while areas with poor seed reserves may take years to recover from major disturbances, such as cyclones and floods (Rasheed et al., 2014). Where light depreviation (e.g. from dredging or flooding) has been the cause of seagrass loss, *Halophila* sp. is able to recover quickly (mainly from seeds) as soon as light conditions have been restored to previous levels (Longstaff et al., 1999).

Zostera muelleri has also shown significant ability to recover (repeatedly) after major disturbances (e.g. storms and floods). For example, over 15 years of regular, quarterly Seagrass-Watch monitoring at Urangan in the Burnett Mary NRM region, Queensland, has seen a *Zostera muelleri* meadow come and go on an irregular basis following major flooding events (e.g. in 1999, 2006 and 2011). After water quality conditions improved, seedlings emerged and patches began re-establishing, resulting in significant recovery of the meadows from July 2000 onwards, as well as in 2008 and again since 2012 (McKenzie and Yoshida, 2015).

Macreadie et al. (2014) reported good recovery of *Zostera muelleri* meadows through asexual rhizome encroachment in Lake MacQuarie (Australia) following small-scale disturbances within <35 weeks, but recovery through sexual recruitment was insignificant. They concluded that, in the absence of a notable seed bank, *Z. muelleri* populations within Lake Macquarie rely entirely on clonal growth to recover from small-scale disturbances.

Findings reported in literature for *Zostera marina*, a species similar to *Zostera muelleri*, may further contribute to our understanding of the environmental conditions required for successful recovery of *Zostera muelleri*. Following major nutrient reductions and improved water quality in Odense Fjord (Denmark), Valdemarsen et al. (2010) found that recovery of *Zostera marina* meadows by recolonization through reproductive dispersal was negatively affected by physical disturbances (such as smothering and dislodgement/uprooting) from drifting macroalgae (contributing 40% to overall seedling mortality), as well as from hydrodynamic exposure (waves/currents) and sediment mobility due to bioturbation, although these latter causes were not quantified in their study. Bintz and Nixon (2001) carried out shading experiments (over 12 weeks) on *Zostera marina* in mesocosms in Narragansett Bay, Rhode Island, USA and concluded that the responses of seedlings to reduced light were similar to those reported for mature *Z. marina* plants. These findings suggest that physical disturbance (uprooting) is likely to be of primary concern for *Zostera muelleri* seedlings (more than in mature plants), similar to what was reported above for other species, whereas the sensitivity of adverse water quality (esp. turbidity) on seedlings is probably similar to mature plants.

Campey et al. (2002) reported significant flower densities for *Heterozostera tasmanica* in mixed meadows on Success Bank, southwestern Australia, in 1997, pointing to potential sexual reproduction as a contribution to the meadow, but the absence of flowers in 1998 and 1999, and the absence of a seed bank within the sediment, suggested that sexual reproduction probably did not contribute significantly to the maintenance of this population. As such, recovery of this meadow in the event of a major disturbance will most likely be through asexual (clonal) vegetative shoot recruitment and horizontal rhizome elongation from existing/remaining patches.

In summary, it is concluded that successful recovery of former seagrass areas through recruitment of propagules and establishment of seedlings primarily depends on the degree of spatial (shelter) or temporal (calmer months) respite from physical/hydrodynamic disturbances (e.g. from waves or storms), offering them a *window of opportunity* to become established and anchored. The chances of uprooting/dislodgment in seedlings are much greater than mature plants. Although this has not been quantified in terms of a critical threshold for the maximum bottom orbital velocity, it is likely to be comparable to the force needed to uproot the smaller, wave-sensitive seagrass species.

For most other environmental variables, the habitat requirements of seedlings appear to be similar to those of mature plants.

[7] Other light model

Some authors have suggested to apply light thresholds based on the overall total quantity of light energy (expressed as annual total PAR) required as a minimum to sustain seagrass growth.

Chartrand et al. (2012 a, b) reported how *Zostera muelleri* required 4.5-12 mol PAR m^{-2} day^{-1} for a minimum of two weeks to survive. This was converted into a trigger for a dredging operation as 6 mol PAR m^{-2} day^{-1} (rolling 14 day-average).

Collier et al. (2012) reported >50% loss of seagrass cover in *Halodule uninervis* (GBR) when 16-18% of days light levels fell below 3 mol PAR m^{-2} day^{-1} over a 3-months period.

Dixon (2000) documented annual water column PAR totals received by *Thalassia testudinum* meadows in Tampa Bay, Florida (USA), to be at or above 4860 mol PAR m^{-2} $year^{-1}$ for sites (shallow) with no evidence of stress and 3730 mol PAR m^{-2} $year^{-1}$ at a light-stressed site (at their maximum depth-limit).

While this is a potentially promising and interesting approach, there is currently not enough quantitative information (published data) to apply this as an alternative methodology to derive thresholds to determine the Habitat Suitability for the different seagrass species in SA.

Cited references

Alagna A, Fernández TV, Anna GD, Magliola C, Mazzola S, Badalamenti F, 2015. Assessing *Posidonia oceanica* Seedling Substrate Preference: An Experimental Determination of Seedling Anchorage Success in Rocky vs. Sandy Substrates. PLoS ONE 10(4): e0125321. doi:10.1371/journal.pone.0125321

Bintz, J. C. and S. W. Nixon. 2001. Responses of eelgrass *Zostera marina* seedlings to reduced light. Mar. Eco. Prog. Ser. 223:133–141.

Bulthuis, D.A., 1983. Effects of in situ light reduction on density and growth of the seagrass *Heterozostera tasmanica* (Martens ex Aschers.) den Hartog in Western Port, Victoria, Australia. J. Exp. Mar. Biol. Ecol. 67: 91-103.

Cambridge, M.L., G.R. Bastyan and D.I. Walker, 2002. Recovery of *Posidonia* meadows in Oyster Harbour, Southwestern Australia. Bulletin of Marine Science 71(3): 1279-1289.

Campey, M.L., Gary A. Kendrick, Diana I. Walker, 2002. Interannual and small-scale spatial variability in sexual reproduction of the seagrasses *Posidonia coriacea* and *Heterozostera tasmanica*, southwestern Australia. Aquatic Botany 74: 287–297.

Chartrand, K.M., Ralph, P.J., Petrou, K., Rasheed, M.A., 2012a. Development of a Light-Based Seagrass Management Approach for the Gladstone Western Basin Dredging Program. DEEDI Publication, Fisheries Queensland, Cairns, p. 92.

Chartrand, K.M., M. Rasheed, K. Petrou and P. Ralph, 2012b. Establishing tropical seagrass light requirements in a dynamic port environment. Proceedings of the 12th International Coral Reef Symposium, Cairns, Australia, 9-13 July 2012, paper 15B 'Seagrasses and seagrass ecosystems'.

Chisholm, W.J., 2009. The stability of shallow coastal sediments with and without seagrasses. PhD thesis, Murdoch University, Perth (Australia).

Clarke S.M. and H. Kirkman, 1989. Seagrass dynamics. In: Larkum A.W.D., McComb A.J. and Shepherd S.A. (Eds.), Biology of Seagrasses. Elsevier, Amsterdam, pp. 304-345.

Collier, C.J., Lavery, P.S., Masini, R.J., Ralph, P.J., 2009. Shade-induced response and recovery of the seagrass *Posidonia sinuosa*. J. Exp. Mar. Biol. Ecol. 370, 89–103.

Collier, C.J., M. Waycott and A. Giraldo Ospina, 2012. Responses of four Indo-West Pacific seagrass species to shading. Marine Pollution Bulletin 65: 342–354.

Collier, C.J., M. Waycott and L.J. McKenzie, 2012. Light thresholds derived from seagrass loss in the coastal zone of the northern Great Barrier Reef, Australia. Ecological Indicators 23: 211–219.

Collier C.J., C. Villacorta-Rath, K.-j. van Dijk, M. Takahashi and M. Waycott, 2014. Seagrass proliferation precedes mortality during hypo-salinity events: a stress-induced morphometric response. PLoS ONE 9(4): e94014. doi:10.1371/journal.pone.0094014

Deltares, 2014. Adelaide Receiving Environment Model – Pilot Model set-up and evaluation. Deltares, Technical Report (version 8), November 2014.

Deltares, 2015. Adelaide Receiving Environment Model – Phase 2 Inception Report. Deltares, Technical Report, April 2015.

Erftemeijer, P.L.A., 2013. Seagrass Habitat Model - Adelaide's Coastal Waters: Literature review of habitat requirements of seagrasses in Adelaide's coastal waters. Sinclair Knight Merz, Technical Report, prepared for Deltares & SA Water, Perth, December 2013, 42 pp.

Fitzpatrick, J. and H. Kirkman, 1995. Effects of prolonged shading stress on growth and survival of seagrass *Posidonia australis* in Jervis Bay, New South Wales, Australia. Marine Ecology Progress Series 127: 279-289.

Gordon DM, Grey KA, Chase SC, Simpson CJ (1994) Changes to the structure and productivity of a *Posidonia sinuosa* meadow during and after imposed shading. Aquat Bot 47:265–275

Hocking, P.J., M.I. Cambridge and A.J. McComb, 1981. The nitrogen and phosphorus nutrition of developing plants of two seagrasses, *Posidonia australis* and *Posidonia sinuosa*. Aquatic Botany 11: 245-261.

Infantes, E., Terrados, J., Orfila, A., Cañellas, B., Álvarez-Ellacuria, A., 2009. Wave energy and the upper depth limit distribution of *Posidonia oceanica*. Botanica Marina 52: 419–427.

Infantes, E., A. Orfila, T.J. Bouma, G. Simarro and J. Terrados, 2011. *Posidonia oceanica* and *Cymodocea nodosa* seedling tolerance to wave exposure. Limnology and Oceanography 56(6): 2223-2232.

Inglis, G.J., 2000. Variation in the recruitment behaviour of seagrass seeds: implications for population dynamics and resource management. Pacific Conservation Biology 5(4): 251-259.

Irving, A.D., 2013. A century of failure for habitat recovery. Ecography 36: 414-416.

Jarvis, J. C. and K. A. Moore. 2010. The role of seedlings and seed bank viability in the recovery of Chesapeake Bay, USA, *Zostera marina* populations following a large-scale decline. Hydrobiologia 649: 55-68.

Kendrick G.A., M. Waycott, T.J.B. Carruthers, M.L. Cambridge, R. Hovey, S.L. Krauss, P.S. Lavery, D.H. Les, R.J. Lowe, O. Mascaró i Vidal, J.L.S. Ooi, R.J. Orth, D.O. Rivers, L. Ruiz-Montoya, E.A. Sinclair, J. Statton, J.K. van Dijk, and J.J. Verduin, 2012. The central role of dispersal in the maintenance and persistence of seagrass populations. BioScience 62(1): 56-65.

Kirkman, H., A. Cohen and H. Houridis, 2012. A seagrass shading experiment to determine the effects of a dredge plume. Victorian Naturalist Vol 129 (3): 97-108.

Kiswara, W., P. van Avezaath, A.H.L. Huiskes, P.L.A. Erftemeijer and T.J. Bouma, 2009. Root architecture of six oligotrophic seagrass species growing in three contrasting habitats. Aquatic Botany 90: 235-245.

Kuo, J. and H. Kirkman, 1990. Anatomy of viviparous seagrasses: seedlings of *Amphibolis* and *Thalassodendron* and their nutrient supply. Botanica Marina 33: 117-126.

Lavery, P.S., K. McMahon, M. Mulligan, A. Tennyson, 2009. Interactive effects of timing, intensity and duration of experimental shading on *Amphibolis griffithii*. Marine Ecology Progress Series 394: 21–33.

Longstaff, B.J., Loneragan, N.R., O'Donohue, M.J., Dennison, W.C., 1999. Effects of light deprivation on the survival and recovery of the seagrass *Halophila ovalis* (R.Br.) Hook. J. Exp. Mar. Biol. Ecol. 234, 1–27.

Mackey, P., C.J. Collier and P.S. Lavery, 2007. Effects of experimental reduction of light availability on the seagrass *Amphibolis griffithii*. Marine Ecology Progress Series 342: 117–126.

Macreadie, P.I., P.H. York and C.D.H. Sherman, 2014. Resilience of *Zostera muelleri* seagrass to small-scale disturbances: the relative importance of asexual versus sexual recovery. Ecology & Evolution, doi: 10.1002/ece3.933.

McKenzie, L.J. and R.L. Yoshida, 2015. Seagrass-Watch: Proceedings of a workshop for monitoring seagrass habitats in the Burnett Mary Natural resource Management Region, University of Southern Queensland, Fraser Campus, Hervey Bay, Queensland, 29-30 August 2015 (Seagrass-Watch HQ, Cairns), 68 pp.

McMahon, K., P.S. Lavery and M. Mulligan, 2011. Recovery from the impact of light reduction on the seagrass *Amphibolis griffithii*, insights for dredging management. Marine Pollution Bulletin 62: 270–283.

Meehan, A.J. and R.J. West, 2004. Seedling development and patch formation of the seagrass *Posidonia australis* in a southeast Australian estuary. Aquatic Botany 79: 1-14.

Neverauskas, V., 1988. Response of a *Posidonia* community to prolonged reduction in light. Aquat. Bot., 31: 361-366.

Orth, R.J., M.C. Harwell and G.J. Inglis, 2006. Ecology of Seagrass Seeds and Seagrass Dispersal Processes. Chapter 5 in: A.W.D. Larkum et al. (Eds) Seagrasses: Biology, Ecology and Conservation, Springer, pp. 111-133.

Paling, E.I and A . J. McComb, 1994. Nitrogen and phosphorus uptake in seedlings of the seagrass *Amphibolis antarctica* in Western Australia. Hydrobiologia 294: 1-4.

Rasheed, M.A., S.A. McKenna, A.B. Carter and R.G. Coles, 2014. Contrasting recovery of shallow and deep water seagrass communities following climate associated losses in tropical north Queensland, Australia. Marine Pollution Bulletin 83: 491–499.

Rivers, D., Kendrick, G., Walker, D.I., 2011. Microsites play an important role for seedling survival in the seagrass *Amphibolis antarctica*. J. Exp. Mar. Biol. Ecol. 401(1): 29–35.

Serrano, O., M.A. Mateo and P. Renom, 2011. Seasonal response of *Posidonia oceanica* to light disturbances. Marine Ecology Progress Series 423: 29-38.

Shepherd S.A. and E.L. Robertson, 1989. Regional studies - seagrasses of South Australia, Victoria and Bass Strait. In: Larkum A.W.D., McComb A.J. and Shepherd S.A. Eds. Biology of Seagrasses. Elsevier, Amsterdam, pp. 211-229.

Statton, J., G.A. Kendrick, K.W. Dixon and M.L. Cambridge, 2014. Inorganic nutrient supplements constrain restoration potential of seedlings of the seagrass *Posidonia australis*. Restoration Ecology 22(2): 196-203.

Vacchi, M., Montefalcone, M., Bianchi, C.N., Morri, C., Ferrari, M., 2012. Hydrodynamic constraints to the seaward development of *Posidonia oceanica* meadows. Estuarine, Coastal and Shelf Science 97: 58–65.

Vacchi, M., M. Montefalcone, C.F. Schiaffino, V. Parravicini, C.N. Bianchi, C. Morri and M. Ferrari, 2014. Towards a predictive model to assess the natural position of the *Posidonia oceanica* seagrass meadows upper limit. Marine Pollution Bulletin 83: 458–466.

Valdemarsen, T., P. Canal-Verges, E. Kristensen, and M. Holmer. 2010. Kristiansen MD, Flindt MR: vulnerability of *Zostera marina* seedlings to physical stress. Mar. Ecol. Prog. Ser. 418:119–130.

Verduin, J.J., A. Seidlitz, M. van Keulen and EI. Paling, 2013. Maximising establishment success of *Amphibolis antarctica* seedlings. Journal of Experimental Marine Biology and ecology 449: 57-60.

Walker, D.I., M.L. Campey and G.A. Kendrick, 2004. Nutrient dynamics in two seagrass species, *Posidonia coriacea* and *Zostera tasmanica*, on Success Bank, Western Australia. Estuarine, Coastal and Shelf Science 60: 251-260.

Wear, R.J., Tanner, J.E., and S.L. Hoare, 2010. Facilitating recruitment of *Amphibolis* as a novel approach to seagrass rehabilitation in hydrodynamically active waters. Mar. Freshw. Res. 61 (10), 1123–1133.

Yaakub, S.M., E. Chen, T.J. Bouma, P.L.A. Erftemeijer and P.A. Todd, 2013. Chronic light reduction reduces overall resilience to further shading stress in the seagrass *Halophila ovalis*. Marine Pollution Bulletin 83: 467-474.

G Simulated HSI and stressors for individual seagrass species

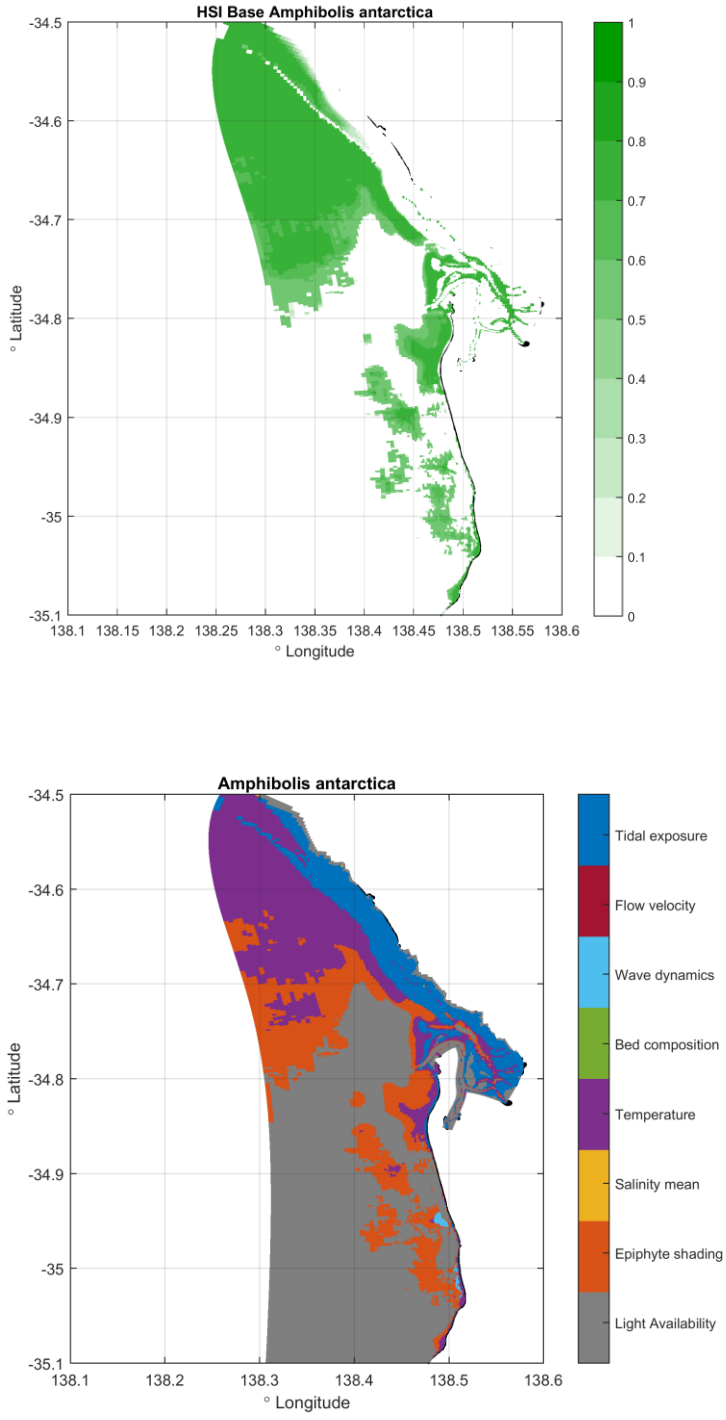

Figure G.1 Habitat suitability index (top) and most limiting environmental condition (bottom) for Amphibolis antarctica

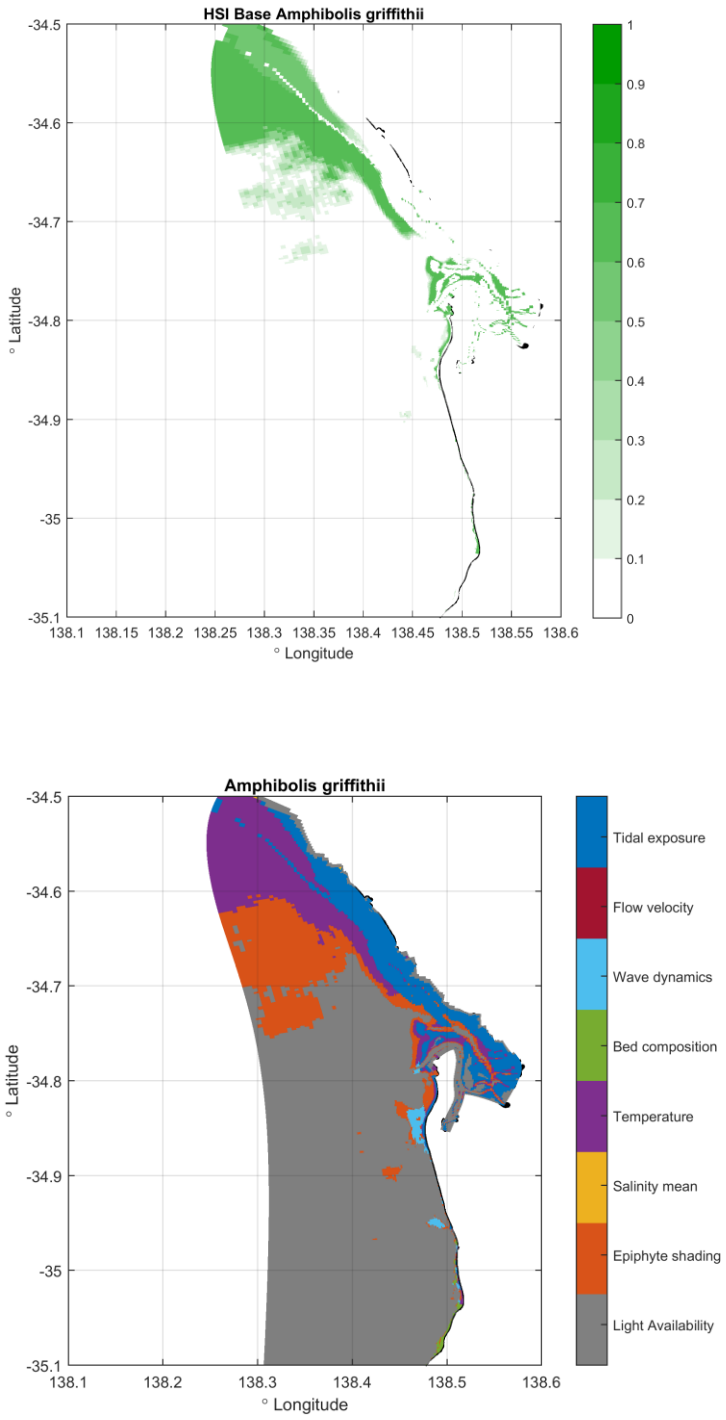

Figure G.2 Habitat suitability index (top) and most limiting environmental condition (bottom) for Amphibolis griffithii

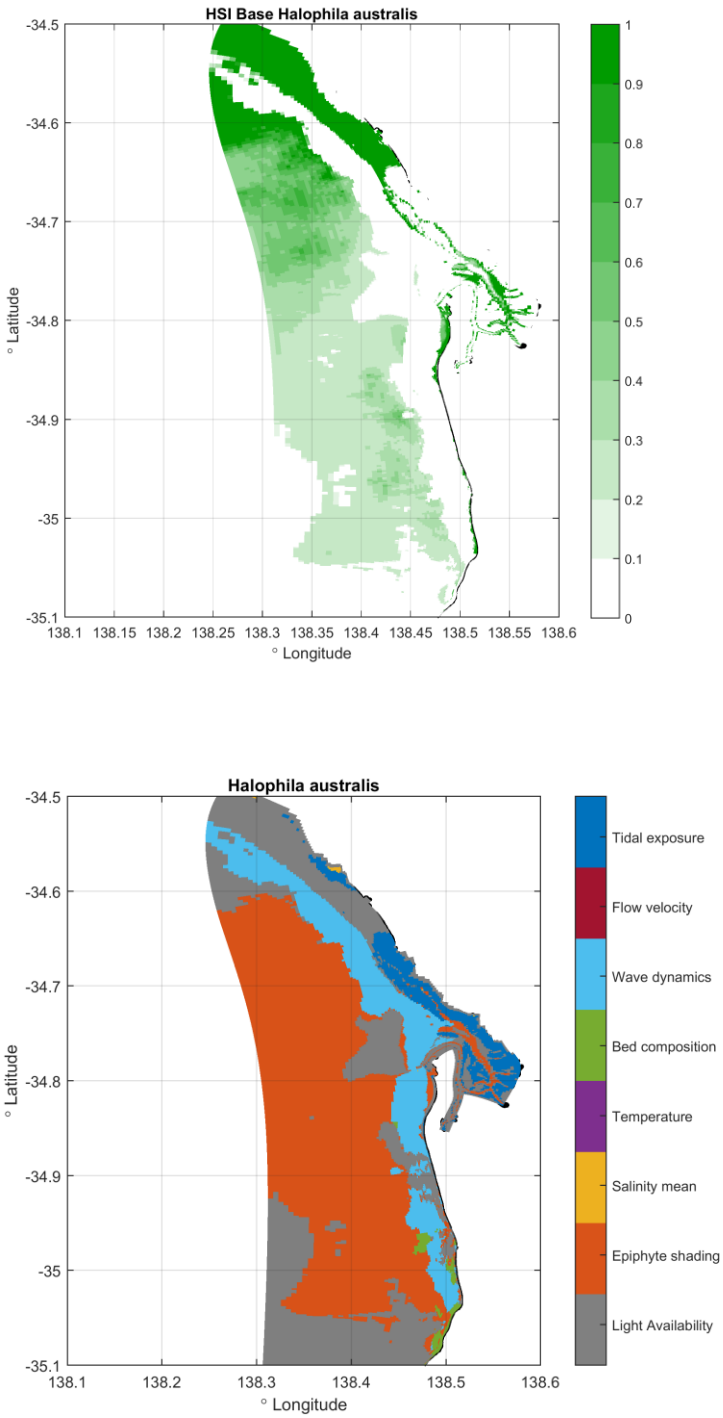

Figure G.3 Habitat suitability index (top) and most limiting environmental condition (bottom) for Halophila australis

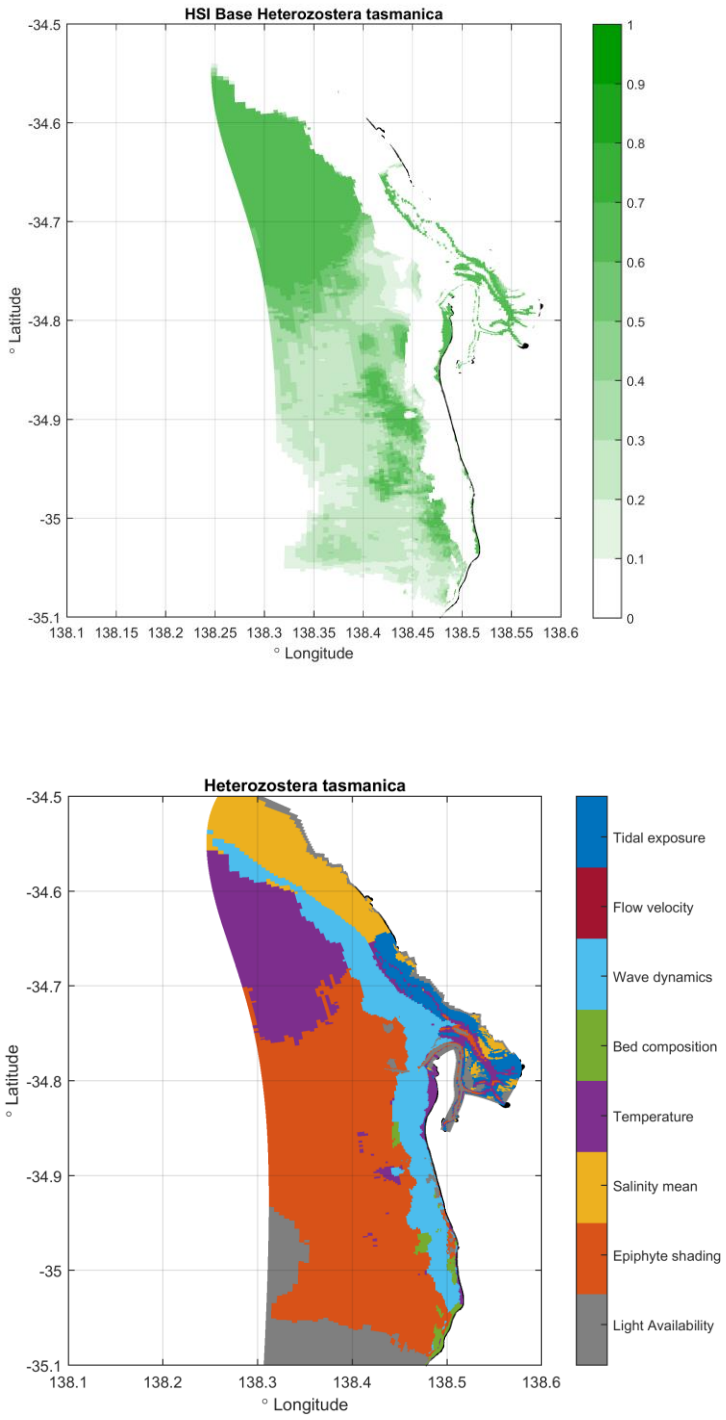

Figure G.4 Habitat suitability index (top) and most limiting environmental condition (bottom) for Heterozostera tasmanica

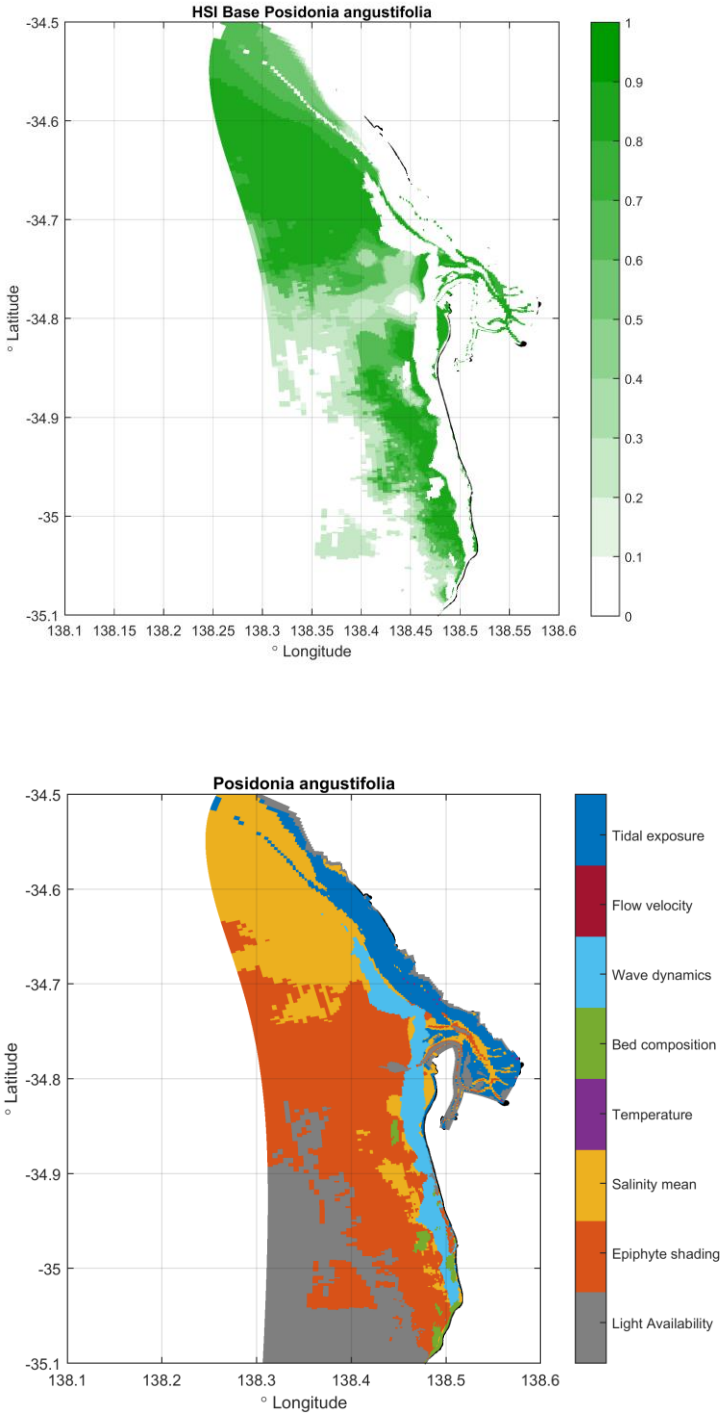

Figure G.5 Habitat suitability index (top) and most limiting environmental condition (bottom) for Posidonia angustifolia

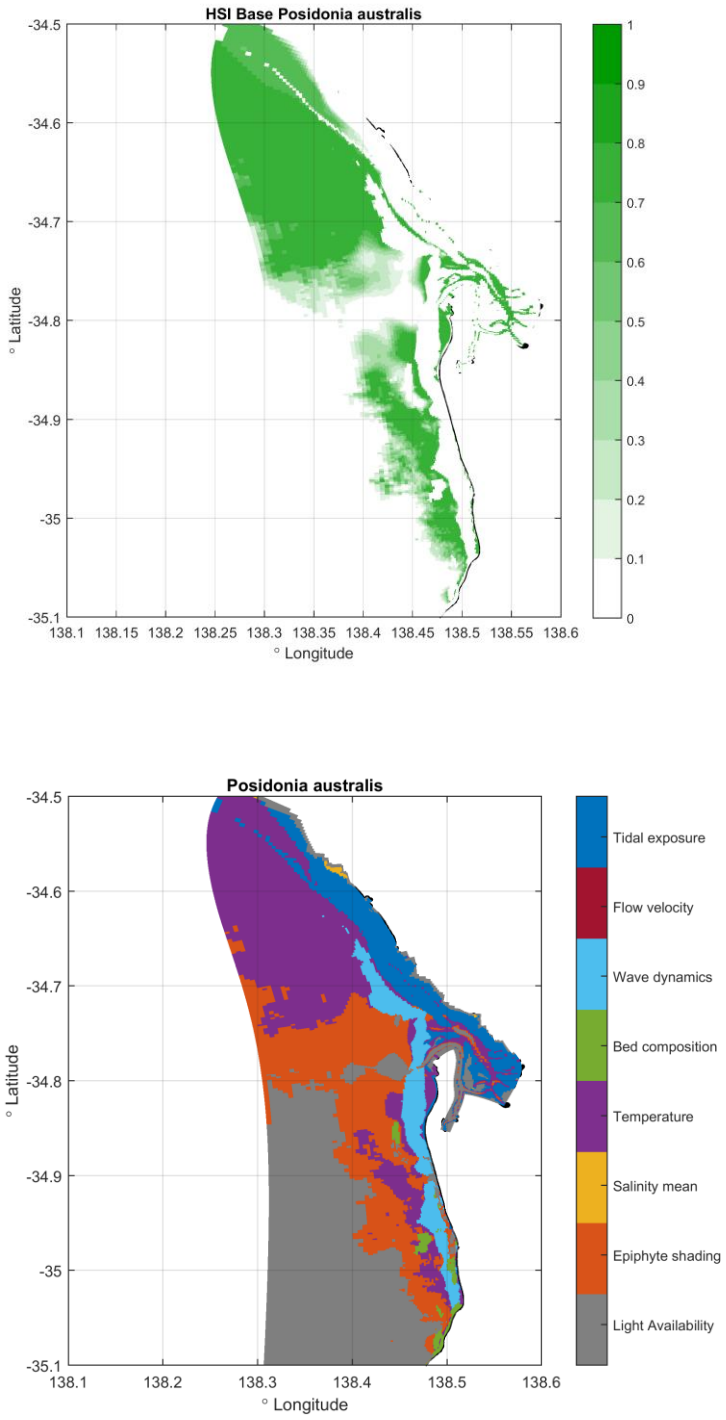

Figure G.6 Habitat suitability index (top) and most limiting environmental condition (bottom) for Posidonia australis

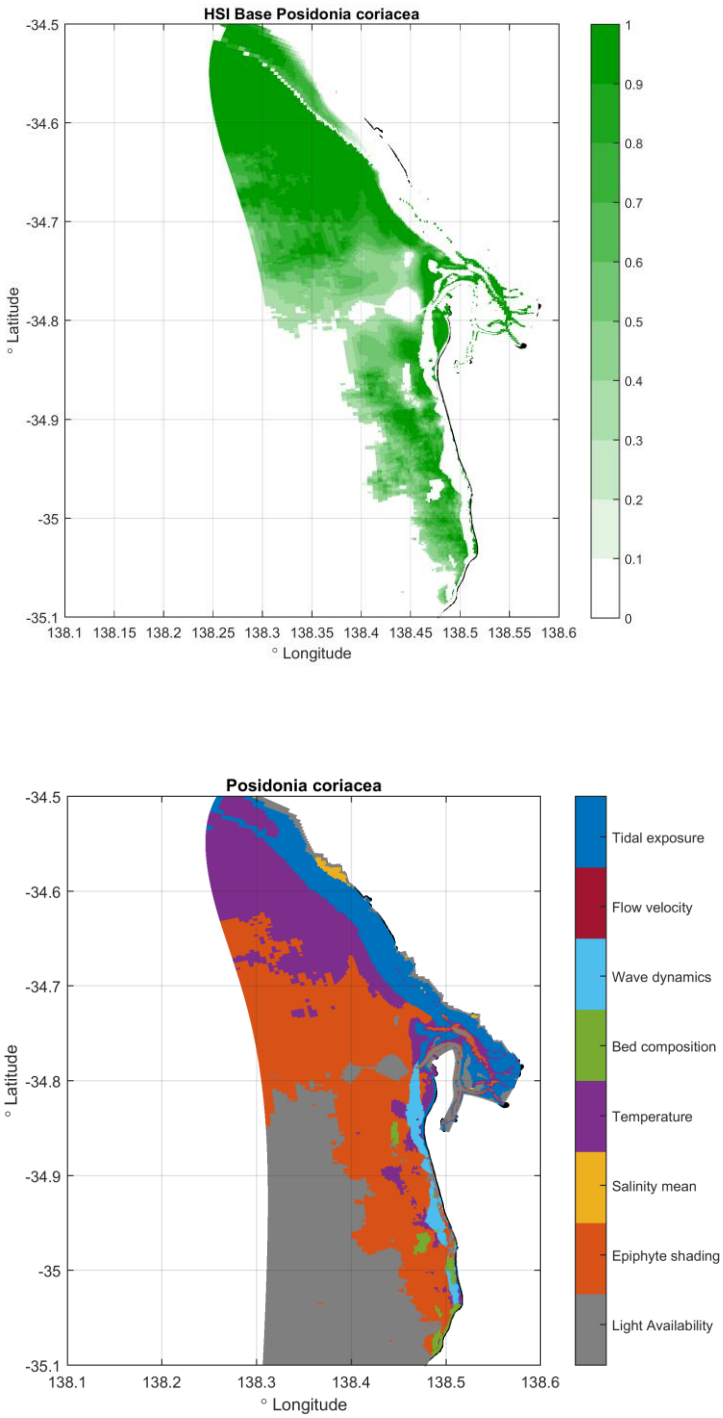

Figure G.7 Habitat suitability index (top) and most limiting environmental condition (bottom) for Posidonia coriacea

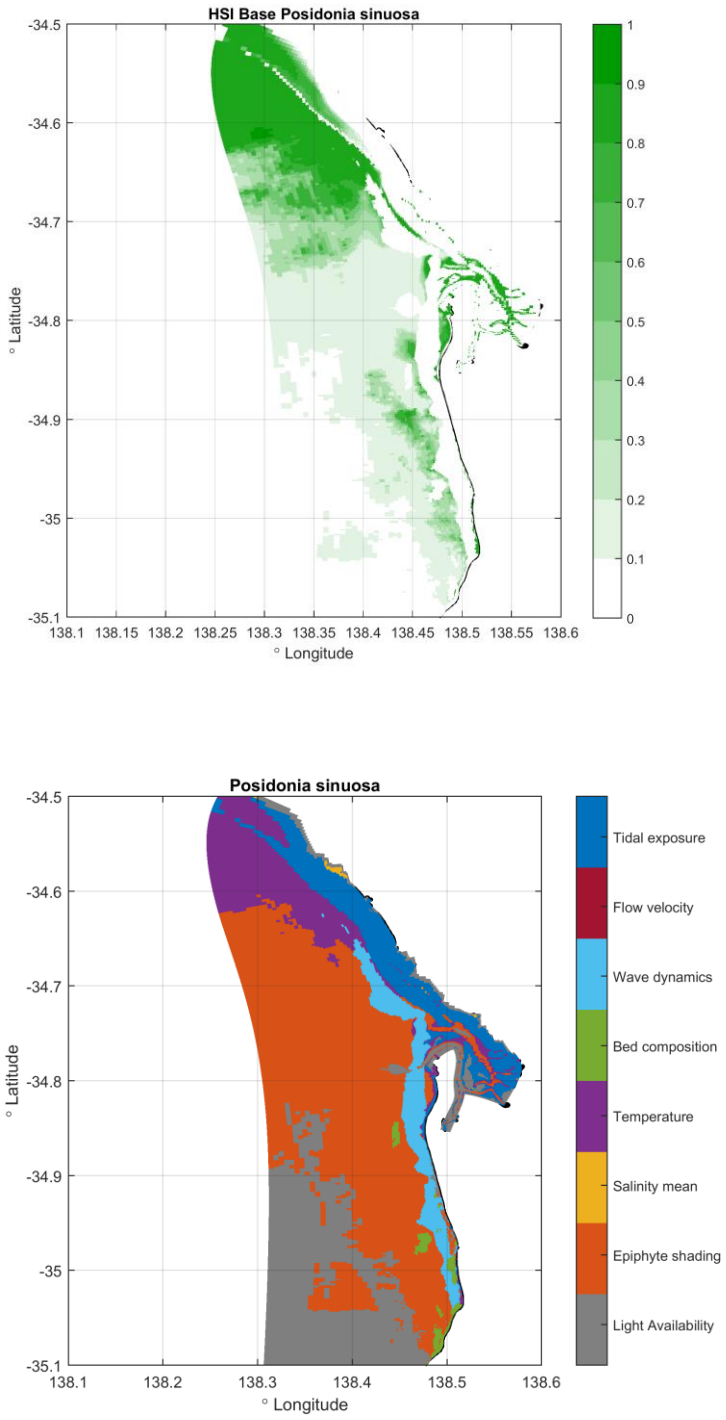

Figure G.8 Habitat suitability index (top) and most limiting environmental condition (bottom) for Posidonia sinuosa

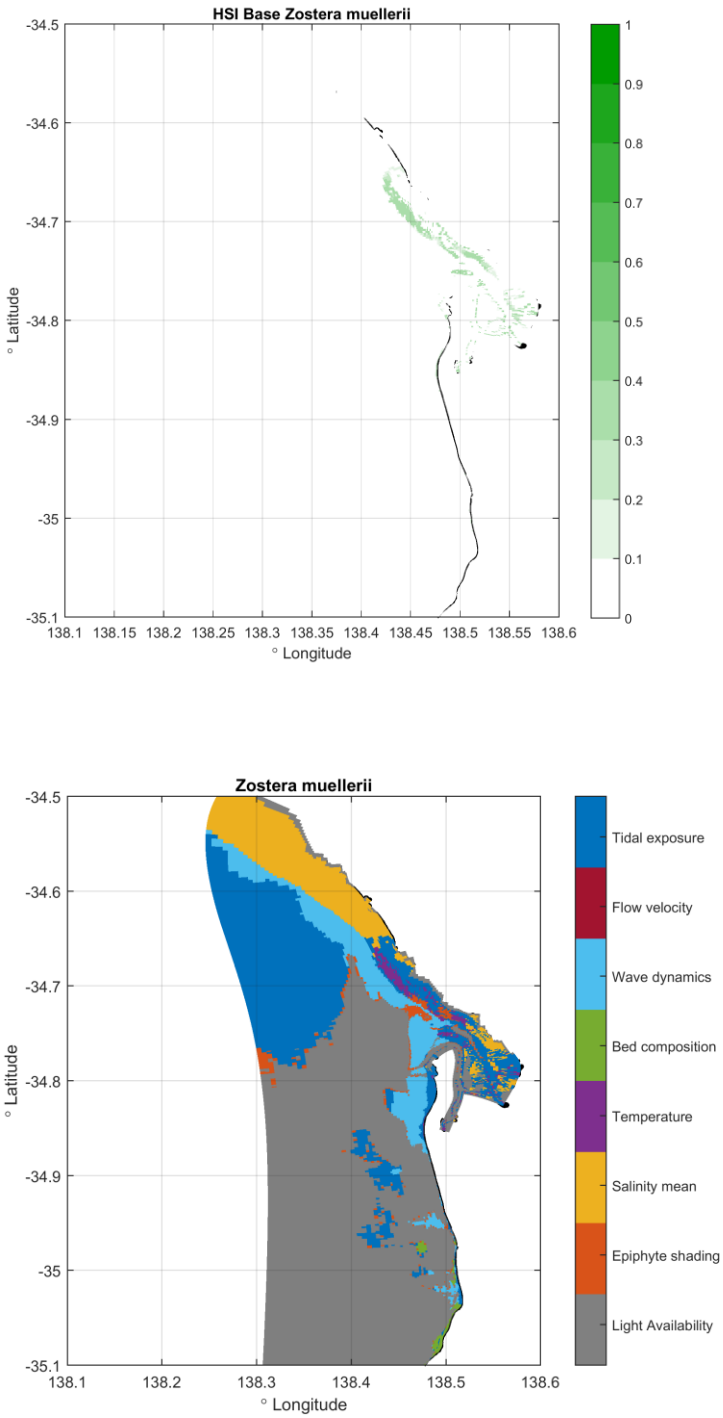

Figure G.9 Habitat suitability index (top) and most limiting environmental condition (bottom) for Zostera muellerii

H The impact of Bolivar Lagoon particle discharges on the downward attenuation of light

H.1 Introduction

Part of the Bolivar WWTP effluents pass a system of lagoons which leads to a change of the nature of particles discharged to the sea. In particular, the particles discharged via the lagoon system have a higher organic content. In this appendix, we investigate what the organic content of the particles means for the impact of the discharge on the downward attenuation of photosynthetically active radiation (PAR), expressed by the K_d coefficient in m^{-1}.

H.2 Method

We calculate the quality of a pocket of water moving with the currents for a period of 10 days (240 hours) after discharge. The quality is undergoing changes due to settling and the decay of the organic fraction. The dilution with ambient water masses is neglected. The concentrations calculated by this approach will in reality be lower, since the discharged material will be mixed over a larger volume. The model can be expressed as follows:

$$\frac{dC}{dt} = -k_{removal}\, C$$

with C (g m^{-3}) the concentration of a fraction of suspended solids and $k_{removal}$ (d^{-1}) the total removal rate by decay and sedimentation:

$$k_{removal} = k_{decay} + \frac{v_s}{Z}$$

with k_{decay} (d^{-1}) the decay rate, v_s (m d^{-1}) the effective settling velocity and Z the water depth. The model is solved numerically by a simple explicit time stepping algorithm:

$$C^{t+\Delta t} = C^t - \Delta t\, k_{removal}\, C^t$$

Table H.1 Modelled fractions of SS and their properties

Fraction		k_{decay} (1/d)	v_s (m/d)	C(t=0) - Case 1	C(t=0) - Case 2
IM1	mg/L	0	0.5	2	1.25
IM2	mg/L	0	2	6	3.75
IM3	mg/L	0	5	32	20
POC1	mgC/L	0.15	1.5	0.8	2
POC2	mgC/L	0.015	1.5	3.2	8
SS	mg/L			50	50

The modelled fractions of suspended matter are listed in Table H.1 with the associated settling velocity and decay rate, as well as the initial concentrations for two cases (1) 20% of SS is organic, and (2) 50% of SS is organic. The fractions distinguished are the same as in the AREM (Chapter 4), and the same holds for their settling velocities and decay rates. The separation of SS in fractions follows the methodology outlined in Chapter 2 for the Bolivar Lagoon discharge. The settling velocities are applied with a correction for the shear stress term (Appendix B) which we set to a value of 0.5. This is a value estimated by expert judgement, since in reality it depends on the depth and the hydraulic conditions. The water

depth has been set to a value of 3m, reflecting the shallowness of the Bolivar discharge receiving waters. The downward attenuation coefficient K_d is finally calculated as discussed in Chapter 3.

H.3 Results

Figure H.1 shows the calculated K_d for cases (1) and (2), as well as the ratio between the two, over a period of 240 hours after release, under the influence of decay of organic matter and settling of particles.

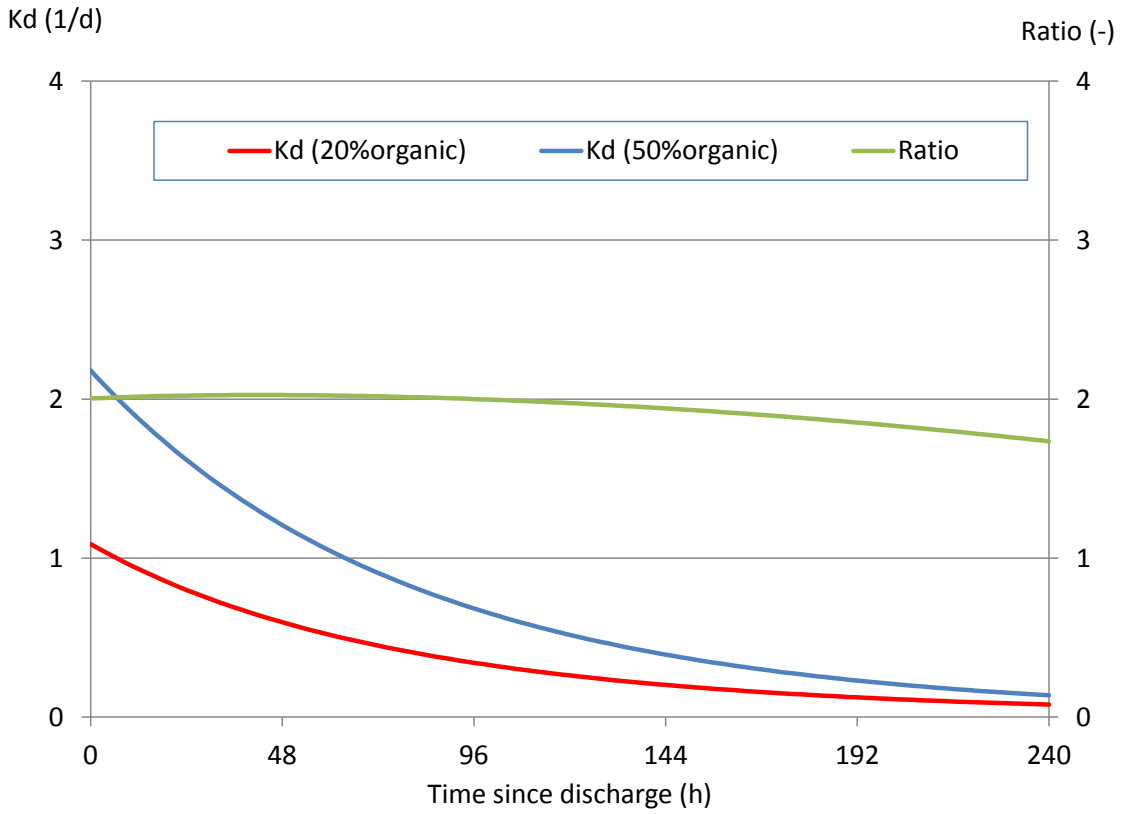

Figure H.1 Calculated K_d assuming an initial concentration of SS equal to 50 mg/L consisting of 50% organic particles and 20 % organic particles respectively, as well as the ratio between the two, over a period of 240 hours after release, under the influence of decay of organic matter and settling of particles.

The results show that in the effluent the K_d is about 2 times higher in case 2 (50% organic matter) than in case 1 (20% organic matter). This ratio remains close to this value during the analysed period of 10 days after discharge. It does not really make sense to continue this assessment over longer periods, since environmental mixing and variable bathymetric and hydrodynamic conditions will gain increasing importance. In summary, the light attenuation properties of suspended matter depend strongly on their composition. Under conditions like those near the Bolivar discharge this dependency is expected to persist also after discharge in the receiving environment.

www.deltares.nl

Deltares